MASTER'S THESIS REPORT

By

Ewa Anna Kunicka

CONCRETE SLAB BENEATH BALLAST BED

An Abatement Measure For Railway Induced Vibration

Graduation committee:

Dr. ir. K.N. van Dalen	*Chairman*	*TU Delft*
Prof. dr. A.V. Metrikine	*Supervisor*	*TU Delft*
Dr. J.M. de Oliviera Barbosa	*Supervisor*	*TU Delft*
Ir. P. Lagendijk	*Supervisor*	*TU Delft*
Ir. J.M. Houben	*Supervisor*	*TU Delft*
Ir. Saeed Hosseinzadeh	*Supervisor*	*Arcadis*

Faculty of Civil Engineering and Geoscience

Delft University of Technology

November 2019

Abstract

In this research project, an assessment of an abatement measure for mitigating railway induced vibrations is carried out. Ground-borne vibrations, which are primarily generated due to wheel-rail interaction, may also result in ground-borne noise in the buildings located in vicinity of railway tracks. An example of adverse environmental impact caused by ground-borne vibration and noise is the annoyance to people living those buildings. Assessing ground-borne vibration and noise is of crucial importance, especially in soft soils in which Rayleigh wave velocity is low and amplification of vibrations is more likely to occur. For mitigating the ground-borne vibration and noise exceeding the threshold values defined by technical standards in each country, abatement measures are applied.

The main objective of this research is assessing the effectiveness of 'concrete slab beneath ballast bed' used as the abatement measure for reducing vibrations. For this purpose, Plaxis 3D based on Finite Element Analysis method is employed. Numerical model is created and validated through measurement data available from field tests conducted in the Netherlands. After having numerical model validated, several simulations are performed in order to study the factors influencing ground-borne vibrations.

From the results of this study, one can conclude that 'concrete slab beneath ballast bed' is effective in reducing vibration strength at all distances when train speed is considerably lower than Rayleigh wave velocity of the uppermost soil layer. It is notable, however, that the application of this measure may bring about amplification of the vibration strength in the vicinity of the track for trains running at hinger speeds. Nevertheless, regardless of the train speed, there is always a reduction in the vibration strength at further distances from the railway track. From practical standpoints, this aspect is of interest for the buildings located in the far field.

From the results of a sensitivity analysis on changes to the width and thickness of the concrete slab, it can be concluded that an optimal solution of concrete slab dimensions can be found. It is observed that by changing concrete slab dimensions, the maximum vibration strength is mostly affected in close proximity to the railway track.

In addition, the dispersion lines and oscillatory moving load in the Wavenumber-Frequency plane are analyzed. Their intersection indicates that the moving oscillatory load excites a wave of frequency and wavenumber given by the intersection point. If these frequencies are harmful for the environment then concrete slab application can diminish their content from response. Sleeper passing frequency content increases when the concrete slab is applied.

The obtained results and recommendations from this study can be used for further studying the other factors influencing the effectiveness of the measure. Examples of these factors include, among others, various ground conditions (e.g., soft soils of different stratifications, local changes in soil properties, etc.), and optimization of concrete slab dimensions, material parameters, as well as, cracked and uncracked concrete stage. The numerical model developed during this research study can be further employed to analyze different aspects of railway induced ground-borne vibrations.

Table of Figures

List of Tables

Contents

1. Introduction

1.1. Problem statement and research motivation

Studying railway induced ground-borne vibration and noise, due to the adverse environmental impact, has gained great attention over the past two decades. Examples of the adverse environmental impact in urban areas can be found in (Connolly, et al., 2016; Janssen, et al., 2015; Tatara & Kozuch, 2017). This is caused by several reasons including, among others, increasing operational train speed and weight of trains, which in return, introduces higher forces acting on the train-track system. An example of this effect is the well documented case of Ledsgård in Sweden, in which excessive vibrations were detected during passage of X-2000 train with the increment of speed up to 200km/h (Madhus & Kaynia, 2000).

One of the challenges to railway projects is the presence of soft soils such as peat or clay where the Rayleigh wave velocity is very low. In these soft soils there is a high risk of amplification of the displacements of the railway track, which increases together with increasing operational train speed (Paul de Vos, 2017; Madhus & Kaynia, 2000). Such phenomenon is common in some European countries such as Sweden or the Netherlands where soft soils are present.

The vibrations generated by the passage of freight and passenger trains might lead to the exceedance of the threshold levels of vibration at dwelling/buildings in the vicinity of railway tracks. Once the threshold levels of vibrations, defined based on national policies and regulations, are exceeded, an abatement measure assessment must be performed. Vibration abatement measures can be studied through three different groups. These include measures at the source of vibration (Deutsche Bahn, 2011), measures through the propagation path which are used between the vibration source and receiver (e.g. (Coulier, et al., 2013; Coulier, et al., 2014; Dijckmans, et al., 2015; Barbosa, 2013)), and measures at the receiver (e.g. (Sadeghi & Hasheminezhad, 2014)).

From practical perspective, it is often favorable to apply the measure at the source of vibration. Examples of these measures include, among others, slab track (Steenbergen, et al., 2007; Gautier, 2015), commonly used resilient pads as well as concrete slab beneath ballast bed. The latter has been applied in the Netherlands. Detailed explanation of abatement measures are contained in section 2.4.

To investigate these measures, researchers used different methods (for the exposition of the methods see section 2.3). Examples of these methods are numerical approaches such as 2D, 2.5D, and 3D models as well as empirical and analytical methods.

The objective of this research is to investigate the effectiveness of the concrete slab beneath ballast as a vibration abatement measure. For this purpose the author employed numerical model in Plaxis3D (Brinkgreve, et al., 2018) which is based on finite element method. The model was verified with available measurements, through numerical simulations investigating the influence of factors such as embankment details, wheel load formulation, changing soil profile, damping ratio for soil stratum and more (see chapter 5). The effectiveness of concrete slab beneath ballast is assessed in terms of changing slab width, thickness, train speed, as well as cracked and uncracked concrete material. Strength of the vibration and frequency content of the response before and after concrete slab application is analyzed.

1.2. Organization of the document

The thesis report begins with the literature review on different aspects of railway induced vibration and noise in Chapter 2. Furthermore, the description of different prediction models of railway induced vibration and noise and their associated difficulties are included.

Next, in Chapter 3 plan of the measurements and equipment used to conduct the test are described. Moreover, the soil profile is established based on the Cone Penetration Test (CPT) and cross-section of the embankment is described. Parameters related to sleepers, rail and fasteners are introduced.

Chapter 4 is the main description of the numerical model developed in this study as well as its associated parameters. These include model size, mesh, simulation phases, boundary conditions settings for particular system elements (e.g. railpad damping parameters). Next, the methods of simulating the moving load in the model are explained.

Chapter 5 focuses on description of the results of the measurements and numerical models where concrete slab is not applied.

The influence of the embankment cross-section layout, soil profile properties and geometry, methods of load simulation, and other particular components is assessed. Frequency and time domain of the signals are investigated.

Chapter 6 focuses on the assessment of effectiveness of concrete slab abatement measure. Its variations were investigated in terms of changing slab thickness, width and train speed.

Conclusions and recommendations for future work are described in Chapter 7.

In Appendix A, more detailed information about parameters of elements described in Chapter 3 are included.

Appendix B includes detailed numerical simulations phases described in Chapter 4.

Appendix C contains the results of some simulation studies discussed in Chapter 5.

In Appendix D results of some simulations performed in Chapter 6 are shown.

2. Literature review

2.1. Theoretical background

In order to understand the process of vibration propagation in soil the theoretical background shall be introduced. In the following section different wave types will be discussed. Next, different types of damping will be presented together with the Rayleigh damping representation of damping ratio. Later the phenomenon of Mach cone will be introduced together with the critical speed. Explanation of what it means for soil will be briefly presented. For more information about waves and another aspect of this sub-section one can refer to (Hall, 2000; Paul de Vos, 2017; van Dalen, 2015; Spijkers, et al., 2005) or another earthquake engineering or soil dynamics text book.

2.1.1. Wave types

Crucial wave types are explained in the section below. They can be divided between surface waves and body waves.

2.1.1.1. Body waves

Compression waves – called also P-waves, where the movement of a single particle is in the longitudinal direction (parallel to the propagation direction). These waves travel through compression and expansion of the material. They have the highest wave speed when compared to the other types of waves. Moreover, they can travel through soil and fluids. They propagate into the soil stratum. The graphical representation is shown in Figure 2.1.

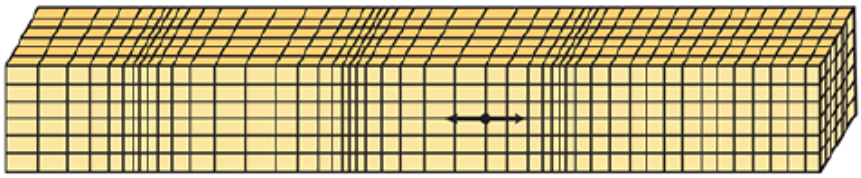

Figure 2.1. P-waves graphical representation. (Paul de Vos, 2017)

Shear waves – known also as S-waves, where the movement of the single particle is perpendicular to the propagation direction. These waves cannot propagate in fluids, but only in ground. They propagate into the soil stratum. Their graphical representation is shown in Figure 2.2.

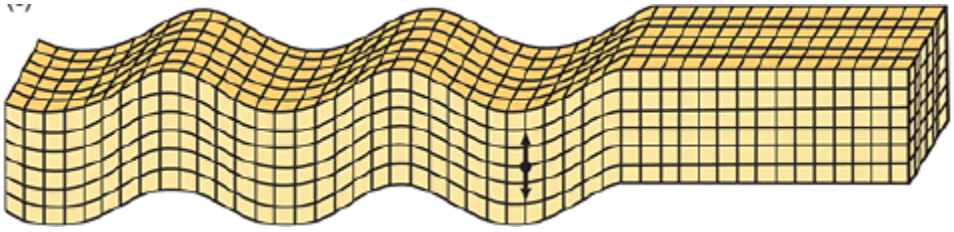

Figure 2.2 S-waves graphical representation. (Paul de Vos, 2017)

2.1.1.2. Surface waves

Surface waves are the result of interaction between body waves P and S, ground surface and upper layers of the ground. The amplitude of surface waves decreases approximately exponentially with depth. (Hall, 2003). They also attenuate faster than body waves. However, they are more damaging than the body waves because they occur at the surface. Surface waves are dispersive meaning that their speed depends on frequency.

Rayleigh waves are propagating only at the free surface. The particles follow an elliptical path in the direction counter clockwise to the direction of wave propagation. Rayleigh waves propagation speed is lower by around 10% comparing to the shear waves (Paul de Vos, 2017). Most of the interest is put into Rayleigh waves, because they can have much larger impact on the structure than the other waves and they do not suffer from geometrical damping (refer to section 2.1.2). Their graphical representation is shown in Figure 2.3.

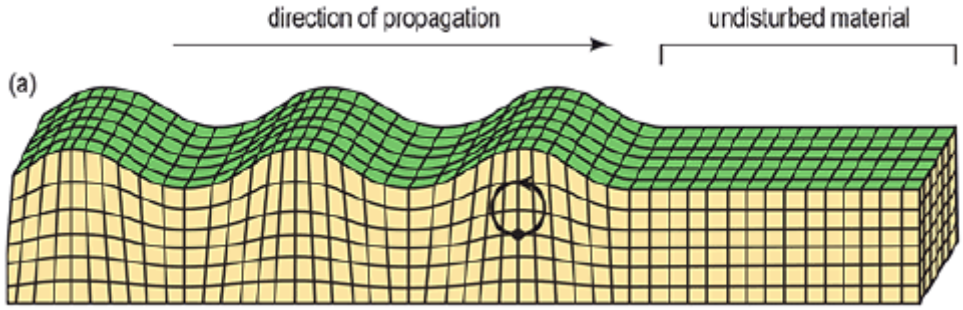

Figure 2.3 Rayleigh waves - graphical representation. (Paul de Vos, 2017)

Love waves are characterized by the so called "zig-zag" motions. The particles are moving transverse to the direction of propagation. Love waves might occur when the top layer has noticeably smaller Young's modulus (what implies smaller wave speed) than the top layer. Then the wave is trapped in the top layer by means of multiple reflections. The graphical representation of Love waves is shown in Figure 2.4.

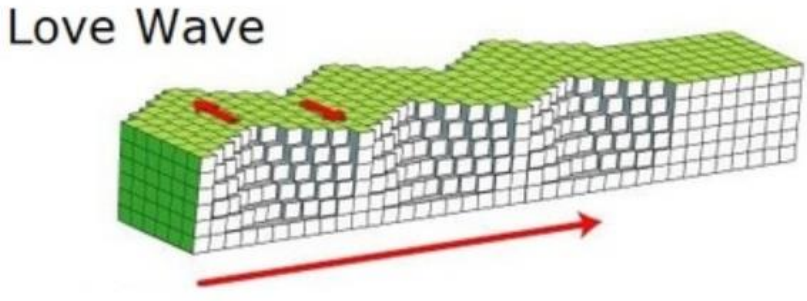

Figure 2.4 Love wave – graphical representation (Waikato, n.d.)

All types of waves decay due to damping. Material and geometrical damping are distinguished and described in the next section.

2.1.2.Types of damping

Geometrical damping is caused by spread of the energy over a larger distance. The simplest example can be ripples at water surface. After throwing a rock in the water ripples start to form. Their amplitude is higher at the point where the stone hit the surface because the energy of the falling stone acts on the limited water volume. With propagation of waves the energy is transferred to larger amount of water and the amplitude of ripples decreases

The reason for material damping are losses of energy during transmission int the medium by means of friction. Material damping is higher in the soft soils, and it increases together with increasing frequencies. It is defined by means of so called coefficient of attenuation, which is the frictional damping characteristics of the soil.

Both types of damping attenuate vibrations. In Equation of Motions (EOM) the damping coefficient is represented by "c" parameter.

In the next section it is briefly explained how to solve EOM for N-dimensional system and what problems come along with "c" parameter. As a handy solution to this problem the approach introduced by Lord Rayleigh will be presented.

2.1.3.Damping coefficient in Equation of Motions

2.1.3.1. Modal analysis for undamped and damped systems

Modal analysis is a method to solve a set of EOM equations in matrix notations. EOM equations once defined and written down are coupled. In other to solve a system in matrix notations one needs to decouple them. Decoupling is performed, because the analysed structure can have thousands of degrees of freedom (DOFs). It is easier to solve N decoupled equations than NxN matrix consisting of coupled equations. Mathematically, coupling means that matrix contains off diagonal elements. The goal is to have the matrix of decoupled equations meaning that only the main matrix diagonal has non-zero values. In order to achieve such matrix, **M** and **K** matrixes need to be pre-multiplied with a transposed and post-multiplied with an eigenmatrix. Eigenmatrix is a matrix consisting of eigen vectors. In matrix notations, the diagonal matrices are written as:

$$\boldsymbol{M}^* = \boldsymbol{E}^T\boldsymbol{M}\boldsymbol{E} \qquad \textit{Eq. 1}$$

$$\boldsymbol{K}^* = \boldsymbol{E}^T\boldsymbol{K}\boldsymbol{E} \qquad \textit{Eq. 2}$$

where:

$\mathbf{M}^*$ - modal mass matrix

$\mathbf{K}^*$ - modal stiffness matrix

E – eigenmatrix

These considerations were done on an undamped system. By adding damping to EOM one obtains a system of coupled equations:

$$\boldsymbol{M}\ddot{\boldsymbol{x}} + \boldsymbol{C}\dot{\boldsymbol{x}} + \boldsymbol{K}\boldsymbol{x} = \boldsymbol{f} \qquad \textit{Eq. 3}$$

As described above, in order to decouple the equations it is necessary to pre and post-multiply by $\mathbf{E}^T$ and **E**. Modal matrixes $\mathbf{M}^*$, $\mathbf{K}^*$, $\mathbf{C}^*$ will be obtained. The problem with damping modal matrix is that it is generally not diagonal, meaning that EOM cannot be decoupled. Lord Rayleigh came up with the idea how to overcome this problem.

2.1.3.2. Proportional (Rayleigh) damping

If the assumption is made that $\mathbf{C}^*$ is a diagonal matrix, the problem can be solved in mathematical sense. Lord Rayleigh proposed the solution which is appropriate for assuring that modal damping matrix is diagonal. The main thought is to make **C** as a combination of **M** and **K** in a certain proportion. In matrix notation:

$$\boldsymbol{C} = a_0\boldsymbol{M} + a_1\boldsymbol{K} \qquad \textit{Eq. 4}$$

Now, it is known that matrixes **M** and **K** can give diagonal matrices by mathematical manipulations. It means that **C** defined as above can also create diagonal matrix.

$$\boldsymbol{C}^* = \boldsymbol{E}^{\boldsymbol{T}}\boldsymbol{C}\boldsymbol{E} \qquad \textit{Eq. 5}$$

Now it is assured that $\mathbf{C}^*$ is diagonal and in such case the solution of the system can be found.

By introducing Modal Damping ratio defined as:

$$\xi_i = \frac{c_{ii}^*}{2m_{ii}^*\omega_i} \qquad \textit{Eq. 6}$$

It is possible to write down the matrixes coefficients in the form:

$$a_0 = \frac{2\omega_1\omega_2(\xi_1\omega_2 - \xi_2\omega_1)}{\omega_2^2 - \omega_1^2} \qquad \textit{Eq. 7}$$

$$a_1 = \frac{2(\xi_2\omega_2 - \xi_1\omega_1)}{\omega_2^2 - \omega_1^2} \qquad \textit{Eq. 8}$$

The assumption is that one who wants to use proportional damping definition knows at least two Modal damping ratios for at least two structure vibration modes.

This method is handy and straightforward. However, it has a big disadvantage. Desired damping ratios are well defined for only some range of frequencies. It is presented in the Figure 2.5.

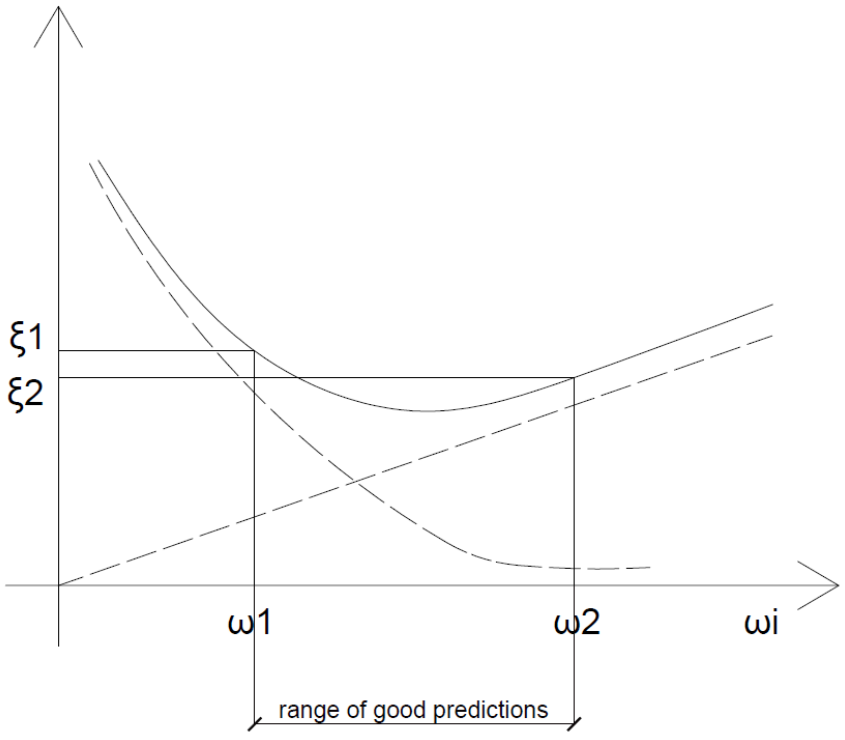

Figure 2.5 Graphical representation of Rayleigh damping for two frequencies and damping coefficients

2.2. Railway induced vibration and noise propagation

2.2.1. Generation mechanisms and transmission paths

In order to describe sources of noise and vibration introduction on types of noise shall be given.

Vibrations once induced by an acting force, propagate through the different mediums. In case of train passage, these mediums are structure (e.g. concrete, wood), ground or the air. This leads to division of noise for structure-borne, ground-borne and air-borne noise.

The first type of noise is generated by structure motion, therefore it is called structure-borne noise. When building gives dynamic response (e.g. due to wind) displacements occur in the system (e.g. building walls) exciting pressure waves in the surrounding air. Pressure wave reaches human ears and that is what is perceived as noise.

Second one is the special case of ground-borne noise. It specifies that building is excited by means of waves travelling earlier in the ground and reaching the foundation. The wave becomes excitation force for the whole structure. It starts from the foundation, forcing the structure to the dynamic response which is in form of walls or celling movement. It generates pressure wave in the air what people perceive as noise.

Finally, the air-borne noise is of the same nature as the two other, but air particles are put in motion directly by the source. The air-borne noise is for instance a conversation between people or breaking of the train wheels, where high-pitched noise comes directly from interaction between wheel and rail.

For more detailed explanation one can refer to for instance (Paul de Vos, 2017).

The graphical representation of above described noise types and its generation mechanism (Hall, 2003) is presented in the Figure 2.6.

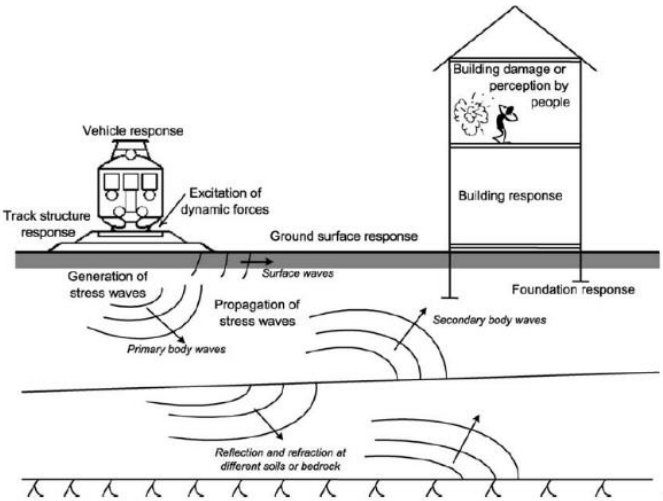

Figure 2.6 Origin of vibration together with their propagation paths and generation of the noise (Hall, 2003)

Different sources of noise are listed in the Table 2.1 (Hall, 2003; Paul de Vos, 2017):

Factors influencing the level and characteristics of train induced vibrations are categorized below.
1) Train (in as a machine sense) related factors • axle weight • axial spacing (distance between wheels) • boogie suspension (spring damper pairs) • wheel defects (eccentricity, imbalance, flats) 2) Train passage related factors: • train speed • breaking accelerating, passing through • unsteady riding (eg. bouncing) 3) Rail related factors • unevenness of the rail • corrugation of the rail • Spacing and interval of the rail joints • Switches 4) Support related factors • sleepers spacing • hanging sleepers • discrete stiffness / changing stiffness along the track • ballast/subballast properties • ground profile • soft spots in the subsoil

Table 2.1 Factors influencing the level and characteristics or train induced vibrations

Reference (Paul de Vos, 2017) Table.1. provides some characteristic values of frequencies which are generated depending on the speed of the train and different vibration generation mechanisms. Same reference in Graph. 5. shows at which frequency ranges what type of noise is important for analysis. It illustrates that in range of 16Hz to approximately 60Hz three phenomena are relevant (that are felt as the building ground vibration, ground-born noise, audible sound). Same reference informs that it is difficult to distinguish if noise is heard or felt for low frequency content signal. This is the reason why ground vibration factor is also of interest for the building analysis.

2.2.2. Phenomenon related to passage of the train

When train speed approaches Rayleigh wave velocity high deformations of the ground are observed due to track-rail resonance, which can lead to derailment of the train or other serious accidents and damages. This phenomenon can be explained by understanding the mechanism of Mach Cone formation.

2.2.2.1. Mach Cone formation

Mach cone is the most known phenomenon from wave propagation in the air. When a plane travels faster than the speed of sound in the air, the sonic boom occurs behind the plane. An insightful article about the Mach Cone and the sonic boom effect can be found in (Seebass, 1969).

When the object is moving through the air it creates the sound wave, which is propagating with the speed of sound in the air in front of the aircraft and behind it. When the aircraft is moving faster than the waves it produces, it leaves both waves behind causing wave interference and amplifications of the amplitude. Graphical representation of the Mach Cone in shown in the Figure 2.7. As seen in the Figure 2.7 the pilot cannot hear the sound waves, because he moves faster than them. The observer from the ground hears louder sound because sound waves superpose and amplify. In case of the subsonic plane, the sound wave has enough time to redistribute before the next wave is produced. The comparison of both cases is illustrated in the Figure 2.8.

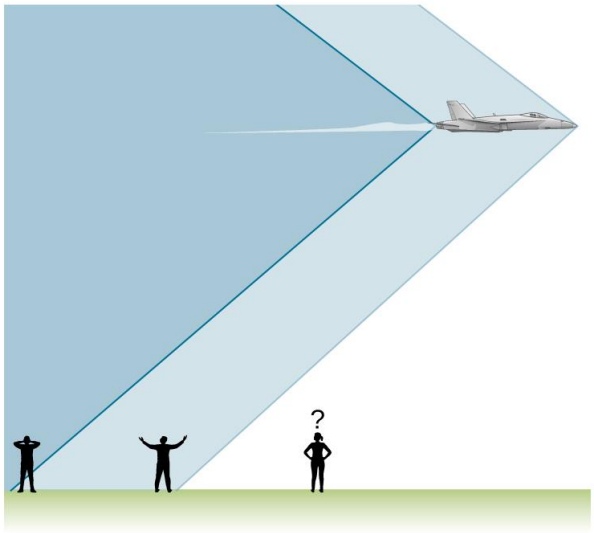

Figure 2.7 Mach Cone formation for supersonic plane (Physics, 2019)

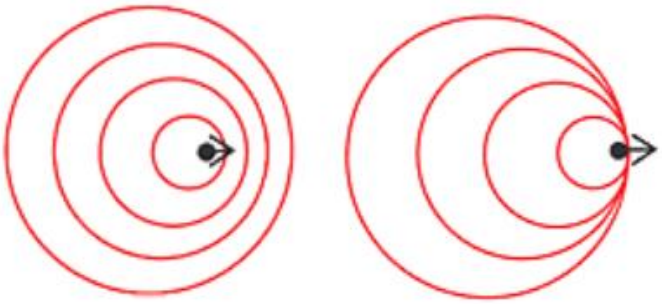

Figure 2.8 From the left subsonic plane travelling with V<sound speed in the air, from the right supersonic plane travelling with sound speed, in other words with Mach 1 speed (Physics, 2017)

The Mach Cone occurs not only in the air but also in any other medium. Another simple example can be a duck swimming in a pond. The duck leaves characteristic cone behind itself. It is because the duck is travelling faster than the wave in the water. Illustration of the effect is seen in Figure 2.9

Figure 2.9 The duck leaving Mach Cone behind (Hermans, 2010)

For the ground the same effect occurs. When the train travels faster than the slowest wave speed, in this case the surface Rayleigh wave, large amplifications are observed due to the Mach Cone formation behind the train.

Before the Mach Cone is observed people can experience another effect called the Doppler Effect.

2.2.2.2. Doppler Effect

When observer is not moving and the source of the sound approaches him with the certain speed, the observer hears higher pitched noise (higher frequency) before the source reaches him and lower pitched noise (lower frequency) after it passes. This effect is called the Doppler Effect.

The most popular example of this is the pedestrian waiting on the crossing and the honking car on the road driving by. Pedestrian hears high pitched noise when the car is approaching him and, in contrast he hears low frequency noise when it passes. The effect is presented in the left graphic of Figure 2.8. Moving plane is generating denser waves in front and less compacted behind. In the paper (Gupta, et al., 2012) the following equation for perceived frequency is written:

$$f_r = f_t\left(\frac{c+V}{c-V}\right) \qquad \textit{Eq. 9}$$

f_r – perceived frequency
f_t – original frequency
c – speed of the sound
V – velocity of the target.

After rewriting the formula for the train case (incoming waves and the ones after train passes) the following equation is obtained:

$$f' = f_0\left(\frac{V+V_0}{V \mp V_s}\right) \qquad \textit{Eq. 10}$$

f'- perceived frequency
f_0 – the actual frequency of moving object
V – Rayleigh wave velocity
V_0 – velocity of the observer (in this case V_0=0, observer is not moving)
V_s – velocity of the train

Eq. 10 is valid for non-dispersive systems. However, for dispersive systems (Rayleigh wave is dispersive in soil) it can serve as indication of the frequencies resulting from the Doppler effect.

It means that for the soils with low a Rayleigh wave velocity and the train travelling with a speed close to it one might observed much higher and lower frequencies content in the signal than the actual frequency of the load.

All effects described in this section are related to the train passage and they are necessary to understand why trains can have the environmental impact. This will be described in the next section.

2.2.3.Damages and nuisances caused by the railway induced vibrations

2.2.3.1. Noise

The environmental impact caused by train networks is becoming more of interest in the recent years. One of the main issues is noise that a train passage generates. It might start at the source and cause air-

borne and ground-borne vibrations. The wave travels through the soil and usually its strength decays with the distance, meaning that energy dissipates during transmission stage from train-track source to the building foundation. From the building foundation the wave propagates through the building causing its vibrational response. Different floors might experience different displacements/velocities/accelerations, which depends on many factors like material that the building is made of, mass of the floors, damping ratio for each floor, floor height, spans and much more related to the structure itself. For more information one can refer to basic course of structural dynamics e.g. (Spijkers, et al., 2005). In paper (Xia, et al., 2009) authors investigate velocity of each of the floors of a 6 story masonry building. One of their conclusions is that the lateral velocity increases monotonically with building elevation while the vertical velocity increases in fluctuating manner. This aspect is important from a practical point of view because the same wave does not have to impact all structure elements in the same manner. As mentioned previously it depends on many different factors. This implies that during analysis of vibration level it is important to not only look into propagation stage in the soil but also at the type of structure. It makes the prediction of the vibrations level and its impact on inhabitants of the buildings a very complex problem, because each situation becomes unique. Not only every structure responses to the same wave differently but also response of elements within the structure varies. Additionally, uncertainty of the ground profile is also involved in the analysis process as it is hard to define exact its layering, and only approximations are estimated. Local effects as a water table, an object in the ground, the tree roots etc. influence the results, which can lead to inaccurate predictions. It is worth mentioning that for the lower frequency bands (below 20Hz) it is difficult to define whether sound is heard or vibration is felt (Paul de Vos, 2017). However, it can cause irritation.

In many countries, specifications have been developed, which define the threshold value for vibration levels. For instance ISO 2631 can serve as the reference norm if national standards are not yet present. ISO 2631 (graph 8) defines threshold values measured in rms of the value of approximately 1 mm/s at 1Hz and 0.1mm/s at 10Hz. In the Netherlands the valid reference is BTS, the Dutch policy for track vibrations. Two values of velocity are of interest. The evaluation is based on maximum velocity recorded at the location of the property V_{max} and the average value of velocity V_{per} recorded during specific period of time during the passage of trains.

2.2.3.2. Damage to the building

Complaints about the effect of passing vehicles have not arose only in the last years. One of the campaigns carried in Canada investigated the influence of trolley bus and buses on the nearby building in 1950 (Sutherland, 1950). Other research works like (Dawn & Stanworth, 1979; Wilson , et al., 1983) talk about increasing complaints and importance of developing vibration abatement measures. In the first article the authors study different rail design parameters and their influence on the nearby buildings. In the second paper the attention is given to the vibrations caused by freight trains and abatement measures such as floating slab track and modification of the design of transit car bogies (changing the geometry in such manner that wheel/rail forces are reduced) It has been shown that proper design of the bogie suspension can significantly reduce the levels of ground-borne noise and vibration.

Since society awareness is increasing and so are the standards is comfort of living, a concern was born amongst people whether or not trains can cause structural damages to the buildings located nearby railway network. A lot of research proves that train circulation is very unlikely to cause any structural damage to the building (Barbosa, 2013; Hall, 2003; Paul de Vos, 2017). However, the quality of life inside such buildings deteriorates significantly. Even though there is no structural damage noise and unpleasant effects like rattling of cutleries are still present.

State of the art (Paul de Vos, 2017) in chapter 4 talks about damage to the buildings. Cosmetic damage can occur in the building for instance due to settlements caused by vibrations in soil. However, if the assumption is made that no settlements occur (trains run on stiff and well compacted ground), then

damage is unlikely because the level of vibration causing cosmetic damage is 8 to 50 times higher than train can induce (Paul de Vos, 2017).

2.2.3.3. Soft soils and associated difficulties

The Netherlands is the one of the most populated countries in Europe, therefore terrains around train stations and railway track become very attractive. Unfortunately, big part of the country has very poor ground conditions such as clay, peat and silty soils in the most upper layers (Cheng-hou, et al., 1990). There is then a lot of interest in investigating level of vibration reaching the building located in proximity to train route in order to meet required noise threshold and achieve optimized train speed.

Soft soils have a relatively low Rayleigh wave velocity which is around 10% slower than a shear wave velocity (Paul de Vos, 2017). This speed is around 50 m/s. Hall in his soil model obtained the value of 45 m/s for shear wave speed in mud (Hall, 2003). Such a low wave velocity put a lot of limitations onto design process of the railway network. The operational speed must be decreased sufficiently so that the resonance of the ground is avoided. For comparison, in granite the Rayleigh wave velocity is around 2286 m/s (Weatherby, et al., 1934), theoretically train could run 50.8 times faster without observing excessive deformations. It is then visible that in soft soils operational speed of the train can be reduced to around 180km/h.

The assessment of vibration levels is often required when a new track is planned in a proximity of existing buildings or when some changes are about to be made in an existing network. There is often a contract clause which says that level of vibrations cannot increase in the building due to changes to be made in the railway system. Usually, when the new residential project close to the existing rail is about to commence, the developer is responsible for providing appropriate level of vibrations in the building. Previous considerations explains that the resonance or excessive vibrations are more likely to occur in soft soils (resonance happens at lower speed) than in hard soils. For the investor it means that he has to be very careful about the level of vibrations in soft soil because building structure closer to the track can experience higher vibrational level and the threshold value might be exceeded. For soft soils the design margin is much smaller than for hard soils. Ensuring compliance with standard requirements can involve additional tests and measurement campaigns or abatement measures. For the developer it means additional cost that can be harmful for the project budget.

In order to avoid excessive vibrations cheaper methods with computer use has been developed. In the next section the overview of the available prediction models will be presented.

2.3. Existing prediction models

There are a couple of different ways to evaluate level of vibrations. First ones are analytical and numerical family of approaches such as Finite Elements Models in 2D, so called 2.5D, 3D, periodical models and solutions based on Winkler foundation and elastic half space. Another type of prediction models is based on field measurements, is the so called empirical models. All of these approaches will be shortly described in the following subsections and in the end compared against each other. Some factors important for the analysis of railway induced vibrations will be explained in more details, because there are many available techniques to account for them.

2.3.1. Empirical models

Empirical models are based on the collection of data from the measurements during certain campaigns. In thesis of (Bahrekazemi, 2004) semi-empirical model which uses database from a set of in field measurements is developed. This approach divides railway stretch for sections depending on

embankment cross section, soil strata and material properties. Then to each of the obtained sections model assigns the most suitable available case from database. There cross-sections are later collected, put all together and further analysed. Based on empirical database the map of potential vibration sensitive areas is created. This method is dedicated especially for the preliminary design. The validation of this method (With, et al., 2006) is based on two field measurements taken in Sweden. The result of this validation was fairly accurate at the embankment but less consistent at the railroad. Authors explain that because the software developed in (Bahrekazemi, 2004) is based on soft or very soft clay measurements, perhaps it would be more appropriate to apply it to similar ground conditions case. The other suggestion made by the authors is to extend the database by continuing measurement on different stiffer geotechnical sites and consequently add them to the database.

In paper (Verbraken, et al., 2011) authors are verifying the method of the Federal Railroad Administration (FRA) of the U.S. Department of Transportation, which predicts vibrational level due to railway traffic by means of empirically derived set of procedures. As the case study the underground construction is taken and verified by analytically formulated coupled FE-BE method. Their results shows a good agreement in terms of RMS (root mean square) of the vibration velocity during the stationary part of train passage in one-third octave band.

2.3.2. Analytical methods

Two analytical methods might be distinguished in this section: elastic halfspace and Winkler foundation solutions. In the work of (Dieterman & Metrikine, 1997) the authors derived steady state wave forms of the Euler-Bernoulli beam smoothly lying on an elastic halfspace. Parameters such as external viscous damping at the critical speed, speed of the load for different characteristics of the beam and halfspace are considered. Four cases were investigated in total, namely halfspace with soft and stiff soil profile and beam representing small and large track-ballast-embankment systems. The results shows that displacements directly under the load are equal to the maximum displacements just for the small velocities, far off from the critical ones. However, with increment of the vehicle speed the maximum displacement occurs behind the load what is due to the application of external damping of the beam. For critical speeds this shift is more substantial due to radiation of the waves. The paperwork and its results are the extension of the paper of (Kenny, 1954) whose model was Euler-Bernoulli beam on viscous-elastic Winkler foundation. In his article also displacements due to the moving constant load were calculated.

Winkler foundation is an infinite beam supported by distributed springs. Due to the simplicity of the system it became very popular to be used. It was used for instance in work of (Patil, 1988) where the effect of mass of the infinite railroad was investigated; (Duffy, 1990) was working on the same problem but he considered also moving and stationary vibrating loads as a function of both the mass and driving frequency of the load as well as the physical properties of the track. Other papers working on the railway induced vibrations with Winkler foundation implementation are for instance: (Lee, 1994; Lee, 1998; Achenbach, 1965).

2.3.3.Numerical approaches

2.3.3.1. 2D methods

2D models are commonly used to perform calculations of tunnels and above ground lines. For the tunnels study case in the paper of (Nejati, et al., 2012) authors use 2D Finite Difference Method (FDM) modelling to obtain ground surface vibrations and to simulate train movements. The studied tunnel is located in a very populated area. Ground conditions are mostly sandy soil. Along model boundaries dashpots are employed in order to avoid spurious wave reflections. The results are compared with analytical model of (Metrikine & Vrouwenvelder, 2000) and satisfying agreement is met in terms of vertical

and horizontal displacements. Effects of axle weight load, spacing of wheel axes and speed of the train are studied in terms of frequency content and load amplitude. Also Finite Element Method (FEM) is very popular to be used in both 2D and 3D models. The study of (Hall, 2003) was made in order to check if it is possible to simulate railway induced vibrations by means of FEM analysis. Validation is performed through comparison with field measurements taken in Ledsgård in Sweden. Study is performed for both frequency and time domain for the embankment and further distances. Ground conditions are mainly soft soils namely, crust, mud and clay (Fig.3. (Hall, 2003)). Boundaries have dashpot in order to avoid spurious reflections. The author concludes that 2D FEM model is a good alternative to study certain phenomenon for instance propagation of waves from the embankment into the soil or track structure response. He also states that for detailed simulation of the problem the 3D model should be used. The work of (Correia, et al., 2007) presents comparison of three different commercial software Diana, Plaxis and Ansys used by three different university teams. The aim of the study was to compare these packages performances in 2D approach. For the validation the measurements from the train Thalys running close to Ath, between Brussels and Paris are used. The study shows that all numerical models are giving results of the same trend but it is not necessarily in line with measurements from the field. To obtain better convergence between numerical 2D models and measurements authors are suggesting further investigation.

2.3.3.2. 3D methods

Another popular method of research is with 3D modelling. Lots of them are based on FEM. For instance, (Hall, 2003) mentioned in the previous paragraph, also used 3D models to study wave propagation. The author arrived to few conclusions. First was that 3D models are capable of simulating vibrations in the embankment and further away from it. Second stresses that waves are not fully evolved when they enter the model but they are fully developed at the exit of it. His next observation was that motion orbits of particles from 3D models indicate that Rayleigh wave is a dominating type outside of the embankment. Another aspect he mentioned was that the entry and exit of the load in the model create a disturbances which may affect the final responses. If a load enters the model from the north end, it would dissipate due to damping before it reaches the other end of the model. It means that models gives better prediction closer to the south end.

Another research (Ruiz, et al., 2016) also focuses on proving that railway induced vibrations predictions can be realized by means of 3D numerical modelling. The goal of the authors was to employ commonly used engineering software and Plaxis 3D was chosen. Numerical results are compared in time and frequency domain with real case measurements induced by Alfa-Pendular train near the city Carregado in Portugal. The train line is conventional above the ground embankment system. The results shows that reasonable agreement between prediction model and measurements can be obtained close to the track as well as away from it.

Not only wave propagation in soil is investigated with help of 3D numerical models. For another example of 3D application one might look into the work of (Oregui, et al., 2016). The main purpose of this work was to investigate vertical damping behaviour of railway tracks with monoblock sleepers. To calibrate the 3D FEM model some parameters were subject to change, namely: stiffness and the damping of railpad and ballast. The numerical results were set such that they match with series of hammer tests conducted on the rail. In this case, rail and sleepers have been modeled from solid elements and subgrade is simplified to spring-dashpot area under each of the sleepers. Authors conclude that for the hammer test the fixation of all degree of freedom at the ends of the rail gives the same results when boundaries are modelled as non-reflective, meaning that reflective waves has no influence for the results. Good agreement between measurements and models is achieved in the frequency range 300-3000Hz. The research can be used as the reference for the design of tracks and its components as well as for derivation of track parameters in unloaded conditions.

2.3.3.3. 2.5D models

The next numerical tool becoming very popular in research is 2.5D models. The technique assumes that the system in longitudinal direction is invariant. By performing Fourier analysis with respect to x-coordinate the results in frequency-wavenumber domain are obtained. It means that for the each wavenumber a 2D problem needs to be solved instead of 3D. Quite often Boundary Elements Method (BEM) is employed in this approach. The method requires only discretization at the boundary of halfspace and eventually at contact surface of different layers if halfspace is layered. It also requires knowing Green's functions. Green's functions are the response of the system due to an impulse force, in more scientific words: Green's function is the inverse Fourier transform of the transfer function related to harmonic steady-state response. The Boundary element due to Green's function is capable of accounting for propagation of waves towards infinity. For more information about Green's functions the reader is referred to e.g. (van Dalen, 2015).

In the article (Aubry, et al., 1994) the 2.5D models method is used to investigate response due to the moving load in the system consisting of infinitely long beam relaying on elastic halfspace. The hybrid 2,5D BEM-FEM (boundary elements plus finite elements) is used in paper (Ruiz, et al., 2016) to verify size of the 3D model constructed in Plaxis. In (Barbosa, 2013) 2,5D FEM-BEM method is used to build a numerical tool allowing analysing railway induced vibrations. (Barbosa, 2013) uses this tool to test the effectiveness of trenches as the countermeasure of the induced vibrations.

Both approaches, FEM and BEM, are attractive from scientific point of view so a lot of research is focusing now on FEM-BEM hybrid and improving its performance. The work of (Galvín, et al., 2010) stresses the importance of developing 2.5D models further by comparing results of two different models. It is a part of the benchmark study. First model consists of the ballast and the embankment placed on an elastic continuum using 2,5D solid elements. Second model is a simplified representation where the ballast is modelled as the spring dashpot distributed pair while the embankment is represented by the Euler-Bernoulli beam. The obtained results of free field vibrations turned out to be very different for higher frequencies between the two approaches. That has been confronted with the field measurements conducted during passage of the TGVA train. Comparison presents that the continuum model no. 1 leads to a reasonably good approximation in low frequencies when quasi-static load component is dominating. Quasi-static component is the static part of the load, namely weight, whereas oscillatory part is called the dynamic part of the load (refer to the section 2.3.3.7. In work of (Yang, et al., 2003) the effect of each of following parameters for the ground response is studied parametrically: the shear wave speed, damping ratio, stratum depth of the supporting soils, moving speed and vibration frequency of the travelling train. The method of the research is also 2.5D finite-infinite elements.

2.3.3.4. Periodic models

Another method of evaluating railway induced vibrations is by periodic models. For instance (Gupta, et al., 2008; Gupta, et al., 2007) use it to evaluate underground traffic. The research accounts for repetitive nonlinearity creating the so called basic cell. The cell can be for instance a piece of a model from sleeper to sleeper, as it is repetitive. By mathematic transformations with respect to longitudinal coordinate it is possible to collect all separate cells and create one infinitely long domain.

The (Gupta, et al., 2008) article is related to building Beijing metro line 4. The author used FEM-BEM periodic model hybrid approach. The main focus of their study was to predict free field vibrations at the surface in the proximity of the Physics Laboratory of Beijing University. The laboratory possesses some vibration sensitive equipment and their concern was that passage of the underground train that could disturb its functionality. The authors validate the model through comparison with the side field measurements from line 1 of Beijing metro between Dongdan station and Juanguomen station. Match

between the predicted model and the measurements is reasonable which allows to make the conclusion that the model can reproduce effectively the railway induced vibrations.

The (Gupta, et al., 2007) article the main motivation for the research was to compare two approaches: semi-analytical three dimensional model with periodic FEM-BEM approach. It is done based on the tunnel study case embedded in homogenous space. Free field response due to harmonic load is computed and compared with both approaches. Both models are giving good match for response in frequency-wavenumber domain. The authors states that semi-analytical approach is plausible in the early stage of the design. It allows to make rational decisions regarding track design in terms of vibration reduction without looking into structural details. Computations are faster than in case of periodic models. However, for accurate predictions of vibrations due to underground traffic with complex geometry and inhomogeneous soil characteristics periodic FEM-BEM model should be considered.

2.3.3.5. Method of fundamental solutions

To make a complete overview of available prediction models meshless technique needs a bit of attention. The method does not require the discretization of the boundary neither of the domain. It becomes promising alternative for analysis of railway induced vibrations. Relatively new approach of Method of Fundamental Solutions (MFS) was used for instance in (Colaço, et al., 2017) where 2.5D FEM-MFS technique was implemented. FEM is used to obtain structural response, namely displacements. They are later on used as an input for studying induced noise in the building (acoustic part of the study case). By means of fundamental solution (MFS technique) re-radiated noise in the building is obtained.

2.3.3.6. Representation of wheel axial load

As stated in Table 2.1 many factors are influencing the level of vibration. This section is focused on how to apply loads in the system. A few approaches can be distinguished: analytical formulation, moving load along specific path, triangular pulses, periodic force function.

Analytical formulation

In the paper (Ruiz, et al., 2016), a point load is applied to each of the sleepers. The way of obtaining dynamic multiplier force signal comes from 2D analytically solved train train-track interaction system. The quasit static component, as well as the dynamic component associated with rail unevenness, and welds are included in the mechanical system. Later, the obtained force-time signal is applied to each sleeper with a certain time offset, simulating the train passage. Rail is not included in the 3D model as its contribution has been already considered in the analytical solution. By that time there was no other option to include rail irregularity in the Plaxis 3D model, also Plaxis was not capable of implementing moving load directly.

Moving point load

In (Steenbergen, et al., 2007) only a single moving load is considered to assess effectiveness of a ballastless slab track system. The model consists of a beam laying on a visco-elastic half-space.

Triangular pulses

In the 3D FEM/FEM-BEM method it is quite common to apply the load in form of triangular pulses because software (Plaxis 3D, Abaqus, Ansys) is not equipped with formulating moving load along specific path (Shahraki, et al., 2014; Hall, 2003; Oregui, et al., 2016). (Hall, 2003) states that a loss of accuracy has been observed by applying load directly to the sleeper instead to the rail through triangular pulses. The applied load was calculated from the static solution of the beam on Winkler foundation. In between sleepers, the rail was divided in four pieces, meaning that every 4th node is connected to the

sleeper. Each of these nodes are points of application of the stationary load. Load distribution applied in the described way depends on the speed of the train and accuracy that is opted for. Too coarse discretization may lead to erroneous results in time and frequency domain.

Periodic function

In the contribution of (Nejati, et al., 2012) the author assumes constant load acting on the sleeper. Load is formulated as rectangular pulse. It begins with the first wheel of bogie and it ends when the second wheel passes. It is presented in the Figure 2.10.

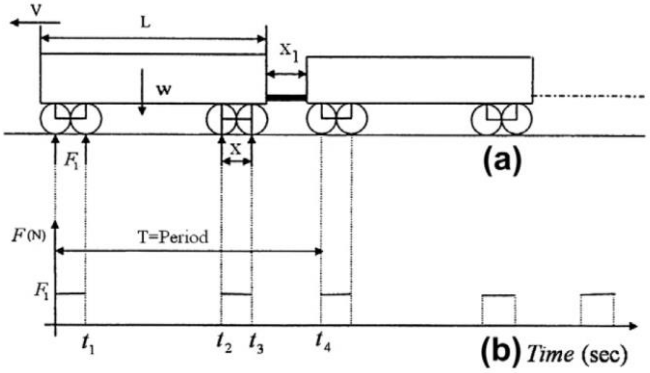

Figure 2.10 (a) Schematic plan of train wagons and (b) normal force variation of wagon wheels. (Nejati, et al., 2012)

In the form of periodic function it might be written as follows:

$$f(t) = \begin{cases} F_1 & 0 \le t \le t_1 \\ 0 & t_1 \le t \le t_2 \\ F_1 & t_2 \le t \le t_3 \\ 0 & t_3 \le t \le t_4 \end{cases} \quad \text{(Nejati, et al., 2012)} \qquad \textit{Eq. 11}$$

2.3.3.7. Characteristics of quasi-static and dynamic part of the load

Another aspect that would need closer attention is the static and oscilatory part of the load. It is of great importance if the load is standing or moving. Short description and explanation of the most important features related to these loads will be shown in this section.

Train experiences varying stiffness due to discretization of the sleepers. Due to unevenness of the track, wheels, possible weak spots in the rail material or in the embankment both systems (train and embankment/rail) experience dynamic excitation and start to vibrate. Another railway induced vibrations causes are listed in the Table 2.1. Some of them are influencing quasi-static load component while some are contributing to the dynamic load part.

Quasi-static component

The load representing the train mass is called quasi-static component. It depends on the speed of the train, axial spacing and, of course, mass. In most of the situations the static component of the load does not contribute much to feelable vibration. Far from the track, this load component induces very small vibrations (Paul de Vos, 2017).

A measurement campaign was performed in Germany (1994, 2005) near Würzburg where oscillations were measured. The result suggested that the static component is responsible for the near field response but due to damping its magnitude decays fast. It was also noted that sleeper passing frequency could be seen in the results meaning that the sleepers act as the harmonic forces which magnitude increases with

speed (Barbosa, 2013). The author in (Milne, et al., 2017) also mentions about sleeper passing frequency seen in the spectral results.

Dynamic component

The dynamic force component of the force causes vibration at further distances. As described in (Paul de Vos, 2017) parametric excitation is usually caused by fixed distance between sleeper, axial spacing and bogie spacing. Another sources of dynamic excitation like unevenness of the track, rail corrugation, track singularities and unevenness of the wheel are causing high vibrations. However, since it is included in the maintenance plan to eliminate these excitation sources, railway networks are not designed in accordance with it. Some of the examples of induced vibration frequencies dependent on speed of the train are presented in the Figure 2.11.

Vehicle Speed	40 kph	80 kph	160 kph
Moving load (axle spacing approx. 1.8 m)	3 Hz	5 Hz	11 Hz
Track unevenness	≥ 1 Hz ≤ 100 Hz	≥ 2 Hz ≤ 200 Hz	≥ 4 Hz ≤ 400 Hz
Rail corrugation	Approx. 500 Hz	Approx. 1000 Hz	Approx. 2000 Hz
Wheel unevenness	≥ 4 Hz	≥ 8 Hz	≥ 15 Hz
Wheel polygonisation (here assuming a wavelength of 0.1 m)	Approx. 100 Hz	Approx. 200 Hz	Approx. 400 Hz
Inter bogie spacing (assuming approx. 8 m)	Approx. 1 Hz	Approx. 3 Hz	Approx. 5 Hz
Sleeper spacing (0.6 m)	Multitudes of 16 Hz	Multitudes of 32 Hz	Multitudes of 64 Hz

Figure 2.11 Frequency of typical vibration for different vibration generation factors depending of the train speed (indicative only) (Paul de Vos, 2017)

Standing and moving load

Difference between moving load and standing load should be mentioned. Standing oscillating load imposes frequency of the response of the system same as its own frequency. Moving load has different frequency component depending on speed of the train. Doppler effect becomes relative because not moving observer (or measurement point) experiences different ranges of frequencies before and after train passage. This effect has been described in section 2.2.2.2.

In work (Karlström, 2006), the author investigate the influence of acceleration and deceleration of the trains. The conclusion is that there is no significant difference in the vertical displacements between the accelerating/decelerating train and the one that passes through. However, differences are observed in the horizontal displacement and they cannot be disregarded.

2.3.3.8. Soil material models

Another important choice that one needs to make during his research is about the soil model. Soft soils are more difficult to work with because of their low Rayleigh wave velocity. As already explained in section 2.2 when the train is travelling faster than Rayleigh the substantial growth of the amplitude and vibrations is observed. Moreover, the so called Mach Cone is formed at the tail of the train. Induced wave is not fast enough to propagate in front of the carriage meaning that train leaves all waves behind causing their interference. This effect leads to excessive displacements causing damage of the rail, its bending and final derailment of the train itself.

In general, when working with stiffer soil one has to struggle with air-borne noise. Frequency content of ground vibrations is higher and decays quickly moving away from the source. This is the contrary to

softer soils, where frequency content of vibrations is placed in lower band. Noise itself is not a difficulty but displacements need attention.

Different soil models were implemented amongst literature. In many papers (Nejati, et al., 2012; Ruiz, et al., 2016; Hall, 2003; Dieterman & Metrikine, 1997) authors are using linear elastic model of soil because their assumption is that passage of the train cannot excite large deformations and thus they are limited to the elastic range. Based on previous considerations, it is necessary to know for what speed and soil profile the solution is searched. For cases where train is travelling with speed close to critical speed, the non-linear soil model might need to be considered. This is because the assumption about small displacements stops being applicable (see section 2.2.2.1).

In (Dong, et al., 2019) the authors are facing a problem related to the non-linear soil model. They developed novel semi-analytical model which can allows the soil stiffness and damping ratio to change as the function of strain. Method is based on iteratively updating soil material properties. Periodic model was used to compute responses. Analytical model serves to compute track response and thin-layer element method is used to obtain ground response. Updates on nonlinearity are done in soil response. Three different soil profiles are analyzed. The case study is proving that displacements of the rail are around 30% higher using the non-linear approach for the case with soft soil overlying the stiff one. Another outcome of the research is the change of critical speed. The non-linear model gives even from 80 to 89% critical soil speed of the linear case. However, these results are based on the single axle load passage and authors emphasize that the dynamic amplification factor is strongly soil profile and train axle load configuration dependent and more variations should be done in the field in order to get the whole picture of the problem.

In (Shahraki, et al., 2014) the authors compare the vertical velocity of the particle using the linear elastic approach and hardening soil(HS)-small model. The differences that authors obtain for the depth-velocity relationship are not that significant. The biggest difference is found at the 5 mm/s vibration speed. Linear elastic model reaches this speed at -1,9m when HS-small approach has such speed at around 1m lower. A brief comparison of all prediction models is presented in the Table 2.2. Explanation about each of the categories is necessary.

2.3.4.Comparison of the prediction models for railway induced vibrations

	Computational cost	Soil non-linearities	Model non-linearities	Theoretical background	Results accuracy
Empirical	Low	All	All	Easy	Depends
Analytical	Low	rather difficult	rather difficult	Medium	Depends
2D	Medium	possible	possible with exceptions	Easy	Depends
3D	High	possible	possible	Easy	Depends
2.5D	Medium	possible	possible with exceptions	Medium	Depends
Periodic	Medium	possible with exceptions	possible with exceptions	Medium	Depends

Table 2.2 Prediction models comparison

2.3.4.1. Computational cost

Empirical models have rather low computational cost. The solution is based on collection of database thus just some simple extrapolations between different site conditions need to be made in order to obtain

the results. In terms of analytical formulations, these are rather short and fast to solve by computer or even by hand. In numerical models category the highest computational cost has 3D approach. It has a lot of nodes and elements, which creates larger matrixes to be solved and therefore convergence is slow. For 2D, 2.5D and periodic models one might say that computational cost is medium but this statement is driven by comparison with high computational demand of 3D models. 2D models are faster to solve than 3D. 2.5D models are analyzing series of 2D problems what is still faster than solving 3D problem. It is similar with periodic models.

In 3D and 2D models the non-reflective boundary conditions in form of dashpots are applied at the boundaries but not all waves can be absorbed at the boundary. For this reason the larger models should be considered allowing redistribution and decaying of the propagating waves.

The rest of the approaches is capable of accounting for the propagation of waves towards infinity. The size of the model is not related to avoiding spurious reflections at the boundaries.

2.3.4.2. Non-linearities

In the empirical model all nonlinearities are included in the results. The problem is that this applies for a very specific ground conditions and flexibility of such model is rather low. Hence, results of different soil layers cannot be obtained and new measurements and database has to be created.

For the rest of the models flexibility is possible to some extent. It is possible for instance to change soil conditions. However for 2D, periodic and 2.5D models applying non-linearity in the longitudinal direction is not possible. In the periodic model the non-linearity might be only included in the basic cell, but then it is repeated in the whole analysis. In the analytical solutions only simple models are considered, thus the nonlinearities are not suitable for this approach. On the contrary, the 3D models can include the non-linearities in form of an object in the ground, changing water table, transient effect or sudden change of stiffness (e.g. train going form the embankment into the bridge).

2.3.4.3. Finding Green's functions

Theoretical background indicates the difficulty of finding Green's function. Sometimes it might become a problem to define it for the halfspace in the periodic and the 2.5D models. In 2D and 3D approach usually software packages are used. FEM and BEM methods are not causing that much problems as finding Green's functions for soil stratum. Also, the method is no that popular in daily engineering practice and its application is so far limited to academic applications.

2.3.4.4. Accuracy

Empirical models are giving the best accuracy from all of the discussed approaches. The difficulty related to this method is that a very good predictions can be obtained but only for cases with conditions similar to the ones available in database (parameters like train, soil profile, track profile etc.). To extend the relatively narrow field of application of the method additional field measurements should be conducted for multiple different soil profiles. It is not desirable solution due to its high cost. On the other hand this method might be useful for instance when investor wants to increase operational train speed. The best price wise solution might be found for the abatement measure with empirical method because of its high accuracy. It might turned out that it is more profitable to fund additional tests suitable for the specific case and save money on optimizing the applied abatement measure.

3D models are generally giving good predictions for waves propagation. Including lots of details, thereby accuracy, is a trade-off for extending computational time.

For 2.5D and periodic models a good accuracy can be obtained but level of nonlinearities is limited as described in the previous section.

For 2D models it is difficult to clearly state their accuracy. Hall in his dissertation thesis and later works (Hall, 2000; Hall, 2003) investigated conversion from 3D to 2D. His conclusion is that certain effects might be investigated by means of the 2D models but for good predictions the 3D models should be employed. In the paper of (Correia, et al., 2007) by using 3 different software packages the author did not obtain results close to the measurements.

On the other hand, (Nejati, et al., 2012) obtained a good match with the analytical model of (Metrikine & Vrouwenvelder, 2000). Then this subject is still open for discussions.

2.3.5. Size of 3D model

Since 3D modelling seems to be a reasonable solution if flexibility of the model and reasonable accuracy are searched for, it is decided to describe how the model size has been established by other researchers. Main disadvantage of the 3D approach is its high computational effort which is strongly related to the model size.

Depending on the area of interest calculation time might be pulled down by reducing the number of elements and nodes. Size of the model is strongly related to the area of study of a train-rail-soil system. In article (Jiang, et al., 2014) authors build up a real scale model 15m x 5m x 6m which was validated through field measurements and the 3D FEM model of dimensions 30m x 30m x 100m. The main focus of study was to predict the slab track and rail velocities behavior. Results were extracted either from track position or roadbed. Then small models might be used because reflections from boundaries have secondary influence for the vibrations right next to the source.

In article (Shahraki, et al., 2014) the 3D modelling in PLAXIS software package was employed. In order to define dynamic multiplier and shear force signal, an auxiliary software called PROKON was used. The model had dimensions of 35mx35mx9,5m. Hall (Hall, 2003) used ABAQUS software for the analysis. His model had dimensions of 65m x 23m x 50m. It is shown that it is possible to simulate ground response in rail proximity. Distances up to 22,5 have been analyzed in his work.

In work of (Ruiz, et al., 2016) the final model has dimensions of 70m x 65m x 30m. Distances are considered up to 45m. Mesh is denser in region of 30m x 45m. In order to redistribute waves propagation was extended 20m each direction.

2.4. Abatement measures

In order to make the full overview of the matter of railway induced vibration the methods of preventing them should be described. There are many possible abatement measurements available. Only some of the most popular will be discussed in this section.

Abatement measures can be divided into three categories: at the source, in the propagation path, and at the building (receiver).

At the source the following abatement measurements solutions are available: track alignment, stiffness pads, under ballast mats, slab track and floating slab track (Paul de Vos, 2017; Lombaert, et al., 2015).

Measurements to mitigate vibrations are much more costly than the one to mitigate noise itself. Only track alignment itself can result in 10 dB reduction.

To reduce vibrations levels one should be looking for low stiffness pads with small difference between dynamic and static stiffness. The softer the pad the better for vibration reduction. Such pads should be

able to reduce vibrational level in high frequency range (above 30Hz). Expectations for the lower frequency band is that due to usage of the soft pad, the magnitude will be amplified. Field tests show reduction of around 8-20dB in higher bands. However, they cannot be too soft because of the requirements for operational safety of the train. Excessive deformations of the pads need to be avoided.

Under ballast mats are used mainly in tunnels but it is possible to apply them in the over ground construction as well. One must be very careful with choosing for stiffness of the pad because it may also lead to amplification of the vibrations. Reduction is observed up to 5dB for well-chosen mats. It might be an alternative to expensive floating slab track. It would mean that the mat is installed under each of the sleepers and it is submerged into the concrete continuous block.

Floating slab track is more common in tunnels than in overground systems. Sleeper is detached from the whole tunnel structure by applying elastomeric pads / bearings. It allows systems to vibrate but vibrations are damped by pads and not transmitted further. It is similar to a mass-spring system. Major disadvantage of this system is its high maintenance cost. Bearings are usually trapped within the structure making them inaccessible after execution stage. Different sources predict reduction of vibrations differently, from 10dB do 20dB.

Non-ballasted slab track is usually the measurement taken in high-speed rails. It means that solid concrete slab is placed on the ballast/subballast.

Many techniques are available for soil improvement and one of them is column stabilization by jet grouting or by pile driving. Concrete piles are embedded in stiffer layers than the one on which embankment relies directly. This method is found to be the most effective for ground-borne noise and vibrations travelling through the soil.

Next type of abutment measure is on propagation path. The main idea is to block travelling waves and prevent them from reaching the building. It is achieved by introducing barriers. Their task is to reflect waves back to the system and to damp passing through waves. Two the most common are concrete barrier and trenches (opened or filled). They are studied in (Jiang, et al., 2013) and (Coulier, et al., 2013). Sometimes also sheet piling is used. Opened trenches are very effective in reducing surface waves, which is especially useful when significant reduction is needed but there is not enough geometrical and material damping provided (Barbosa, 2013). In both, trench and concrete barrier waves could bend at the edge of the barrier. It would imply that barrier must be deep enough in order to be effective.

The last way to reduce excessive vibrations is at the receiver: the building. A few ideas are listed here. Worth mentioning are vertical elastic layer around foundation or foundation on bearings (often abatement for earthquake impact). In case of the wooden floors, adding extra cross beams will make the floor stiffer and less sensitive (of lower mobility) for vibrations.

More information can be found at project RIVAS website (Anon., n.d.). Also RENVIB project and catalogue for Railway Vibration produced by Grontmij for ProRail are good source of information.

3. Site investigation

In the following chapter the overview of the properties established based on field investigations are presented. Soil profile layering, embankment cross-section, sleepers layout, fastener system, equipment used to conduct tests and its collocation in the field are briefly described. The most important parameters of aforementioned are introduced.

3.1. Ground conditions

Based on the CPT test conducted near to the place of measurement the parameters of the soil layers up to 30m depth are derived and presented in Table 3.1. Parameters E, G, V_s and V_p are obtained by using Eq. 12 to Eq. 15. Groundwater table is found at -1m.

	γ_{uns} $[\frac{\text{kN}}{\text{m3}}]$	γ_{sat} $[\frac{\text{kN}}{\text{m3}}]$	ρ $[\frac{\text{kg}}{\text{m3}}]$	Poisson's ratio [-]	E_{oed}^{ref} [MPa]	E [MPa]	G [MPa]	V_s $[\frac{m}{s}]$	V_p $[\frac{m}{s}]$	thickness [m]
loosely packed sand upper layer	17	19	1732.93	0.22	16	14	5.74	57.57	96.09	1
Sand, loosely or moderately packed, upper layer	18	20	1834.86	0.22	81	71.12	29.15	126.04	210.37	2.5
Sand, very loosely packed, weak to extremely silent	17	19	1732.93	0.22	40	35.11	14.39	91.12	152.08	2
Sand, loosely or moderately packed, lower layer	18	20	1834.86	0.22	50	43.88	17.98	99.00	165.24	3.5
loosely packed sand lower layer	17	19	1732.93	0.22	24	20.97	8.60	70.43	117.55	4
Sand, moderately packed	18	20	1834.86	0.22	36	32	13.08	84.43	140.91	17

Table 3.1 Property of soil stratum derived based on CPT test

$$E = E_{oed}^{ref} \cdot \frac{(1+\nu)(1-2\nu)}{(1-\nu)}; \quad \textit{Eq. 12}$$

$$G = \frac{E}{2\,(1+\nu)}; \quad \textit{Eq. 13}$$

$$V_s = \sqrt{\frac{G}{\rho}}; \quad \textit{Eq. 14}$$

$$V_p = \sqrt{\frac{E_{eod}^{ref}}{\rho}}; \quad \textit{Eq. 15}$$

3.2. Measurements

3.2.1. Description of the equipment used to perform measurements

For performing measurements piezo electric acceleration sensors are used. The vibrations expressed through liquid acceleration [m/s^2] are transmitted via an amplifier to the computer and post-processed by an dedicated software. Sensors measure acceleration in 3 directions namely, in-plane and out of plane. They are placed in the field such that movements normal, transverse and parallel to the rail and parallel to the rail are recorded.

Representative train passages are running with the constant speed. Measurements are conducted a site location in the Netherlands.

3.2.2. Situational plan of the measurements

Measurements are taken for 5 different buildings located in the same area. Each of them has assigned five measurement points (MP1-5). They line up in a cross section which is perpendicular to the longitudinally running train track. For all the buildings the sensor placement convention is as follows:

Measurement Point 1: as close to the rail as possible, ground level

Measurement Point 2: intermediate point between MP1 and MP3, ground level

Measurement Point 3: sensor placed in front of the building, ground level

Measurement Point 4: sensor placed on the wall of the building, 10cm above the ground level

Measurement Point 5: inside the building, floor level

Detailed and representative layout of sensors is shown in the Figure 3.1. All 5 buildings and their distances to the track are presented in the Figure 3.2.

In reality, not all of the 5 buildings have simple rectangular geometry. Some of them have multiple stories and irregular shape. At this stage of research careful analysis of the buildings and their situational plan is made. As the result, building number 1 is chosen for the validation of the numerical model. Selection process and justification of the choice is listed below:

- Simplicity of shape – building has only one story and simple rectangular shape
- Sensors proximity to the rail –sensors for building no. 1 are the closest to the vibration source of the other available buildings
- She distance at which the acceleration is recorded – for building no. 1 the ratio between distance at which the acceleration is recorded and the distance from MP1 to the source is higher than for other buildings. For building no. 1 distance at which accelerations are recorded is 8 times longer than the distance from MP1 to the source. For the buildings 3 and 5 the distance between MP1 and the source is 2-3 times longer than the distance at which accelerations are measured.
- Scatter effect – building is not surrounded by other structures, meaning that there is less reflected waves influencing the measurement results
- Reliability – taking into consideration all listed factors, simplicity of the building, proximity to the rail and no surrounding structures, building no. 1 signal will provide the most reliable data from all available measurement points

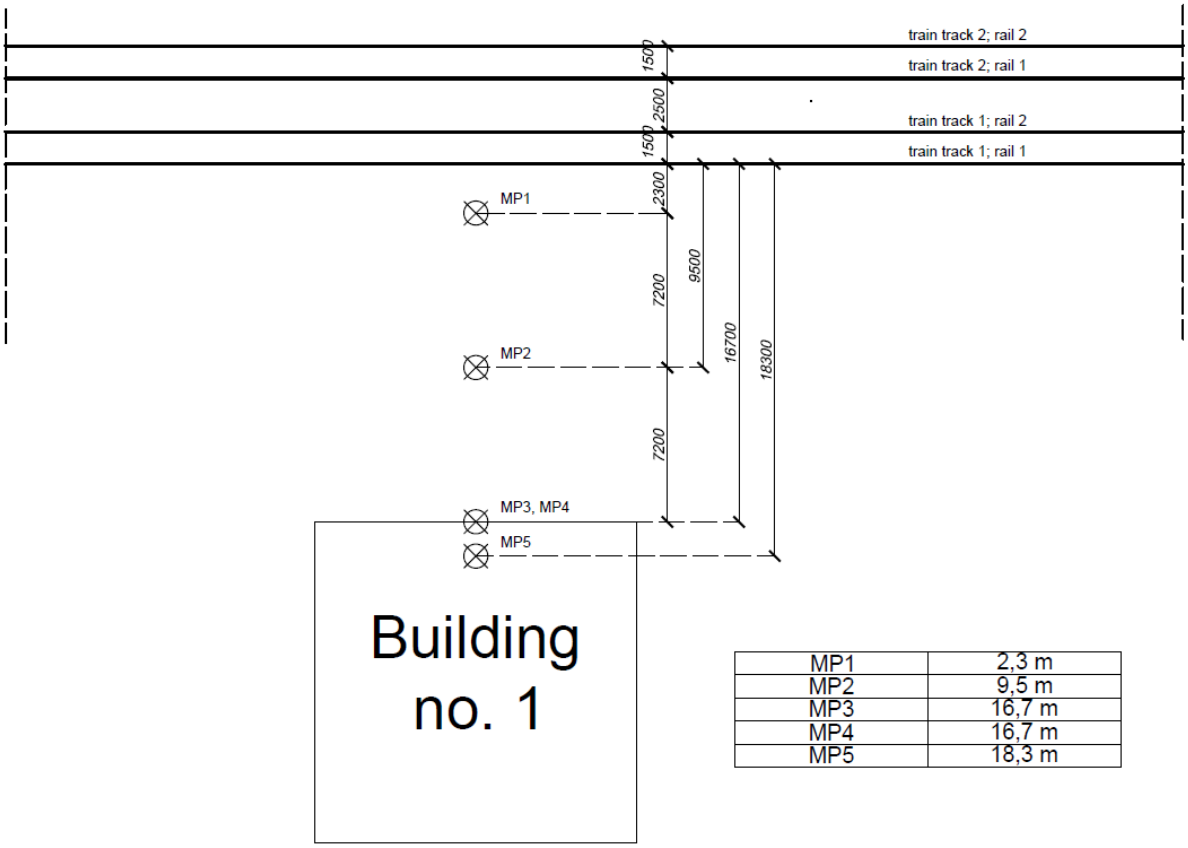

Figure 3.1 Detailed notation of building number 1. Same concept is applied to the rest of the buildings.

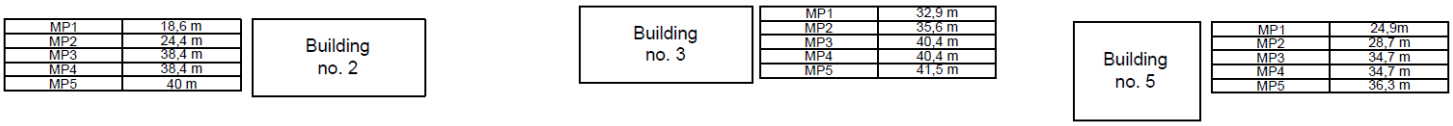

Figure 3.2 Situational plan with distances to the closest train track

3.3. Embankment cross section and its material properties

The cross section of the built in field embankment from were used. Small differences between design and implementation stage might occur. For this reason, engineering approximations must have been done in order to establish geometry and parameters of the embankment materials for the numerical analysis. The cross-section of the embankment used throughout the presented research is illustrated in the Figure 3.3. Properties of the embankment layers are presented in Table 3.2.

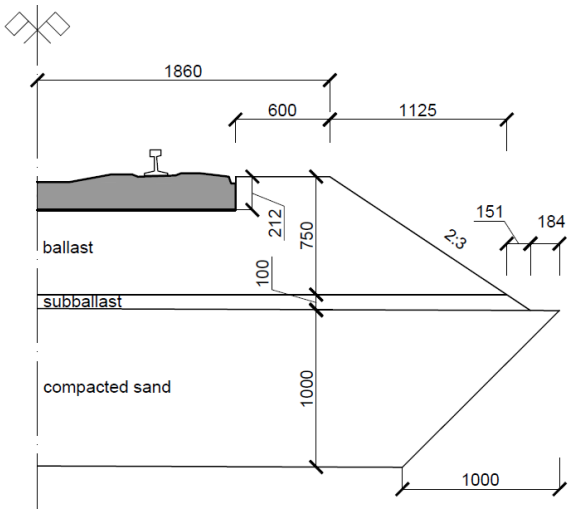

Figure 3.3 Embankment cross-section, dimension in mm

	$\gamma\ [\frac{\mathrm{kN}}{\mathrm{m3}}]$	$\gamma_{sat}\ [\frac{\mathrm{kN}}{\mathrm{m3}}]$	$\rho\ [\frac{\mathrm{kg}}{\mathrm{m3}}]$	Poisson's ratio [-]	E [MPa]	G [MPa]	$V_s\ [\frac{m}{s}]$	$V_p\ [\frac{m}{s}]$
ballast	16	17	1733	0.15	130	56.52	186.2	290.1
subballast – crushed stone 31.5/60	22	23	2243	0.22	180	73.77	181.4	302.7
subballast - asphalt	24	25	2548	0.33	11500	4324	1329	2639
compacted sand	20	22	2038	0.3	74.3	28.57	118.4	221.5

Table 3.2. Embankment layers material properties

Values of E parameter for asphalt are taken from (Real, et al., 2015) Table 2. There are uncertainties regarding the materials used in embankment, namely material used for subballast. Moreover, presence of the compacted sand beneath ballast bed is not confirmed.

3.4. Sleepers properties

The distance of 35m away from cross-section where measurements were performed is considered. At this distance different sleeper profiles of varying masses are present (see Table 3.3). The layout of the sleepers along 70m is shown in Figure 3.4. Sleeper profile is either NS90 or 14-002. Their main dimensions and weight are presented in the Table 3.3. To the left from the cross-section are 12 of 14-002 and 47 of NS90 sleepers, to the right are 22 of 14-002 and 36 of NS90 sleepers.

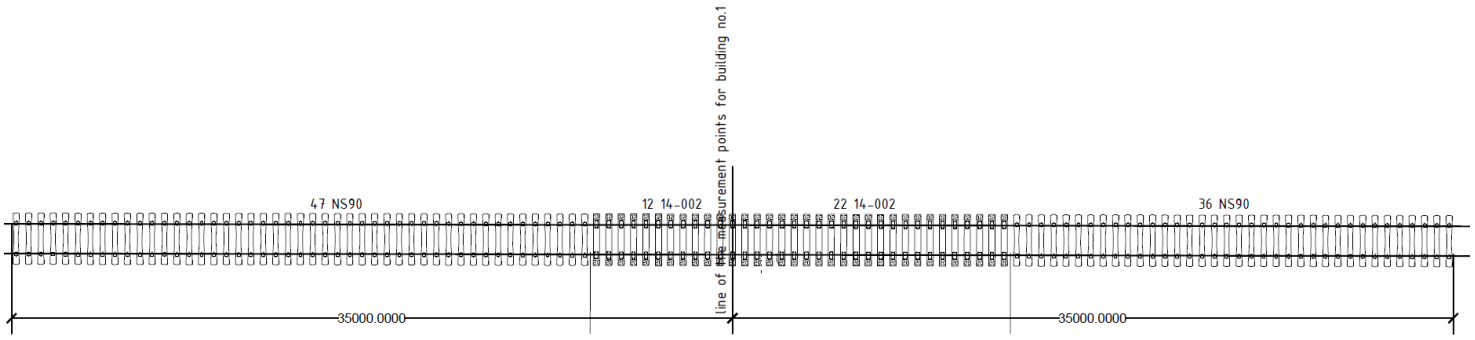

Figure 3.4. Sleepers distribution along 70m distance. Cross-section where measurements are taken is indicated by the vertical line

	Length [mm]	Width [mm]	Height [mm]	Weight [kg]
NS90	2520	300	214/175	276
14-002	2500	300	200	369

Table 3.3 Main properties of sleeper NS90 and 14-002. For full set of sleepers properties please refer to AP. A Figure 1 and AP. A Figure 2

This sleepers layout was implemented into the final numerical model. For further implementation in modeling, only one dimension, namely 14-002 sleeper, has been considered. To account for difference in mass, sleepers NS90 have different density. Dimensions of each sleeper are set to: 2500mm x 300mm x 200mm. Its volume is 0.15m^3.

$$\rho_{14-002} = \frac{369kg}{0.15\ m^3} = 2420\,\frac{kg}{m^3}; \quad \rho_{NS90} = \frac{276kg}{0.15\ m^3} = 1830\,\frac{kg}{m^3}$$

3.5. Rail

In accordance with available information about situation at the site rail profile is 54E1, which is equivalent of UIC54. Using specification from one of the manufacturers available on the market, properties of the rail were established (Arcelor Mittal, n.d.). They are shown in Appendix A in AP. A Figure 3.

3.6. Railpad and fasteners

In (Oregui, et al., 2016) the author modelled the fastener-railpad system as the district spring-damper pair. Through model calibration, stiffness of the railpad was obtained and set to 1560 MN/m. As the rule of thumb, in the Dutch train network the stiffness of the railpad should be around 1300 MN/m (personal communication from 26.04.2019) which is in line with the value obtained by the referenced article. However, if one would decide for modelling the fastener-railpad pair as volume the Eq. 16 can be used. By proper selection of the parameters stiffness k can be recreated during numerical modelling process what is described in more details in section 4.3.4.

$$k = \frac{EA}{L} \qquad \textit{Eq. 16}$$

where:
$L - height\ of\ railpad$
$A - area\ or\ railpad$

Railpad can be simulated by means of discrete spring and dashpot. In (Oregui, et al., 2016) the author provides a value of damping coefficient equal to c = 67.5kNs/m. The other approach was implemented in paper of (Shahraki, et al., 2014) where Plaxis 3D software is used. In that article fasteners are modelled but without railpad. They are simulated by node to node anchor element which has different tensile and compressional resistance assigned what leads to non-linear behavior. However, the approach introduced in the referred article cannot be implemented in this research because in both cases fastener type and properties remain unknown. Therefore, proper adaptation of real system into the numerical model is not possible.

3.7. Summary of Chapter 3

The most important information discussed in Chapter 3 is listed below in form of bullet points

- Soil profile at the site location consists of loose to medium sandy layers. Full overview of parameters is available in the Table 3.1.
- Some uncertainties regarding embankment cross-section are involved such as compacted sand presence and subballast material. They will be calibrated at the later stage of this report
- Building no. 1 is for model validation purpose.
- Out of 5 measurement points MP1-5 per building only MP1-3 can be used.
- Two types of sleepers are present in the model, namely NS90 and 14-002
- Rail profile is UIC54.
- In Dutch train network stiffness of the railpad is estimated to be 1300MN/m.

4. Numerical modelling

This chapter focuses on numerical model settings, therefore few subjects are discussed. First concerns adaptation of properties of soil, embankment, sleepers, railpad and rail to the numerical model. Moreover, justification of the size of: model, mesh, time step and area from which the results are extracted is presented. Next issue addressed is load representation as triangular pulses and as moving point load. Additionally, finite elements available in Plaxis database are discussed. In the end the settings of each phase in staged construction mode in Plaxis are shown. Model is considered to be linear elastic. Shear modulus is not updated during any of the model phases.

4.1. Size of the model

Size of the 3D numerical model has already been discussed in section 2.3.5 and sleeper layout at this distance is depicted in 3.4. For the present work the dimensions of the numerical model take pattern from the ones implemented in research of (Ruiz, et al., 2016). The reasons to use aforementioned reference is that authors employ the same numerical tool as for the presented research study, namely Plaxis 3D. The verification of the 3D model in (Ruiz, et al., 2016) was made through 2.5D technique derived by same authors. In their article (Ruiz, et al., 2016), distances up to 45m away from the track were investigated. To avoid spurious reflections of the waves from the boundaries model was extended beyond the area of interest by 20m in X direction (both sides, towards X_{min} and X_{max}, total 70m of the model), and by 20m in Y direction. Considered depth was 30m.

In presented research the interest is in distances up to approximately 20m away from the track. Following the methodology described above, the model should have dimensions of around 70m x 40m x 30m. It was then decided to implement model dimensions of 70m x 55m x 30m. If model in XY plane is of the shape of narrow rectangle more spurious reflections will be experienced in the considered cross-section instead of redistributed (they will reflect from Y_{max} plane). For this reason width of the model is equal to 55m instead of 40m. The model used through the rest of the presented research is presented from Figure 4.1 to Figure 4.3.

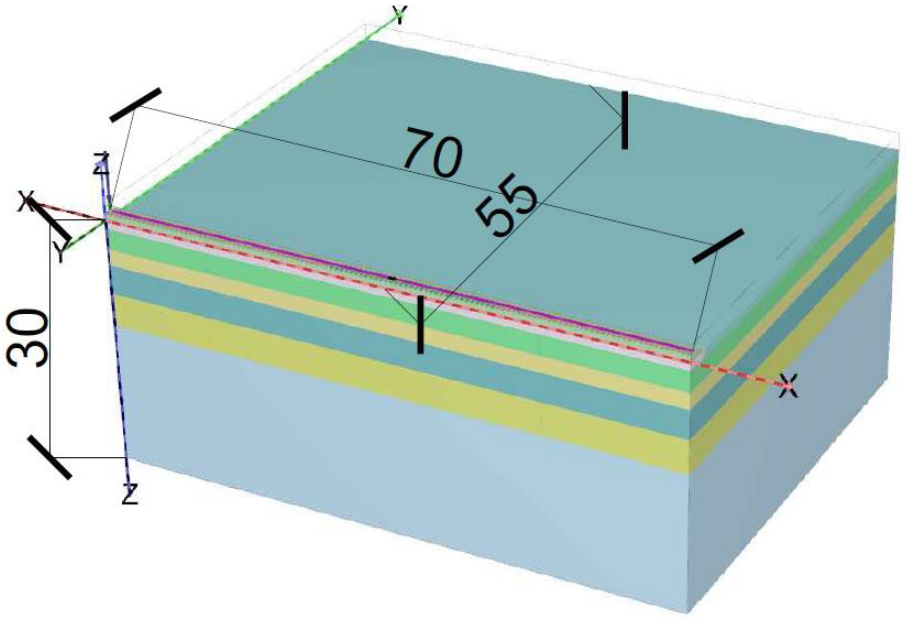

Figure 4.1 Overview for the implemented model. Dimensions are 70m (length-X) x 55m (width-Y) x 30m (depth-Z)

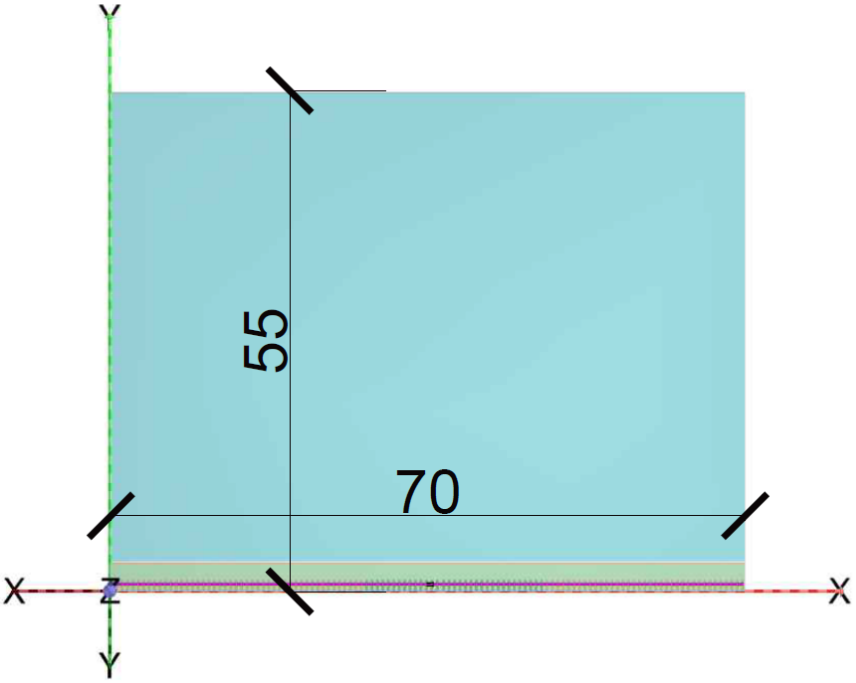

Figure 4.2 Top view of the model, XY plane

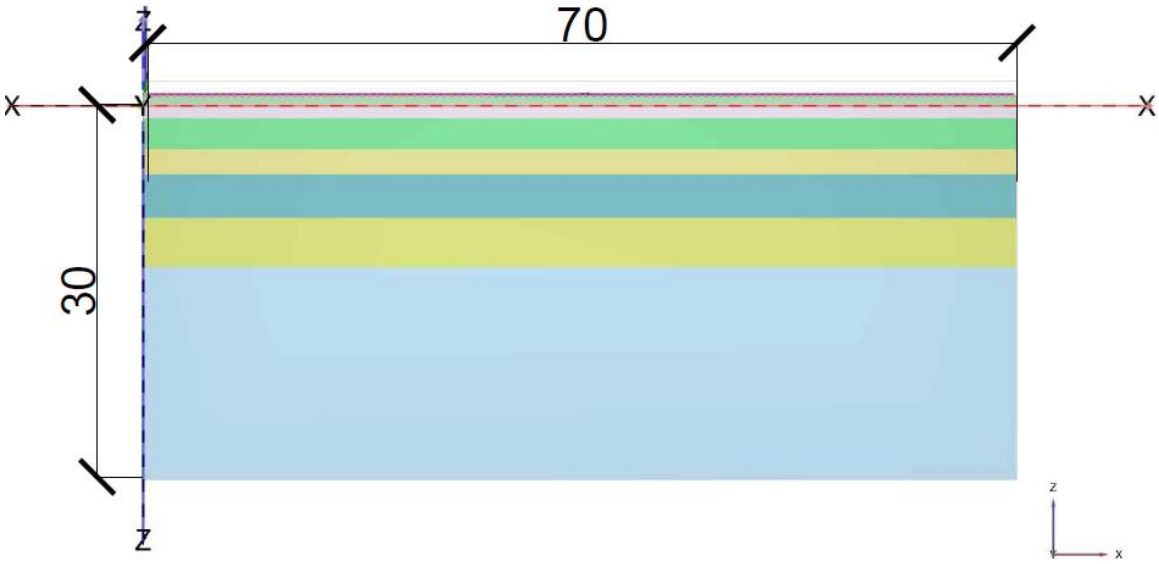

Figure 4.3 Side view of the model, XZ plane

4.2. Boundary conditions

Because symmetry model is applied the following boundary conditions (BC) are used:

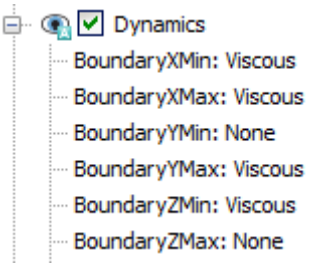

Figure 4.4 Dynamic boundary conditions

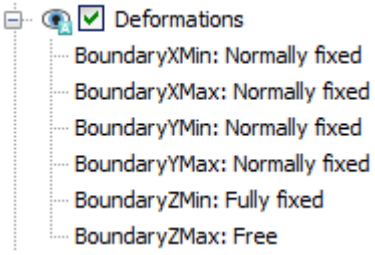

Figure 4.5 Static boundary conditions

Dynamic BC overwrites static BC (deformations). If dynamic BC are set to "none", then static BC are applied.

- X_{Min} – that is left surface of the model, ZY plane, Viscous boundary conditions in order to avoid reflections of spurious waves
- X_{Max} – right surface of the model, ZY plane, rest same as X_{min}
- Y_{min} – front surface of the model, XZ plane, fixed boundaries conditions applied due to symmetry of the model.
- Y_{max} - rear surface of the model, XZ plane, Viscous boundary conditions in order to avoid reflections of spurious waves
- Z_{max} – top surface of the model, YX plane, free boundaries conditions applied as top surface of the ground is free to deform in reality
- Z_{min}- bottom surface of the model, YX plane, viscous boundary conditions applied no change of the soil material is expected at the bottom of the model, meaning that sand layer continues beyond the model.

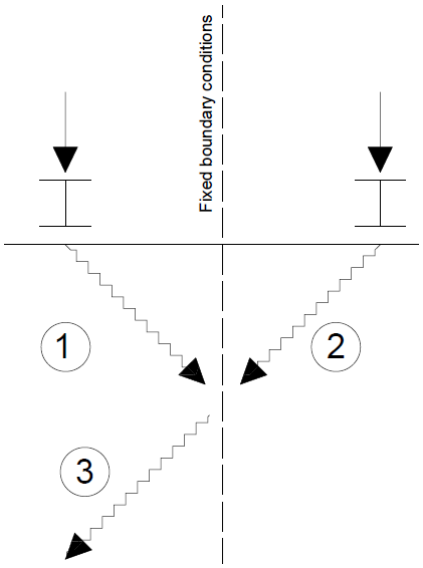

Figure 4.6 Propagation of waves with application of different boundary conditions

Boundary condition Y_{min} needs some explanation because it is set to "none" meaning that XZ plane is "normally fixed". Symmetry model is implemented and only one axle load is considered. However, in the reality soil experiences influence of both train wheels. This scheme is presented in the Figure 4.6. From the left side axle load induces wave (1) but from the other side there is an incoming wave (2) induced by the other wheel of the train which is not modelled. In reality wave (2) is present in the model. It can be artificially simulated in symmetry model by having fully reflective boundary condition at the symmetry plane. Reflection of wave (1) becomes wave (3) representing the continuation of wave (2) propagation path.

Some concerns might arise regarding Z_{min} BC. After personal communication with Plaxis support the advice was to model Z_{min} as non-reflective boundary if the impedance between materials is high, for instance if there is transition from soft clay to a very stiff rock. Unless otherwise the viscous BC is probably more appropriate (personal communication with Plaxis support, April 2019). In this research, the very bottom soil layer extends beyond considered 30m depth and no reflections into the system are expected. Hence, viscous boundary is chosen.

4.3. Modelling of the system elements procedure

In this subsection it will be briefly explained how soil, embankment, sleepers, railpad and rail are modelled in Plaxis 3D in this research study. Moreover, the finite elements employed for discretization of aforementioned will be shortly explained. For more scientific information and mathematical formulation about the finite elements refer to (Brinkgreve, et al., 2018).

4.3.1.Elements available in Plaxis 3D database library

4.3.1.1. 10-node tetrahedral element

This element has 10 nodes where every single one of them has 3 translational degrees of freedom: u_x, u_y, u_z. This is the only element available to model soil volume because Plaxis 3D does not allow to choose another one. The element is presented in Figure 4.7.

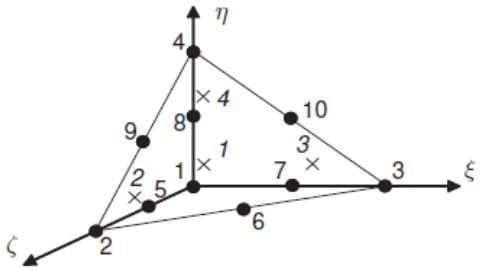

Figure 4.7 10-noded tetrahedral element, x- integration point, ⋆ –nodes (Brinkgreve, et al., 2018)

4.3.1.2. Beams

Beam elements serve for creating slender objects with significant flexural and axial rigidity. They are one dimensional. Each element consists of 3 nodes and every single one of them has 6 degrees of freedom, namely: three translations, u_x, u_y, u_z, and three rotations φ_x, φ_y, φ_z. The example of 3-noded Beam elements is presented in Figure 4.8.

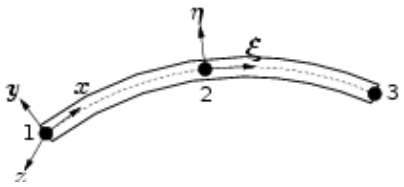

Figure 4.8 3-noded beam element *(Brinkgreve, et al., 2018)*

4.3.1.3. Plates

Plate in Plaxis 3D is in fact a shell. It has 6 nodes each of them has 5 degree of freedom: three translations u_x, u_y, u_z, and two rotations φ_y, φ_z. No so called "drilling DOF" is available for this element. Plate element is presented in Figure 4.9.

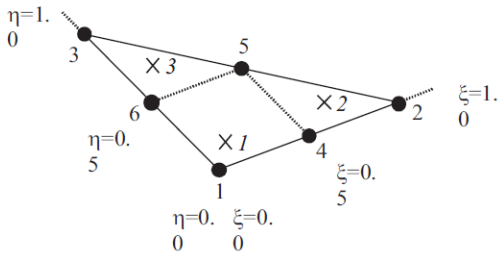

Figure 4.9 6-noded plate triangle, x- integration point, ⋆ –nodes (Brinkgreve, et al., 2018)

4.3.1.4. Interface elements

Interface element is a special kind of finite element. Unlike the other elements, it is consis of pairs of nodes. Each node has 3 degrees of freedom, namely three translations, u_x, u_y, u_z,. This element allows for differential displacements between pairs, meaning that gapping and sliding can be simulated. The distance between pair of nodes is equal to zero. They are triangular 6 noded elements. However, it is one pair thus in total one triangular interface element has 12 nodes.

4.3.2. Soil and embankment

Soil profile and embankment were formed by applying borehole pairs. Since model is invariant in longitudinal direction same boreholes profiles were used to opposite sides X_{min} and X_{max}. The example is presented in Figure 4.10. As already mentioned in section 4.3.1.1 for modelling the soil volume 10-noded tetrahedral elements are the only possibility allowed.

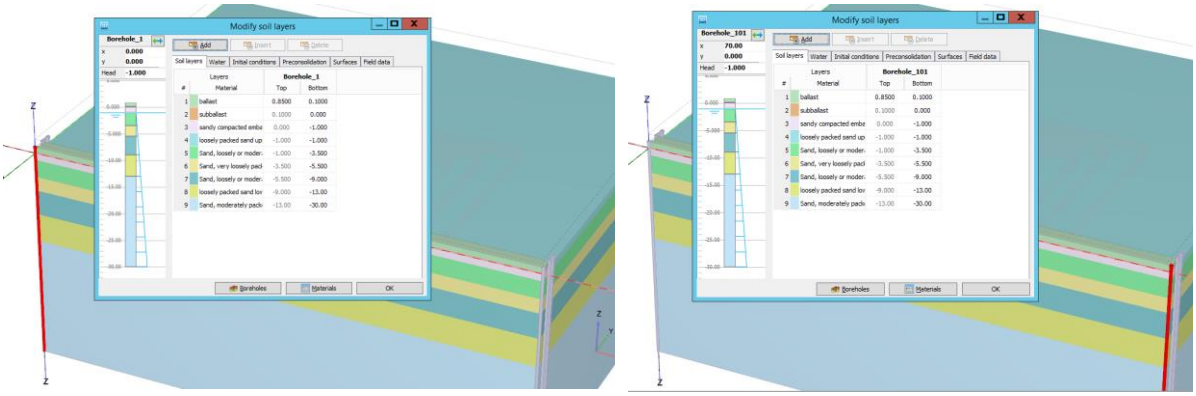

Figure 4.10 Boreholes pairs example, selected borehole is highlighted in red

4.3.3.Sleepers

As described in section 3.6, all sleepers have the same dimensions but different density to make distinction between mass of two sleeper types used along considered distance. Schematic drawings of sleepers layout are shown from Figure 4.11 to Figure 4.13. Dimensions of the modelled sleepers are same as sleeper 14-002, namely: 2500mm x 300mm x 200mm. The centre to centre distance of the sleepers is 0.6m.

Plaxis as default connects rigidly any overlying objects. At the beginning of this research it was planned to model railpad as plate only. In that case rail would be at the same level as the top of the sleeper. In order to avoid fixations between any volume elements and rail (modelled as a beam) sleeper has been risen up by 5cm. This action would assure that rail is supported in a discrete way and transmission of the force is through the sleeper to the soil, not through the soil and sleeper simultaneously when axle load is in between sleeper position. At the later stage of the project it turned out that it is more appropriate to model railpad as a volume, not plate (refer to section 4.3.4). The final situation is presented in the Figure 4.12. If the top surface of the sleeper was at the same level as the ground level, rail would have been still discretely supported by railpad. It means that rising sleeper up by 5cm was not necessary. More about the railpad design is included in the section 4.3.4.

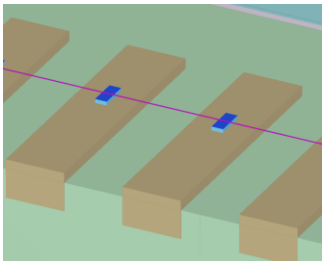

Figure 4.11 Schematic view at the sleeper and railpad in the 3D model

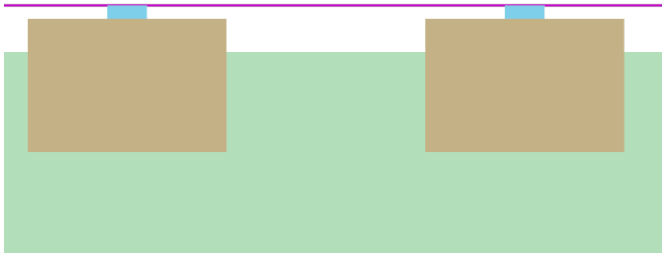

Figure 4.12 Side view for the sleeper and railpad. Light blue – railpad volume, pink line - rail

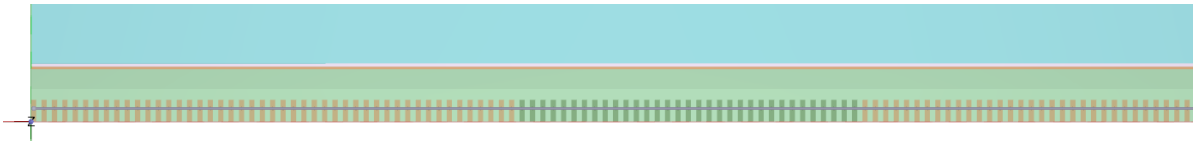

Figure 4.13 Top view at all sleepers

In practice it is advised to reduce the interface interaction between concrete structure (such as sleeper) and the soil. Interface element related to strength reduction factor is reduced to 80%. Based on article (Ruiz, et al., 2016) Rayleigh damping is set to 1% in frequency ranges from 10Hz to 50Hz. Properties of sleepers are presented in the Table 4.1. For more details refer toAP. A Figure 1 and AP. A Figure 2.

	γ_{unsat} [kN/m^3]	Rayleigh α [-]	Rayleigh β [-]	R_{inter} [-]	E' [kN/m^2]	ν [-]
NS90	18.30	1.67	0.000053	0.8	30 000 000	0.2
14-002	24.20	1.67	0.000053	0.8	30 000 000	0.2

Table 4.1 Properties of sleepers NS90 and 14-002 established for research study

4.3.4.Railpad

The easiest way to model the rail-railpad (fastener) connection would be in form of the plate with certain Young's modulus, dimensions and damping ratio and rail relying on it fully. However, railpad and rail do not share rotational degree of freedom around the axe perpendicular to the rail. At later stage of the research, it turned out that in Plaxis 3D no option of releasing this rotational degree of freedom shared between rail and plate (railpad) is possible. It forces full fixation between them while in reality connection is not fully rigid. Since Plaxis 3D makes rigid connections by default it would lead to rail being fixed along whole width of the sleeper. For modelling purposes, in order to simulate hinge mechanism in the best way possible, the area of railpad is highly reduced to limit the fixed part of the rail (by reducing the area of railpad it is possible to get closer to discrete spring-dashpot representation). However, after conversion of dimensions stiffness has to remain the same. The method to do that was already discussed in section 3.6 by means of using Eq. 16.

Two elements should be considered during modelling of fastener system, namely clips and railpad. Firstly, the intention was to establish stiffness of each of the aforementioned, sum them up and obtain equivalent stiffness value for volume block. Damping in the fastening system is mostly dictated by railpad then no summation is needed for this parameter. However, range of stiffness of different railpads at different frequencies is wide. In Article (Maes, et al., 2006) in section 3.2. properties of sample railpads provided by manufacturer are given. Difficulties in choosing one specific railpad arise from lack of the information about the fastener system properties applied on the site. Taking into account above considerations and uncertainties the average value for Dutch network (see 4.3.4) is assumed and equal to k = 1300 MN/m.

Size of the railpad is 15cm x 6cm x 2cm what is driven by feasibility of mesh. If railpad was smaller, mesh error occurs. The layout of the railpad can be seen in Figure 4.11 and Figure 4.12. Light blue indicates railpad volume. Dark blue represents the plate element which functions are described in the latter part of this sub-section.

As previously discussed, parameters used in Eq. 16 need to be properly converted. At this moment only E-modulus is missing for full formulation:

$$\frac{kL}{A} = E \rightarrow E = \frac{1300 \cdot 10^3 \frac{kN}{m} \cdot 0.02m}{0.06 \cdot 0.15\, m^2} = 2.89 \cdot 10^6 \frac{kN}{m^2}$$

$$E = 2.89 \cdot 10^6 \frac{kN}{m^2}$$

Young's modulus value of $2.89 \cdot 10^6 \frac{kN}{m^2}$ is assumed in all calculations numerical simulations.

No literature reference could be found regarding the amount of damping ratio in railpad. Only values of damping coefficient c could have been found in for instance (Oregui, et al., 2016) and its value is c = 67.5 kNs/m. Assuming mass of railpad equal to zero coefficient from Eq. 4 a_1 can be derived. The following holds:

$$c = a_0 m + a_1 k; m = 0$$

$$a_1 = \frac{c}{k} = \frac{67.5 \frac{kNs}{m}}{1300 \cdot 10^3 \frac{kN}{m}} = 0.052 \cdot 10^{-3}$$

This value is used for calculations in all of the models putting zero mass to railpad volume.

Since in reality rail relies on the whole railpad, there should be an element which simulates rail base. In order to distribute loads evenly to the railpad, not only locally, fictitious plate is used on top of whole pad, what is indicated in the Figure 4.11 by dark blue colour. The properties of the plate element plate are shown in Table 4.2. The plate element has 138 times higher stiffness than railpad and it is twice as stiff as steel. Due to high stiffness and relatively small load, plate do not bend but it transfers the whole load to the railpad in more evenly distributed manner.

	d [m]	w [m]	l [m]	γ [kN/m^3]	E [kN/m^2]
fictitious plate	0.03	0.06	0.15	1.00	400 000 000

Table 4.2 Properties of fictitious plate providing even distribution of the load to the railpad

4.3.5.Rail

As already discussed in section 3.5 UIC54 profile is used as presented in the AP. A Figure 3.

Properties given in Plaxis 3D are presented in the Table 4.3

	A [m^2]	I_2 [m^4]	I_3 [m^4]	γ [kN/m^3]	E [kN/m^2]
UIC54	$6.877 \cdot 10^{-3}$	$4.190 \cdot 10^{-6}$	$0.0234 \cdot 10^{-3}$	78.5	200 000 000

Table 4.3 Railpad properties, direction of I_2 and I_3 are indicated in the Figure 4.14

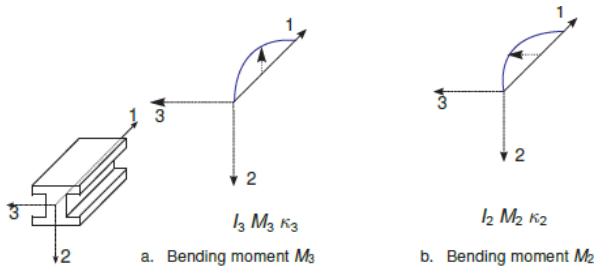

Figure 4.14 Local axes of 3D beam and directions of different cross-section properties

4.4. Load representation

4.4.1. Train model and load

It is known that the train type VIRM is running along considered track. The exemplary picture of such train is presented in the Figure 4.15. VIRM train consists of front, intermediate and back carriages. Train specification is taken from (Somda nl, 2010) where the load of the train is approximated with max 21.3t. Since symmetry model is used half of the load is necessary to be applied. For simplicity, after rounding up, 105.5kN is assumed to be the wheel load. During modelling only the intermediate carriages are considered as their exact configuration is not known.

Figure 4.15 The example of VIRM train type (Bombardier, n.d.)

The schematic sketch of wheel distances is presented in the Figure 4.16. For more detailed information about train and specification please refer to AP. A Figure 6.

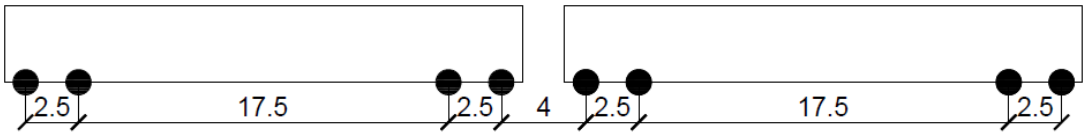

Figure 4.16 Wheel distances in VIRM train implemented in the numerical model

4.4.2.Triangular pulses static load

For the start, it was decided to account for the static moving load which can only be done by properly designed series of point loads. The rail is discretized between the sleepers and a point load is applied to each node. By means of activating and disactivating point loads the movement of the wheel can be simulated. The load distribution for point loads is linear. The interpolation function takes then shape of a triangle which can be seen in Figure 4.17. From this point they will be called "triangular pulses". In Figure 4.17 two blue point loads applied to the nodes at 0.6m and 0.9m are shown. The triangular functions represents the magnitude of the point load depending on the position of the wheel.

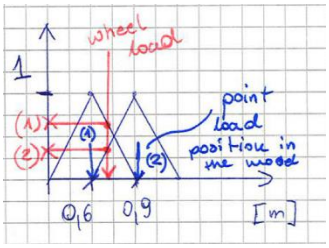

Figure 4.17 Linear function for load dynamic multiplier when wheel is located in between nodes

For instance, if the wheel is at the 0.7m position, value (1) is assigned to the point load (1) and equal to 2/3 while for the point load (2) magnitude (2) is assigned and equal to 1/3. It the wheel was at 0.6m then point load (1) would have magnitude equal to 1 assigned and point load (2) would have 0 magnitude. Wheel load is represented by summation of the magnitudes of the two adjusting point loads. This method is commonly used amongst researchers, refer to Figure 4.18 and Figure 4.19.

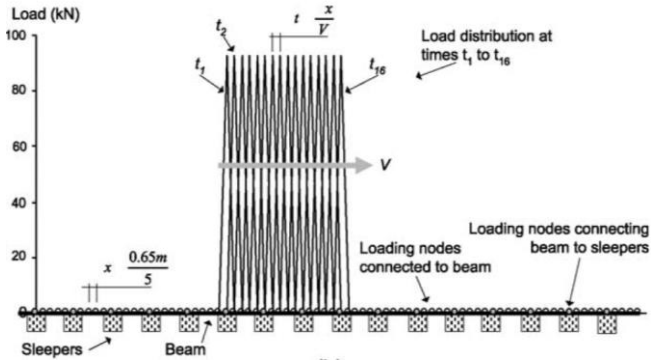

Figure 4.18 Load distribution of moving point load (Fig.19 (b) (Hall, 2003))

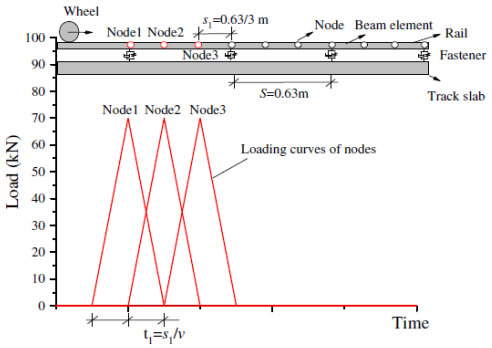

Figure 4.19 Moving load formulation (Fig. 4 (Jiang, et al., 2014))

To apply time function in Plaxis 3D to each of the point loads the dynamic multiplier can be used. It is formulated by applying the table with time and value specified. For this sake table in Excel has been created. Its overview can be seen in the Figure 4.21.

First column consists of numbers is the constitutive time step considered. Second column is the distance that the first wheel travels and it is set to 0.1m in one step. Third column represents time, at which the wheel load is present at specific position. Fourth column represents the dynamic multiplier value for specific time moment for the first point load applied to the node. Next columns are also dynamic multipliers but for the rest of the point loads, 2nd, 3rd, 4th etc. The other wheel and implemented into the dynamic multiplier such, that value 1 occurs at the time when the first wheel travelled distance between the first wheel and the one considered. In the example, in Figure 4.21 value 1 is seen at the same row as distance 2.5 m, the distance between first and second wheel (Figure 4.16). It means then, that the second wheel is exactly in the position of the first point load, when the first wheel travels 2.5m. When the train is moving forward then the wheel leaves position of the first point load and moves by 0.1 m meaning that first point load “feels” now 2/3 of this load, when 1/3 is felt by the second point load. Where the value 1 should be put in the dynamic multiplier column is presented in the Figure 4.22. How the signal looks for the point number 1 can be seen in

Figure 4.23. Comparison of time-load magnitude signal can be seen in Figure 4.24. In Figure 4.21 the cells highlighted in orange cells indicate the distance at which point load occurs (refer also to Figure 4.20) and the ones in bold frame indicate sleepers position.

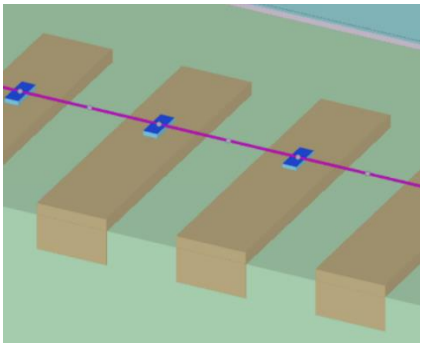

Figure 4.20 Division of rail in between sleepers, one intermediate point

Train geometry	x [m]
First wheel	0
Second wheel	2.5
Third wheel	20
Fourth Wheel	22.5
Fifth wheel	26.5
Sixth wheel	29
Seventh wheel	46.5
Eight Wheel	49
Ninth wheel	53
Tent hwheel	55.5
Eleventh wheel	73
Twelveth Wheel	75.5

Figure 4.22 Load dynamic multipliers

	distance [m] first wheel	0	1.000	2.000	3.000
1	0	0.0000000	0.333	0.000	0.000
2	0	0.0032727	0.667	0.000	0.000
3	0	0.0065455	1.000	0.000	0.000
4	0.10	0.0098182	0.667	0.333	0.000
5	0.20	0.0130909	0.333	0.667	0.000
6	0.30	0.0163636	0.000	1.000	0.000
7	0.40	0.0196364	0.000	0.667	0.333
8	0.50	0.0229091	0.000	0.333	0.667
9	0.60	0.0261818	0.000	0.000	1.000
10	0.70	0.0294545	0.000	0.000	0.667
11	0.80	0.0327273	0.000	0.000	0.333
12	0.90	0.0360000	0.000	0.000	0.000
13	1.00	0.0392727	0.000	0.000	0.000
14	1.10	0.0425455	0.000	0.000	0.000
15	1.20	0.0458182	0.000	0.000	0.000
16	1.30	0.0490909	0.000	0.000	0.000
17	1.40	0.0523636	0.000	0.000	0.000
18	1.50	0.0556364	0.000	0.000	0.000
19	1.60	0.0589091	0.000	0.000	0.000
20	1.70	0.0621818	0.000	0.000	0.000
21	1.80	0.0654545	0.000	0.000	0.000
22	1.90	0.0687273	0.000	0.000	0.000
23	2.00	0.0720000	0.000	0.000	0.000
24	2.10	0.0752727	0.000	0.000	0.000
25	2.20	0.0785455	0.000	0.000	0.000
26	2.30	0.0818182	0.333	0.000	0.000
27	2.40	0.0850909	0.667	0.000	0.000
28	2.50	0.0883636	1.000	0.000	0.000
29	2.60	0.0916364	0.667	0.333	0.000
30	2.70	0.0949091	0.333	0.667	0.000
31	2.80	0.0981818	0.000	1.000	0.000
32	2.90	0.1014545	0.000	0.667	0.333
33	3.00	0.1047273	0.000	0.333	0.667
34	3.10	0.1080000	0.000	0.000	1.000

Figure 4.21 Dynamic multiplier input for many loads

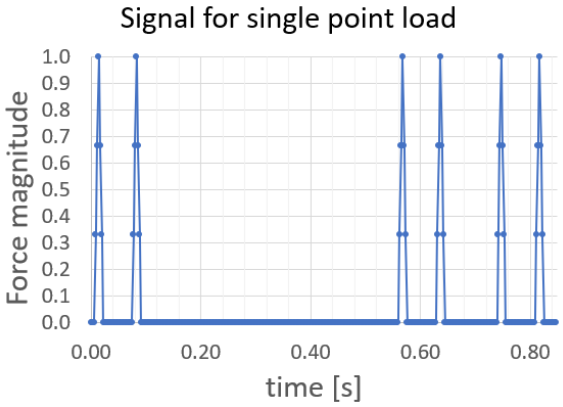

Figure 4.23 Time signal for point load number 1

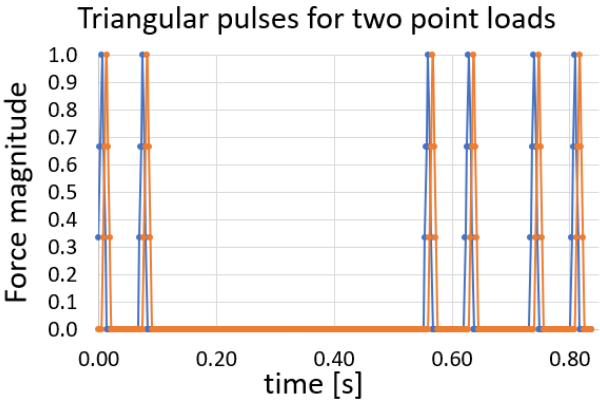

Figure 4.24 Time signal for two different point loads. Time shift visible, simulation of the moving load shown.

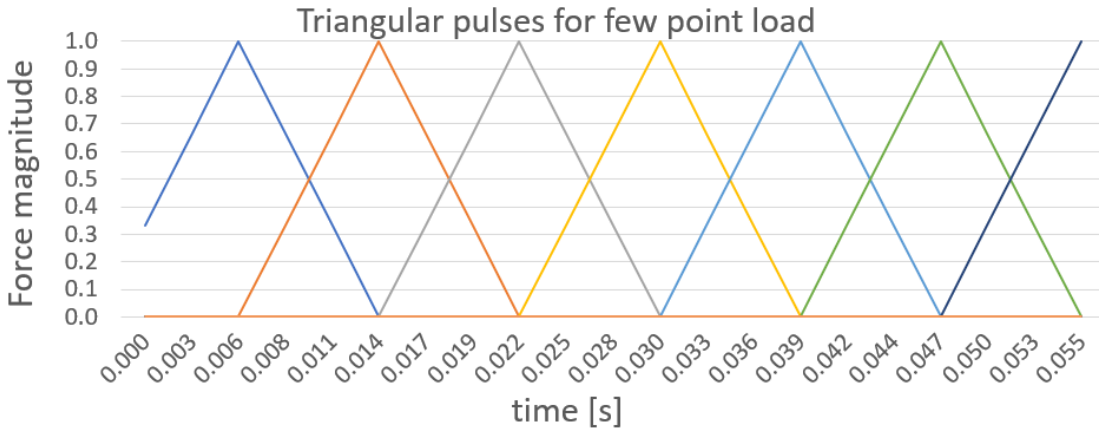

Figure 4.25 Linear function for simulation of moving point load

If one plots a few point loads time-dynamic relation in one graph, Figure 4.25 is obtained. The passage of the wheel load could be clearly seen.

Since the exact train speed at the site location is not known different train speeds were studied. These include 100, 115 and 130 km/h. As previously mentioned in this section, only static load component is considered.

The model with implemented point loads is shown in Figure 4.26. In total 233 point loads are created in the model. Only dynamic part of the load is selected in point load components which is presented in Figure 4.27. Static load has to be deselected because it cannot have assigned time-magnitude function.

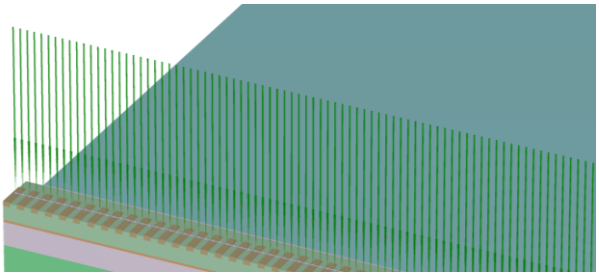

Figure 4.26 Implementation of the point loads simulating train passage in Plaxis 3D

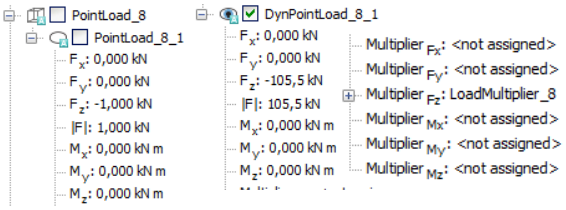

Figure 4.27 Settings for point load number 8

4.4.3. Oscillatory moving load

The option available in Plaxis 3D software since the end of 2018 is the moving point load along the specified path. In this way also oscillatory part of the load can be easily implemented. User needs only to know frequency of the oscillations and the force. The application of feature in this research is presented in the Figure 4.28.

To simulate train passage, loads need to start moving with a certain time offset driven by vehicle geometry and speed. To execute it in Plaxis each of the loads has to be applied to the separate node otherwise, they will be merged. For instance, if there is 15 different loads applied to the same node, Plaxis in the end will merge them into one point load. Then, it is not possible to activate them at different time. To overcome this difficulty loads are arranged as 12 separate point loads applied to 12 nodes (Figure 4.29, Figure 4.31).

Because of the two different parts of the load (what is explained at the latter part of this section) the extra set of dynamic load is applied in form of 12 dynamic point loads. In total 24 loads are active in the model. The distance between each of the loads is 1mm. Moving load needs such parameters as movement function and path. In this case path is rail for all of the loads. Movement function activates the movement of the point load at the certain time. The example are movement function 2 and 3 which are related to point load 2 and 3. Because one wheel load is divided into two separate parts the set of moving loads is employed. That is presented in the Figure 4.31. The red loads consist of quasi-static component and 60Hz sleeper passing frequency. The blue loads represent oscillations of the natural frequency of the train what is assumed to be 2Hz. Both oscillating loads are having 5% of the axle load what is equal to 5.275kN. The value is established by means of an educated guess. It should not exceed around 10% of the dead load, and for the start assumption was 5%. In chapter 5 of this research variation of this value is shown and details about results are presented.

It is important to mention that load oscillating with train natural frequency should be considered during analysis only when rail irregularities are accounted for. In this research this factor is not taken into account what implies that 2Hz component should not be included in the load. However, it will be shown later in section 5.3.2.5 that this load component has very small influence on the response signal. Therefore, the presented research remains valid.

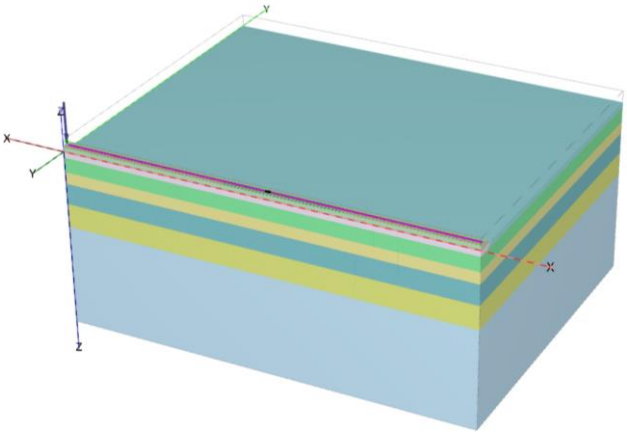

Figure 4.28 Model with moving load implemented

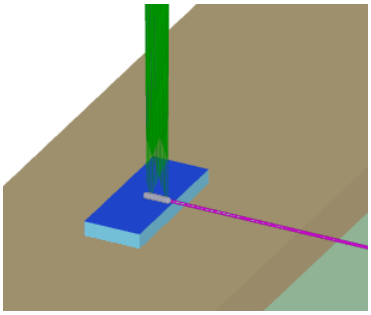

Figure 4.29 Inset to the point of moving loads application

a)

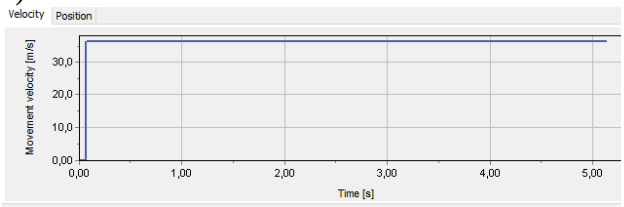

b)

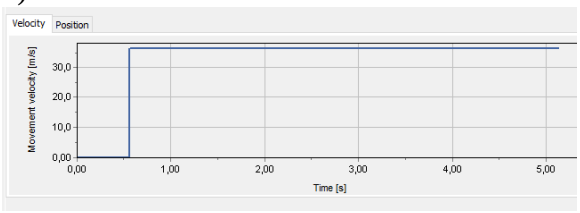

Figure 4.30 Movement function for (a) point load 2 and 14 (b) for point load 3 and 15

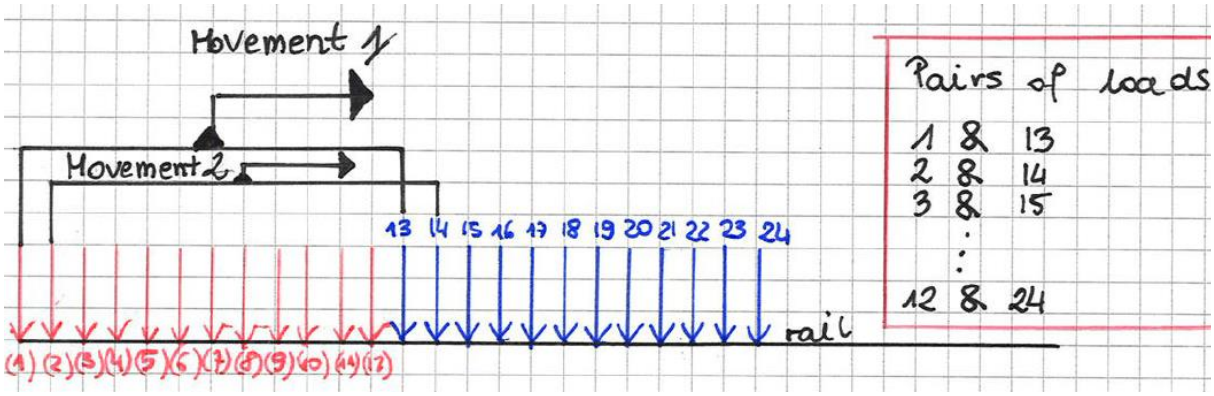

Figure 4.31 Movement function assignment, layout of load sets

Quasi-static component of the load

As previously explained in 2.3.3.7 quasi-static component is related to the weight of the vehicle. In considered case VIRM train type axle load for symmetry model is equal to 105.5kN.

Dynamic component of the load

For dynamic part of the load first sleeper passing frequency is taken into account. The frequency of oscillations is formulated in the following way:

$$\frac{V}{a} = f \qquad \textit{Eq. 17}$$

where:

a – distance between sleepers

V – train velocity

From Eq. 17 it is clear that the faster the train runs the higher is the frequency it is imposing on the system. For instance, for considered speed of 130km/h:

$$\frac{130\frac{1000m}{3600s}}{0.6m} = 60{,}18Hz \approx 60Hz$$

Also another component of train natural frequency is taken into account by applying 2Hz oscillations to loads 13-24.

4.5. Mesh and time step

It is expected based on the work of for instance (Ruiz, et al., 2016) that the dominant frequency component will be located up to around 40 Hz. That means that the wave length that needs to be fully captured is:

$$\Delta l = \frac{V_s}{f} \qquad \textit{Eq. 18}$$

where:

$\Delta l - wavelength$

$V_s - the\ slowest\ shear\ wave$

$f - upper\ frequency\ limit$

Based on Eq. 18 and the fact that 40Hz frequency is wanted to be simulated properly it is obtained:

$$\Delta l = \frac{V_s}{f} = \frac{57.57\frac{m}{s}}{40\frac{1}{s}} = 1.44m$$

For each wavelength at least 9-10 points are needed in order to follow the wave shape. 10-noded tetrahedral elements are used and they have 3 nodes at each edge. It means that around 4-5 elements of this kind are necessary to properly model wave shape. That is illustrated in the Figure 4.32. The element size should not have larger dimensions than 1.44m / 4 = 0.36m. Plaxis formulates basic size of the elements based on the model size what is described in more details in section 7.1.1 of (Brinkgreve, et al., 2018) and a piece of settings related to mesh size is shown in Figure 4.33. By using mesh function and specifying if it should be “fine”, “very fine” or medium one can manipulate with generic element size. When local coarseness factor is specified the element dimension is multiplied by it and mesh is generated according to modified dimension. For instance factor 0.12 with element dimension from Figure 4.34 will generate 10-noded tetrahedral elements of dimensions approximately 2.365m$\cdot$0.12=0.28m. Figure 4.34 represents what is the coarseness factors for elements, and in what areas what factor is used. Factor 0.12 generates the element size which is (in accordance with Eq. 18) able to reproduce properly waves of frequencies up to 51Hz. Also higher frequencies can be captured but with smaller accuracy.

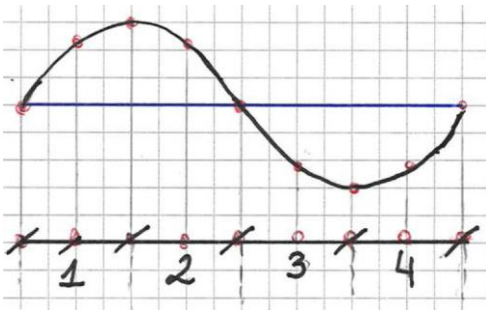

Figure 4.32 Discretization of single wavelength, red points are nodes. Numbers gives the idea of the 10-noded tetrahedral element amount necessary to describe wave length

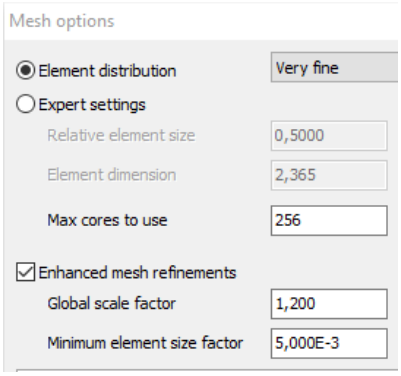

Figure 4.33 Mesh settings

The area of interest is located in the middle of the model and has dimensions of 30m x 20m. At this area it is important to have proper propagation of waves. However, outside this area, waves need to be only redistributed and high accuracy is not necessary. It allows for larger element size. The size of the element is modified by the intermediate coarseness factors as displayed in Figure 4.34. Smooth transition is provided in order to avoid sudden changes in mesh. The mesh considered in this study is presented in Figure 4.35 and Figure 4.36.

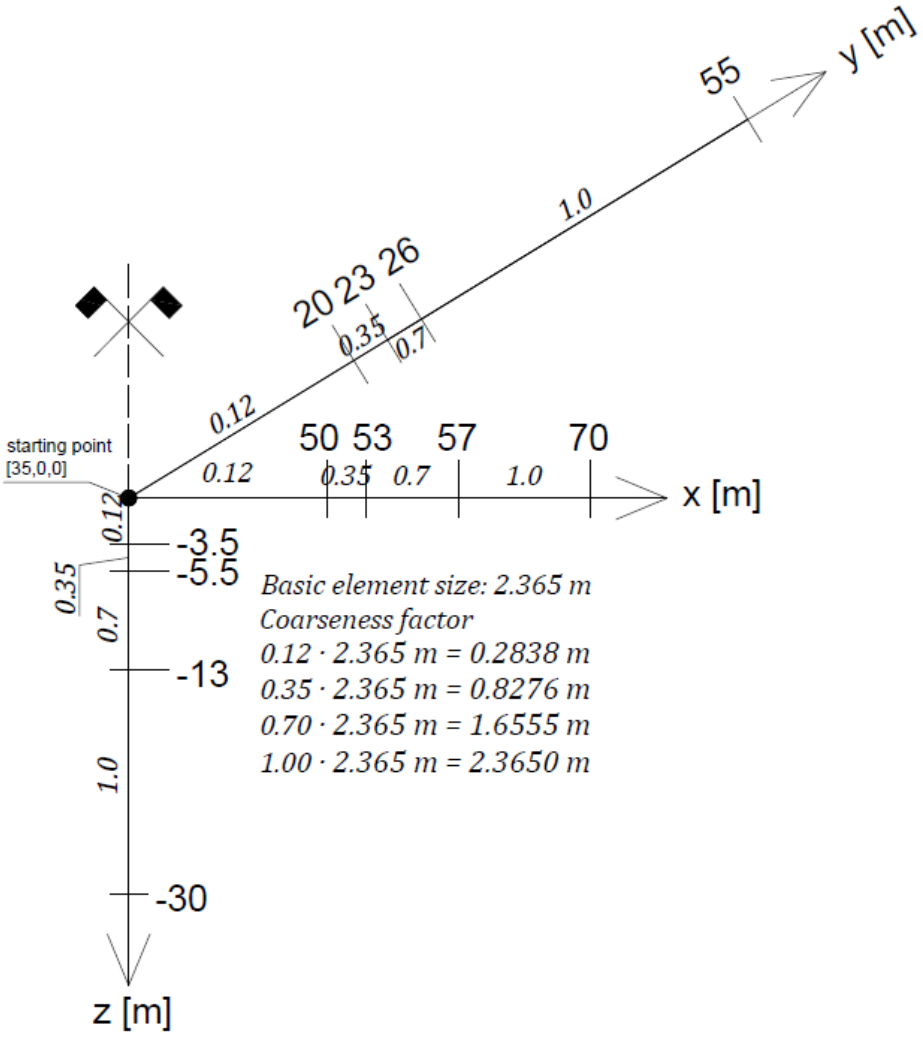

Figure 4.34 Mesh coarseness factors and element size

For proper simulation of waves not only element size should be small enough but also time sampling should be appropriate. For this case for each wavelength also around 9 to 10 time points are necessary. For frequency 40Hz it means that time sampling should be approximately 1 / 400 = 0.0025s.

Final mesh size consists of 715 739 elements and 1 000 113 nodes. The depth of fine mesh is limited to 3.5m otherwise the number of the elements is too high and no mesh can be generated.

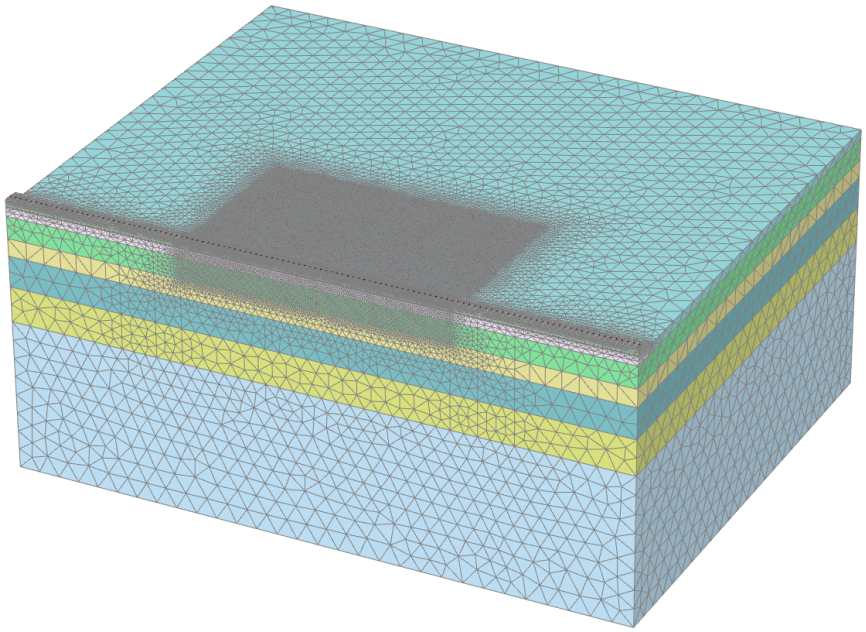

Figure 4.35 Mesh in Plaxis 3D

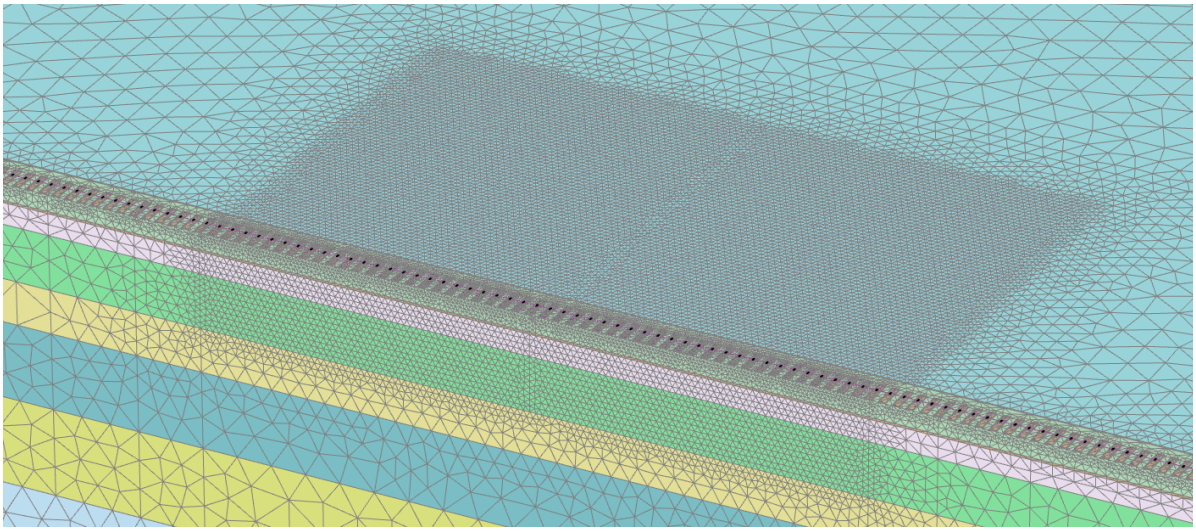

Figure 4.36 Inset into the dense mesh part where element size is small

4.6. Simulation stages

In Plaxis 3D there is a certain order of creating a model. First soil profile has to be defined, after that one can move to creating objects section, for instance sleepers or rail. Next, user can move to the construction mode where the sequence of erecting the structure/system is defined

The general rule used in research for establishing simulation phases is activating one element of the model at the time. Naming of phases is in order but their numbers are random. It is dictated by the fact that once the phase is created its original name cannot be changed, then after deleting one of them, number is still missing. Following phases are present in the model: Initial phase, Phase_1, Phase_3-9, Phase_19-22, Phase_24-28. Table 4.4 gives an overview of the element activated during each of the non-dynamic phases. In order to avoid numerical errors, which might occur due to high number of elements, non-dynamic parts are split into many phases.

	Activated	settings	Model Figure	Settings details
Initial Phase	soil stratum	default	Figure 4.37	Appendix B
Phase 1	compacted sand		Figure 4.38	
Phase 3	subballast		Figure 4.39	
Phase 4	ballast		Figure 4.40	
Phase 5	sleepers		Figure 4.41	
Phase 6	railpads		Figure 4.42	
Phase 7	railpad plates		Figure 4.43	
Phase 8	rail		Figure 4.44	
Phase 9	nothing		Figure 4.45	

Table 4.4 The overview of activated elements respectively in Phases 1, 3-9, phases settings

Phase 19 and the rest of dynamic phases

In this phase all loads are active. Calculation type is set to dynamic. Model at this phase is presented in Figure 4.46. The most important features will be described in this paragraph. Settings for this phase are displayed in the Figure 4.47.

Approximately 2.75 - 3s dynamic time simulating of train passage is analyzed. This dynamic time duration is dictated by the fact that many simulations were necessary to be performed in order to achieve model calibration. It was found that 3s simulation time gives reasonable approximations of the results in comparison with 6.5s. If longer time interval is considered then calculation time increases significantly without improvement of the results but calculation time increases around 3 times.

Dynamic time simulation was divided into a few phases of smaller time intervals in order to prevent losing the results due to the software unforeseen errors.

All dynamic phases are formulated in the same way. The only difference is in the first dynamic phase in which displacements are reset to zero. In this way the influence of train passage only is included in the obtained numerical results.

In order to have desired time step one must switch to “Manual” time step determination. If as in the Figure 4.47 dynamic time interval is set to 0.5s in order to obtain 0.0025s time step, max steps should be set to 200. In this way 0.5s / 200 = 0.0025s the wanted time interval is obtained. Max number of steps to be stored is set to low value otherwise result files are taking too much space (for instance 150GB) what is difficult to be stored. Number of sub-steps is set to 3. It defines how many sub-steps in each of 200 steps software needs to consider in order to meet wanted accuracy. Rest of the parameters is left as default.

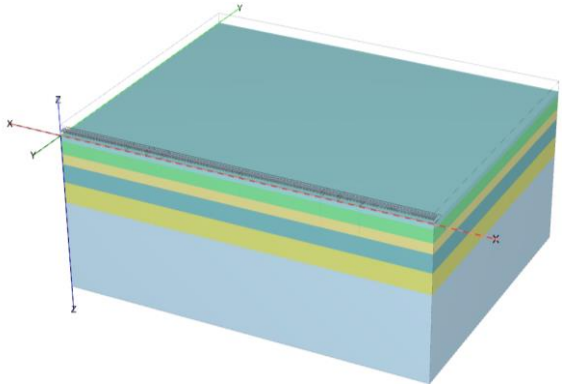

Figure 4.37 Initial phase model

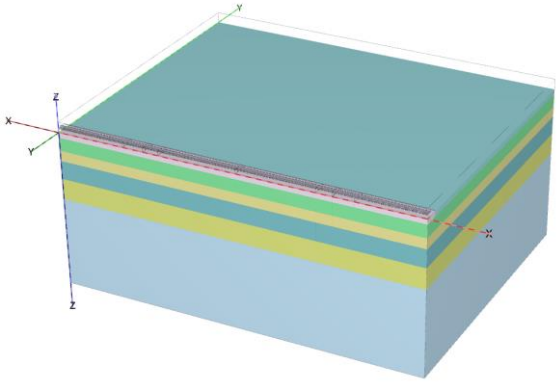

Figure 4.38 Phase_1 model

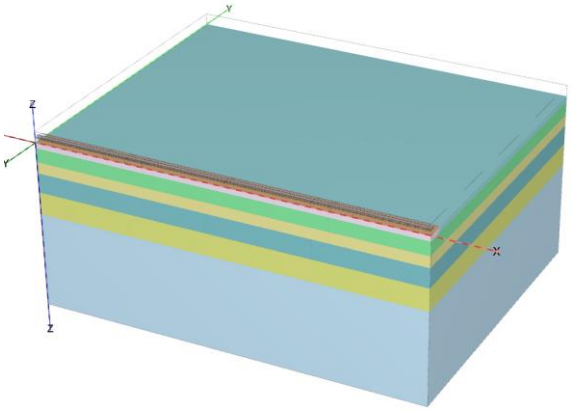

Figure 4.39 Phase__3 model

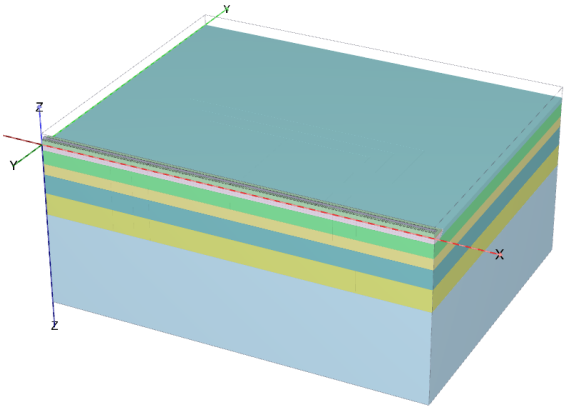

Figure 4.40 Phase_4 model

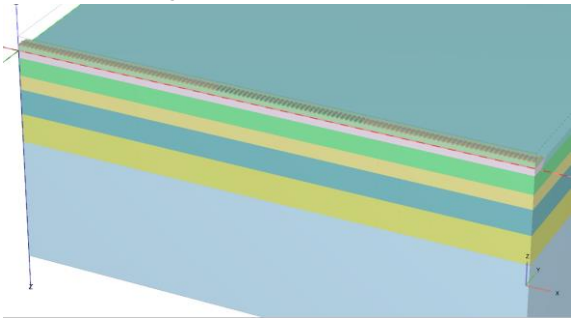

Figure 4.41 Phase_5 model

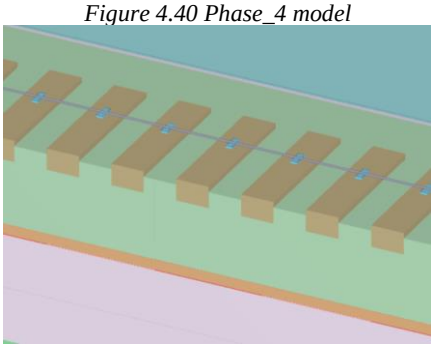

Figure 4.42 Phase_6 model

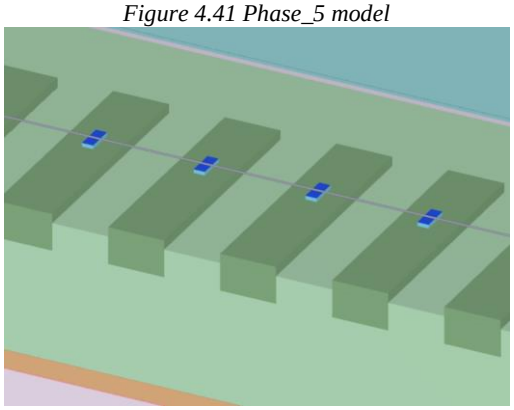

Figure 4.43 Phase_7 model

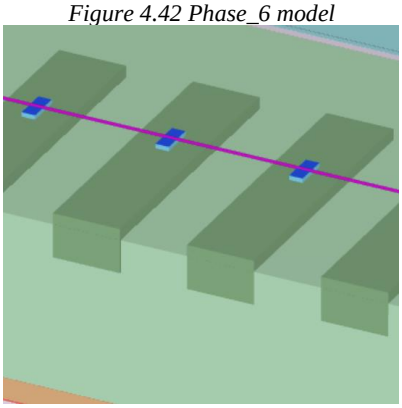

Figure 4.44 Phase_8 model

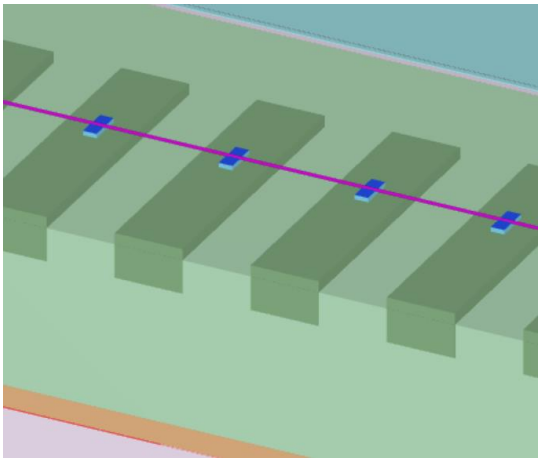

Figure 4.45 Phase_9 model

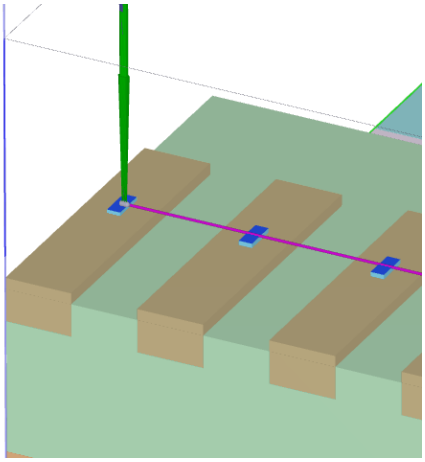

Figure 4.46 Phase_19 model

Name	Value
General	
ID	Phase_19
Start from phase	Phase_9
Calculation type	Dynamic
Loading type	Staged construction
Pore pressure calculation type	Use pressures from p
Dynamic time interval	0,5000 s
First step	17
Last step	216
Special option	0
Deformation control parameters	
Ignore undr. behaviour (A,B)	☐
Reset displacements to zero	☑
Reset small strain	☑
Reset state variables	☐
Reset time	☐
Updated mesh	☐
Ignore suction	☑
Cavitation cut-off	☐
Cavitation stress	100,0 kN/m²

Numerical control parameters	
Solver type	Picos (multicore iterative)
Max cores to use	256
Max number of steps stored	2
Use default iter parameters	☐
Max steps	200
Time step determination	Manual
Number of sub steps	3
Tolerated error	0,01000
Max unloading steps	5
Max load fraction per step	0,5000
Over-relaxation factor	1,200
Max number of iterations	60
Desired min number of iterations	6
Desired max number of iterations	15
Use line search	☐
Use gradual error reduction	☐

Dynamic control parameters	
Alpha - Newmark time integration	0,2500
Beta - Newmark time integration	0,5000
Mass matrix	0,000
Reached values	
Reached total time	5,787E-6 day
CSP - Relative stiffness	1,000
ForceX - Reached total force X	0,000 kN
ForceY - Reached total force Y	0,000 kN
ForceZ - Reached total force Z	0,000 kN
Pmax - Reached max pp	0,000 kN/m²
ΣM_{stage} - Reached phase proportion	0,000
ΣM_{weight} - Reached weight proportion	1,000
ΣM_{sf} - Reached safety factor	1,000

Figure 4.47 Settings for Phase_19

4.7. Summary of Chapter 4

The most important information discussed in Chapter 4 will be listed below in form of bullet points

- Size of the model is set to 70m x 55m x 30m (length, width, depth respectively).
- Boundary BC at symmetry plane are set to normally fixed, top surface BC is set to free, BC for other planes is set to viscous
- Two sleeper types are considered. In the numerical model they are distinguished by different mass. Their dimensions are 2500mm x 300mm x 200mm. properties are presented in Table 4.1
- Sleepers spacing is 0.6m.
- Railpad had dimension of 150mm x 60mm x 20mm. It is massless. Young's modulus is set to $2.89 \cdot 10^6$ kN/m^2. Parameters needed for Rayleigh damping are $\alpha=0$ $\beta=0.052 \cdot 10^{-3}$.
- Fictitious plate is applied on top of the railpad in order to distribute the moving point load evenly to the railpad. Its properties are shown in Table 4.2.
- In triangular pulses representation of the moving load, only quasi-static axle load related to the dead weight of the vehicle is present and equal to 105.5kN
- In the moving point load model, three load components are taken into account. Quasi-static load component is equal to 105.5 kN, dynamic load component is oscillating with frequency of 60Hz (train is travelling at 130km/h speed) and of 2Hz (first natural frequency of the train). It should be stressed that 2Hz oscillatory load component should not be taken into account

because rail irregularities are not considered during analysis. However, in this research 2Hz load has secondary effect on the response and results are reliable.

- Dynamic loads components are consisted of the force equal to 5% of the axal load.
- In order to simulate properly wave propagation up to 40Hz the element size cannot be larger than 0.36m. Finally in the area of interest which is 30m x 20m x 3.5m element size is equal to 0.28m which can simulate waves up to 51Hz. The element size in the whole mesh is presented in the Figure 4.34
- Duration of dynamic simulation is 3s.
- Time step is set to 0.0025s

5. Validation of the numerical results

Focus of this chapter is on the description of the results obtained from numerical simulations. It starts from explaining available measurement signal necessary for model calibration. Next, validated model and all simulations performed to achieve it are discussed. Flow chart schematically describing each of performed simulation is shown in Figure 5.1.

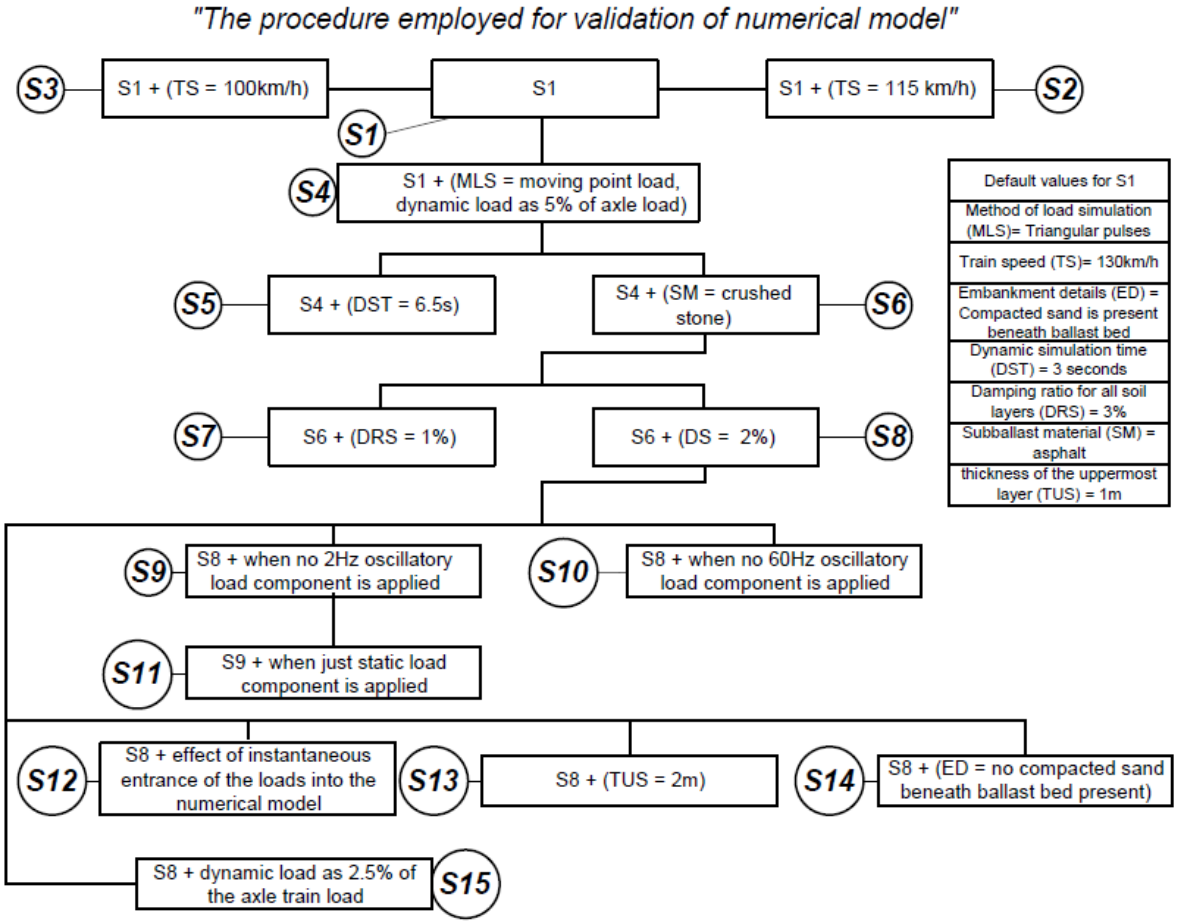

Figure 5.1 Schematic description of numerical simulations performed to obtain the best match with measurements results

5.1. Measurement results

In order to eliminate excessive vibrations due to vehicle factor (e.g. flat wheel) two available from measurements signals are analysed. In this way, by comparing them, abnormalities related to the train vehicle can be easily spotted. The results of measurements results in time and frequency domain are presented from Figure 5.2 to Figure 5.4 and from Figure 5.5 to Figure 5.7 respectively.

In general, by looking at the results in time domain, it is possible to observe and distinguish passing wheels. In Figure 5.2 which depicts MP1 acceleration in time domain, in signal 1 (blue) high peaks of $\pm$ 4.5 m/s^2 can be treated as vehicle related and disregarded. This conclusion is made upon single occurrence of the peak in the signal. When other train wheels are passing much smaller accelerations are recorded meaning that the cause of the very high peaks is local and associated with particular, non-repetitive axle load. It is known that wheel irregularities are enhancing higher frequencies, what also causes higher accelerations, at least close to the track. Therefore, it might be concluded based on the above, that high acceleration value is most probably caused by the wheel irregularities.

Moreover, such high peaks do not appear in signal 2 (red) at any time what is the next argument to disregard them. Another aspect observed at MP1, is that signal 2 gives more higher acceleration peaks than signal 1. When combining this observation with acceleration spectrum presented in Figure 5.5 the conclusion might be that the higher acceleration values from signal 2 are caused by higher content of high frequencies in the signal (range of around 130-150Hz). That once again can be assigned to the vehicle rather than the soil or rail because in signal 1 which is the result of another train passage on the same embankment, such high frequency content is not recorded. When analyzing MP2 results, it is visible from Figure 5.6 that high frequency content (around 100-180Hz) decays with the distance for both signals. Acceleration results from signal 1 and 2 are now very similar in their magnitude. The same holds for MP3. High frequencies excited probably by the irregularities of the wheel are influencing the area in the source vicinity. Their content decays faster than low frequencies content and for further distances their influence is not that significant. It is observed that the frequency content of the highest magnitude occurring further from the source is in range of approximately 55Hz to 80Hz.

The time shift between two signals is observed in the time domain for all measurement results. The reason for this is manually started recording of the train passage. It happened that the vehicle passage was recorded at different time intervals within 20s of the recording duration.
Since accelerations are the only available data, validation of the numerical model is done by comparing them and theirs spectrums. Measurement points MP4 and MP5 involve building factor, therefore they are excluded from validation process. Building is not present in the model, only one variation at later stage of this work is investigated. The tolerance in expected results is rather high since there are uncertainties about several parameters such as weight of the train, speed, configuration of carriages. Therefore, it is easier to talk about target range than a specific number. Based on the interpretation of the available data, the values that are expected to be obtained from numerical model simulations are put together in Table 5.1. In the next sections only signal 1 will be compared with results from the numerical analysis.

	MP1	MP2	MP3
Acceleration a_z [m/s^2]	1.6 - 2	0.6 - 0.8	0.2 - 0.25
Frequency range (the highest magnitude) [Hz]	55 - 100	55 - 80	55 - 80

Table 5.1 The range of expected values from the numerical simulations based on available signals

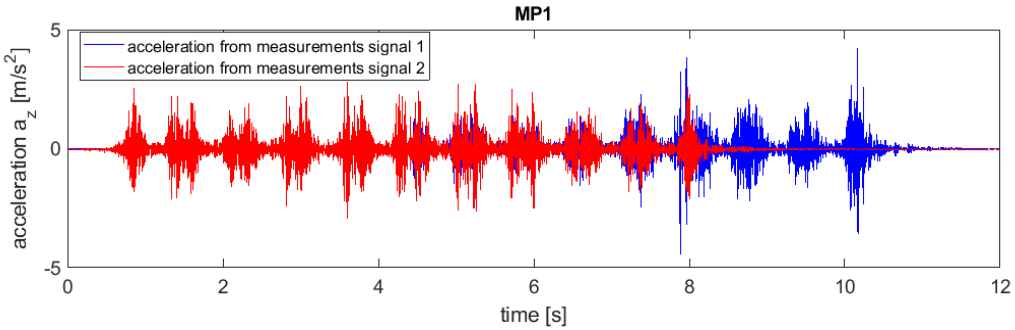

Figure 5.2 Measured acceleration at MP1 for two recorded train passages

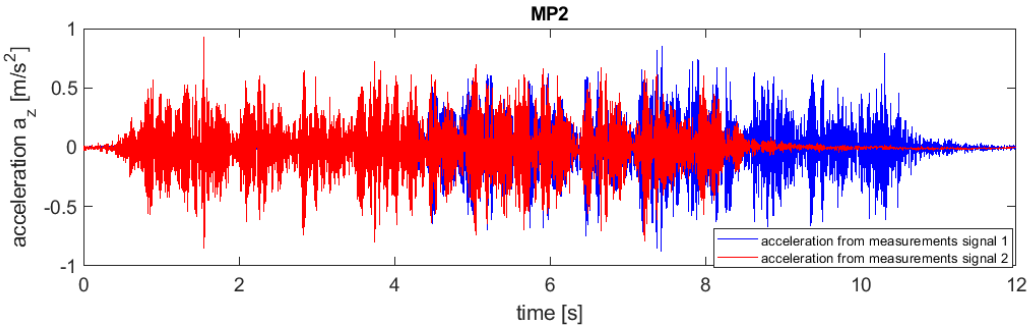

Figure 5.3 Measured acceleration at MP2 for two recorded train passages

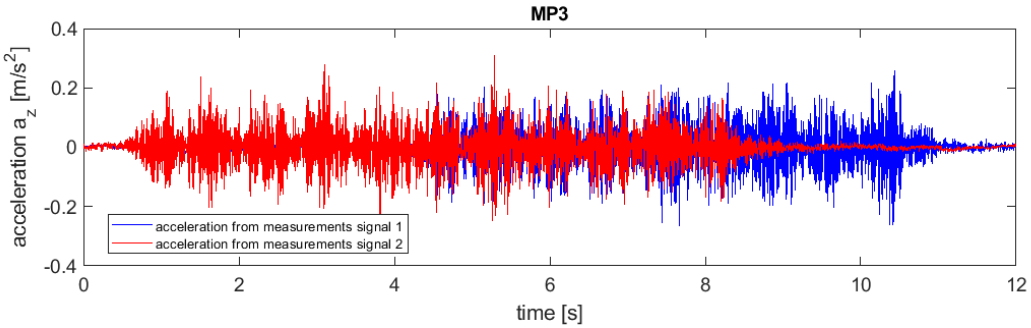

Figure 5.4 Measured acceleration at MP3 for two recorded train passages

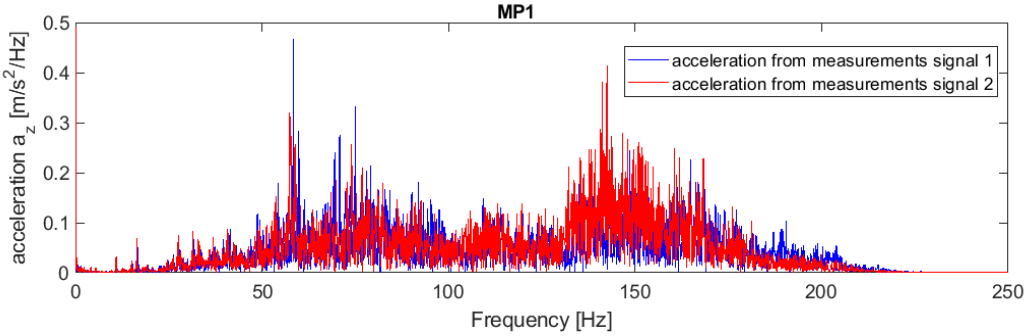

Figure 5.5 Acceleration spectrum at MP1 for two recorded train passages

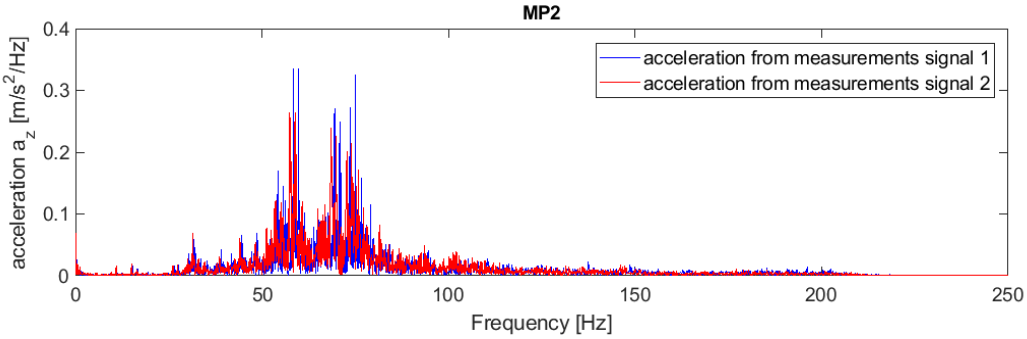

Figure 5.6 Acceleration spectrum at MP2 for two recorded train passages

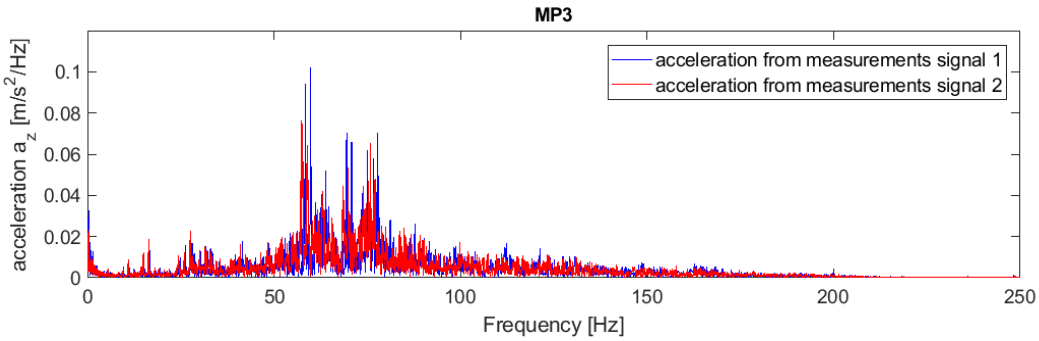

Figure 5.7 Acceleration spectrum at MP3 for two recorded train passages

5.2. Validated model (S8)

Many simulations were run in order to find the best match between measurement results and numerical simulations. In these simulations considered aspects are load simulation as triangular pulses and moving point load (see 4.4 and 5.3.2.1), different subballast material, varying damping ratio for soil stratum, long and short duration of dynamic simulation, influence of each load component on the results, instantaneous entrance of the load into the model, change of dynamic oscillating force value, change of soil profile uppermost layer, presence of compacted sand beneath ballast bed. In this subsection, only the results of the validated model are discussed (S8). It was mentioned previously in Chapters 3 and 4 that the exact cross-section of the embankment is not fully known. In the end geometry consisted of compacted sand and crushed stone as subballast gives the best agreement with the measurements. Nevertheless, the other simulations that were performed to verify numerical model are treated as the variation study and described in the next chapter. How model is established is described in Chapters 3 and 4. Damping parameters which were used in this variation for different elements are listed in Table 5.2.

	α	β	damping ratio [%]
Sleeper	1.67	0.000053	1
Ballast	8.94	0.000283	6
Subballast	6.14	0.000195	4
soil – all layers	3.25	0.0001025	2

Table 5.2 Damping values for different layers for the validated model

The results of acceleration in time and frequency domain are presented from Figure 5.8 to Figure 5.10 and from Figure 5.11 to Figure 5.13 respectively. Numerical models were run for approximately 3s.

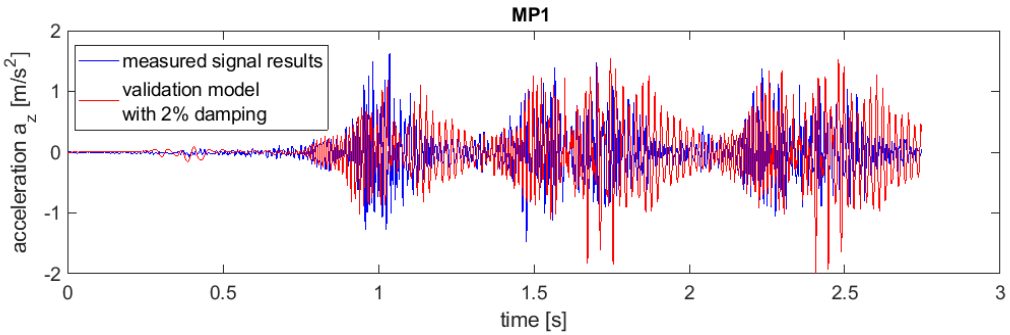

Figure 5.8 Comparison of accelerations of validated numerical model with measurement results at MP1

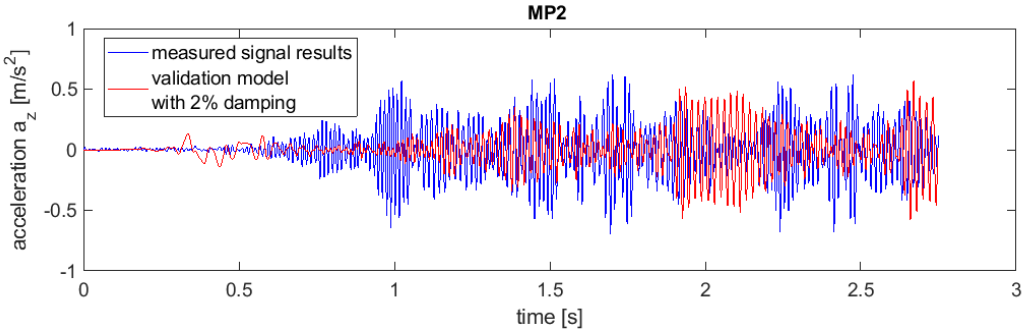

Figure 5.9 Comparison of accelerations of validated numerical model with measurement results at MP2

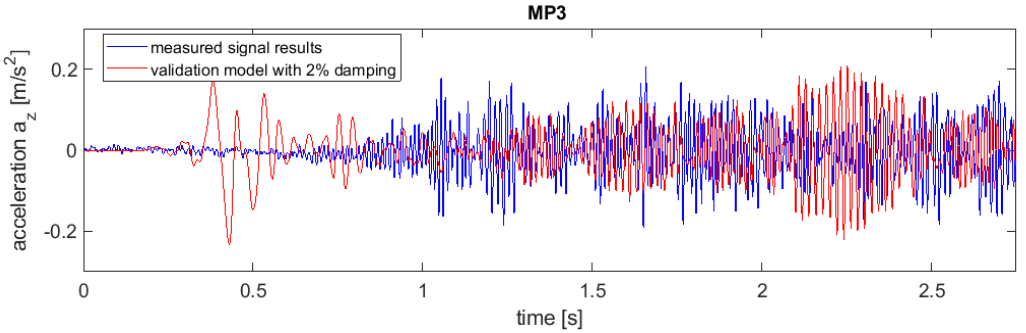

Figure 5.10 Comparison of accelerations of validated numerical model with measurement results at MP3

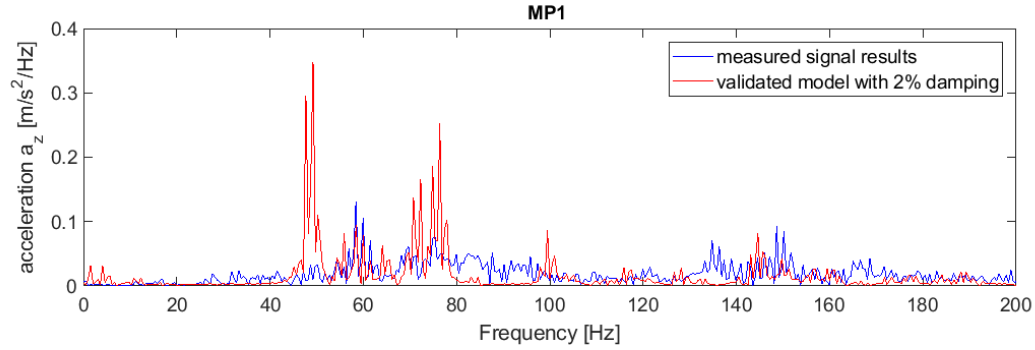

Figure 5.11 Comparison of acceleration spectrums of validated numerical model with measurement results at MP1

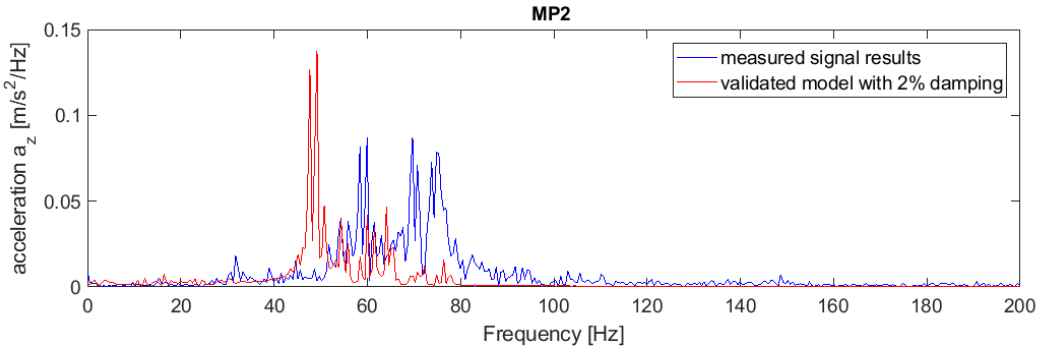

Figure 5.12 Comparison of acceleration spectrums of validated numerical model with measurement results at MP2

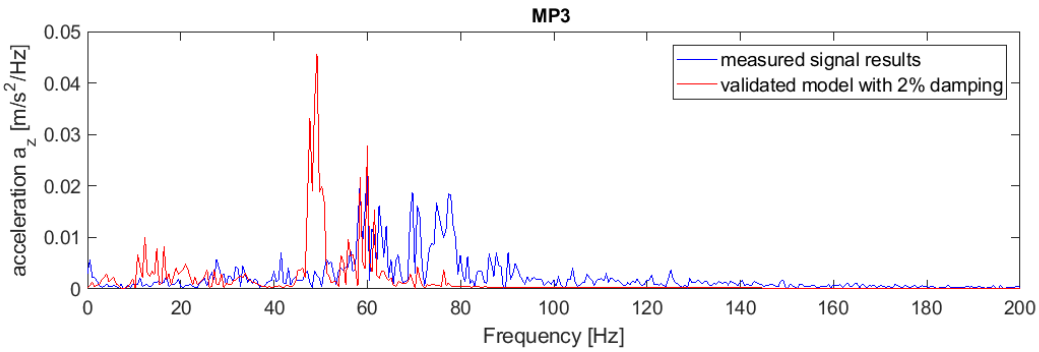

Figure 5.13 Comparison of acceleration spectrums of validated numerical model with measurement results at MP3

	MP1	MP2	MP3
Maximum acceleration amplitude a_z from numerical model [m/s^2]	-2	-0.59	-0.22
looked for ranges from Table 5.2	1.6 - 2	0.6 - 0.8	0.2 - 0.25
Within the target range [Yes/No]	Yes	Yes	Yes

Table 5.3 Comparison of numerically obtained accelerations with target values from Table 5.2

Acceleration

The first part of the computed signal at MP2 and MP3 is not taken into consideration during analysis of the obtained values (Table 5.3) because it is the effect of the sudden load entrance in the model. As visible in Figure 5.9 and Figure 5.10

The high peak in acceleration decays before the repetitive signal pattern starts to develop. This phenomenon will be explained in more details in subsection 5.3.2.8. What can be seen from the Table 5.3 is that obtained acceleration results from the numerical modeling show a very good agreement with the results of the measurements. From the results it is also possible to verify speed at which train is travelling. In the model it is set to 130km/h. From Figure 5.8 to Figure 5.10 it can be seen that oscillations obtained numerically are in good agreement with measurement results in terms of duration. It means that speed of the train is correctly adjusted. Another observation is that numerical model goes back to equilibrium slower than the measured system. Oscillations after train passage are higher than the measured ones.

Acceleration spectrum

Sleeper passing frequency at 60Hz occurs in both, the measurements and the numerical results. The agreement between both models is very good for MP1 and MP3. However, for MP2 60Hz frequency content is less accurate. That can be caused, for instance, by locally changing top soil layer. If in the uppermost layer clay occurs between points MP1 and MP2 it will influence results of MP2. However, information about locally changing profile is not investigated during measurement campaign. Therefore, due to lack of information about soil profile located around considered cross-section, improvement of results related to 60Hz frequency content for MP2 is very difficult. Furthermore, the low frequency content is present in MP3 spectrum but it is again caused by the sudden entrance of the load into the model what will be discussed later (see 5.3.2.8). Same is observed at locations MP1 and MP2 but the effect is not as prominent as for MP3.

Another aspect following from spectrum results is unexpected peak at position of approximately 50Hz at all points. Additionally, only at point MP1 significant frequency content is noticed at 70-80Hz and it does not appear in the measurements spectrum. The reason for the fast decay of frequency content 80Hz

for further distances of the numerical model can be related to definition of damping. Rayleigh damping is frequency dependent what implies that each frequency is being damped bit differently. For range 10-50Hz damping ratio can be treated as constant and in case of the soil stratum for validated model it is equal to approximately to 2% (Table 5.2). However, outside of that range the ratio starts increasing. For 80Hz it reaches approximately 3%. This might be also the reason why magnitude of high frequency content (above 100Hz) in numerical results is almost equal to 0 at all points. It will be shown in later stage of this research that damping ratio is very influential parameter for the analysis (see .

Nevertheless, the origin of both high frequency contents is investigated further. It is been established that top layer thickness, damping ratio, load speed, subballast material etc. (see section 5.3) are not responsible for generation of aforementioned frequencies. It was decided to have a closer look into the dispersion lines for the existing soil profile.

Dispersion lines / guided waves

By plotting dispersion lines in Frequency-Wavenumber plane for the soil profile presented in Table 3.1 the Figure 5.14 is obtained. In this graph oscillatory moving load is represented by the kinematic invariant. Dispersion lines become one line in Figure 5.14 for certain combination of wavenumber and frequency. Intersection of this formed line and kinematic invariant indicates that moving oscillatory load excites a wave of frequency and wavenumber given by the intersection point. From Figure 5.14 it is seen that kinematic invariant intersects dispersion lines at frequencies approximately 48Hz and 75Hz. These frequencies correspond to peaks occurring in acceleration spectrum what explains their origin. The dispersion lines were calculated with the Thin-layer method in accordance with (Kausel, 1986).

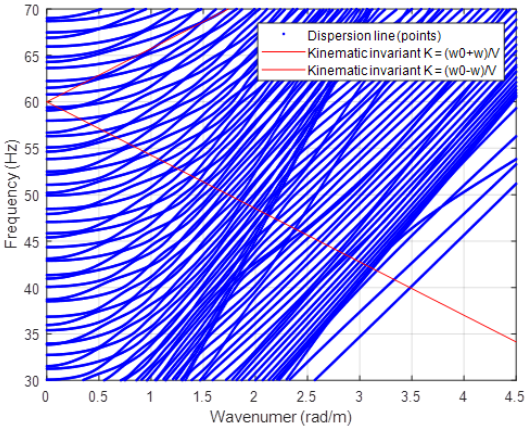

Figure 5.14 Dispersion lines with kinematic invariant for train running 130 km/h and soil profile from Table 3.1. Intersection points of kinematic invariant and dispersion lines, indicates that moving oscillatory load excites a wave of a wavenumber and frequency given by the intersection point. Waves of a wavenumber and frequency following from intersection of congestion of dispersion lines and kinematic invariant are more visible in the obtained spectrum shown in Figure 5.11-Figure 5.13.

5.3. Variation studies

5.3.1. Triangular pulses load representation results with static load only (S1-S3)

The load in form of triangular pulses is already discussed in section 4.4.2. The motivation to represent force in this way was number of scientists (as already described in section 2 of this document) who obtained satisfactory predictions of vibrations using that approach. It was the first model analysed during this research. Only quasi-static part of the load is included in triangular pulses method. Parameters for this variation are as for the validated model case except for the load and the flowing parameters:

- damping ratio for soil stratum is equal to 3%, α=4.8 and β=0.000152
- asphalt as subballast (properties in Table 3.2) damping ratio is equal to 4%, damping parameters α=6.14 and β=0.000195.

The speed of the train was unknown. The approach to establish it was to run three simulations where train travels with velocity 100, 115 and 130 km/h. Furthermore, response of the system for varying speed was needed in order to have establish the direction that needs to be taken when running next simulations. Based on the obtained results of the speed variations it could be seen which model match the best with the measured signal in terms of acceleration amplitude and duration of oscillations.

Accelerations

Clear pattern cannot be defined from the results in time domain (shown in Appendix C, AP. C Figure 1 to AP. C Figure 6). The obtained acceleration amplitudes are shown in the Table 5.4. Numerical results are far off from the target values for all the points. At points MP2 and MP3 the vibrations are barely feelable. The best result (meaning the closest to the value obtained during measurements) is obtained in this iteration for point MP1 for 130km/h and equal only to $0.8/2 \cdot 100\%=40\%$ of the target value.

	MP1	MP2	MP3
Acceleration a_z [m/s^2] 100km/h	0.35	0.05	0.01
Acceleration a_z [m/s^2] 115km/h	0.67	0.02	0.03
Acceleration a_z [m/s^2] 130km/h	0.81	0.03	0.04
ranges from Table 5.2 [m/s^2]	1.6 - 2	0.6 - 0.8	0.2 - 0.25

Table 5.4 Acceleration results of triangular pulses model load for speed 100, 115 and 130km/h

From the Table 5.4 it is visible that vibrations decay very quickly with the distance what was expected based on discussion from section 2. Quasi-static load component influences only the nearest field located around the source. In next simulations oscillatory dynamic load component will be added on top of quasi-static part.

Acceleration spectrums

By comparing spectrums of measured signal and numerical simulation it is visible that frequency ranges do not match. At MP1 by increasing train speed from 100km/h to 130km/h to the main frequency content shifts from 80Hz to around 100Hz. However, for measured signal it is located between 20 and 80 Hz. Sleeper passing frequency is not visible in the numerical simulation results.

Another interesting finding from this simulation is made through analysing scaled spectrum of the train. Each of the signals in the frequency domain presented from AP. C Figure 4 to AP. C Figure 6 is divided by its train velocity and Figure 5.15 to Figure 5.17 are obtained. At MP1 peaks for all signals are located at the same point, namely 2.8 [1/m] Taking the reverse of it the distance in [m] is obtained and equal to 1 / 2.8 = 0.357 m. This results indicates the repetitive location of the cause for peaks. It is similar to the distance between nodes where the load is applied. The conclusion is that discretization of the load for triangular load representation model is of very high importance because it influences significantly the spectrum. In order to obtain better results one should apply finer discretization of the distance between sleepers.

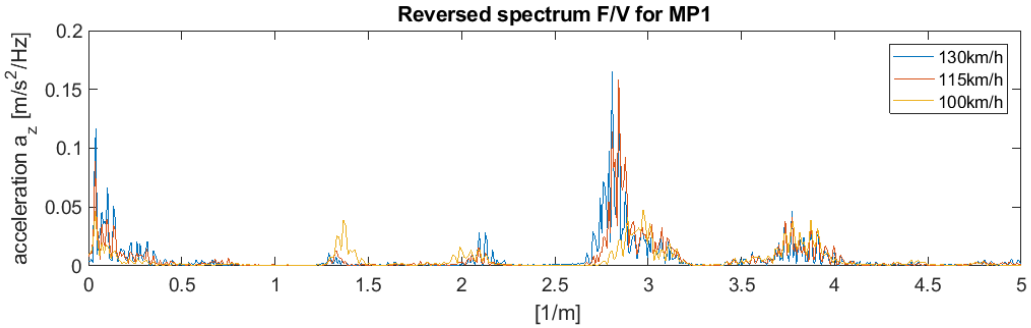

Figure 5.15 Scaled spectrum of the train with triangular load representation for different velocities at MP1

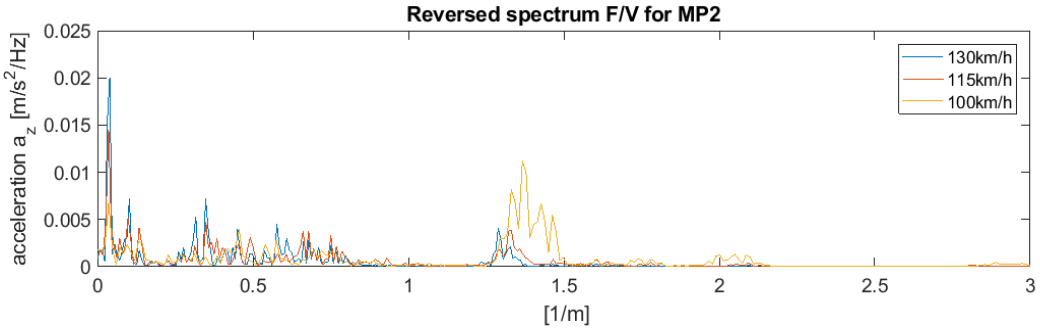

Figure 5.16 Scaled spectrum of the train with triangular load representation for different velocities at MP2

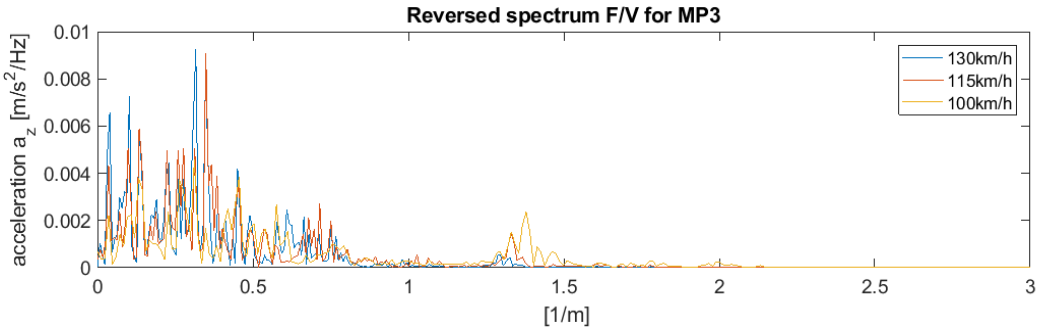

Figure 5.17 Scaled spectrum of the train with triangular load representation for different velocities at MP3

5.3.2.Moving load models

All investigated models have the load as described in 4.4.3, namely 5% of the axle load (5.275kN) oscillating with frequencies 60Hz and 2Hz.

5.3.2.1. Comparison between quasi-static triangular pulses load (S1-S3) and combined action of moving quasi-static plus dynamic load component (S4)

This model has the same properties as the one described in section 5.3.1 except for load formulation what is indicated above in 5.3.2. The models with two different ways of incorporating the load into the system are compared and presented in Appendix C from AP. C Figure 7 to AP. C Figure 12.

Accelerations

The results of maximum acceleration are shown in the Table 5.5. The acceleration amplitudes increases at all points. The percentage tells how smaller the results are from the target. It is clear that by adding dynamic component significant improvement of results is observed in comparison with triangular pulses consisted only in the quasi-static part. For the track vicinity (MP1) the maximum acceleration amplitude is closer to the target value. Furthermore, the oscillations are clearly noticeable at MP2 and MP3. Pattern of the signal became more similar to the measurement.

Point	Expecta-tions[m/s^2]	triangular pulses [m/s^2]	off from range (with respect to the upper bound)	Moving loads [m/s^2]	off from range (with re-spect to the upper bound)
MP1	1.6-2	0.8	60%	1.36	32%
MP2	0.6 - 0.8	0.04	95%	0.28	75%
MP3	0.2 - 0.25	0.04	84%	0.06	76%

Table 5.5 Comparison of maximum acceleration a_z between model with triangular pulses with quasi-static load implementation and moving point load model with dynamic and quasi-static load component incorporated

Acceleration spectrum

From Figure 5.11-Figure 5.13 it is visible that the desired frequency content from 40Hz to 80Hz has appeared in contrast to the model from subsection 5.3.1. That is in line with the measurements within the same range of frequencies. With the increasing distance from the source frequencies from 65Hz to 80Hz decay. The peak at 50Hz is caused by the wave excitation by the moving oscillatory in considered soil profile (see section 5.2). The prediction of the results becomes more accurate using the model including dynamic load component because oscillations away from the source occurs what is in line with the measurements.. However, results are still quite far off from the measurements then the further improvement is necessary.

5.3.2.2. Longer duration of the signal (S5)

It was decided to check whether 12 axle loads and approximately 3s of signal duration are sufficient to obtain accurate predictions. In previous model 24 point loads were applied. Now 72 loads representing in total 9 wagons are incorporated. The procedure of modelling loads is analogical to the one described in 4.4.3. Loads are not activated all at once. Excessive displacement at the beginning of the model wanted to be avoided. Instead, three sets of 24 loads are activated in three rounds. One set at the time. The sequence is presented in the Figure 5.18. Results are presented in Appendix C from AP. C Figure 13to AP. C Figure 18.

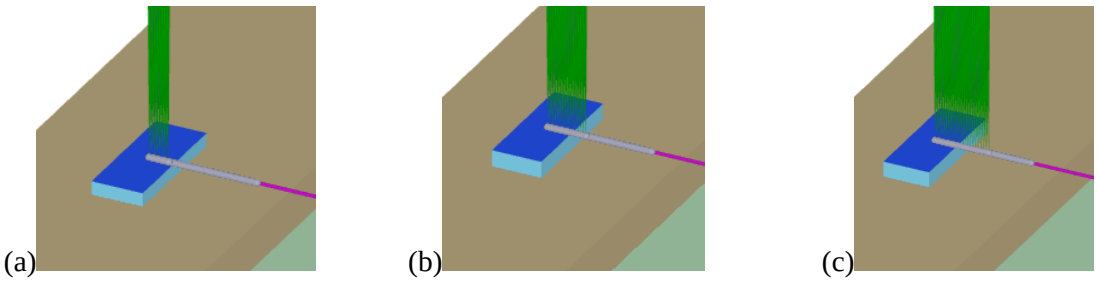

Figure 5.18 Load sets activation (a) first 3 wagons, activated at 0s (b) second 3 wagons, activated at 2s (c) third 3 wagons, activated at 4.25s.

Acceleration

In Table 5.6 values of acceleration for model with shorter and longer duration are compared. The difference in results is small and decreases with increasing distance. Signals in time domain overlap (From AP. C Figure 13 to AP. C Figure 15) and shorter duration results (blue) are barely visible. It implied that the pattern of vibrations remains unchanged.

	Short signal [m/s^2]	Long signal [m/s^2]	Difference [%]
MP1	1.36	1.46	7%
MP2	0.28	0.29	3%
MP3	0.06	0.06	0%

Table 5.6 Acceleration amplitude values for the models with longer (6.5s) and shorter (2.75s) duration

Furthermore, quite high peaks (the ones that do not match the general signal trend) in acceleration vs. time graphs for longer duration at MP2 and MP3 are locally spotted. Investigating their exact time of occurrence it turns out that at MP2 they appear at time 0.33s, 2.33s, 4.58s. Each of the peaks occur exactly 0.33s after activation of the particular load set. For MP3 it is similar situation. Peaks occur at: 0.38s, 2.37s, 4,63s. They do not match the rest of the results and occur with the certain time offset. The conclusion is that they are the results of the instantaneous entrance of the load in the system (load sets activation), therefore they can be disregarded during analysis.

The uneven beats that stand out from the rest of the response are disregarded because there was an input error in the numerical model. The rest the signal gives reasonable results. It is decided not to repeat the simulation due to its long duration (more than a week).

Acceleration spectrum of the shorter and longer signal

In spectrum results of all points the peaks occur at the same frequencies. Duration of the signal does not influence spectrum pattern. However, peaks are more distinct for short signal close to the track. In contrast, away from the source the situation reverses but only for the peak at 50Hz. Sleeper passing frequency content is at all points higher in shorter signal.

The difference between shorter and longer signal in calculation time is around 5 days. For this reason it is decided to continue with shorter models which calculations takes around 2 days.

5.3.2.3. Change of subballast material from asphalt to crushed stone (S6)

As already mentioned, it is not known what subballast precisely was used in the embankment. Two possibilities are tested and the difference between using asphalt and crushed stone is quantified. The following iteration shows how important this parameter is for the sake of the project.

All settings and properties of the models are the same as described in chapter 3 except for subballast. Its properties are listed in Table 3.2. Results of both simulations are shown in the Appendix C are shown from AP. C Figure 19 to AP. C Figure 25.

Acceleration

Acceleration amplitudes obtained in this iteration are presented in Table 5.7. The noticeable difference (around 30%) between two models occurs for the near field but it decreases with the distance. At MP3 vibrations are already very little, therefore it is difficult to state clearly that the difference between two models it is as much as 25%. From the figures showing acceleration in time domain (AP. C Figure 19 to AP. C Figure 22) it can be noticed that crushed stone subballast is more sensitive to vibrations. Namely, it goes back to equilibrium slower than stiff asphalt. Pattern is the same but peaks are larger.

	MP1	MP2	MP3
Asphalt acceleration [m/s^2]	1.36	0.26	0.065
Crushed stone acceleration [m/s^2]	1.8	0.28	0.082
Difference between asphalt and crushed stone [%]	32%	8%	26%

Table 5.7 Results and differences between crushed stone and asphalt subballast models

Acceleration spectrum

Frequency content does not experience a lot of changes after switching from asphalt subballast material to crushed stone. The magnitude of accelerations differs slightly in value at the peak, although they occur at the same frequencies for both models. Sleeper passing frequency has higher magnitude for the asphalt subballast.

Because the improvement of results in time domain is noticed while there is almost no deterioration in frequency domain it was decided to proceed with crushed stone as the subballast material for the rest of the performed simulations.

5.3.2.4. Soil damping calibration (S6-S8)

Since results were not satisfactory enough iterations are continued to run. For the beginning it was chosen to set soil stratum damping to 3% (Simulations S6 in Figure 5.1) what came from research of (Ruiz, et al., 2016) where the authors use the same value. However, naturally at the considered location damping ratio might be different and calibration of the model by changing this specific parameter material is justified. For this reason simulations based on the model described previously in section 5.3.2.3 where crushed stone is used as the subballast material are run(S6 in Figure 5.1). Soil damping is set to 1%, 2% and 3% (S6-S8 in Figure 5.1). The values used to simulate this ratio are presented in the Table 5.8.

	α	β
1%	1.67	0.000053
2%	3.25	0.0001025
3%	4.8	0.000152

Table 5.8 Values used for Rayleigh damping representation in soil stratum

The influence of damping ratio on vibration propagation in soil is presented from Figure 5.19 to Figure 5.28. Maximum accelerations obtained from three models are presented in the Table 5.9.

max acceleration a_z / location	MP1	MP2	MP3
1% damping ratio	2.31 m/s^2	1.15 m/s^2	0.57 m/s^2
Over / under expectations	Over by 15%	Over by 44%	Over by 128%
2% damping ratio	2 m/s^2	0.59 m/s^2	0.22 m/s^2
Over / under expectations	Within rage	Within range	Within range
3% damping ratio	1.78 m/s^2	0.28 m/s^2	0.08m/s^2
Over / under expectations	Under by 11%	Under by 65%	Under by 68%

Table 5.9 Acceleration values for models with soil damping 1%, 2%, 3%. Comparison is made with regards to the upper bound. Targets values are presented in Table 5.1

max acceleration a_z / location	MP1	MP2	MP3
1% damping ratio	2.31 m/s^2	1.15 m/s^2	0.57 m/s^2
2% damping ratio	2 m/s^2	0.59 m/s^2	0.22 m/s^2
Reduction in comparison to 1% damping ratio	13%	47%	61%
3% damping ratio	1.78 m/s^2	0.28 m/s^2	0.08 m/s^2
Reduction in comparison to 2% damping ratio	11%	52%	62%

Table 5.10 Reduction of acceleration amplitude depending on changing damping ratio

Based on Table 5.9 it is shown that 1% and 3% of soil damping acceleration values match the measurements less than 2%, thus they are not the correct damping ratios. For 1% the soil transmits too much vibrations while for 3% it seems that too much energy dissipates with the distance.

Acceleration

With regards to maximum accelerations results of the three simulations, their relation with damping ratio seems to be linear within the range of investigation what is seen from the Table 5.10. Varying damping ratio influences the most the distant points. For MP1 increasing damping ratio from 2% to 3% gives reduction of 11% but for MP3 it is already 62%. It is visible that it is of the great importance to establish correct damping ratio for soil stratum but especially when the response far away from the source is of interests.

However, if the damping ratio increment does not reduce accelerations linearly, it cannot be clearly stated that the further increment of damping ratio will reduce accelerations by a certain percentage. It implies that damping ratio cannot be foreseen a priori with high accuracy but needs to be calibrated by means of the iterative procedure for the specific case. It is advised to consider this effect carefully for another than presented in this research range of investigation because system response is very sensitive for changes made in damping ratio for soil.

From the Figure 5.19 - Figure 5.24 it is seen that accelerations peaks occur mostly at the same time. However, the amplitude differs significantly, hence damping ratio variations influence only the amplitude but not the pattern of the vibrations. Furthermore, for the most the time models with 1% and 2% have very similar acceleration amplitude but only for point MP1. It is also reflected in the spectrum results for MP1, as very small change of frequency magnitude for specific frequencies is observed.

Acceleration spectrum

From spectrum results presented from Figure 5.25 to Figure 5.28 it is clear that the magnitude of acceleration spectrum increases when the damping ratio decreases. Although, it is not a linear relation. The difference in acceleration signal frequency content is larger between 1% and 2% than between 2% and 3% soil damping.

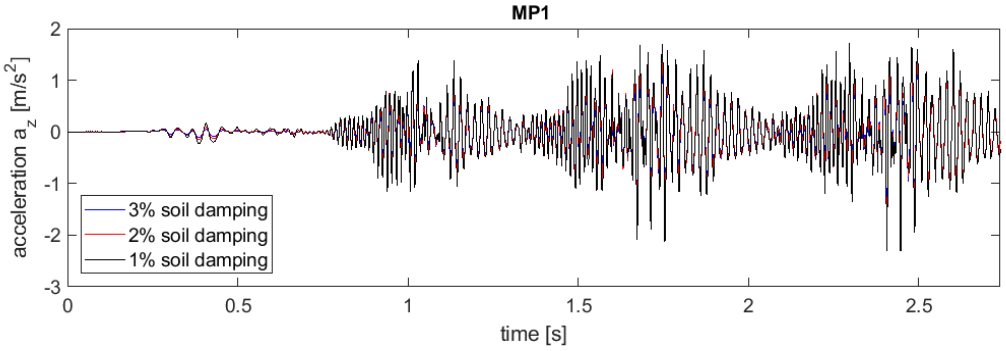

Figure 5.19 Comparison of acceleration in time domain between three models, with 1%, 2% and 3% damping at MP1

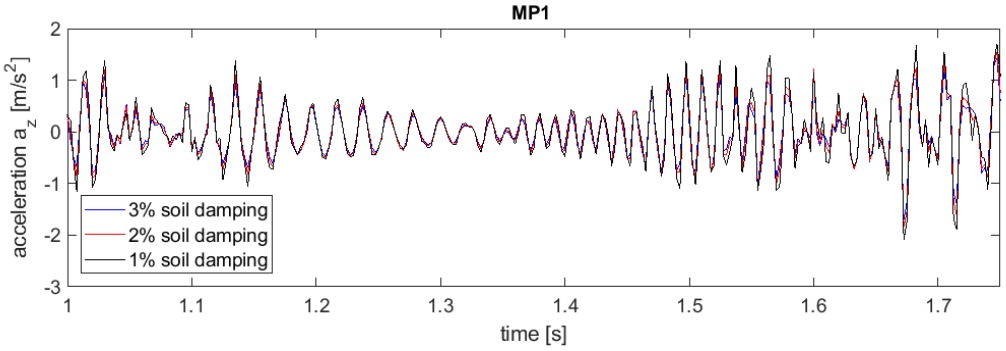

Figure 5.20 Inset into Figure 5.19.

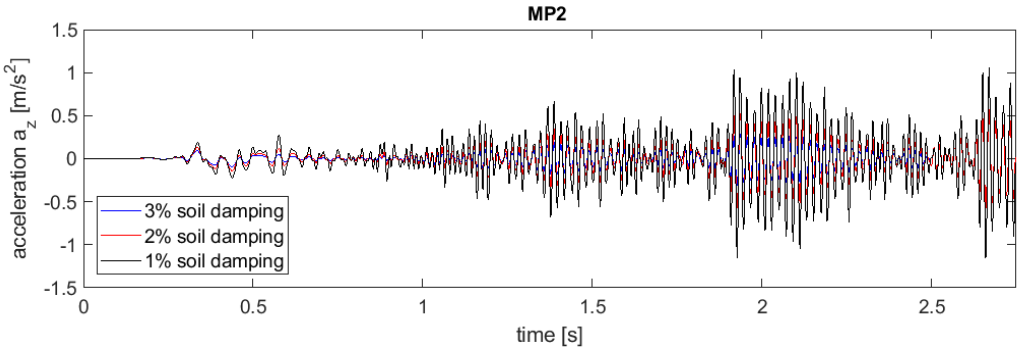

Figure 5.21 Comparison of acceleration in time domain between three models, with 1%, 2% and 3% damping at MP2

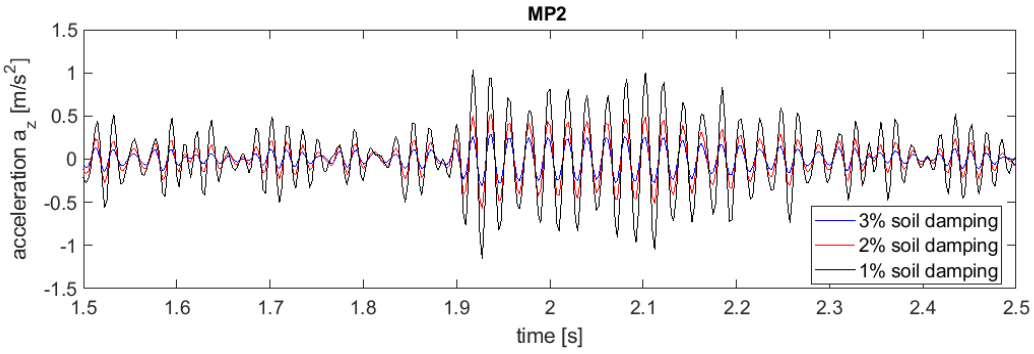

Figure 5.22 Inset into Figure 5.21

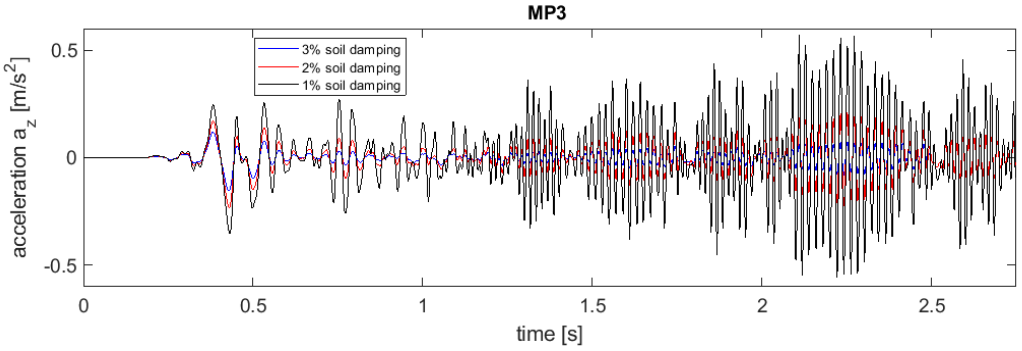

Figure 5.23 Comparison of acceleration in time domain between three models, with 1%, 2% and 3% damping at MP3

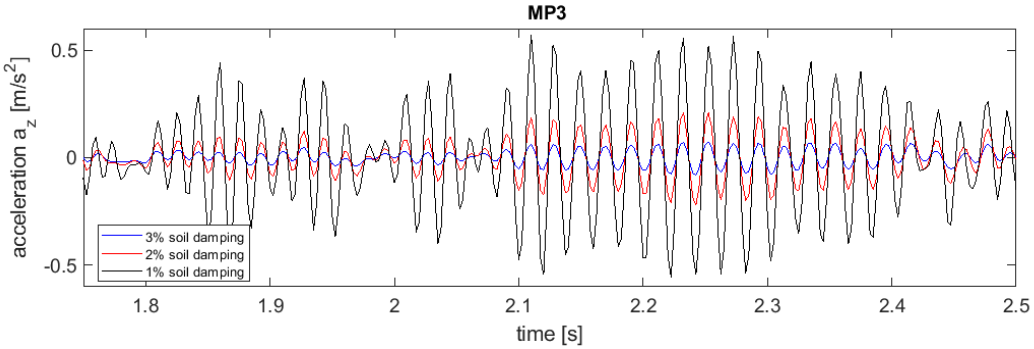

Figure 5.24 Inset into Figure 5.23

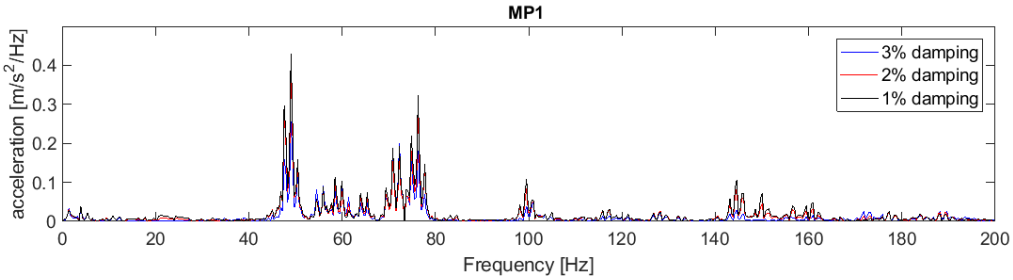

Figure 5.25 Comparison of spectrums between three models, with 1%, 2% and 3% damping at MP1

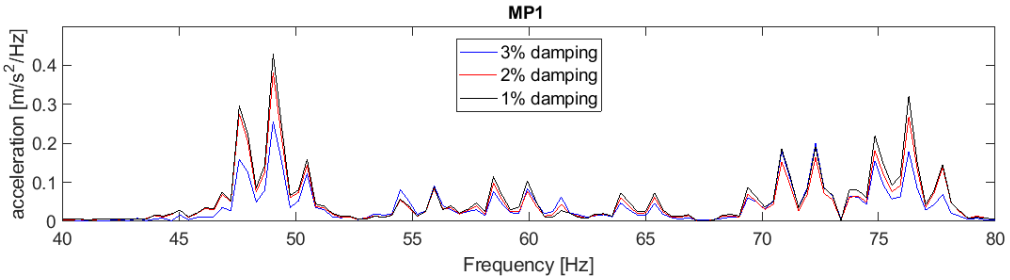

Figure 5.26 Inset into Figure 5.25

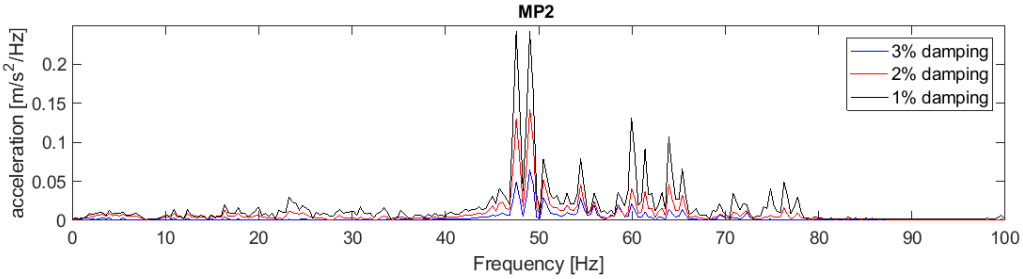

Figure 5.27 Comparison of spectrums between three models, with 1%, 2% and 3% damping at MP2

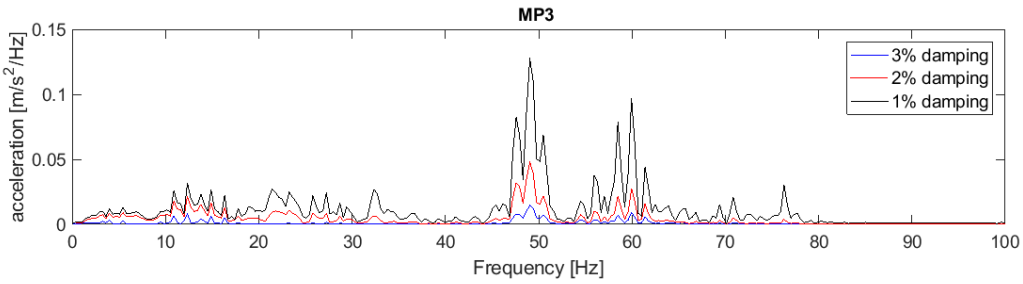

Figure 5.28 Comparison of spectrums between three models, with 1%, 2% and 3% damping at MP3

5.3.2.5. Influence of 2Hz oscillatory load for the results (S9)

Since unexpected peaks are obtained at the frequencies of around 50Hz and 80Hz it is decided to investigate separately the effect of each load components. In this way is possible to establish what part of the force generates this frequency content.

Hence, firstly 2Hz component is removed from the load. The obtained results are presented in Appendix C from AP. C Figure 26 to AP. C Figure 31. Based on these graphs big difference is not observed between both responses. The results from simulations almost overlap. It means that dynamic component of 2Hz does not contribute substantially to the system response. That can be caused by several factors. One of them is accounting for the damping through Rayleigh damping. It attenuates highly low frequencies. As the outcome the influence of 2Hz frequency for the results is highly limited and might be underestimated. Oscillatory force value is equal to 5% of the total weight of the train, thus its influence as the quasi-static load for the near field is relatively small.

5.3.2.6. Influence of 60Hz oscillatory load for the results (S10)

The same operation as in 5.3.2.5 is repeated in order to establish the contribution of 60Hz oscillatory load to the total system response. Therefore, this dynamic load component is removed from the analysis. Only 2Hz together with the quasi-static load is now present in the model. The results of the simulations are presented from Figure 5.29 to Figure 5.34.

Accelerations

As seen from graphs plotted in time domain (Figure 5.29-Figure 5.31), the force without 60Hz dynamic component influences only close field and only little oscillations are observed further from the source. It might be stated that in considered case higher frequency content is responsible for propagation of the waves further away from the track. At MP2 and MP3 some disruptions are visible at the beginning of the signal, what is caused by instantaneous load application in the system.

Acceleration spectrum

Frequencies from range 40Hz-80Hz are not induced at any of the points (Figure 5.32-Figure 5.34) when the load from which dynamic force component oscillating with 60 Hz is excluded. The conclusion is that responsible part for the peaks at 50Hz and 80Hz is the dynamic force oscillating with the sleeper passing frequency.

Low frequency content is observed at MP3 but both static and oscillating with 2Hz load might be responsible for this content. In the next section it will be investigated what is the effect of the static load only because it will help to define what is the exact 2Hz load influence for the results.

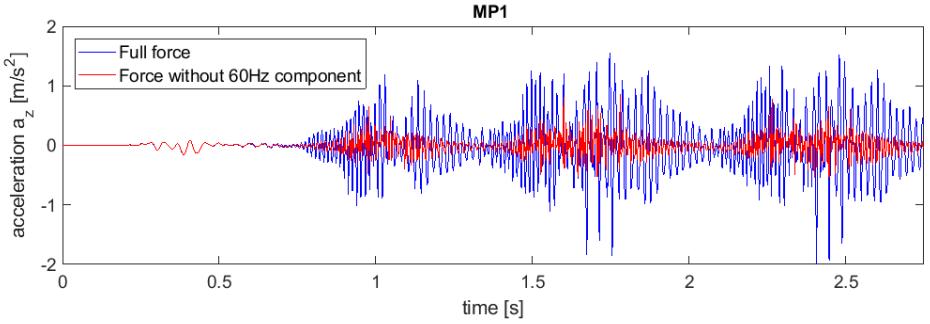

Figure 5.29 Comparison of accelerations in time domain between models with 60Hz oscillating component included and excluded at MP1

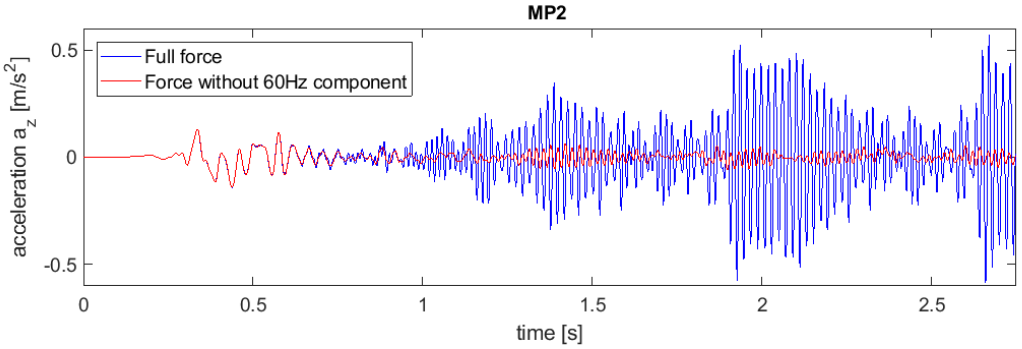

Figure 5.30 Comparison of accelerations in time domain between models with 60Hz oscillating component included and excluded at MP2

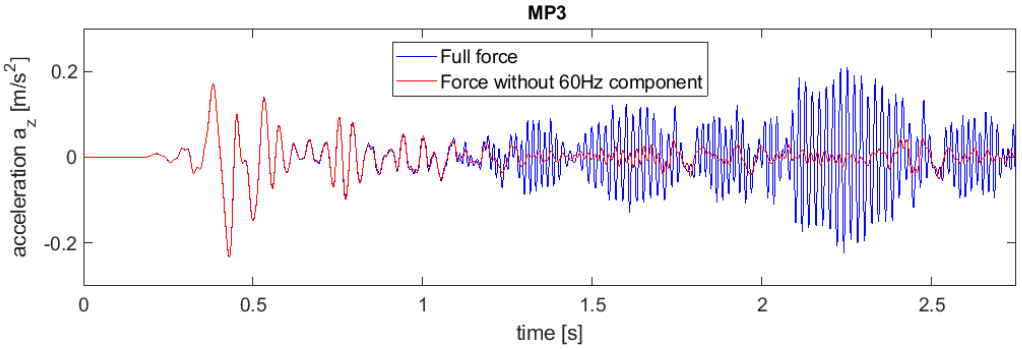

Figure 5.31 Comparison of accelerations in time domain between models with 60Hz oscillating component included and excluded at MP3

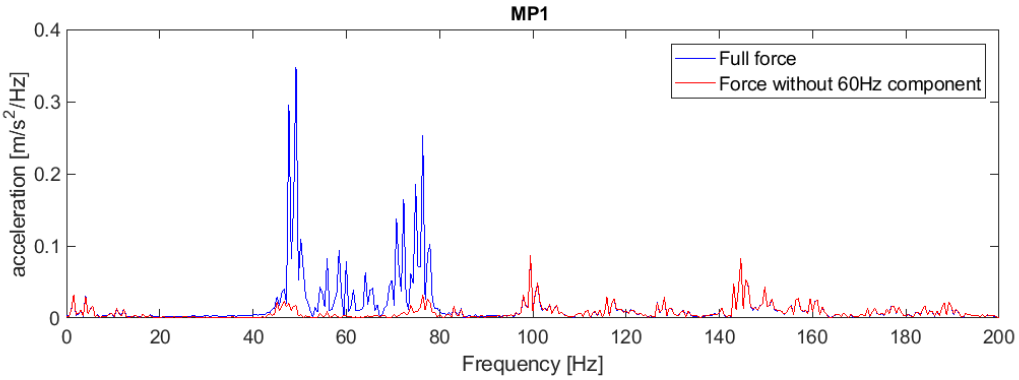

Figure 5.32 Comparison spectrums between models with 60Hz oscillating component included and excluded at MP1

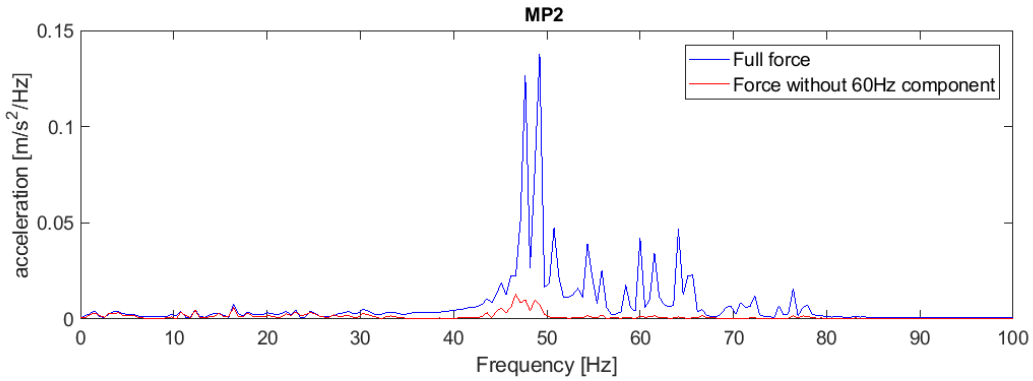

Figure 5.33 Comparison spectrums between models with 60Hz oscillating component included and excluded at MP2

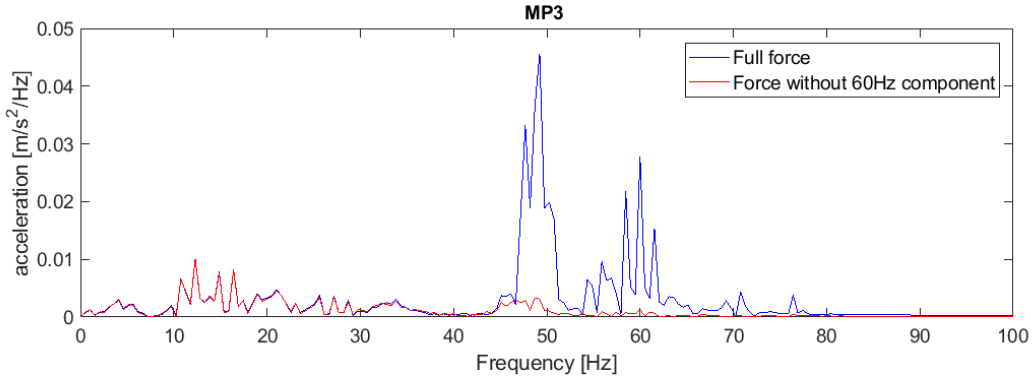

Figure 5.34 Comparison spectrums between models with 60Hz oscillating component included and excluded at MP3

5.3.2.7. Static moving load only (S11)

The influence of only quasi-static load acting on the system is investigated and put in graphs against load without 60Hz component (subsection 5.3.2.6). The results are presented in Appendix C from AP. C Figure 32 to AP. C Figure 37.

Accelerations

From the results in time domain it is visible that there is almost no difference between both curves. Since the only difference between both models is presence of 2Hz it concludes that this load component has secondary effect on the results.

In next section the effect of the sudden entrance of the load in to the system will be investigated.

5.3.2.8. The effect of the instantaneous entrance of the point load into the system (S12)

The firsts peak values of the acceleration occurring in the signal were disregarded during interpretation of the results because they are the result of the instantaneous entrance of the loads in the system. This effect is described in the following section.

The model considers quasi-static load component only. Once point loads are activated they remain in the same place for the whole time of the simulation. Moreover, they are not deleted at any stage of calculations because the extra vibrations would be observed. Soil would displace due to application of 12 static loads at first, but if one removes them suddenly, soil would go back to equilibrium (0 displacement) through oscillations. In all considered models no sudden removal of the force is made, hence it is important to keep the loads throughout the whole simulation. In this way it is possible to investigate

the effect of instantaneous entrance of the loads in the system without the effect of their sudden removal. The results of the iteration are presented from Figure 5.35 to Figure 5.40.

Accelerations

From these figures it is clear that the first part of the response almost overlaps. The small difference is caused by the fact that another 24 loads which are in total equal to 1.2 of one static axle load (dynamic force is not included, namely 2Hz and 60Hz, each of them has F=5% of the static axle load) are excluded from the model. They were not applied because the interpretation would become more difficult and less straightforward.

Acceleration spectrums

Frequency content in range 1Hz-30Hz is similar between both models. At each considered point most of the low frequency content coincides. It means that this content might be disregarded during interpretation. It is especially important for MP3 because low frequency content is more prominent at this point.

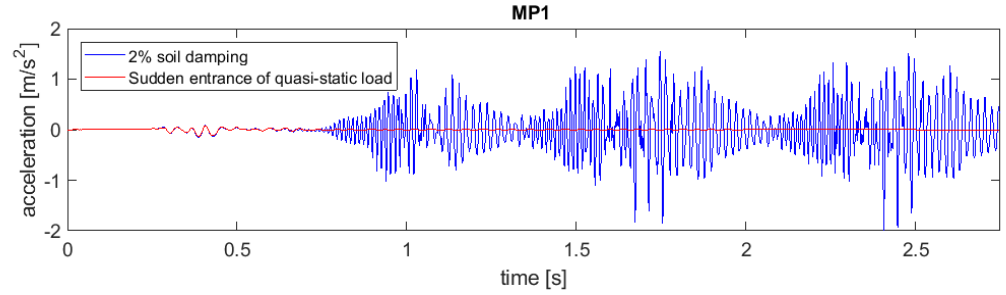

Figure 5.35 The effect of the sudden entrance of the loads into the system for acceleration in time domain at MP1

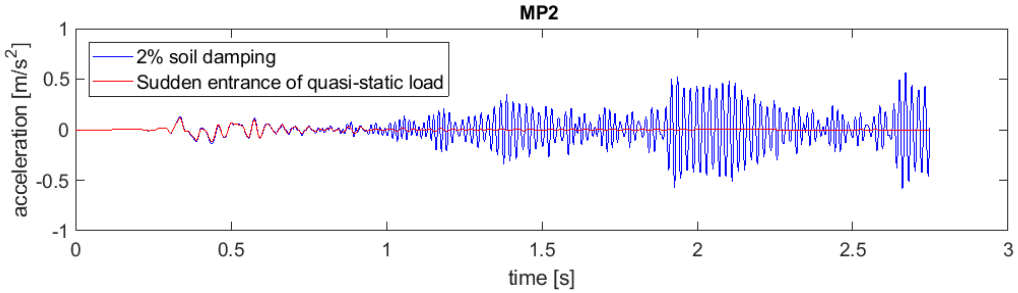

Figure 5.36 The effect of the sudden entrance of the loads into the system for acceleration in time domain at MP2

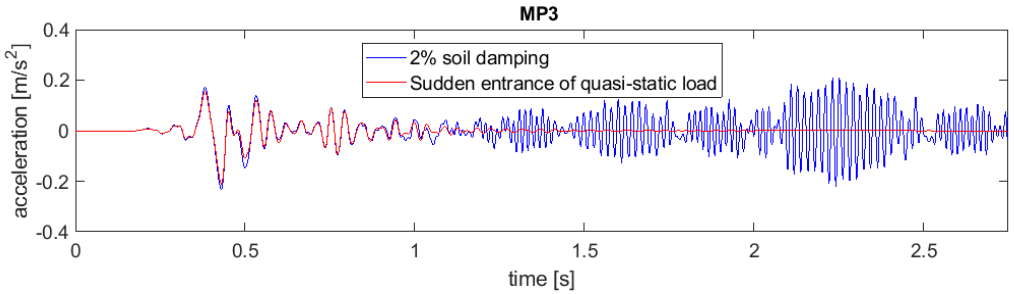

Figure 5.37 The effect of the sudden entrance of the loads into the system for acceleration in time domain at MP3

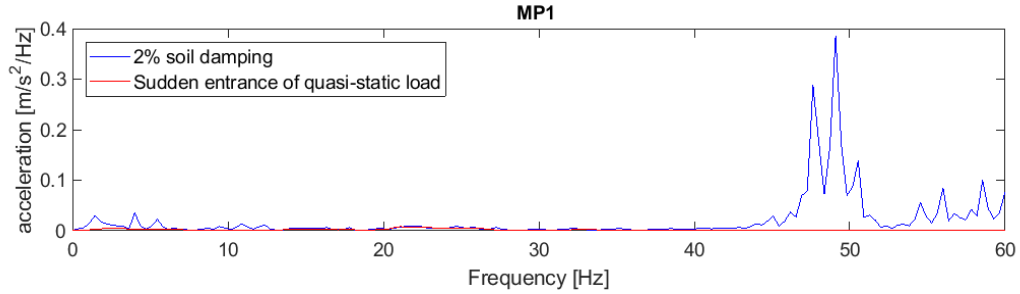

Figure 5.38 The effect of the sudden entrance of the loads into the system for acceleration in frequency domain at MP1

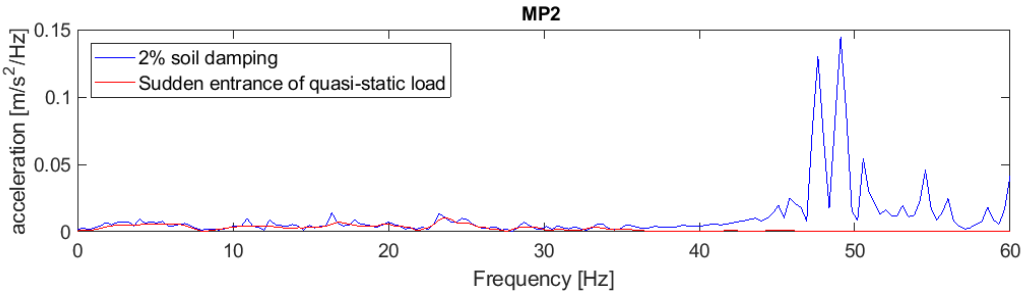

Figure 5.39 The effect of the sudden entrance of the loads into the system for acceleration in frequency domain at MP2

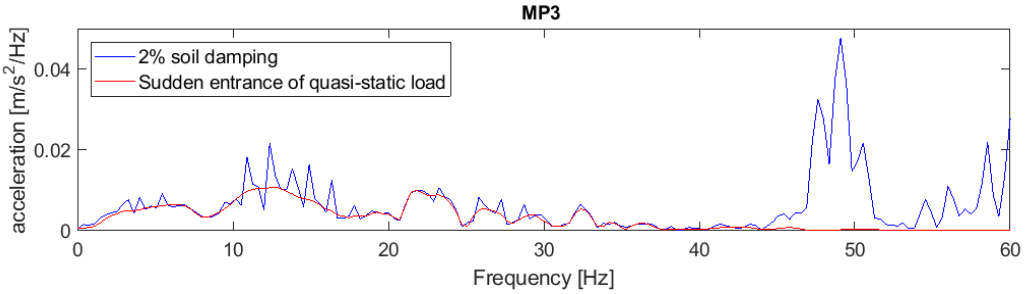

Figure 5.40 The effect of the sudden entrance of the loads into the system for acceleration in frequency domain at MP3

5.3.2.9. The uppermost layer from 1m to 2m thickness (S13)

The soil profile probably differs from the one established based on the available CPT test. Parameters of soil stratum used during this research are presented in the Table 3.1. The attempt to improve accuracy of the soil profile has been made by changing the upper most layer thickness.

This layer should have the highest influence on the results because Rayleigh waves propagates in it. It is known that the surface waves have crucial impact for the dynamic response of the system. This layer has also the lowest Young's modulus and the slowest shear wave velocity from the whole soil profile. The effect of the thickness change of the top layer from 1m to 2m will be investigated. The results are presented in Appendix C AP. C Figure 32 to AP. C Figure 37.

Accelerations

Thicker top layer of soft sand is working for a favour of accelerations as they decrease by approximately 20% what is shown in the Table 5.11. Furthermore, at some points values of both models overlap but at the peaks, the acceleration for the model with 2m of soft top layer is considerably smaller.

	MP1	MP2	MP3
top layer 1m thick, max acceleration [m/s^2]	2	0.59	0.22
top layer 2m thick, max acceleration [m/s^2]	1.56	0.46	0.18
Difference between both models	22%	22%	18%

Table 5.11 Results of maximum acceleration for models with where top layer is 1m and 2m thick

Acceleration spectrum

The peak at 50Hz is less prominent at all locations for the model with top layer 2m thick. Moreover, sleeper passing frequency loses its importance especially at MP3. On the one hand, the decrease of frequency content located around 50Hz is profitable and matches measurements better. In contrast, sleeper passing frequency content becomes less influential for distant points what is not in accordance with the measurements. Increasing thickness of the top sandy layer from 1m to 2m is a trade-off between improving frequency content results concentrated around 50Hz and decreasing sleeper passing frequency importance.

It is possible that such situation occurs. Thicker soft top layer gives higher accelerations as a rule of thumb because it is more sensitive for vibrations. On the contrary, it damps high frequencies more than thinner layer. High frequencies are responsible for higher acceleration values. In this specific case it turned out that the second effect outbalance the first one. However, for different soil profile the result of such change might come out differently.

This iteration does not clearly improve the frequency spectrum but it deteriorates acceleration results. It was decided not to change the layers thicknesses.

5.3.2.10. No compacted sand under the embankment (S14)

There were some uncertainties involved during defining the properties of sand beneath the embankment (its presence in the actual situation is questionable). This section will investigate what is the response of the system when no compacted sand is used. The results are presented in Appendix C from AP. C Figure 44 to AP. C Figure 49.

Accelerations

Removing compacted sand gives an increment of the acceleration amplitude by 37% close to the track but at the intermediate point the decrease of 37% is observed. For MP3 hardly any difference is noticed. All results are presented in the Table 5.12. For most part of the signal duration system where sand is not applied gives smaller response than the one where sand is present. By removing compacted sand from beneath the embankment, response of the system is locally higher. On the contrary, accelerations decrease globally.

	MP1	MP2	MP3
compacted sand beneath embankment present, max acceleration [m/s^2]	2	0.59	0.22
compacted sand beneath embankment not applied, max acceleration [m/s^2]	2.65	0.37	0.21
Difference between both models	increase by 33%	decrease by 37%	decrease by 5%

Table 5.12 Results of maximum acceleration for models with and without compacted sand beneath the embankment

Acceleration spectrum

An increase of the sleeper passing frequency is observed at MP1 point when compacted sand is removed. On the other hand, at MP2-3 this frequency magnitude decreases slightly. Moreover, significant increase of frequency 80Hz appears at MP1 but it decays almost completely with the distance. Peak at 50Hz becomes smaller for all frequencies but it is not a substantial drop. This simulation does not improve results. Removing compacted sand deteriorates the results by increasing content of 80Hz and sleeper passing frequency at MP1. For MP1 sleeper passing frequency content already matches measurements well with compacted sand applied. Moreover, peak at 50Hz is still present.

5.3.2.11. Applying 2.5% vehicle weight as the oscillatory load (S15)

The oscillating force value is an educated estimate. It gives good prediction of vibrations what is described in subsection 4.4.3. Nevertheless, it is decided to compare results of 2.5% with 5% of the train weight. The results are presented in Appendix C from AP. C Figure 50 to AP. C Figure 55.

Accelerations

The obtained values from both models are presented in the Table 5.13. Almost linear decrease in comparison with force value is observed in the results. For point MP1 smaller reduction is noticed because response at this point is largely driven by the quasi-static load component which does not change significantly. Nevertheless, for points where results are mainly dependent on the dynamic force the relation is linear.

	MP1	MP2	MP3
5% train weight, max acceleration [m/s^2]	2	0.59	0.22
2.5% train weight,, max acceleration [m/s^2]	1.25	0.3	0.11
Difference between both models	38%	50%	50%

Table 5.13 Results of maximum acceleration for models with dynamic force equal to 5% and 2.5% of the total train weight

Acceleration spectrum

Spectrum results behave analogically to the accelerations.

Since the results of changing dynamic force value are predictable it is concluded that 5% of the axle train load is a reasonable value for the dynamic load. By increasing the force value higher acceleration and frequencies magnitude would have been obtained. That would deteriorate already found approximation.

5.3.2.12. Short summary of Chapter 5

The most important findings of Chapter 5 are listed below:

- Two measured train passages acceleration signals are available, therefore by their comparison, it is possible to eliminate results associated with vehicle factor e.g. uneven wheel.
- Validation of the model is achieved.
- The origin of peaks at 50Hz and 80Hz in acceleration spectrum is explained by the wave excitation by the moving oscillatory load in soil profile. This effect is related to the dispersion lines found for the considered soil profile.
- Numerical model goes back to equilibrium slower than the real system. Oscillations after train passage are higher than the measured ones.

- Triangular pulses consisted of quasi-static component influence the nearest track field only.
- In triangular pulses load formulation method sleeper passing frequency is not noticed.
- In triangular pulses load formulation method the rail discretization is too coarse and has noticeable impact for frequency content. The discretization of the rail is reflected in spectrum.
- Dynamic force is equal to 5% of the axle load what is a good approximation for the current case.
- 3s of simulation is sufficient to obtain reasonable approximations.
- Change of the subballast material from asphalt to crushed stone influences only area in source vicinity, for further distances the effect is negligible.
- Model with asphalt used as subballast material shows higher sleeper passing frequency content than crushed stone
- Damping ratio of the soil stratum is the most influential parameter amongst all investigated. Modification of soil damping ratio might change the acceleration results even by 128%.
- Calibration of soil stratum damping is important especially for the far field.
- Within the range of investigations acceleration amplitude has linear relation with soil damping ratio. Nevertheless, response of soil depends on the damping ratio in a complicated way. Therefore, it is advised to consider this effect carefully for other than presented in this research range of investigation because system response is very sensitive for changes made in this parameter.
- Change of soil damping ratio influences the amplitude but not the pattern of acceleration.
- Dynamic load component oscillating with 2Hz frequency has negligible influence for the results.
- Dynamic load component oscillating with 60Hz (sleeper passing frequency) is responsible for waves propagation to the further distances.
- Instantaneous entrance of the static loads into the numerical model has noticeable effect on the results. However, the wave passes before the loads reach cross-section of interest. Therefore, acceleration results are reliable.
- Increasing thickness of the soft uppermost layer from 1m to 2m gives reduction of the acceleration amplitude.
- By removing compacted sand from beneath the ballast bed the response increases in the nearest field, decreases for the intermediate point and does not change in the far field.
- Relation between dynamic force load component and acceleration amplitude is linear (within the range of investigations) for the field where mainly dynamic load is responsible for the vibration of the system.

6. Concrete slab beneath ballast bed as an abatement measure

This chapter considers all simulations performed to assess effectiveness of concrete slab beneath ballast. Variations of abatement measure in terms of thickness, width and vehicle speed are discussed. Moreover, the situation where the slab is cracked is investigated.

Embankment layout with concrete slab applied is presented in the Figure 6.1. Its dimensions can be seen in Table 6.1 as V1.

V1 is the basic system from which the rest of variations will be formulated. The overview of slab dimensions in each variation is presented in the Table 6.1. Slab is invariant in longitudinal direction.

Variation no.	Variation case	Thickness [m]	Width [m]
V1	basic concrete slab design	0.5	3.5
V2	thickness variations	0.25	3.5
V3		0.35	
V4		0.60	
V5	width variations	0.5	4
V6			4.5
V7			5

Table 6.1 Overview of performed variations for concrete slab beneath ballast bed

Since from numerical models it is possible to extract velocities and displacements, these two parameters will be also considered during concrete slab variation studies. Concrete slab is assumed to be made of concrete with Young's modulus equal to E=30 000 MPa. The damping ratio is assumed to be same as for concrete sleepers, namely 1% (Table 4.1).

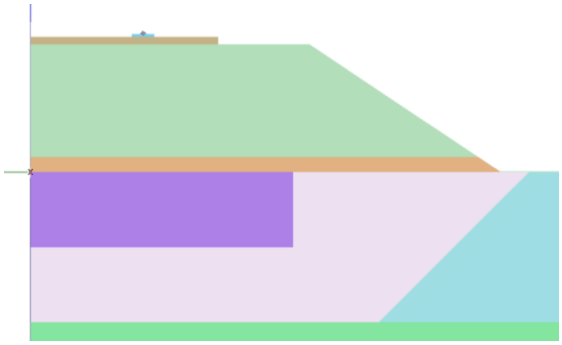

Figure 6.1 Model layout from Plaxis 3D. Cross section with all dimensions is presented in the Figure 3.3. Dark purple rectangular is slab track of dimensions 1.75mx0.5m (half model, in reality slab has 3.5m x 0.5m)

6.1. Variation 1 (V1) width 3.5m thickness 0.5m

The first variation is the basic concrete slab case. Its dimensions are 0.5m x 3.5m. Since symmetry model is used only half of the width is modelled. The results of acceleration amplitudes are presented in the Table 6.2.

Accelerations

From the Table 6.2 reduction of around 20-30% is observed for distances further from the source. Furthermore, at point MP1 peaks occur at different positions after application of concrete slab but the maximum amplitude of accelerations remains the same. Also, system with concrete slab goes back to

the equilibrium quicker in comparison to the one without it. After passage of the train oscillations amplitude decreases faster.

Next, for MP2 there is reduction of 29% of maximum acceleration. Moreover, the oscillations are much shorter in time, system goes back to the equilibrium faster as well as in MP1. Same applies to the MP3 location, although reduction is approximately 23%. Additionally, the general trend seen in the results is in form of "beats". Soil oscillates right before and right after passage of the axle load. It might have an important outcome for the annoyance study because the amount of higher peaks is substantially reduced. Acceleration in the time domain are shown from Figure 6.2 to Figure 6.4.

Acceleration	MP1	MP2	MP3
Numerical model without abatement measure [m/s^2]	-2	-0.59	-0.22
Numerical model with concrete slab abatement measure [m/s^2]	2	0.42	0.17
effectiveness, reduction	0%	29%	23%

Table 6.2 Acceleration comparison between numerical model with ad without concrete slab beneath ballast bed

Acceleration spectrum

For all investigated points the frequency content changes after concrete slab application. When concrete slab is implemented, sleeper passing frequency becomes more pronounced at all distances. Its content in the acceleration signal increases approximately twice.

Moreover, the frequencies related to the wave excitation by the moving oscillatory load in considered soil profile (around 50Hz and 80Hz) completely disappear from spectrum results. Only in the source vicinity higher frequency content around 70Hz is observed. Acceleration spectrums are depicted from Figure 6.5 to Figure 6.7.

This result suggest that application of stiff concrete slab at the source influences the dispersion lines of the system and it causes their upward shift. With this abatement measure applied, the amplification of the system response due to presence of the guided waves would occur at the higher frequencies but these are not excited by the load.

This effect is important for the rail planning. If frequencies resulting from intersection of the dispersion lines and kinematic invariant are harmful for the neighborhood the application of stiff slab can be a solution to eliminate them. Without changing train velocity the undesired frequency content disappears.

Velocity

Analysis of the obtained velocity values cannot be made in a straightforward manner. At some peaks the reduction is visible but at others it is an increment. The only possibility is to describe general trends occurring in the results.

At MP1 at most of the peaks the amplitude of the velocity decreases. The pattern remains the same regardless presence of the abatement measure. It is possible to talk about reduction yet it varies depending on the peak.

At MP2 oscillations duration shortens by application of the concrete slab. Clear wheel passage response is visible in form of beats. Overall, the system oscillation amplitude decreases.

At MP3 same conclusions apply as for MP2.

Results of velocity in time domain are depicted from Figure 6.8 to Figure 6.13

Velocity Spectrum

The same conclusion as for acceleration spectrum are made. Results are shown from Figure 6.11 to Figure 6.13.

Displacements

Concrete slab hardly has any influence on the displacements. Results are depicted from Figure 6.14 to Figure 6.16.

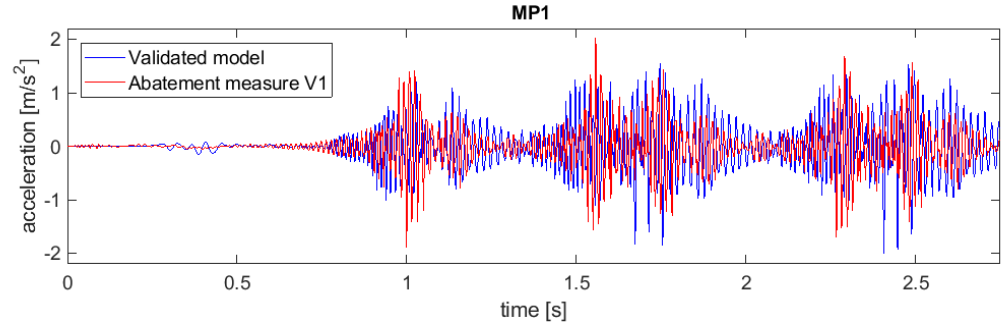

Figure 6.2 Acceleration of numerical models with and without concrete slab at MP1

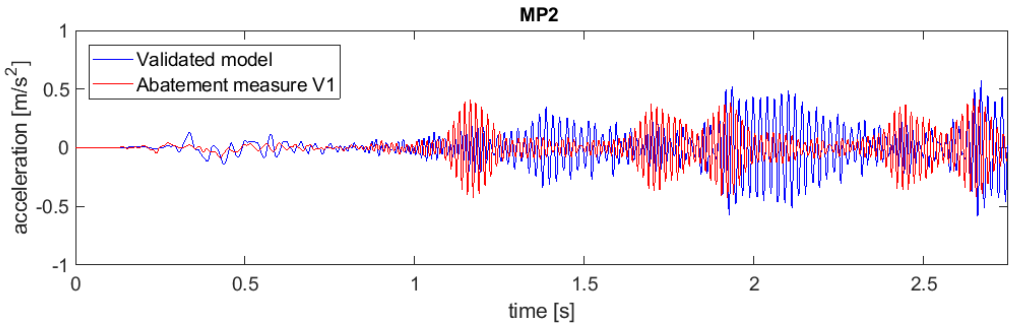

Figure 6.3 Acceleration of numerical models with and without concrete slab at MP2

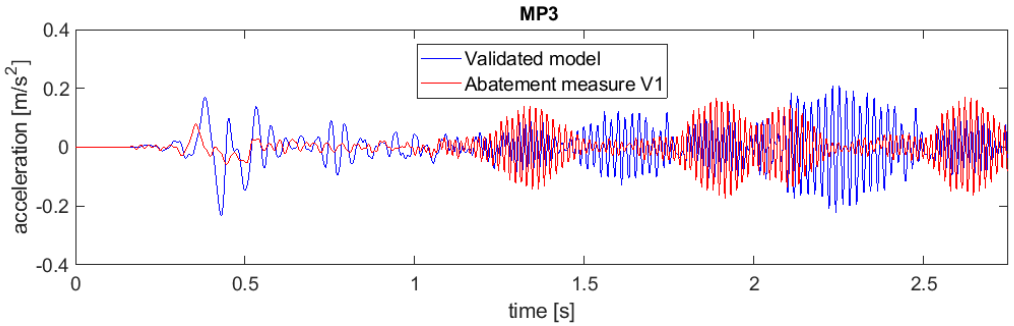

Figure 6.4 Acceleration of numerical models with and without concrete slab at MP3

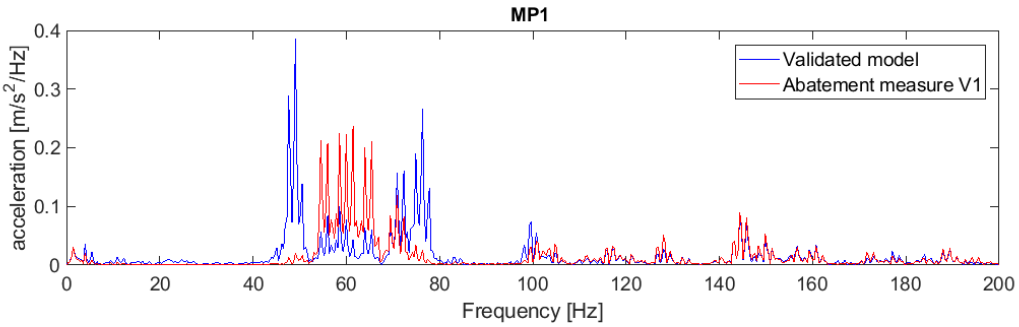

Figure 6.5 Acceleration spectrum of numerical models with and without concrete slab at MP1

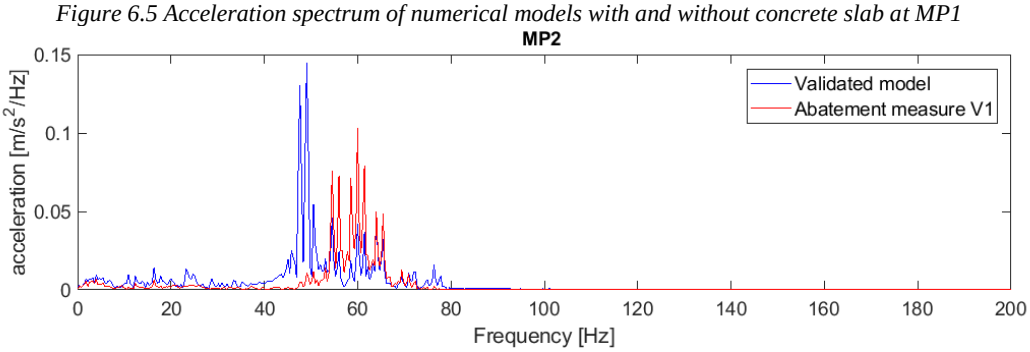

Figure 6.6 Acceleration spectrum of numerical models with and without concrete slab at MP2

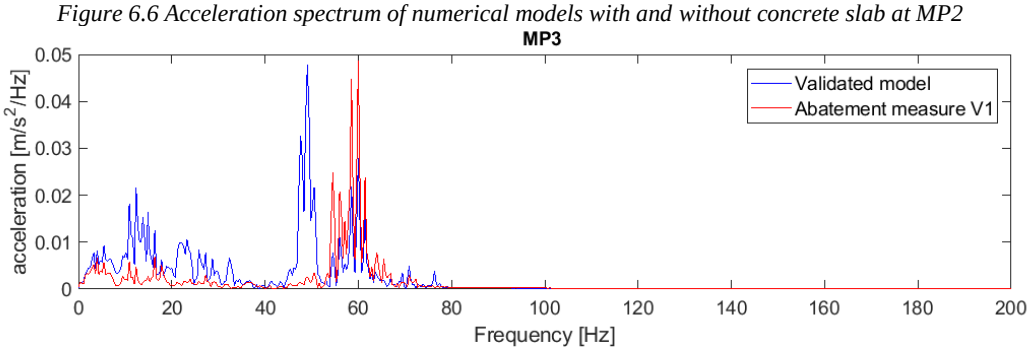

Figure 6.7 Acceleration spectrum of numerical models with and without concrete slab at MP3

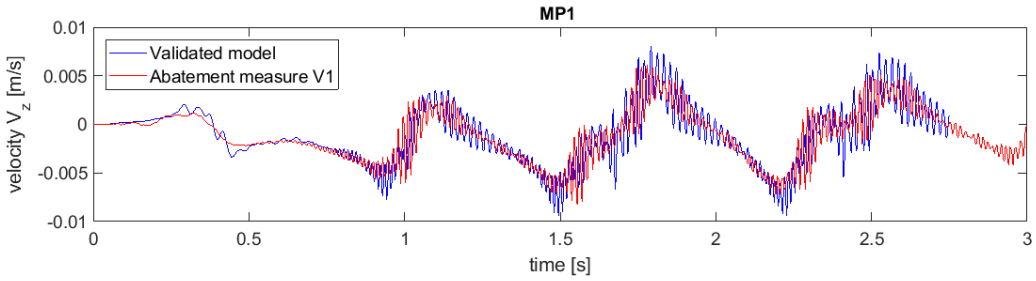

Figure 6.8 Velocity of the measured signal, numerical model with and without concrete slab at MP1

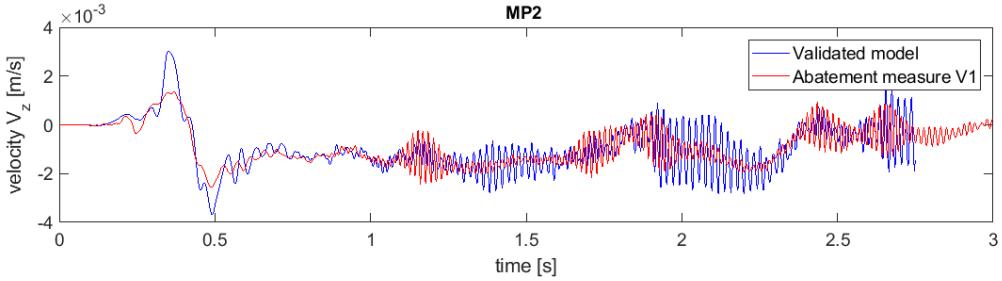

Figure 6.9 Velocity of the measured signal, numerical model with and without concrete slab at MP2

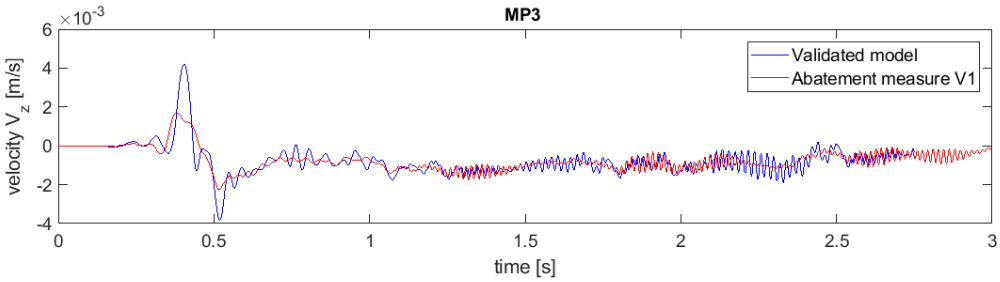

Figure 6.10 Velocity of the numerical model with and without concrete slab at MP3

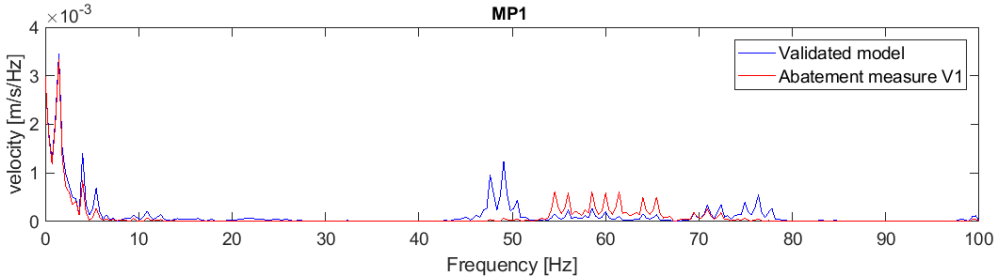

Figure 6.11 Spectrums of velocity of the numerical model with and without concrete slab at MP1

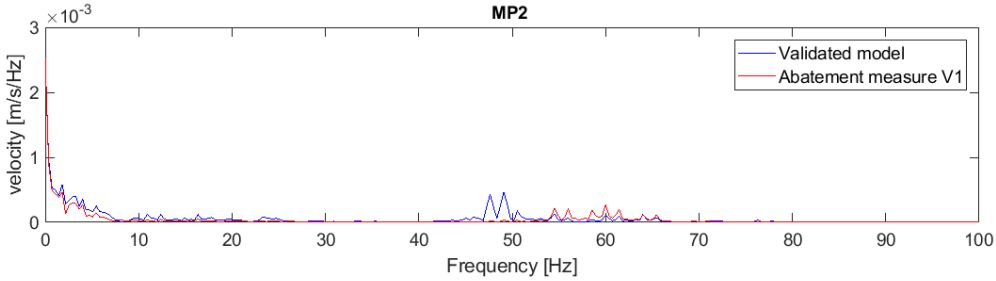

Figure 6.12 Spectrum of velocity the numerical model with and without concrete slab at MP2

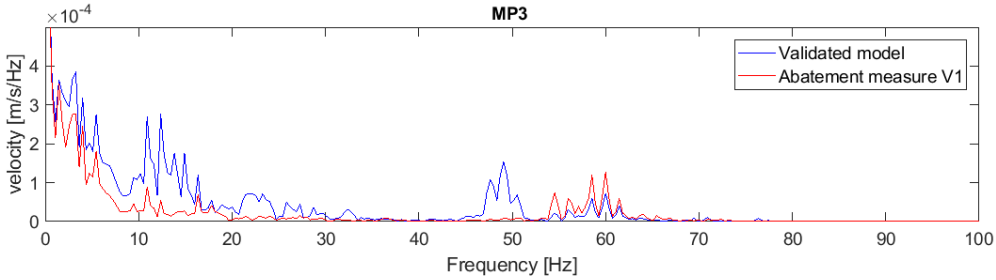

Figure 6.13 Spectrums of velocity the numerical model with and without concrete slab at MP3

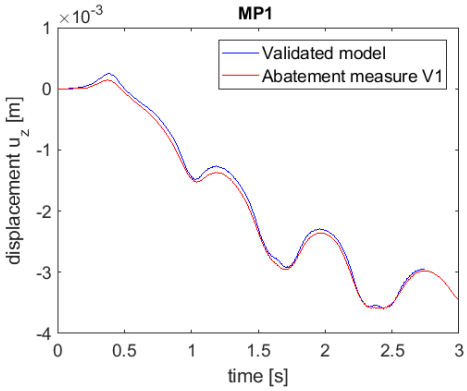

Figure 6.14 Displacements of numerical models with and without concrete slab at MP1

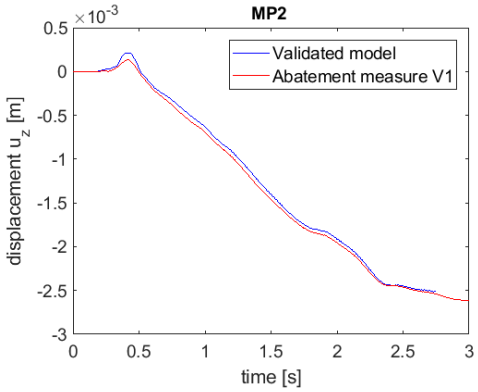

Figure 6.15 Displacements of numerical models with and without concrete slab at MP2

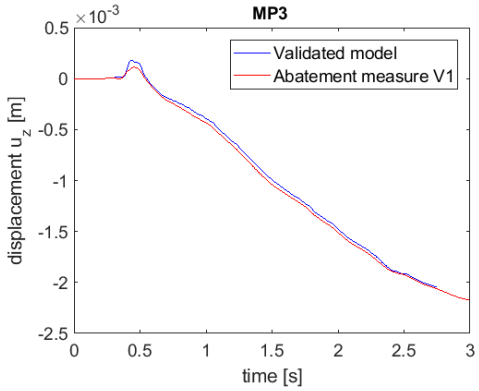

Figure 6.16 Displacements of numerical models with and without concrete slab at MP3

6.2. Thickness Variations (V2, V3, V4)

Acceleration

There is no clear pattern observed in the results presented in the graphs in Appendix D (AP. D Figure 1 to AP. D Figure 3). Nevertheless, a slight decrease of the amplitude is seen with the thickness increment (Table 6.3). Acceleration amplitudes are amplified at some points but at others they are reduced.

Nonetheless, it might be noticed that soil goes back faster to the equilibrium (between wheels) when thicker concrete slab is used but improvement of this effect is observed up to 35cm thickness.

	MP1 Acceleration [m/s^2]	MP2 Acceleration [m/s^2]	MP3 Acceleration [m/s^2]
t = 25cm	-2.13	0.43	0.17
t = 35cm	2	0.42	0.18
t = 50cm	2	0.42	0.17
t = 60cm	1.93	0.42	0.16

Table 6.3 Max values of acceleration for variation studies V1-4 (varying thickness)

Acceleration spectrum

It is visible that the thicker the slab the smaller the content of the dispersive frequency of the soil profile with peaks at 50Hz and 72Hz. Reduction is observed up to 50cm thickness, after that adding extra centimeters to slab thickness does not have an influence.

Furthermore, slight increase of sleeper passing frequency content is observed. Results are depicted in Appendix D from AP. D Figure 4 to AP. D Figure 6.

Velocity

At some peaks reduction of velocity is observed but at the others that is the increment. However, the reduction is seen with thickness growth but just up to 50cm and for MP1 location what is presented in Table 6.4. These results are related only to the lower bound of velocity amplitude. Another observation is that, for points further from the source hardly any difference is visible meaning that thickness variations do not influence velocity at further distances.

The results are shown in Appendix D from AP. D Figure 7 to AP. D Figure 9.

	MP1 [$m/s \cdot 10^{-3}$]
no slab track	9.5
t = 25cm	9.8
t = 35cm	9
t = 50cm	8.2
t = 60cm	7.6

Table 6.4 Comparison of velocity values for numerical models with and without concrete slab

Velocity spectrums

Results for velocity spectrum lead to the same conclusion as acceleration spectrums. The results are presented in Appendix D from AP. D Figure 10 to AP. D Figure 12.

Displacement

Concrete slab thickness variation does not have the influence on the displacements. The results are presented in Appendix D from AP. D Figure 13 to AP. D Figure 15.

6.3. Width Variations (V5, V6, V7)

Acceleration

When slab becomes wider the acceleration amplitude decreases till some point what is depicted in Table 6.5. The visible decrease of the amplitude is seen especially between w = 3.5m and w = 4m. Additionally, reduction at some peaks is more pronounced than at the others (refer to AP. D Figure 16 - AP. D Figure 18).

Moreover, for the points MP2-3 reduction by around 14% in acceleration is observed but further increase of width does not change the results (Table 6.5). It implies that same reduction of acceleration for further distances is obtained by applying slab of 4m width and 5m width. For track vicinity increasing width of the slab might result in the smaller effectiveness of the abatement measure.

The conclusion from this variation study in terms of acceleration is that increasing the width of the slab is beneficial but only till some point, meaning that optimal solution might be found. For this particular case the it is concrete slab of width 4.5m.

Furthermore, 5m concrete slab width results in higher acceleration amplitude when the load is approaching what is perceived as deterioration of the vibrations.

	MP1 [m/s^2]	MP2 [m/s^2]	MP3 [m/s^2]
w = 3.5m	2.025	0.425	0.17
w = 4m	1.72	0.375	0.143
w = 4.5m	1.48	0.34	0.15
w = 5m	1.525	0.345	0.145

Table 6.5 Maximum amplitude values of acceleration for all variation models V1, V5-7

Acceleration spectrum

Acceleration frequency content for the response at different locations is presented in Appendix D from AP. D Figure 19 to AP. D Figure 21.

At first, magnitude of sleeper passing frequency increases in the close field (by 30% between V1 and V7) when width increases but further away the situation is opposite. The wider track gets the smaller is the influence of the sleeper passing frequency at MP2 and MP3 (20% reduction between V1 and V7).

Next, when increasing the width of the slab, frequencies content concentrated around 70Hz diminishes.

Velocity

As for the rest of the velocity results, also in this case, the influence of the varying concrete slab width cannot be formulated explicitly. Again, at some points reduction is observed and at the others increment. The results are presented in Appendix D from AP. D Figure 22 to AP. D Figure 24.

Velocity spectrum

Results for velocity spectrum lead to the same conclusion as acceleration spectrums. Results are presented in Appendix D from AP. D Figure 25 to AP. D Figure 30.

Displacements

No influence of changing slab track width is noticed in displacement results. The results are presented from AP. D Figure 31 to AP. D Figure 33.

6.4. Effectiveness of concrete slab as abatement measure for train passing at different speed

The abatement measure in form of the concrete slab can have different effectiveness depending on the speed of the train. In this section this effect will be further investigated also for speed 110km/h and 150km/h.

6.4.1. Effect of concrete slab application for the train running with speed 110 km/h

Sleeper passing frequency has been adopted and for 110km/h it is equal to 51Hz.

Acceleration

The results of the accelerations are all presented in the Table 6.6. Graphs can be seen in Appendix D from AP. D Figure 34 to AP. D Figure 36.

The reduction of approximately 30% of acceleration amplitude for all three points is observed.

Moreover, as in case of train running with 130km/h, concrete slab changes pattern of the vibrations. Axle load passing can be clearly distinguished and soil responses in short beats. Oscillation duration shortens.

110 km/h	MP1	MP2	MP3
no concrete slab	2.1	0.67	0.23
with concrete slab	1.54	0.48	0.156
Reduction (R)/Increase (I)	R - 26%	R - 28%	R - 32%

Table 6.6 Maximum values of acceleration for model with train running at 110 km/h speed

Acceleration spectrum

Concrete slab for all points eliminates frequency peak at 42Hz and 60-66Hz. Also, at all distances sleeper passing frequency content increases with comparison to the case without concrete slab being used, except for point MP3 where sleeper passing frequency is comparable for both cases. Graphs for acceleration spectrum are placed in Appendix D from AP. D Figure 37 to AP. D Figure 39.

Velocity

In velocity results no substantial reduction is observed. In general at some points reduction is significant, but at others amplification is observed. Much less oscillations occurs but magnitude remains similar as before. As in case of accelerations, signal takes form of beats and axle loads becomes easy to be distinguished. Results are presented in Appendix D from AP. D Figure 40 to AP. D Figure 42.

Velocity – frequency domain

The results of frequency content in velocity response are analogical to acceleration. Velocity spectrums are placed in Appendix D from AP. D Figure 43 to AP. D Figure 45.

Displacement

No significant difference occurs between results of the system with and without slab track applied when train is running with speed 110km/h. The results are in Appendix D from AP. D Figure 46 to AP. D Figure 48.

6.4.2.Effect of concrete slab application for the train running with speed 150 km/h

The same set of data and comparisons as in 6.4.1 will be presented in the following section. Sleeper passing frequency is now equal to 70Hz.

Acceleration – time domain

The maximum acceleration values for both systems with and without concrete slab are presented in the Table 6.7. Graphs can be seen in Appendix D from AP. D Figure 49 to AP. D Figure 51.

150 km/h	MP1	MP2	MP3
no concrete slab	2.1	0.49	0.1
with concrete slab	2.97	0.25	0.07
Reduction (R)/Increase (I)	I - 42%	R - 49%	R - 30%

Table 6.7 Maximum values of acceleration for model with train running at 150 km/h speed

Concrete slab causes significant increment of the acceleration amplitude for distances close to the track (by 42%). However in the mid-distance at MP2 the reduction is 49% and if one goes even further from the track it is around 30% (MP3).

It means that concrete slab solution in terms of acceleration reduction might be beneficial for the far field from the track distances. However, amplification close to the source can be expected.

Acceleration spectrum

Concrete slab for all points eliminates frequency peak at 55Hz and a little bit at 90Hz.

Moreover, at all points sleeper passing frequency content increases with comparison to the case without concrete slab being used. Sleeper passing frequency magnitude for 150km/h is more pronounced than for train travelling with 110km/h.

Furthermore, for MP1 peak the increment of frequencies 80Hz – 85Hz is noticed.

The results are presented in Appendix D from AP. D Figure 52 to AP. D Figure 54.

Velocity

In velocity results no substantial reduction or amplification is observed. In general, at some points reduction is significant, but at others severe amplification occurs.

Another observation is that at MP1 when concrete slab is present the oscillations become more rapid and actually locally amplification is seen. At MP2 results are very similar to the one without any mitigation system but oscillations are smaller in between wheel passage. At MP3 results from both models look very similar one to another. Again, wheel passage response clarifies in a sense that beats related to the passing axle load are formed and oscillation duration shortens. Results are depicted in Appendix D from AP. D Figure 55 to AP. D Figure 57.

Velocity spectrum

The conclusions following from velocity spectrum are the same as for acceleration signal. Results are placed in Appendix D from AP. D Figure 58 to AP. D Figure 60.

Displacement – time domain

No significant difference occurs between results of the system with and without concrete slab applied when train is running with speed 150km/h. The results are presented Appendix D from AP. D Figure 61 to AP. D Figure 63.

6.4.3.Comparison of the result at train traveling with 110, 130 and 150 km/h

6.4.3.1. Numerical results without concrete slab applied

Acceleration – time domain

Acceleration comparison of models where trains run with different velocity is in the Table 6.8. It concerns the cases where concrete slab is not used.

MP1 acceleration close to the track is unchanged regardless speed of the vehicle. Since driving factor for the close field response is the quasi-static load component such outcome is not very surprising. Static loads are the same in all three models.

Furthermore, the faster the train the smaller maximum acceleration value for further field. For points MP2 and MP3 it is visible that reduction occurs for train running with 150 km/h. It can be explained based on the frequency content. Higher speed enhances higher frequencies which are decaying faster with the distance in comparison with lower frequencies excited by the slower train. It might mean that the faster the train the smaller influence is visible for the far field (where usually buildings are present).

	MP1	MP2	MP3
110km/h [m/s^2]	2.1	0.67	0.23
130km/h [m/s^2]	2	0.59	0.22
150km/h [m/s^2]	2.1	0.49	0.1

Table 6.8 Comparison of maximum acceleration amplitudes for speed, 110km/h, 130km/h and 150km/h when no abatement measure is applied

Acceleration signal for three train speeds can be seen in Appendix D from AP. D Figure 64 to AP. D Figure 66.

Acceleration spectrum

The results for all three train speeds are similar one to another.

For MP1 sleeper passing frequency of train running with 110km/h and 150km/h has similar magnitude while for 130km/h this frequency content is smaller in comparison with two others.

Next, at MP2 sleeper passing frequency of 70Hz is very little in comparison with two others, this frequency decays much faster. The frequencies resulting from intersection soil profile dispersion lines and kinematic invariant for the specific case are also of the similar magnitude. Same observation is made for MP3.

Sleeper passing frequency of 70Hz seems to decay faster than 50Hz and 60Hz what can be caused by the damping ratio formulation as Rayleigh damping. Each of these frequencies has bit different damping ratio but 70Hz is already outside "constant damping range" and damping for this value is bit higher than for 50Hz and 60Hz. Graphs of acceleration spectrums are depicted in Appendix D from AP. D Figure 67 to AP. D Figure 69.

Velocity

At MP1 the maximum value of velocity is comparable between all of the speeds but it rises up slightly with increasing speed. At some places the amplification occurs but it is difficult to state that there is any reduction or increase in velocity. Same applies to MP2 and MP3 however for 150km/h less oscillations is observed, the velocity is more stable.

Results can be seen in Appendix D from AP. D Figure 70 to AP. D Figure 72

Velocity spectrum

The observations are the same as for acceleration spectrum. Results can be seen in Appendix D from AP. D Figure 73 to AP. D Figure 75.

6.4.3.2. Results with concrete slab applied in the system

Acceleration

Accelerations from three simulations with abatement measure present in the system is shown in the Table 6.9.

The acceleration amplitude at points close to the track increases together with increasing speed, further from the track the situation is reversed, lower speed induces the highest acceleration at MP2 and MP3. The highest acceleration comes out from 110 km/ at MP2 and at MP3 130 km/h variation induces the higher acceleration.

The conclusion is that application of the concrete slab is a trade-off and it depends on the speed of the train. Usually, the railway network is designed for the highest allowed train speed. If interest is in reduction of the vibration for the further distances and concrete slab is used as an abatement measure, it turns out that the crucial for vibrations is the lower not the higher speed. Therefore, if for the new network it is planned to have on the regular basis trains running at 150km/h and at 100km/h both cases have to be investigated.

The results are shown in Appendix D from AP. D Figure 76 to AP. D Figure 78.

	MP1	MP2	MP3
110km/h [m/s^2]	1.54	0.48	0.156
130km/h [m/s^2]	2.025	0.425	0.17
150km/h [m/s^2]	2.97	0.25	0.07

Table 6.9 Maximum acceleration values for train speed 110km/h, 130km/h and 150km/h with concrete slab as abatement measure in the system

Acceleration spectrum

Train running at 150km/h with 70Hz sleeper passing frequency has much higher magnitude close to the track than other two velocity cases. On the contrary, for further points this frequency content decreases significantly for 150km/h simulation and becomes the smallest amongst three considered variations cases. Furthermore, at MP2 110km/h case has the highest magnitude of sleeper passing frequency and for MP3 it is 130km/h.

As already explained in previous subsection 6.4.3.1 such effect can be the result of damping formulation as for this research it is Rayleigh Damping.

The results are shown in Appendix D from AP. D Figure 79 to AP. D Figure 81.

Velocity

Velocity increases together with train speed for point in source vicinity. However, for points located further away velocity maximum value is almost unchanged regardless speed variations.

Nonetheless, beats are becoming narrower and more compacted for the far field when speed is increasing. In other words, for MP2 the average value of velocity increases, hence the oscillations are smaller but the value remains the same for all cases.

The results for velocity are shown in Appendix D from AP. D Figure 82 to AP. D Figure 84.

Velocity spectrum

The conclusions for the velocity spectrum are analogous to acceleration spectrum findings.

The results for velocity are shown in Appendix D from AP. D Figure 85 toAP. D Figure 87.

6.5. Scatter effect

Detailed elaboration about the model settings and calculations followed up by numerical results is presented in Appendix D. In this subsection only general findings and motivation of performing this iteration are included.

The motivation of including the building in the model is to quantify the importance for locations MP1-3 of the effect of waves reflecting from the building foundation. Measurements for the wall (MP4) and floor (MP5) are available, therefore by modelling the structure it is possible to obtain the response numerically and compare its accuracy. The difficulty associated with this model is the fact that no information about the building is available.

The attempt of fulfilling the above motivation was unsuccessful because obtained values from numerical model did not match the measurements.

Small increment in acceleration is observed at point MP1 (from 2 to 2.15 m/s^2). However, for MP2 it is the opposite as the response is smaller at some peaks. Nerertheless, in general it is very similar to the model where building was not included.

Furthermore, for MP3 the reposnse is considerably smaller for the model with the building included. For points MP4 (wall) and MP5 (floor) the results are very far off from the measurements. Moreover, results obtained from numerical model of MP4 and MP5 are very similar to each other. The reason for this can be too heavy and too stiff building. Calculation time of this model is 6-7 days. Therefore, due to many uncertantities invloved in this iteration and long time needed to investigate this effects no more simulations are performed.

6.6. Slab track effectiveness with cracked concrete and varying damping ratio

The investigation based on concrete slab changing parameters has been made. Based on the research (Irvine, 2004) cracked concrete slab can have damping values with fully developed crack width pattern anywhere between 3% and 6%. Two models, with $E_{cracked}=1/3\ E_{uncracked}$ and 4% and 6% damping ratio has been developed and calculated. The rest of the parameters is the same as for the model from sub-section 5.2.

Acceleration

As seen from the Table 6.10 the reduction or amplification is hardly visible for further distances (MP2 and MP3). The biggest reduction is obtained at the point close to the track, when concrete is cracked and 4% damping ratio is assumed. In this case the reduction of acceleration is equal to 8.5%. Between models assuming 4% and 6% reduction of the acceleration is equal to only 2%. Increasing damping of the concrete slab did not give any further decrease of acceleration.

This results means that even though the slab is cracked no deterioration of its performance is noticed because the acceleration value remains at the same level. Moreover, even slight improvement of the results is observed.

Acceleration [m/s^2]	MP1	MP2	MP3
uncracked 1% damping	2	0.42	0.17
cracked 4% damping	1.83	0.4	0.15
cracked 6% damping	1.79	0.4	0.15

Table 6.10 Maximum acceleration for different slab track models, train running with 130 km/h speed

Acceleration spectrum

The results of range 0-80Hz are shown in Appendix D from AP. D Figure 91 to AP. D Figure 93. No substantial difference is noticed in spectrum results. The only observation is that cracked concrete slabs are having higher frequency magnitude in the range 67-73Hz especially in track vicinity.

Velocity

The results are almost the same for all locations. Sometimes the amplification at peaks occurs and sometimes there is a reduction. The results from the cracked slab are almost the same for 4% and for 6%. The difference between results from cracked and uncracked cases reaches 0.1 m/s. Results are depicted in Appendix D from AP. D Figure 94 to AP. D Figure 96.

Velocity spectrum

It has the same trends as for acceleration spectrums. Results are presented in Appendix D from AP. D Figure 97 to AP. D Figure 99.

6.7. Short summary of Chapter 6 and the most important findings

Comparison between systems with and without abatement measure in which train runs at 130km/h

- Abatement measure gives reduction in acceleration maximum amplitude of around 20-30% for distances further from the source.
- Response pattern changes after concrete slab application. Namely, acceleration signal takes form of beats which represents the direct response to the wheel passage. Moreover, system goes back to the equilibrium faster, less oscillations are noticed – same applies to velocity
- When concrete slab is implemented, sleeper passing frequency becomes more pronounced at all distances. Its content in the acceleration signal increases approximately twice.
- The influence of the frequencies where dispersion lines intersect with kinematic invariant disappear from the spectrum.
- Velocity is reduced but only for MP1if slab track is applied.

Comparison between systems with and without abatement measure in which train runs at 110km/h

- For train running at 110km/h speed concrete slab of dimensions 3.5m x 0.5m gives reduction of about 30% of acceleration maximum value at all locations.
- Same as for train running at 130km/h speed, response (velocity and acceleration) is in form of beats. Moreover, sleeper passing frequency becomes more pronounced for all distances, peaks associated with intersection of dispersion lines and kinematic invariant diminish almost completely from the spectrum.

Comparison between systems with and without abatement measure in which train runs at 150km/h

- Concrete slab solution in terms of acceleration reduction might be beneficial for the far field from the track distances (reduction at MP2 is 49% and at MP3 30%) . However, amplification close to the source can be expected (increase of acceleration amplitude at MP1 is 42%)
- Same as for train running at 130km/h speed, response (velocity and acceleration) is in form of beats. Moreover, sleeper passing frequency becomes more pronounced for all distances, peaks associated with intersection of dispersion lines and kinematic invariant diminish almost completely from the spectrum.

Variations thickness for concrete slab design

- Beats response forms up for further distances at any considered slab thickness. However, for MP1 this effect is observed from 35cm thick slab.
- For the variation where concrete slab is 35cm thick (V3) smaller oscillation for amplitude in terms of acceleration is noticed but further increment of thickness does not give reduction.
- Concrete slab thickness variations influence mainly track vicinity, reduction between system with 25cm and 60cm concrete slab thickness is little for accelerations and equal to 10%.
- Increasing thickness reduces velocities at MP1. The difference can be even as high as 20% but it is applicable just for the lower bound values. On the other hand, at some points there is no reduction observed at all.
- For points further away from the source hardly any difference in velocity is visible while slab thickness is varying. It implies that thickness variations do not influence velocity at further distances.

- Concrete slab thickness variations are influencing mainly track vicinity; it means that the same maximum acceleration amplitude if observed in further distance whether 25cm or 60cm slab is applied.

Variations width for concrete slab design

- Almost same reduction of acceleration for further distances is obtained by applying slab of 4m width and 5m width. For track vicinity increasing width of the slab might result in the smaller effectiveness of the abatement measure, the optimal solution should exist and in this particular case it is 4.5m width.
- 70Hz content decreases at MP1 when increasing width.
- Sleeper passing frequency content increases together with increasing width for MP1 but for MP2 and MP3 it decreases.
- Concrete slab width variations do not influence displacements.

How system behaves without any abatement measure for the trains running ay speed 110, 130 and 150km/h – comparison between speeds

- MP1 acceleration close to the track remains unchanged regardless of the speed.
- The faster the train the smaller the maximum acceleration value for further distances (MP2, MP3).
- Sleeper passing frequency for train running at speed 150km/h is equal to 70Hz. This frequency content decreases much faster with the distance than sleeper passing frequency of 130km/h and 110km/h. That can be associated with the fact that higher frequency content decays faster than the lower frequency content. On the other hand Rayleigh damping is used and frequency dependent what can mean that 70Hz has higher damping ratio than sleeper passing frequency of 60Hz and 50Hz.

How system behaves for the trains running at speed 110, 130 and 150km/h when abatement measure is applied – comparison between speeds

- The acceleration amplitude at points close to the track increases together with increasing speed. However, further from the track the situation is reversed, lower speed induces the highest acceleration at MP2 and MP3.
- Train running at 150km/h with 70Hz sleeper passing frequency has much higher magnitude close to the track than other two velocity cases. On the contrary, for further points this frequency content decreases significantly for 150km/h simulation and becomes the smallest amongst three considered variations cases.
- Velocity increases together with train speed for points in source vicinity. However, for points located further away velocity maximum value is almost unchanged regardless speed.

Cracking of concrete slab

- Cracking of slab does not lead to deterioration of its performance as far as this abatement measure is considered. Moreover, even slight improvement of the results is observed.
- Cracked concrete slabs have higher frequency content, especially in track vicinity, in the frequency range 67-73Hz than non-cracked .
- When slab cracks the system gives almost the same values of maximum acceleration for 4% and 6% damping ratio of the concrete slab.

7. Conclusions and recommendations for future research

7.1. Conclusions

The focus of this report is on vibrations induced by a train passage and an abatement measure to mitigate them. Concrete slab beneath ballast bed is the choice for the abatement measure, and its effectiveness is assessed through this work. Plaxis 3D, finite element method software, is used to perform numerical analysis. The report can be divided in three parts, namely calibration of the model, variation studies without concrete slab and investigation of the influence of concrete slab on the vibration strength. For validation procedure measurement data obtained from tests conducted at one of the sites in the Netherlands are used.

At the beginning of research it is important to assess the situation at which the available measurement data was obtained. Things such as building shape simplicity, measurement point being surrounded by reflective elements, length of the recorded path, sensors distance to the rail, certainty of the soil profile, are significant factors to be considered during decision making process.

Furthermore, numerical model size is crucial for research. In this paper model has size of 70m x 55m x 30m. No erroneous reflections were noticed in the results meaning that redistribution of the waves and model size is well-chosen. Also, area of fine mesh has to be strongly limited, otherwise model cannot be created. Due to large number of nodes and elements in order to reduce calculation time linear elastic material behaviour is assumed for all elements and soils.

One of the most important factors for the analysis is the way of incorporating the axle wheel load in to the model. Two approaches are considered in the research, namely triangular pulses consisted of quasi-static load only and moving point load consisted of dynamic as well as quasi-static load component. It turns out that triangular pulses tend to generate frequency associated with the rail discretization distance but sleeper passing frequency is not recorded in results obtained by this method. Moreover, if dynamic load component is not included waves do not propagate away from the track. In that case only the direct vicinity of the rail can be studied using this approach. In addition, the discretization of the sleeper spacing should be relatively fine to avoid erroneous frequencies.

Since the train is not modelled as a whole vehicle its dynamic rail-train interaction due to changing stiffness should be accounted for in the model artificially. This can be done through adding in the model a point load of a certain force oscillating with sleeper passing frequency. Through the engineering judgement the oscillating force should not be larger than 10% of the weight of the train. It turned out that 5% of the axle load gives good results. Also 2.5% axle load force is investigated and the linear relation between dynamic force and vibration strength is found at the distances where quasi-static load does not have an influence, namely for further distances. It implies that the response after changing force magnitude can be easily predicted when results from one simulations are available.

This effect is similar to the effect of changing damping ratio for the soil stratum as it indicates to have the linear relation with acceleration strength. This relation is observed within range of investigations. However, response of the system depends on the damping ratio in a complicated way. Therefore, it is advised to consider this effect carefully for another than presented in this research range of investigation because system response is very sensitive for changes made in this parameter.

Furthermore, damping ratio of the soil stratum has been found the most important and influential parameter amongst all investigated. Change of soil damping ratio from 2% to 1% gives already 128% difference between results (at MP3). Additionally, damping ratio is especially important for the far field, as for the track vicinity field the biggest different found between results is 13%. It implies that if researcher is trying to predict vibrations in the far field and he is not sure about the damping ratio value

and has no data available to calibrate the model, there is a great chance that results he obtains will not be correct. For this reasons, it is necessary to either have measurements to calibrate damping value available or good approximation of damping ratio e.g. by means of conducting lab tests. In reality, damping is one of the most difficult parameters to be determined.

Sometimes uncertainties of the actual on-site situation are involved in the project. They may be for instance, related to the cross-section of the embankment what is also the case in this research. However, these uncertainties might not have big a impact on the result and insightful, time consuming simulations are unnecessary. Hence, the importance of two factors is studied.

First one is a subballast material. The comparison is made between asphalt and crushed stone from which the first one is ten times stiffer than the second. The outcome of numerical simulations for this iteration is that the change of subballast material influences only area in source vicinity, for further distances the effect is negligible. Also stiffer material gives in its spectrum higher content of imposed load frequency.

Second uncertainty that is came across is the presence of compacted sand beneath ballast bed. By removing compacted sand the system response increases in the nearest field, decreases for the intermediate point but does not change in the far field.

These two points brings us to the conclusion that if researcher is interested in the response in the track vicinity then the exact cross section of the embankment is important, otherwise, probably not too much attention should be paid to being very precise about the embankment cross section and reasonable approximations can be made without deterioration of the results.

In the end, validation of the model is achieved. However, in the spectrum response of the numerical results two large peaks occur which do not match the measurements. Their origin is investigated. The dispersion lines of the soil profile and kinematic invariant are drawn. It is expected that when two aforementioned intersects the wave of a frequency resulting from this intersection will be excited. In the considered case, high peaks occur at these frequencies

This considerations might help in improving soil profile approximation if one is needed. Firstly, the approximated model can be made. Then, both numerical and measurement spectrums can be compared and necessary adjustments in soil profile can be made to define the closer to the reality soil stratum layering. Instead of conducting field tests to improve accuracy of the soil profile, numerical approach can be performed. However, this process might be very time consuming as effect of changing soil layers is difficult to be predicted.

The attempt to improve the soil profile spectrum is made. The top layer which has the smallest Young's modulus, is changed from 1m to 2m thick. It turned out that by doing this, the accelerations decreased by 20%. Moreover, dispersive frequency decreases and matches measurements better. In contrast, sleeper passing frequency content becomes less influential for distant points what is not in accordance with the measurements. Increasing thickness of the top sandy layer from 1m to 2m is a trade-off between improving frequency erroneous content and decreasing sleeper passing frequency importance.

One important conclusion is made for the modelling itself. Loads have to be introduced into the model at some point instantaneously. When it is done, the spurious wave is created. During analysis of the results it is important to ensure that oscillations coming from this effect are not included in the representative acceleration/velocity value (or are negligible). For this reason, load movement should be activated after some time from activating the static load. In this way, the spurious wave passes before the wheel starts influencing the investigated area. The other solution is to make model long enough that the spurious wave decays before it can even reach the point of interest. In that case the signal response does not include the effect of sudden entrance of the load in the model.

The contribution of the loads components into the signal is also checked. The results shows that sleeper passing frequency is responsible for propagation of the waves towards further distances and 2Hz has secondary influence on the results. Small effect of 2Hz frequency can be caused by the way the damping ratio is formulated, namely Rayleigh damping. In this method the low frequencies are highly damped and the actual influence of the low frequencies might be underestimated.

Conclusions for concrete slab beneath ballast bed abatement measure

Few factors that concrete slab beneath ballast bed is influencing are presented in the Table 7.1. As seen in the Table 7.1 sleeper passing frequency content increases after concrete slab application. Peaks related to the to intersection of the dispersion lines and kinematics invariant disappears from spectrum. This is caused by the upwards shifting of the dispersion lines. Now amplification of results might be expected at the higher frequencies which are not enhanced. In this way it is possible to control frequency content of the response. If some frequencies are known to be harmful for the building and they might be excited by the moving oscillatory load and soil profile interaction by the application of abatement measure it is possible to diminish these frequency content.

Aspects influenced by application of concrete slab beneath ballast bed	110 km/h	130 km/h	150 km/h
Sleeper passing frequency content in acceleration and velocity spectrum increases	Yes	Yes	Yes
Peak frequency related to intersection of the dispersion lines and kinematics invariant disappears from spectrum	Yes	Yes	Yes
Reduction of acceleration amplitude	Around 30%	MP1 – no MP2/3 – 20-30%	MP1 – amplification by 42% MP2/3 – red. 40%
Reduction of velocity amplitude	No	MP1 – reduction 20-30% MP2/3 – sometimes reduction sometimes amplification	No
Reduction of vibrations duration	Yes	Yes	Yes
Velocity and acceleration response takes form of beats which indicate directly wheel passage	Yes	Yes	Yes

Table 7.1 Summary of the effect of concrete slab for system with three different train speeds. Comparison is made in reference to situation where no abatement measure is present

Furthermore, the response takes form of beats after concrete slab application. The system reacts during the short time, directly before and after wheel passage. Oscillations decay faster. This outcome might be helpful during annoyance study as higher oscillations are present but for shorter period of time.

In terms of the reduction, concrete slab gives reduction of 20% to even 40% of the maximum acceleration value for further distances. However, close to the track acceleration might increase when train is running bit faster. At MP1 42% of amplification is noticed for train with speed of 150 km/h. Nevertheless, for train running with 110 km/h reduction is seen for all the points while for 130 km/h no change is observed for close field. It concludes that abatement measure is the most effective for relatively slow trains. On the other hand, if the response close to the track is not of interest and researcher is only interesting in looking into further distances, concrete slab could be reasonable solution for mitigation of vibrations.

By looking into the models where abatement is present but train speed varies some interesting findings might be pointed out. In fact, acceleration for the close field increases significantly with increasing speed but further from the track the situation is the opposite. Train running with the lower speed results in higher amplification far away from the track. It might happen that the railway network is designed for the highest allowed train speed. Since buildings are placed in the far field the crucial turns out to be not the train running with the high speed but the one travelling with the low speed. Therefore, if for the new network it is planned to have on the regular basis trains running at 150km/h and at 110km/h both cases have to be investigated as one is governing for the close field and the other one is decisive for far field.

For comparison, when no abatement measure is applied, the response close to the track is almost the same regardless of the speed but with the distance the fastest train gives the smallest acceleration value. For the intermediate point slower train induces higher acceleration but for far field 110 km/h and 130km/h train causes the same acceleration.

The effect of varying width and thickness of the abatement measure is investigated. However, only one of the parameter varies at the time and only train speed of 130 km/h is considered. The basic system for the simulation was concrete slab of dimensions 3.5m x 0.5m.

Concrete slab thickness variations are influencing mainly track vicinity meaning that the same maximum acceleration amplitude if observed in further distance whether 25cm or 60cm thick slab is applied. However, with increasing thickness only 10% reduction of acceleration value obtained from system with 25cm thick slab and 60cm is observed. To sum up thickness variations, this parameter does not change much in the signal response.

The increasing width of the slab is effective especially for the track close field. In this research at MP1 reduction is equal to 25%. However, almost same reduction of acceleration for further distances is obtained by applying slab of 4m width and 5m width. For track vicinity increasing width of the slab might result in the smaller effectiveness of the abatement measure because in this case acceleration for width 4.5m is smaller than for 5m. The optimal solution should exist and in this particular case it is 4.5m width.

The effect of concrete cracking, therefore a change of concrete damping and Young's modulus parameters is addressed in the research as well. Simulation where Young's modulus decreases to 1/3 of the original value is run and varying damping is considered. After slab cracking the reduction of acceleration in close to the rail area is only 8.5%. For further distances no change is observed. It concludes that cracking of the slab does not deteriorate the its performance. Moreover, the difference between damping ratio of 4% and 6% for the concrete slab has negligible effect meaning that establishing the detailed damping ratio of concrete slab has high tolerance.

7.2. Recommendations for future research

The following further studies related to this work would be of interest.

- Calculation time for each of the models is at least 2.5 days what is the biggest disadvantage of this method. It does not allow to run many simulations. The approach to reduce computational time is needed. It is of interest to investigate parametrically the changing model size and its influence on the results as well as the size of the area where fine mesh has to be applied.
- Same studies could be performed for another system of similar properties to confirm findings presented in the research.
- Importance of damping ratio is shown only for sandy soils. It would be beneficial to investigate this effect for soil profile of different characteristics and for changing speed of the train.

- All effects described above are investigated in one or two iterations and for sandy soil profile only. In order to have the whole spectrum of information about the specific effect, simulations for more parameters and different soil characteristics should be investigated.
- Simulation with different damping formulation, namely constant damping which is frequency independent should be performed. In this research it is possible that influence of the low frequencies is underestimated. Also, for the wide range of frequencies (meaning wide range of speed) it is not possible to have constant damping ratio of soil stratum. This is another argument to perform similar studies with constant damping.
- The parameters of the concrete slab in cracked conditions are assumed. The detailed concrete design which can simulate these conditions is needed.
- Similar analysis as presented in this report should be done also for freight trains. For this reason measured signal due to freight train passage is needed.
- Study for what kind of buildings this abatement measure is effective would give the whole picture of concrete slab effectiveness.
- It has been indicated during the research that uncertainties associated with exact embankment cross-section are influencing mainly close field response. However, only two elements were studied in only one iteration. How system behaves depending on embankment changing materials and geometry in the close and far field could be established.

8. Bibliography

Achenbach, J. D. a. C.-t. S., 1965. Dynamic response of beam on viscoelastic subgrade.. *Journal of the Engineering Mechanics Division 91, no. 5* , pp. 61-76.

Anon., n.d. *RIVAS.* [Online]
Available at: http://www.rivas-project.eu/

Arcelor Mittal, n.d. [Online]
Available at: https://rails.arcelormittal.com/pages/162-54e1-uic54-rail
[Accessed 10 06 2019].

Aubry, D., Clouteau, D. & Bonnet, G., 1994. Modelling of wave propagation due to fixed or mobile dynamic sources. *In Workshop Wave,* pp. Vol. 94, pp. 109-121.

Bahrekazemi, M., 2004. *Train-induced ground vibration and its prediction PhD diss,* Byggvetenskap: s.n.

Barbosa, J. M. d. O., 2013. *Analysis and mitigation of vibrations induced by the passage of high-speed trains in nearby buildings,* s.l.: s.n.

Bombardier, n.d. *Bombardier.* [Online]
Available at: https://www.bombardier.com/en/home.html
[Accessed 21 10 2019].

Brinkgreve, R. et al., 2018. *Plaxis Scientific Manula 2018,* s.l.: Plaxis bv.

Brinkgreve, R. et al., 2018. *Plaxis 3D Reference Manual 2018.* Delft: Plaxis bv.

Cheng-hou, et al., 1990. A new classification chart for soft soils using the piezocone test. *Engineering Geology 29, no. 1,* pp. 31-47.

Colaço, A. et al., 2017. Mitigation of vibrations and re-radiated noise in buildings generated by railway traffic: a parametric study. *Procedia engineering, 199,* pp. 2627-2632.

Connolly, D. et al., 2016. The growth of railway ground vibration problems—a review. *Science of the Total Environment vol. 568,* p. 276–1282..

Correia, et al., 2007. Dynamic analysis of rail track for high speed trains. 2D approach.. *5th Intl Worksop on Application of Computational Mechanics on Geotechnical Engineering 4.*

Correia, et al., 2007. Dynamic analysis of rail track for high speed trains. 2D approach.. *5th Intl Worksop on Application of Computational Mechanics on Geotechnical Engineering 4.*

Coulier, P. et al., 2013. *Stiff wave barriers for the mitigation of railway induced vibration,* s.l.: Proc. IWRN 11, Uddevalla.

Coulier, P. et al., 2014. Design and performance of a stiff wave barrier in the soil. *In Proceedings of International Symposium on Railway Geotechnical Engineering, vol. 2,,* pp. 505-514.

Coulier, P., François, S., Degrande, G. & Lombaert, G., 2013. Subgrade stiffening next to the track as a wave impeding barrier for railway induced vibrations. *Soil Dynamics and Earthquake Engineering 48,* pp. 119-131.

Dawn, T., (1983). Ground vibrations from heavy freight trains.. *Journal of sound and vibration 87, no. 2* , pp. 351-356..

Dawn, T. & Stanworth, C., 1979. Ground vibrations from passing trains. *Journal of sound and vibration 66, no. 3,* pp. 355-362.

Deutsche Bahn, A. G. a. T. H.-J., 2011. *State of the Art Review of Mitigation Measures on Track Deliverable D3. 1.,* Paris: International Union of Railways.

Dieterman, H. A. & Metrikine, V., 1997. Steady-state displacements of a beam on an elastic half-space due to a uniformly moving constant load.. *EUROPEAN JOURNAL OF MECHANICS SERIES A SOLIDS 16,* pp. 295-306..

Dijckmans, A. et al., 2015. Mitigation of railway induced ground vibration by heavy masses next to the track. *Soil Dynamics and Earthquake Engineering 75,* pp. 158-170.

Dong, K. et al., 2019. Non-linear soil behaviour on high speed rail lines. *Computers and Geotechnics 112,* pp. 302-318.

Duffy, D. G., 1990. The response of an infinite railroad track to a moving vibrating mass. *Journal of applied mechanics 57(1),* pp. 66-73.

Galvín, P. et al., 2010. A 2.5 D coupled FE-BE model for the prediction of railway induced vibrations. *Soil Dynamics and Earthquake Engineering 30.12,* pp. 1500-1512.

Gautier, P.-E., 2015. Slab track: Review of existing systems and optimization potentials including very high speed. *Construction and Building Materials 92,* pp. 9-15.

Gupta, S. et al., 2007. A comparison of two numerical models for the prediction of vibrations from underground railway traffic.. *Soil Dynamics and Earthquake Engineering, 27(7),* pp. 608-624.

Gupta, S. et al., 2008. Prediction of vibrations induced by underground railway traffic in Beijing. *Journal of sound and vibration 310(3),* pp. 608-630.

Gupta, S., Morris, D., Patel, S. & Tan, D., 2012. Soundwave: using the dopples effect to sense gestures. *Proceedings of SIGCHI Conference on Human Factors in Computing Systems,* pp. 1911-1914.

Hall, L., 2000. *Simulations and analyses of train-induced ground vibrations,* Stockholm 4: Division of Soil and Rock Mechanics, Royal Institute of Technology.

Hall, L., 2003. Simulations and analyses of train-induced ground vibrations in finite element models. *Soil Dynamics and Earthquake Engineering 23, no. 5,* pp. 403-413.

Hermans, l. (., 2010. Physics in daily life: brave ducks. *Europhysics News Vol. 41, No. 3,* p. 29.

Irvine, T., 2004. Damping properties of materials, revision D. *Magnesium 5000, no. 3100,* pp. 10-4.

Janssen, S. et al., 2015. Annoyance due to vibration from freight railway lines in the Netherlands and Poland. *10th European Congress and Exposition on Noise Control Engineering.*

Jiang, H. et al., 2014. Simulating train moving loads in physical model testing of railway infrastructure and its numerical calibration. *Acta Geotechnica,* pp. 11(2), 231-242..

Jiang, J. et al., 2013. *Reducing railway induced ground-born vibrations by using trenches and burried soft barriers,* s.l.: Proc. IWRN 11, Uddevalla.

Karlström, A., 2006. An analytical model for ground vibrations from accelerating trains. *Journal of Sound and Vibration 293, no. 3-5* , pp. 587-598.

Kausel, E., 1986. Wave propagation in anisotropic layered media.. *nternational Journal for Numerical Methods in Engineering, 23(8),* pp. 1567-1578.

Kenny, J., 1954. Steady state vibrations for moving load. *Journal of Applied Mechanics 76,* pp. 359-364.

Lee, H. P., 1994. Dynamic response of a beam with intermedite point constrains subject to a moving load. *Journal of sound and vibration 171, no. 3* , pp. 361-368.

Lee, H. P., 1998. Dynamic response of a Timoshenko beam on a Winkler foundation subjected to a moving mass.. *Applied Acoustics 55, no. 3,* pp. 203-215.

Lombaert, G., Degrande, S. François, and D. J. , G., François, S. & Thompson, D. J., 2015. *Ground-borne vibration due to railway traffic: a review of excitation mechanisms, prediction methods and mitigation measures*.. Berlin, Heidelberg,, Springer, pp. 253-287.

Madhus, C. & Kaynia, A., 2000. High-speed railway lines on soft ground: dynamic behaviour at critical train speed. *Journal of Sound and Vibration 231(3),* pp. 689-701.

Maes, J., Sol, H. & Guillaume, P., 2006. Measurements of the dynamic railpad properties. *Journal of Sound and Vibration 293, no. 3-5,* pp. 557-565.

Metrikine, A. V. & Vrouwenvelder, A. C. W. M., 2000. Surface ground vibration due to a moving train in a tunnel: two-dimensional model.. *Journal of Sound and vibration 234, no. 1,* pp. 43-66.

Metroor, n.d. *The monoligger type brand 2 (14-002).* [Online]
Available at: https://www.meteoor.nl/producten/heavyrail/dwarsliggers-heavyrail/monoliggers-type-merk-2/
[Accessed 03 03 2019].

Milne, et al., 2017. Properties of train load frequencies and their applications. *Journal of Sound and Vibration 397,* pp. 123-140.

Nejati, H. R., Morteza, A. & Hashemolhosseini, H., 2012. Numerical analysis of ground surface vibration induced by underground train movement. *Tunnelling and Underground Space Technology 29,* pp. 1-9.

Oregui, M., Zili, L. & Rolf, D., 2016. An investigation into the vertical dynamics of tracks with monoblock sleepers with a 3D finite-element model. *Proceedings of the Institution of Mechanical Engineers, Part F: Journal of Rail and Rapid Transit 230.3,* pp. 891-908.

Patil, S. P., 1988. Response of infinite railroad track to vibrating mass.. *Journal of engineering mechanics 114, no. 4* , pp. 688-703.

Paul de Vos, S., 2017. *Railway induced vibration, state of the art,* s.l.: International Union of Railways.

Physics, B. T. S. B. -. T., 2017. *steemit.* [Online]
Available at: https://steemit.com/science/@cjrc97/breaking-the-sound-barrier-the-physics?fbclid=iwar3emgo95wpl4aw4w_62nd5knqbig6ydrj6zrlqu56hmb9qutldvm1pbr9w
[Accessed 26 10 2019].

Physics, O. U., 2019. *University Physics Volume 1.* s.l.:s.n.

Poznan, K., 2015. *Konbet Poznan.* [Online]
Available at: http://www.konbet.com.pl/SYSTEMY_STROPOWE_TERIVA_FAMILY,1682.html
[Accessed 09 2019].

Rail.one - the way to go, 2014. *concrete sleepers,* Neumarkt: s.n.

Real, T. et al., 2015. 1525. Optimized design of an asphalt mixture railway track for vibration attenuation. Study of the dynamic performance. *Journal of vibroengineering 17, no. 1* .

Ruiz, J. F. et al., 2016. Study of ground vibrations induced by railway traffic in a 3D FEM model formulated in the time domain: experimental validation. *Structure and Infrastructure Engineering,* pp. 13(5), 652-664.

Sadeghi, J. & Hasheminezhad, A., 2014. Railway-induced Vibration Mitigation Measures in Urban Areas. *Caspian Journal of Applied Sciences Research 3, no. 5* .

Seebass, R., 1969. Sonic boon theory. *Journal of Aircraft 6, no. 3,* pp. 177-184.

Shahraki, M., Sadaghiani, ,. M. R. S., Witt, K. J. & Meier, T., 2014. 3D Modelling of Train Induced Moving Loads on an Embankment. *Plaxis Bulletin 36,* pp. 10-5.

Somda nl, 2010. *RailWiki.* [Online]
Available at: https://www.railwiki.nl/index.php?title=IRM_(InterRegio_Materieel)&action=info
[Accessed 10 03 2019].

Spijkers, J., Vrouwenvelder, A. & Klaver, E., 2005. *Structural Dynamics CT 4140 Part 1 - Structural Vibrations.* s.l.:Delft University of Technology Faculty of Civil Engineering and Geosciences.

Steenbergen, M., Metrikine, A. & Esveld, C., 2007. Assessment of design parameters of a slab track railway system from a dynamic viewpoint. *Journal of Sound and Vibration 306, no. 1-2* , pp. 361-371.

Sutherland, H. B., 1950. A study of vibrations produced in structures by heavy vehicles. *Proceedings of the Thirtieth Annual Meeting of the Highway Research Board 30,* pp. 406- 419..

Takemiya, H., 2003. Simulation of track-ground vibrations due to a high-speed train: the case of X-2000 at Ledsgard. *Journal of Sound and Vibration 261(3),* pp. 503-526.

Tatara, T. & Kozuch, B., 2017. The environmental impact of the vibration induced by the passage of trains at various speeds. *Procedia engineering 199,* pp. 2693-2698.

van Dalen, K. N., 2015. *Lecture notes CIE5340 Soil Dynamics, part B: Body waves in an elastic continuum & Rayleigh waves at the free surface.* s.l.:TU Delft.

Verbraken, H., Lombaert, G. & Degrande, G., 2011. Verification of an empirical prediction method for railway induced vibrations by means of numerical simulations.. *Journal of Sound and Vibration 330, no. 8 (,* pp. 1692-1703..

Waikato, U. o., n.d. *Science Learning Hub - Pokapu Akoranga Putaiao.* [Online]
Available at: https://www.sciencelearn.org.nz/images/353-earth-waves
[Accessed 11 2019].

Weatherby, B., Born , W. & Harding, R., 1934. Granite and limestone velocity determinations in Arbuckle Mountains, Oklahoma.. *AAPG Bulletin 18, no. 1,* pp. 106-118..

Wilson , G., Saurenman, H. & Nelson, J., 1983. Control of ground-borne noise and vibration. *Journal of Sound and Vibration 87 no.2,* pp. 339-350.

With, C., Bahrekazemi, M. & Bodare, A., 2006. Validation of an empirical model for prediction of train-induced ground vibrations.. *Soil Dynamics and Earthquake Engineering 26, no. 11,* pp. 983-990..

Xia, H. et al., 2009. Experimental investigation of railway train-induced vibrations of surrounding ground and a nearby multi-story building.. *Earthquake engineering and engineering vibration 8, no. 1,* pp. 137-148.

Yang, Y., Hung, H. H. & Chang, D., 2003. Train-induced wave propagation in layered soils using finite/infinite element simulation. *Soil Dynamics and Earthquake Engineering, 23(4),,* pp. 263-278.

Appendix A

Material properties

Appendix A contains additional information to Chapter 3 and 4. Rail and sleepers properties are presented in more details by providing manufacturer specifications. Moreover, how these parameters are inserted to Plaxis 3D is shown. Additionally, detailed drawing of VIRM train is presented.

A1 – Sleepers NS90 and 14-002 properties

Parameters	Unit
Permissible axle loads	25 t
Maximum speed	250 km/h
Concrete grade	C 50/60
Concrete volume	112 l
Weight (without fastenings)	276 kg
Length (L)	2520 mm
Width (W)	300 mm
Sleeper height (H)	232.9 mm
Height of centre of rail base (h_1)	214 mm
Height of sleeper centre (h_2)	175 mm
Support surface (total)	6537 cm²
Standard application	Main-track sleeper

AP. A Figure 1 NS90 sleeper type (Rail.one - the way to go, 2014) and its properties

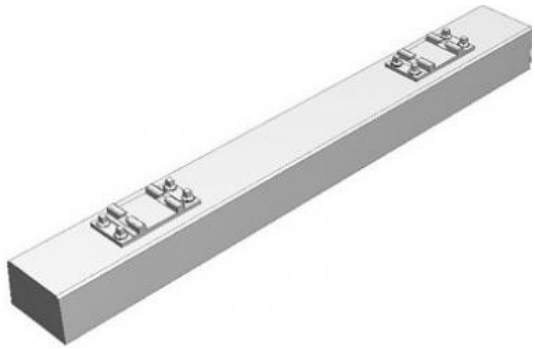

	Length	Width	Thickness	Weight
Brand type 2	2500 mm	300/280 mm	200 mm	369 kg

Concrete quality	C50 / 60
Environmental class	XC4, XD3, XS1, XF4
Certification	SPC00094 and NEN-EN 13230-1 & 4

AP. A Figure 2 14-002 (Metroor, n.d.) type sleeper and its properties

A2 – Cross-section and properties of rail UIC54

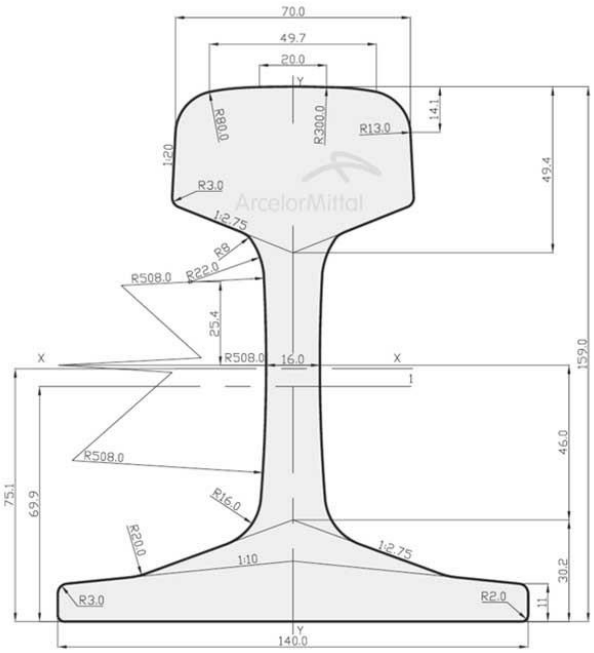

Type of Rail	Standard	Dimensions mm					Section S	Mass m
		H	B	C	D	E	cm²	kg/m
54E1 (UIC54)	EN 13674 - 1	159,00	140,00	70,00	49,40	16,00	69,77	54,77

AP. A Figure 3 Rail UIC54 and its properties (Arcelor Mittal, n.d.)

A3 – Addressing sleepers properties in Plaxis 3D

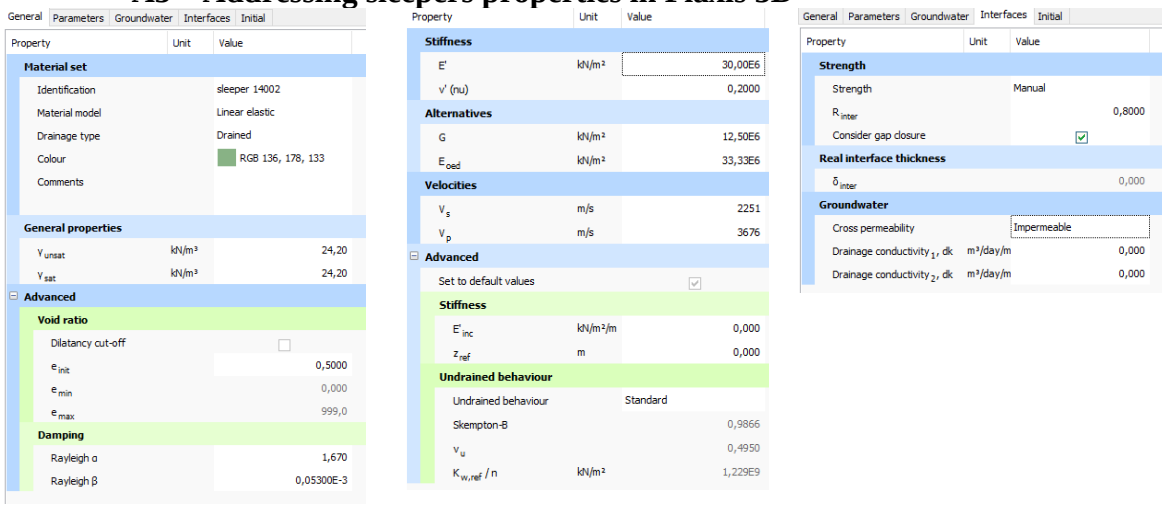

AP. A Figure 4 Properties of 14-002 sleeper

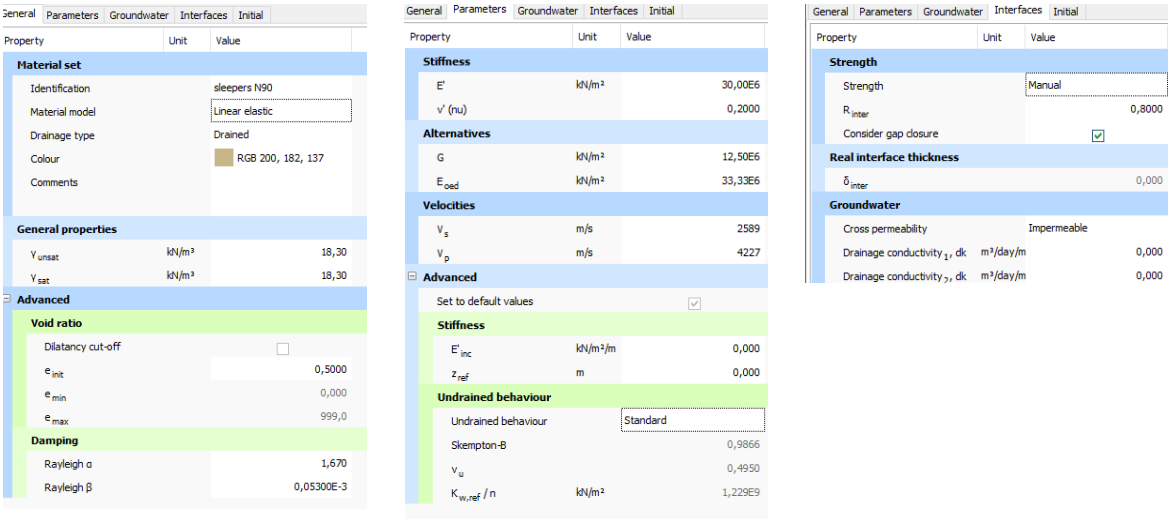

5 Properties of NS90 sleeper

A3 – VIRM train drawing

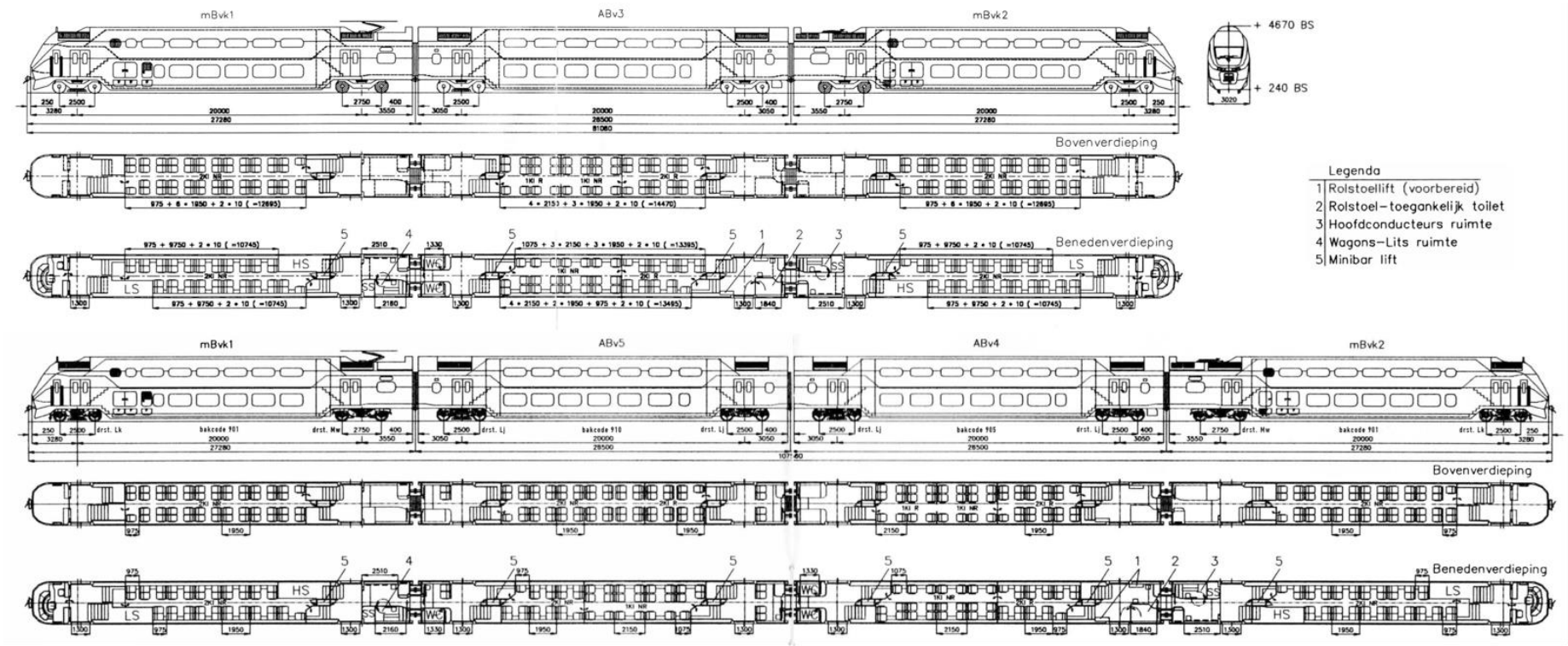

AP. A Figure 6 Detailed drawings of the VIRM train carriages (Somda nl, 2010)

Appendix B

Simulations steps settings

Appendix B includes settings of non-dynamic simulation stages which are performed before activation of the load. It is an extension of section 4.6 where each phase is described in more details.

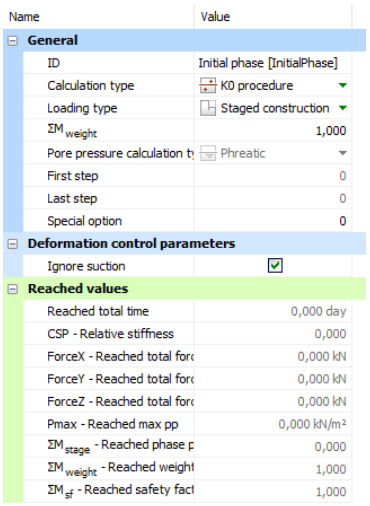

Name	Value
General	
ID	Initial phase [InitialPhase]
Calculation type	K0 procedure
Loading type	Staged construction
ΣM_{weight}	1,000
Pore pressure calculation ty	Phreatic
First step	0
Last step	0
Special option	0
Deformation control parameters	
Ignore suction	☑
Reached values	
Reached total time	0,000 day
CSP - Relative stiffness	0,000
ForceX - Reached total forc	0,000 kN
ForceY - Reached total forc	0,000 kN
ForceZ - Reached total forc	0,000 kN
Pmax - Reached max pp	0,000 kN/m²
ΣM_{stage} - Reached phase p	0,000
ΣM_{weight} - Reached weight	1,000
ΣM_{sf} - Reached safety fact	1,000

AP. B Figure 1 Settings for Initial Phase

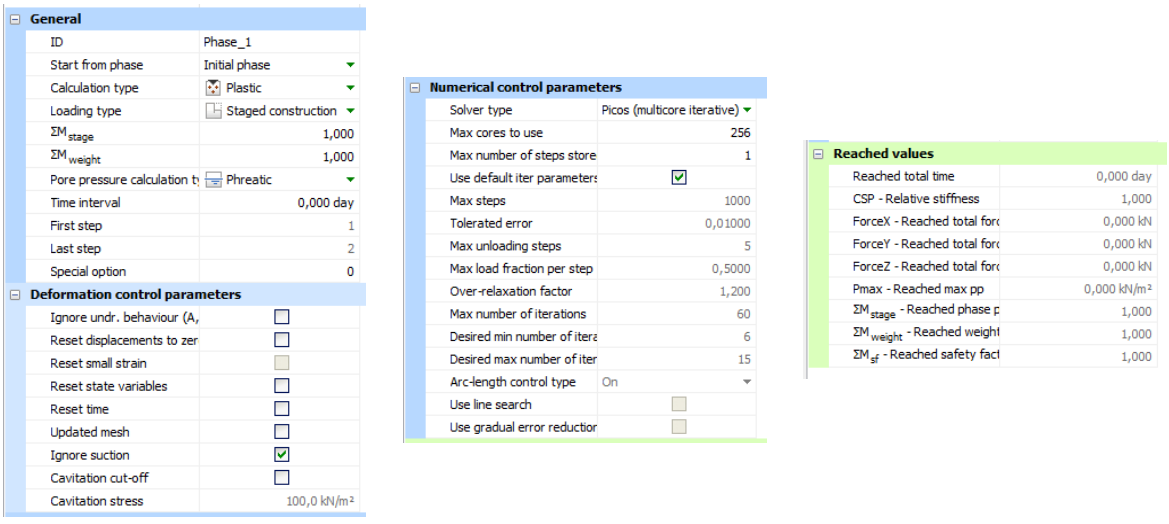

General	
ID	Phase_1
Start from phase	Initial phase
Calculation type	Plastic
Loading type	Staged construction
ΣM_{stage}	1,000
ΣM_{weight}	1,000
Pore pressure calculation ty	Phreatic
Time interval	0,000 day
First step	1
Last step	2
Special option	0
Deformation control parameters	
Ignore undr. behaviour (A,	☐
Reset displacements to zer	☐
Reset small strain	☐
Reset state variables	☐
Reset time	☐
Updated mesh	☐
Ignore suction	☑
Cavitation cut-off	☐
Cavitation stress	100,0 kN/m²

Numerical control parameters	
Solver type	Picos (multicore iterative)
Max cores to use	256
Max number of steps store	1
Use default iter parameters	☑
Max steps	1000
Tolerated error	0,01000
Max unloading steps	5
Max load fraction per step	0,5000
Over-relaxation factor	1,200
Max number of iterations	60
Desired min number of itera	6
Desired max number of iter	15
Arc-length control type	On
Use line search	☐
Use gradual error reductior	☐

Reached values	
Reached total time	0,000 day
CSP - Relative stiffness	1,000
ForceX - Reached total forc	0,000 kN
ForceY - Reached total forc	0,000 kN
ForceZ - Reached total forc	0,000 kN
Pmax - Reached max pp	0,000 kN/m²
ΣM_{stage} - Reached phase p	1,000
ΣM_{weight} - Reached weight	1,000
ΣM_{sf} - Reached safety fact	1,000

AP. B Figure 2 Settings for Phase_1

Name	Value
General	
ID	Phase_3
Start from phase	Phase_1
Calculation type	Plastic
Loading type	Staged construction
ΣM_{stage}	1,000
ΣM_{weight}	1,000
Pore pressure calculation t	Phreatic
Time interval	0,000 day
First step	3
Last step	4
Special option	0
Deformation control parameters	
Ignore undr. behaviour (A,	☐
Reset displacements to zer	☐
Reset small strain	☐
Reset state variables	☐
Reset time	☐
Updated mesh	☐
Ignore suction	☑
Cavitation cut-off	☐
Cavitation stress	100,0 kN/m²

Numerical control parameters	
Solver type	Picos (multicore iterative)
Max cores to use	256
Max number of steps store	1
Use default iter parameters	☑
Max steps	1000
Tolerated error	0,01000
Max unloading steps	5
Max load fraction per step	0,5000
Over-relaxation factor	1,200
Max number of iterations	60
Desired min number of itera	6
Desired max number of iter	15
Arc-length control type	On
Use line search	☐
Use gradual error reductior	☐

Reached values	
Reached total time	0,000 day
CSP - Relative stiffness	1,000
ForceX - Reached total forc	0,000 kN
ForceY - Reached total forc	0,000 kN
ForceZ - Reached total forc	0,000 kN
Pmax - Reached max pp	0,000 kN/m²
ΣM_{stage} - Reached phase p	1,000
ΣM_{weight} - Reached weight	1,000
ΣM_{sf} - Reached safety fact	1,000

AP. B Figure 3 Settings for Phase_3

General	
ID	Phase_4
Start from phase	Phase_3
Calculation type	Plastic
Loading type	Staged construction
ΣM_{stage}	1,000
ΣM_{weight}	1,000
Pore pressure calculation t	Phreatic
Time interval	0,000 day
First step	5
Last step	6
Special option	0
Deformation control parameters	
Ignore undr. behaviour (A,	☐
Reset displacements to zer	☐
Reset small strain	☐
Reset state variables	☐
Reset time	☐
Updated mesh	☐
Ignore suction	☑
Cavitation cut-off	☐
Cavitation stress	100,0 kN/m²

Numerical control parameters	
Solver type	Picos (multicore iterative)
Max cores to use	256
Max number of steps store	1
Use default iter parameters	☑
Max steps	1000
Tolerated error	0,01000
Max unloading steps	5
Max load fraction per step	0,5000
Over-relaxation factor	1,200
Max number of iterations	60
Desired min number of itera	6
Desired max number of iter	15
Arc-length control type	On
Use line search	☐
Use gradual error reductior	☐

Reached values	
Reached total time	0,000 day
CSP - Relative stiffness	1,000
ForceX - Reached total forc	0,000 kN
ForceY - Reached total forc	0,000 kN
ForceZ - Reached total forc	0,000 kN
Pmax - Reached max pp	0,000 kN/m²
ΣM_{stage} - Reached phase p	1,000
ΣM_{weight} - Reached weight	1,000
ΣM_{sf} - Reached safety fact	1,000

AP. B Figure 4 Settings for Phase_4

General	
ID	Phase_5
Start from phase	Phase_4
Calculation type	Plastic
Loading type	Staged construction
ΣM_{stage}	1,000
ΣM_{weight}	1,000
Pore pressure calculation t	Phreatic
Time interval	0,000 day
First step	7
Last step	8
Special option	0
Deformation control parameters	
Ignore undr. behaviour (A,	☐
Reset displacements to zer	☐
Reset small strain	☐
Reset state variables	☐
Reset time	☐
Updated mesh	☐
Ignore suction	☑
Cavitation cut-off	☐
Cavitation stress	100,0 kN/m²

Numerical control parameters	
Solver type	Picos (multicore iterative)
Max cores to use	256
Max number of steps store	1
Use default iter parameters	☑
Max steps	1000
Tolerated error	0,01000
Max unloading steps	5
Max load fraction per step	0,5000
Over-relaxation factor	1,200
Max number of iterations	60
Desired min number of itera	6
Desired max number of iter	15
Arc-length control type	On
Use line search	☐
Use gradual error reductior	☐

Reached values	
Reached total time	0,000 day
CSP - Relative stiffness	1,000
ForceX - Reached total forc	0,000 kN
ForceY - Reached total forc	0,000 kN
ForceZ - Reached total forc	0,000 kN
Pmax - Reached max pp	0,000 kN/m²
ΣM_{stage} - Reached phase p	0,9999
ΣM_{weight} - Reached weight	1,000
ΣM_{sf} - Reached safety fact	1,000

AP. B Figure 5 Settings for Phase_5

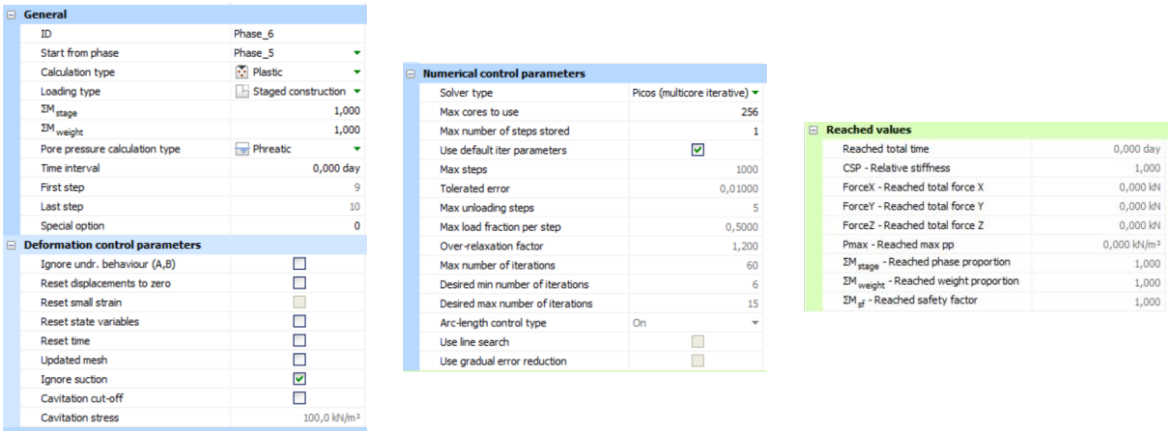

General	
ID	Phase_6
Start from phase	Phase_5
Calculation type	Plastic
Loading type	Staged construction
ΣM_{stage}	1,000
ΣM_{weight}	1,000
Pore pressure calculation type	Phreatic
Time interval	0,000 day
First step	9
Last step	10
Special option	0

Deformation control parameters	
Ignore undr. behaviour (A,B)	☐
Reset displacements to zero	☐
Reset small strain	☐
Reset state variables	☐
Reset time	☐
Updated mesh	☐
Ignore suction	☑
Cavitation cut-off	☐
Cavitation stress	100,0 kN/m²

Numerical control parameters	
Solver type	Picos (multicore iterative)
Max cores to use	256
Max number of steps stored	1
Use default iter parameters	☑
Max steps	1000
Tolerated error	0,01000
Max unloading steps	5
Max load fraction per step	0,5000
Over-relaxation factor	1,200
Max number of iterations	60
Desired min number of iterations	6
Desired max number of iterations	15
Arc-length control type	On
Use line search	☐
Use gradual error reduction	☐

Reached values	
Reached total time	0,000 day
CSP - Relative stiffness	1,000
ForceX - Reached total force X	0,000 kN
ForceY - Reached total force Y	0,000 kN
ForceZ - Reached total force Z	0,000 kN
Pmax - Reached max pp	0,000 kN/m²
ΣM_{stage} - Reached phase proportion	1,000
ΣM_{weight} - Reached weight proportion	1,000
ΣM_{sf} - Reached safety factor	1,000

AP. B Figure 6 Settings for Phase_6

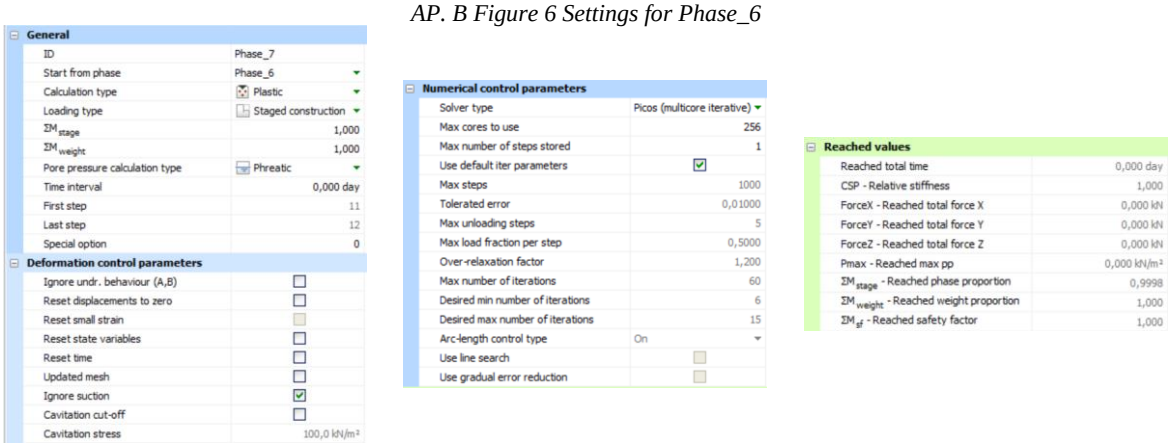

General	
ID	Phase_7
Start from phase	Phase_6
Calculation type	Plastic
Loading type	Staged construction
ΣM_{stage}	1,000
ΣM_{weight}	1,000
Pore pressure calculation type	Phreatic
Time interval	0,000 day
First step	11
Last step	12
Special option	0

Deformation control parameters	
Ignore undr. behaviour (A,B)	☐
Reset displacements to zero	☐
Reset small strain	☐
Reset state variables	☐
Reset time	☐
Updated mesh	☐
Ignore suction	☑
Cavitation cut-off	☐
Cavitation stress	100,0 kN/m²

Numerical control parameters	
Solver type	Picos (multicore iterative)
Max cores to use	256
Max number of steps stored	1
Use default iter parameters	☑
Max steps	1000
Tolerated error	0,01000
Max unloading steps	5
Max load fraction per step	0,5000
Over-relaxation factor	1,200
Max number of iterations	60
Desired min number of iterations	6
Desired max number of iterations	15
Arc-length control type	On
Use line search	☐
Use gradual error reduction	☐

Reached values	
Reached total time	0,000 day
CSP - Relative stiffness	1,000
ForceX - Reached total force X	0,000 kN
ForceY - Reached total force Y	0,000 kN
ForceZ - Reached total force Z	0,000 kN
Pmax - Reached max pp	0,000 kN/m²
ΣM_{stage} - Reached phase proportion	0,9998
ΣM_{weight} - Reached weight proportion	1,000
ΣM_{sf} - Reached safety factor	1,000

AP. B Figure 7 Settings for Phase_7

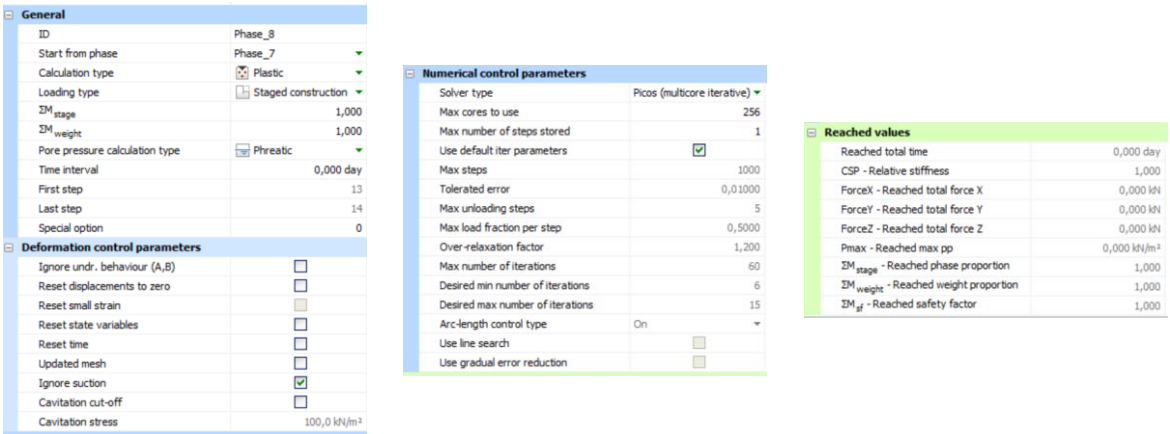

General	
ID	Phase_8
Start from phase	Phase_7
Calculation type	Plastic
Loading type	Staged construction
ΣM_{stage}	1,000
ΣM_{weight}	1,000
Pore pressure calculation type	Phreatic
Time interval	0,000 day
First step	13
Last step	14
Special option	0

Deformation control parameters	
Ignore undr. behaviour (A,B)	☐
Reset displacements to zero	☐
Reset small strain	☐
Reset state variables	☐
Reset time	☐
Updated mesh	☐
Ignore suction	☑
Cavitation cut-off	☐
Cavitation stress	100,0 kN/m²

Numerical control parameters	
Solver type	Picos (multicore iterative)
Max cores to use	256
Max number of steps stored	1
Use default iter parameters	☑
Max steps	1000
Tolerated error	0,01000
Max unloading steps	5
Max load fraction per step	0,5000
Over-relaxation factor	1,200
Max number of iterations	60
Desired min number of iterations	6
Desired max number of iterations	15
Arc-length control type	On
Use line search	☐
Use gradual error reduction	☐

Reached values	
Reached total time	0,000 day
CSP - Relative stiffness	1,000
ForceX - Reached total force X	0,000 kN
ForceY - Reached total force Y	0,000 kN
ForceZ - Reached total force Z	0,000 kN
Pmax - Reached max pp	0,000 kN/m²
ΣM_{stage} - Reached phase proportion	1,000
ΣM_{weight} - Reached weight proportion	1,000
ΣM_{sf} - Reached safety factor	1,000

AP. B Figure 8 Settings for Phase_8

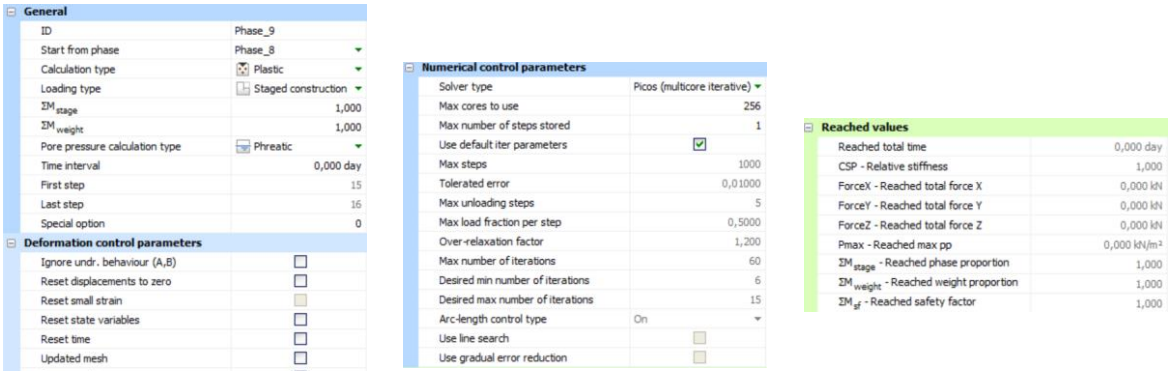

General	
ID	Phase_9
Start from phase	Phase_8
Calculation type	Plastic
Loading type	Staged construction
ΣM_{stage}	1,000
ΣM_{weight}	1,000
Pore pressure calculation type	Phreatic
Time interval	0,000 day
First step	15
Last step	16
Special option	0

Deformation control parameters	
Ignore undr. behaviour (A,B)	☐
Reset displacements to zero	☐
Reset small strain	☐
Reset state variables	☐
Reset time	☐
Updated mesh	☐
Ignore suction	☑
Cavitation cut-off	☐
Cavitation stress	100,0 kN/m²

Numerical control parameters	
Solver type	Picos (multicore iterative)
Max cores to use	256
Max number of steps stored	1
Use default iter parameters	☑
Max steps	1000
Tolerated error	0,01000
Max unloading steps	5
Max load fraction per step	0,5000
Over-relaxation factor	1,200
Max number of iterations	60
Desired min number of iterations	6
Desired max number of iterations	15
Arc-length control type	On
Use line search	☐
Use gradual error reduction	☐

Reached values	
Reached total time	0,000 day
CSP - Relative stiffness	1,000
ForceX - Reached total force X	0,000 kN
ForceY - Reached total force Y	0,000 kN
ForceZ - Reached total force Z	0,000 kN
Pmax - Reached max pp	0,000 kN/m²
ΣM_{stage} - Reached phase proportion	1,000
ΣM_{weight} - Reached weight proportion	1,000
ΣM_{sf} - Reached safety factor	1,000

AP. B Figure 9 Settings for Phase_9

Appendix C

Results of the variation study

Content of each of the subsection included in this appendix is briefly presented in AP. C Table 1. Results are shown for acceleration in time and frequency domain.

Model	Comparison
C1	comparison between three cases where train speed varies and load is simulated as triangular pulses
C2	comparison between models where load is simulated as triangular pulses and as moving point load
C3	comparison of models with shorter and longer duration of train passage
C4	comparison of models where subballast material is modelled as asphalt and crushed stone
C5	comparison of result for model where load is with and without 2Hz dynamic oscillatory component
C6	comparison between models where load has quasi static component only and quasi-static + 2Hz dynamic oscillatory load
C7	Results of the model where upper most layer is changed from 1m to 2m thick
C8	Results of models with and without compacted sand beneath ballast

AP. C Table 1 Overview of Appendix C content

C1 – Models in which load is simulated as triangular pulses

In this section results are presented for three models in which train runs at speed 100km/h, 115km/h and 130km/h. Graphs show acceleration value in time and frequency domain for points MP1-MP3. In these models load is simulated as series of triangular pulses.

For conclusions and graphs description reader is referred to section 5.3.1.

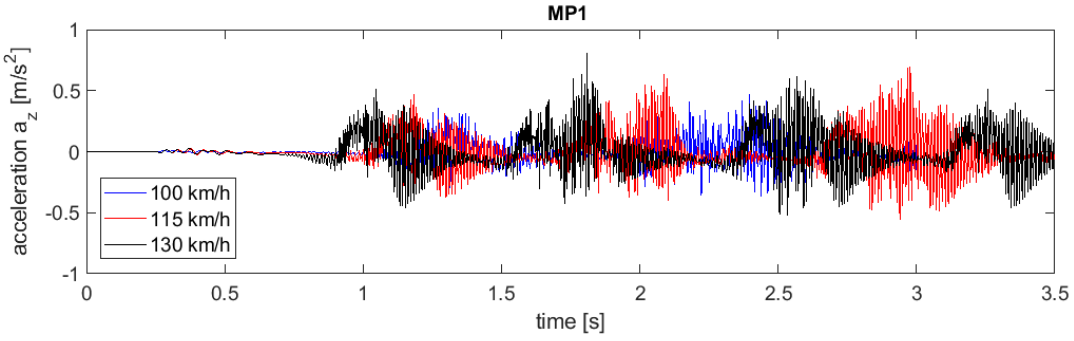

AP. C Figure 1 Acceleration at MP1 for numerical models with load representation as triangular pulses. Simulated train runs at speed 100, 115 and 130 km/h

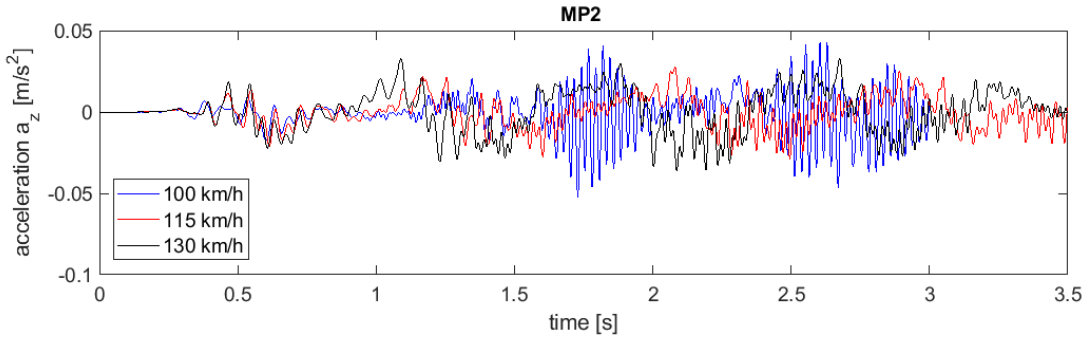

AP. C Figure 2 Acceleration at MP2 for numerical models with load representation as triangular pulses. Simulated train runs at speed 100, 115 and 130 km/h

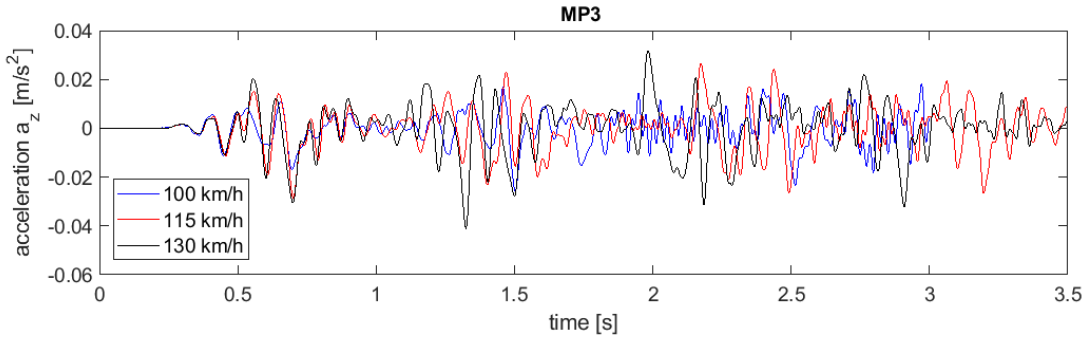

AP. C Figure 3 Acceleration at MP3 for numerical models with load representation as triangular pulses. Simulated train runs at speed 100, 115 and 130 km/h

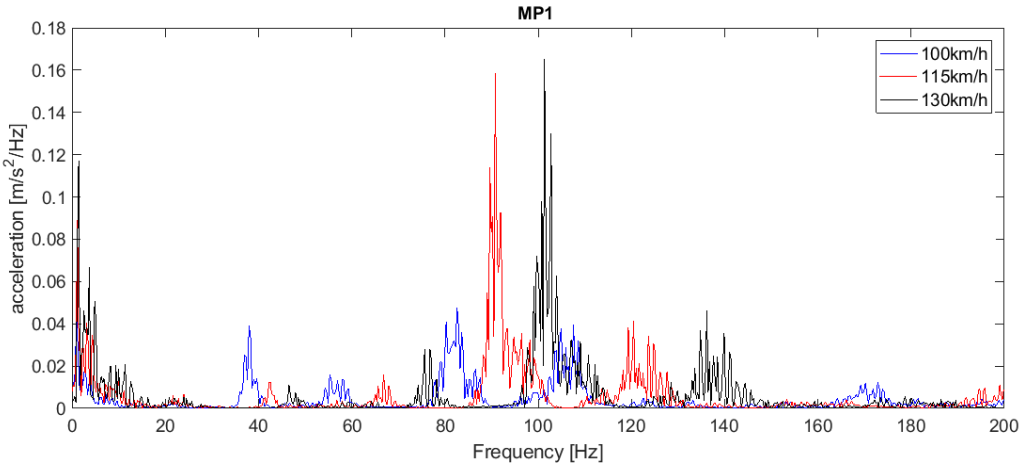

AP. C Figure 4 Spectrum of train with triangular load representation for different velocities at MP1

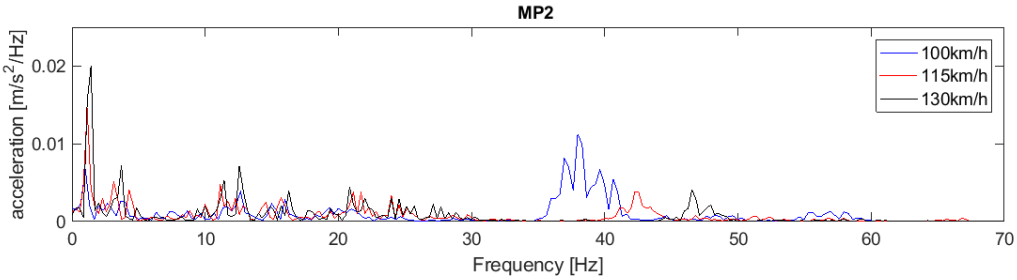

AP. C Figure 5 Spectrum of train with triangular load representation for different velocities at MP2

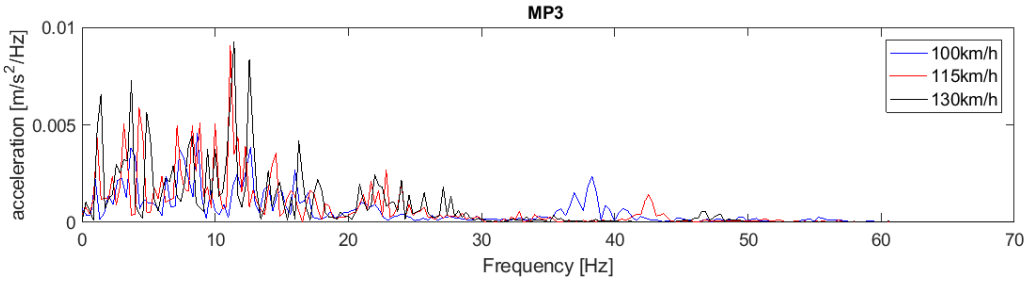

AP. C Figure 6 Spectrum of train with triangular load representation for different velocities at MP3

C2 – Comparison between model in which load is simulated as triangular pulses and model in which it is simulated as a moving point load

In this subsection graphs are presented for two models in which load is simulated differently. In first model load is defined as triangular pulses. In second model load is simulated as moving point load. In both cases train runs at speed 130 km/h. Triangular pulses include only quasi-static part of the load whereas in moving point load quasi-static as well as dynamic oscillatory load (with frequencies 60Hz and 2Hz) components are included. Acceleration results in time and frequency domain are considered.

For conclusions and graphs description reader is referred to section 5.3.2.1

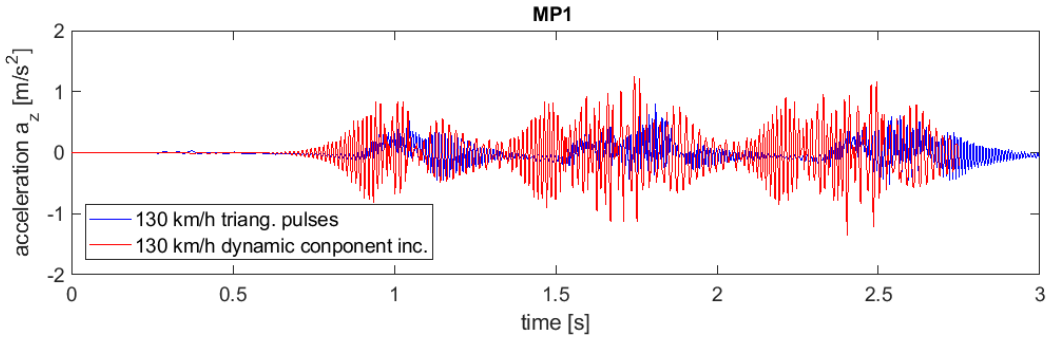

AP. C Figure 7 Comparison of acceleration in time domain at MP1 between model where loads are quasi-static and modelled as triangular pulses and model where loads have quasi-static and dynamic component modelled as moving point loads

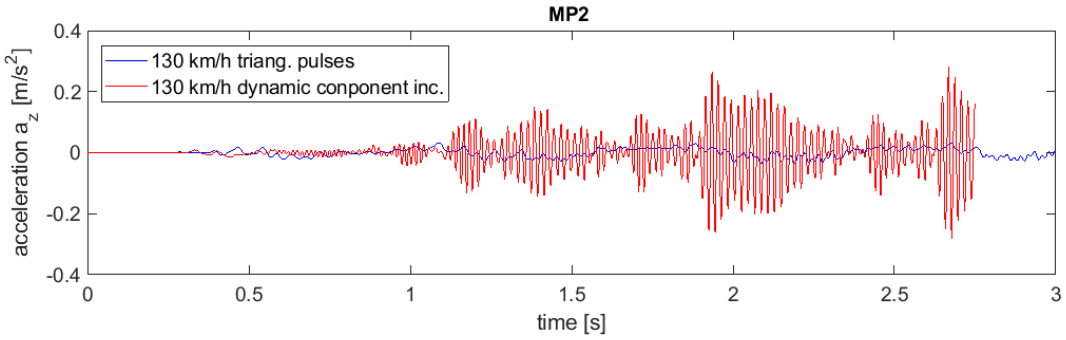

AP. C Figure 8 Comparison of acceleration in time domain at MP2 between model where loads are quasi-static and modelled as triangular pulses and model where loads have quasi-static and dynamic component modelled as moving point loads

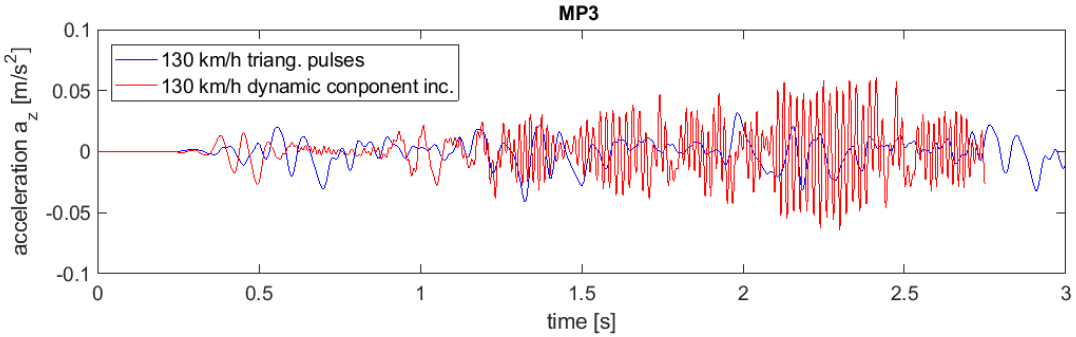

AP. C Figure 9 Comparison of acceleration in time domain at MP3 between model where loads are quasi-static and modelled as triangular pulses and model where loads have quasi-static and dynamic component modelled as moving point loads

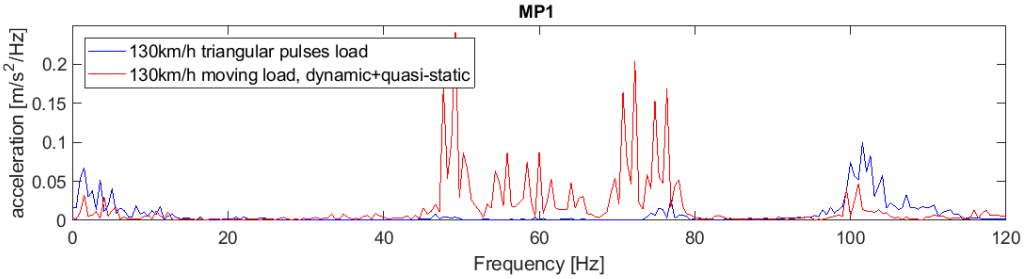

AP. C Figure 10 Comparison of acceleration in frequency domain at MP1 between model where loads are quasi-static and modelled as triangular pulses and model where loads have quasi-static and dynamic component modelled as moving point loads

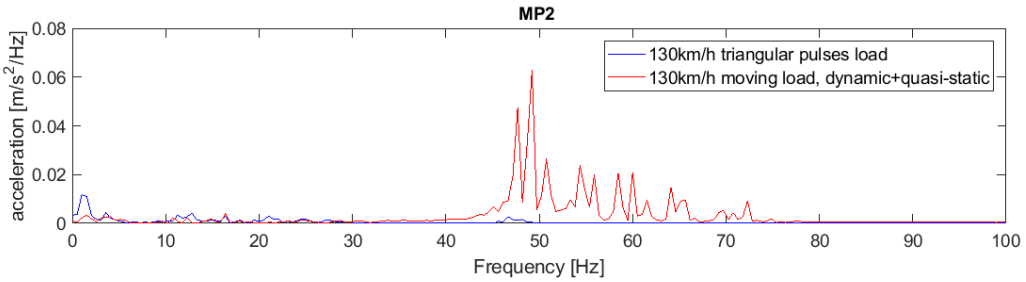

AP. C Figure 11 Comparison of acceleration in frequency domain at MP2 between model where loads are quasi-static and modelled as triangular pulses and model where loads have quasi-static and dynamic component modelled as moving point load

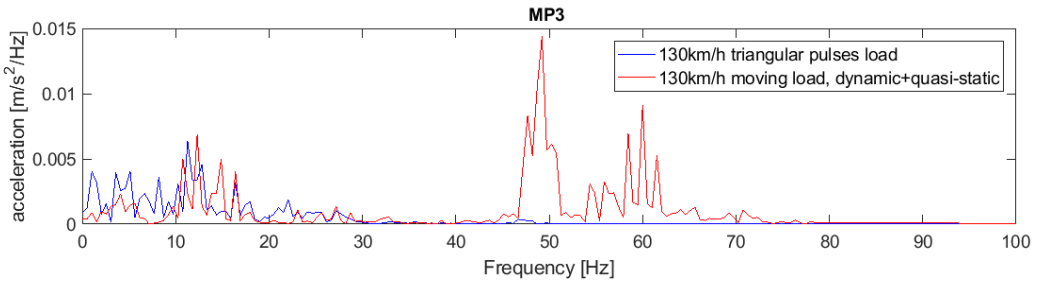

AP. C Figure 12 Comparison of acceleration in frequency domain at MP3 between model where loads are quasi-static and modelled as triangular pulses and model where loads have quasi-static and dynamic component modelled as moving point load

C3 – Longer duration of the simulation

In this section results of acceleration in time and frequency domain for longer and shorter train passage are shown. Longer signal lasts for 6.5s and 7 train wagons passes during this time, whereas short signal duration is 2.75s and 3 wagons passes. The load is simulated as moving point load consisted of quasi-static and dynamic oscillatory point load.

For conclusions and graphs description reader is referred to section 5.3.2.2.

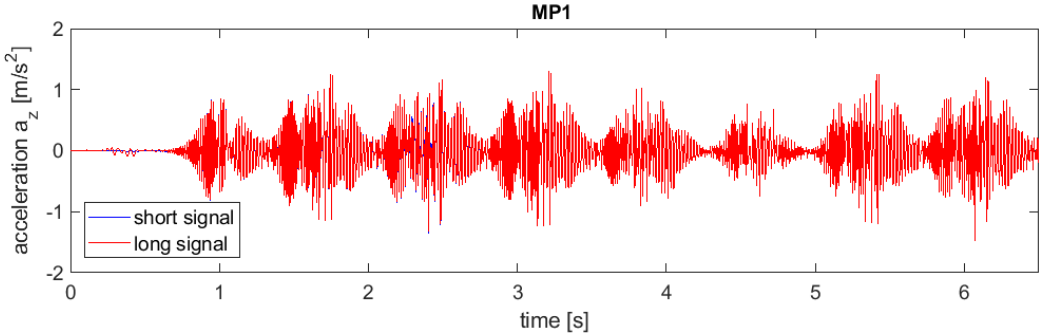

AP. C Figure 13 Comparison of the acceleration in time domain at MP1 for shorter and longer duration of the signal

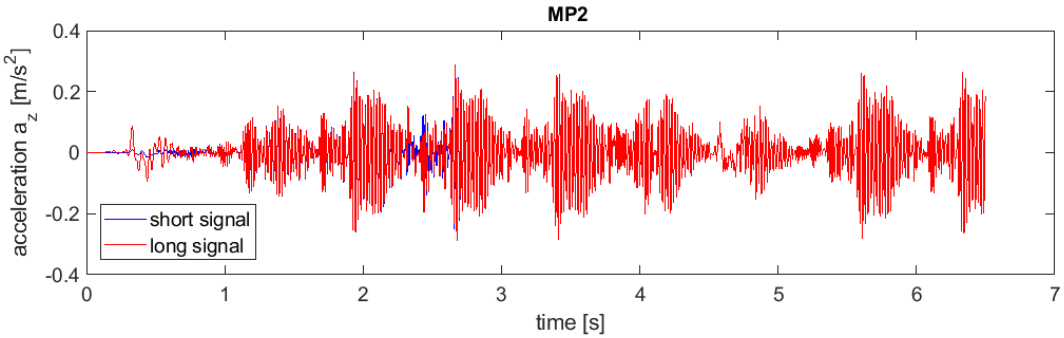

AP. C Figure 14 Comparison of the acceleration in time domain at MP2 for shorter and longer duration of the signal

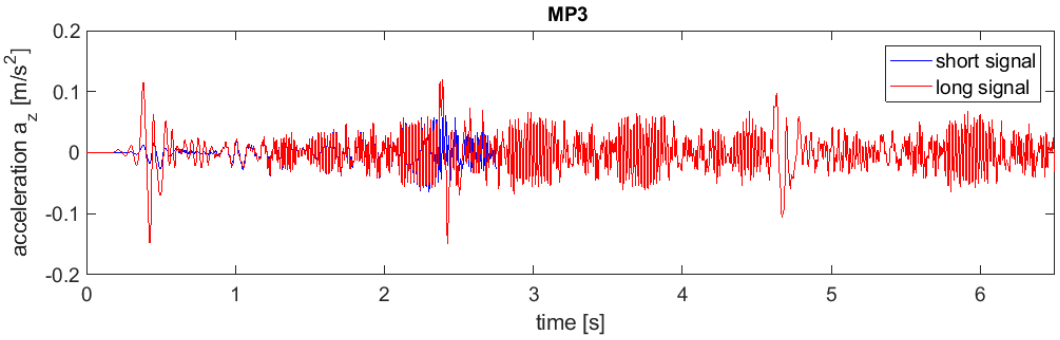

AP. C Figure 15 Comparison of the acceleration in time domain at MP3 for shorter and longer duration of the signal

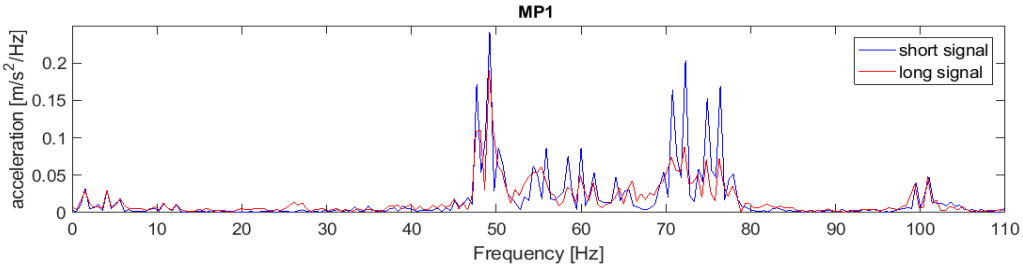

AP. C Figure 16 Comparison of the spectrum in frequency domain at MP1 for shorter and longer duration of the signal

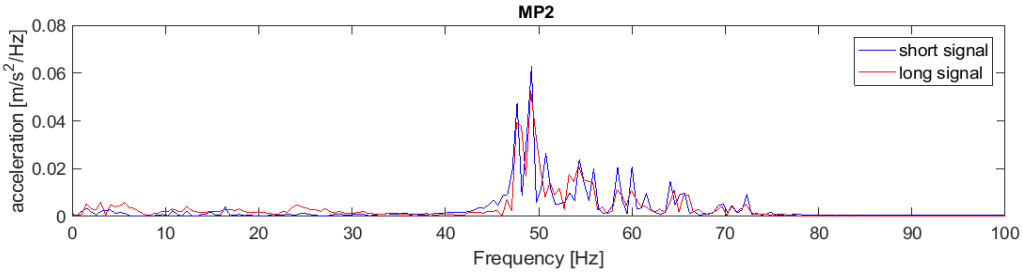

AP. C Figure 17 Comparison of the spectrum in frequency domain at MP2 for shorter and longer duration of the signal

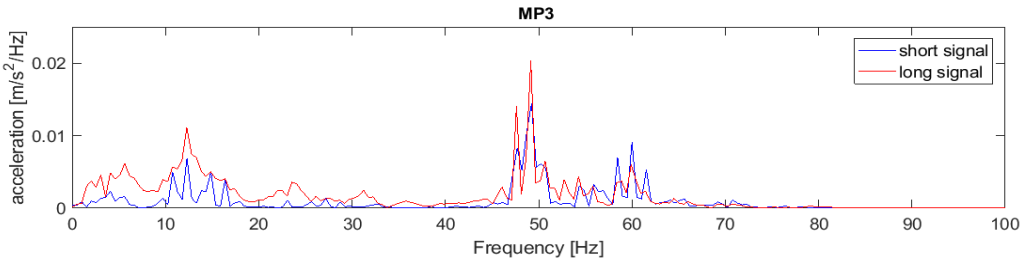

AP. C Figure 18 Comparison of the spectrum in frequency domain at MP3 for shorter and longer duration of the signal

C4 – Change of subballast material from asphalt to crushed stone

This subsection presents graphs where comparison between two models that differ only in subballast material. In first model subballast material is asphalt, in second one it is crushed stone. Materials parameters can be found in Table 3.2. Acceleration results in time and frequency domain are depicted for points MP1-3.

For conclusions and graphs description reader is referred to section 5.3.2.3.

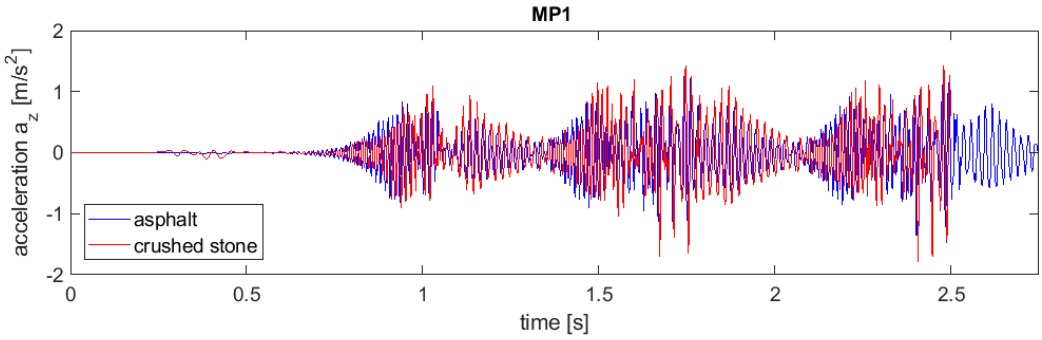

AP. C Figure 19 Comparison of acceleration at MP1 between system with asphalt or crushed stone used as subballast

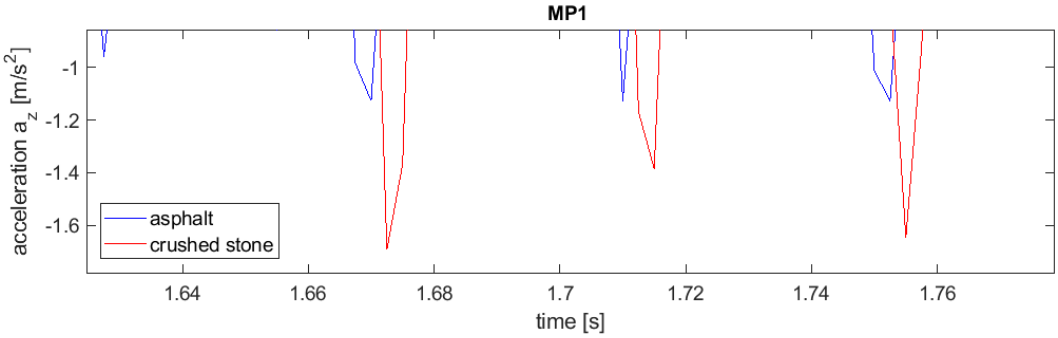

AP. C Figure 20 Inset of AP. C Figure 19

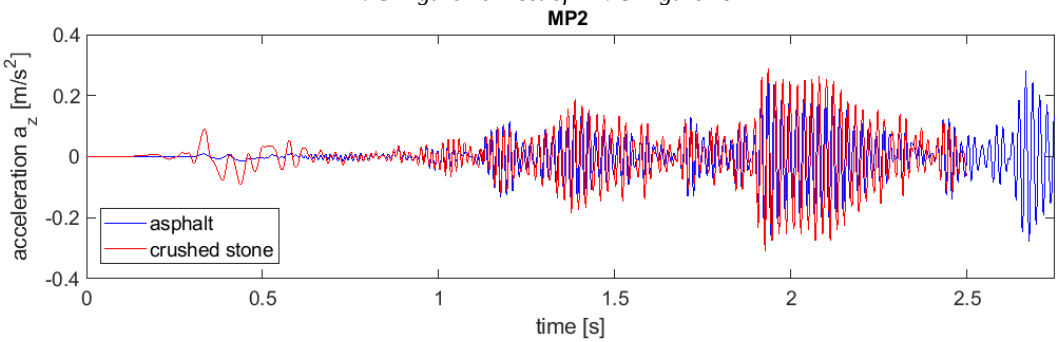

AP. C Figure 21 Comparison of acceleration at MP2 between system with asphalt or crushed stone used as subballast

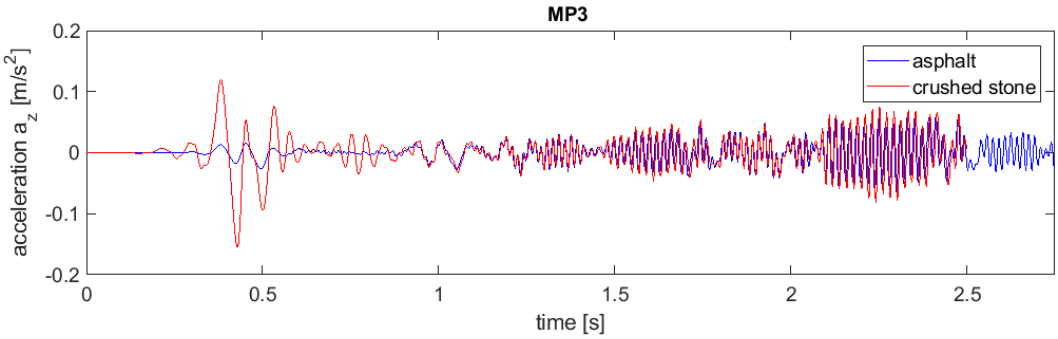

AP. C Figure 22 Comparison of acceleration at MP3 between system with asphalt or crushed stone used as subballast

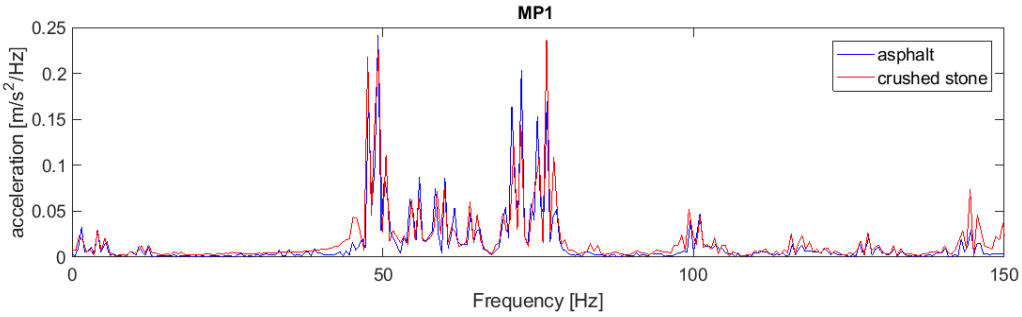

AP. C Figure 23 Comparison of spectrum at MP1 between system with asphalt or crushed stone used as subballast

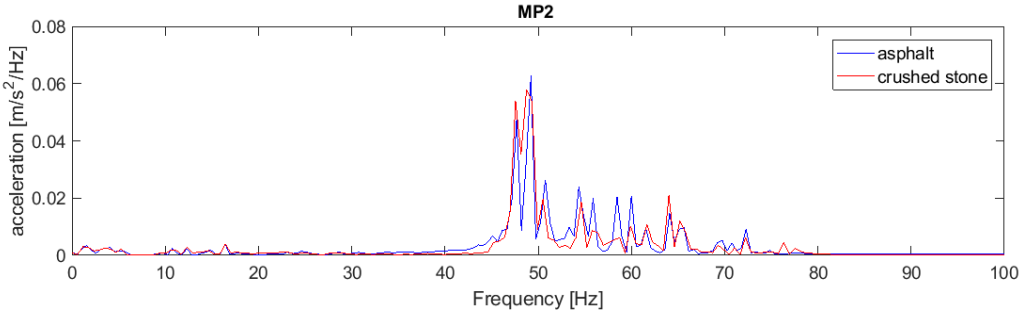

AP. C Figure 24 Comparison of spectrum at MP2 between system with asphalt or crushed stone used as subballast

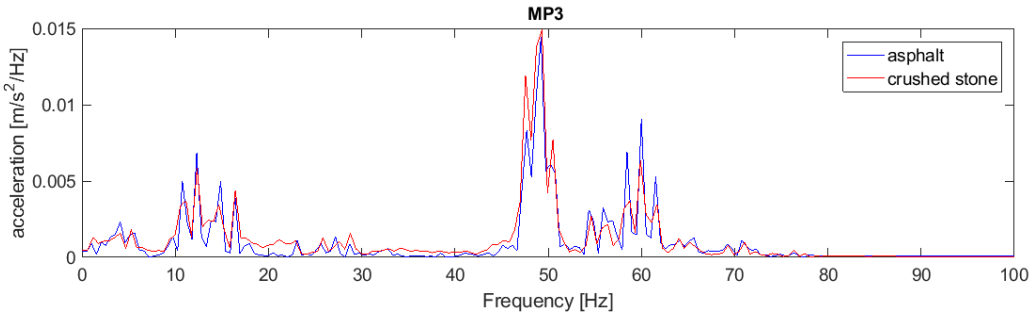

AP. C Figure 25 Comparison of spectrum at MP3 between system with asphalt or crushed stone used as subballast

C5 – Results of moving point load without 2Hz component

In the following section the results of models where load includes and excludes 2Hz oscillatory component are presented. Acceleration values are plotted in time and frequency domain for points MP1-3.

For conclusions and graphs description reader is referred to section 5.3.2.5.

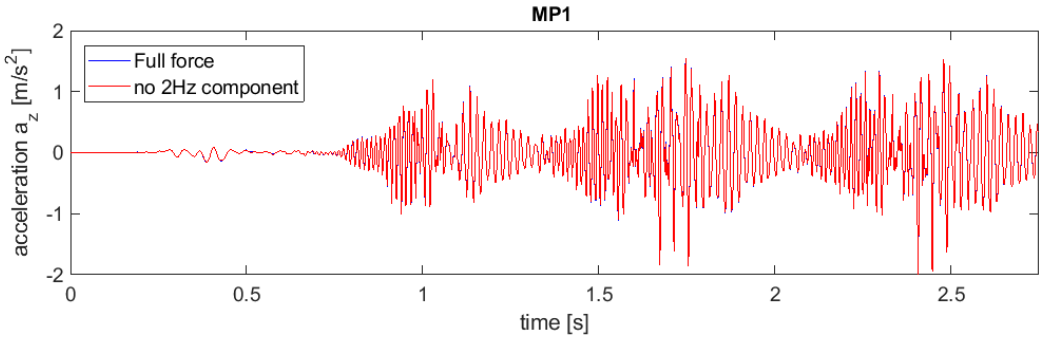

AP. C Figure 26 Comparison of accelerations in time domain between models with 2Hz oscillating component included and excluded at MP1

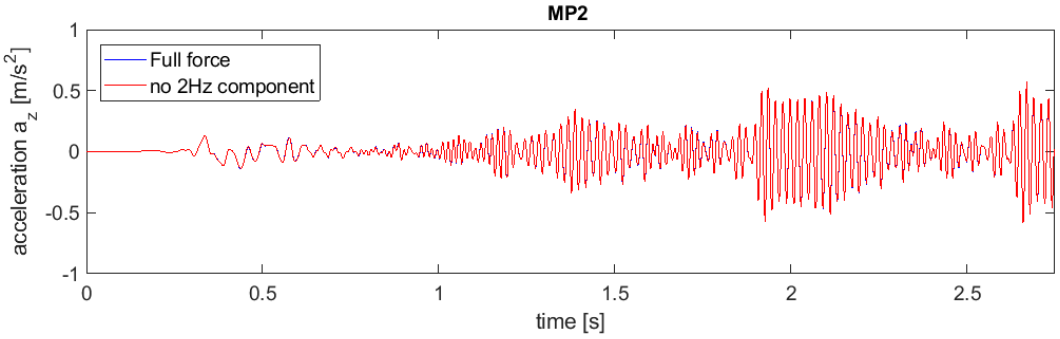

AP. C Figure 27 Comparison of accelerations in time domain between models with 2Hz oscillating component included and excluded at MP2

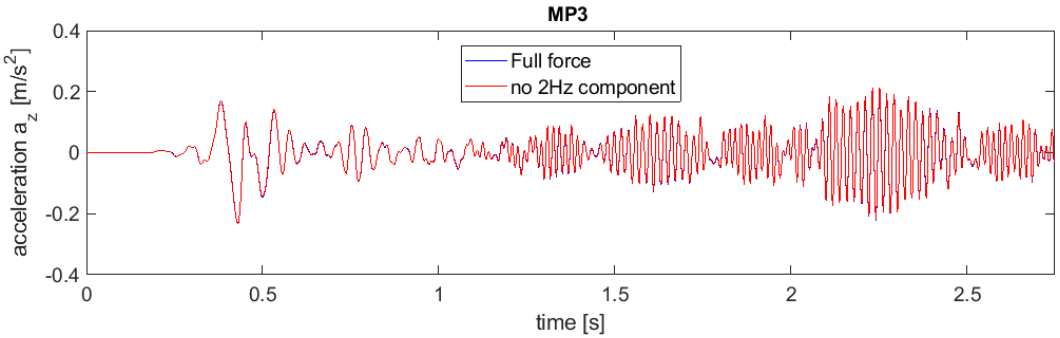

AP. C Figure 28 Comparison of accelerations in time domain between models with 2Hz oscillating component included and excluded at MP3

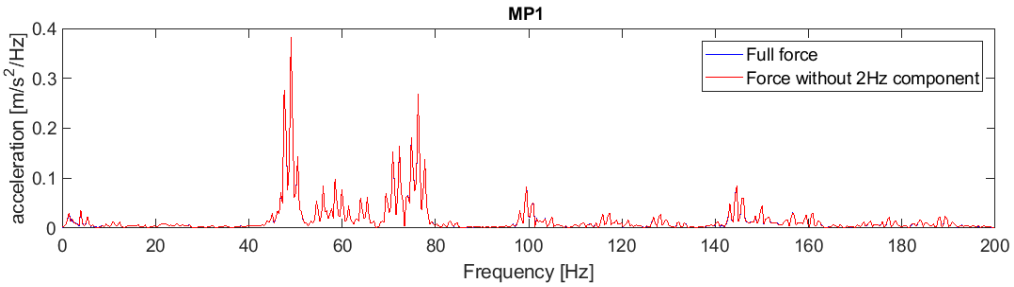

AP. C Figure 29 Comparison spectrums between models with 2Hz oscillating component included and excluded at MP1

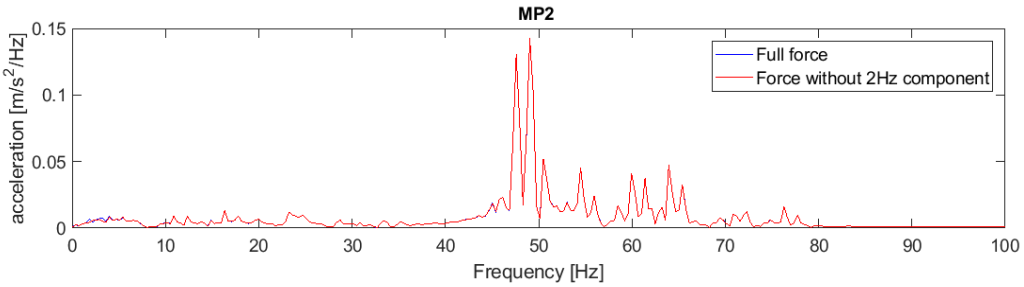

AP. C Figure 30 Comparison spectrums between models with 2Hz oscillating component included and excluded at MP2

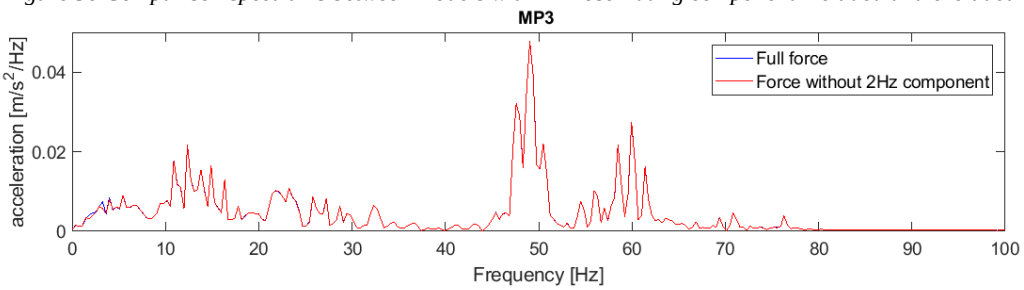

AP. C Figure 31 Comparison spectrums between models with 2Hz oscillating component included and excluded at MP3

C6 – Results of moving point load without dynamic component

In the following section the comparison is made between models in which moving point load has only quasi-static load component and the one where load consists of quasi-static and 2Hz dynamic oscillatory load components. Acceleration values are plotted in time and frequency domain for points MP1-3.

For conclusions and graphs description reader is referred to section 5.3.2.7.

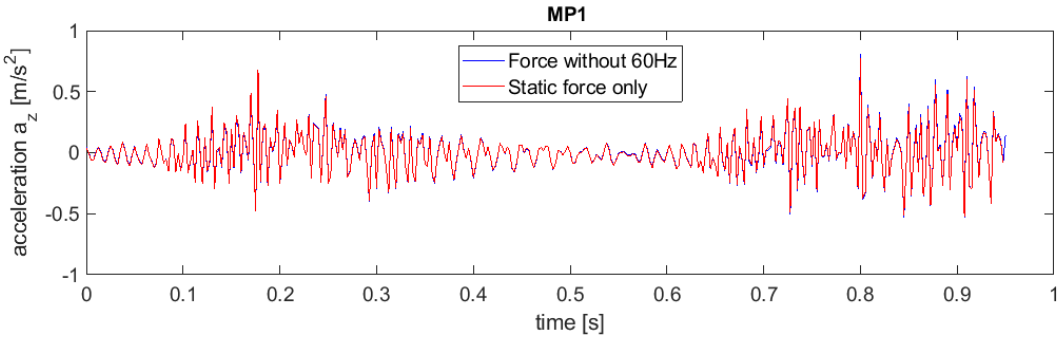

AP. C Figure 32 Comparison of accelerations in time domain between model with force including 2Hz oscillating and quasi-static component and model with quasi-static component included only at MP1

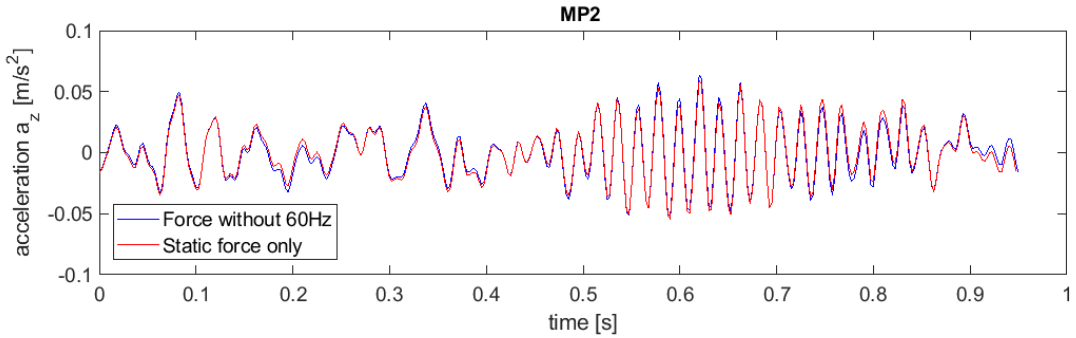

AP. C Figure 33 Comparison of accelerations in time domain between model with force including 2Hz oscillating and quasi-static component and model with quasi-static component included only at MP2

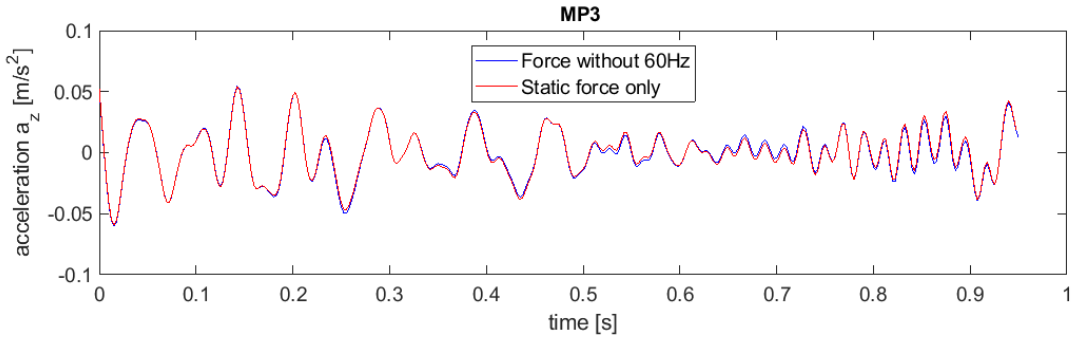

AP. C Figure 34 Comparison of accelerations in time domain between model with force including 2Hz oscillating and quasi-static component and model with quasi-static component included only at MP3

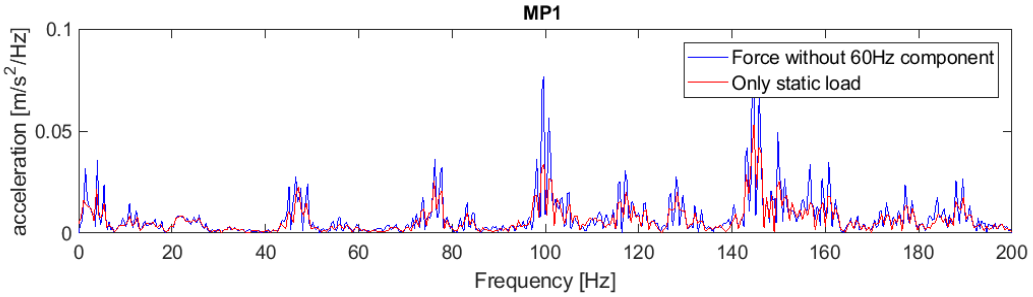

AP. C Figure 35 Comparison of acceleration spectrums in time domain between model with force including 2Hz oscillating and quasi-static component and model with quasi-static component included only at MP1

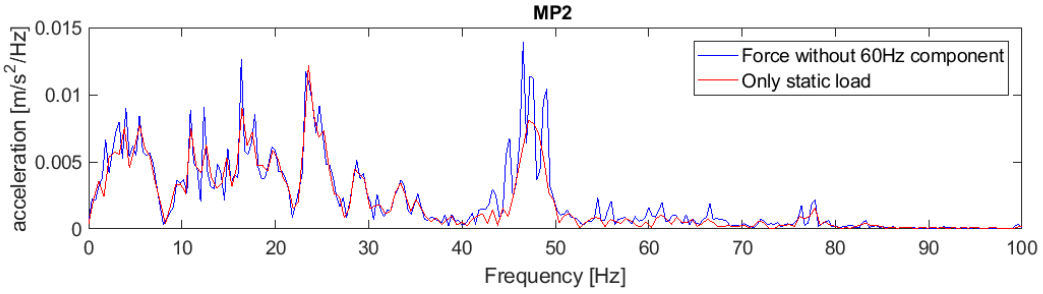

AP. C Figure 36 Comparison of acceleration spectrums in time domain between model with force including 2Hz oscillating and quasi-static component and model with quasi-static component included only at MP2

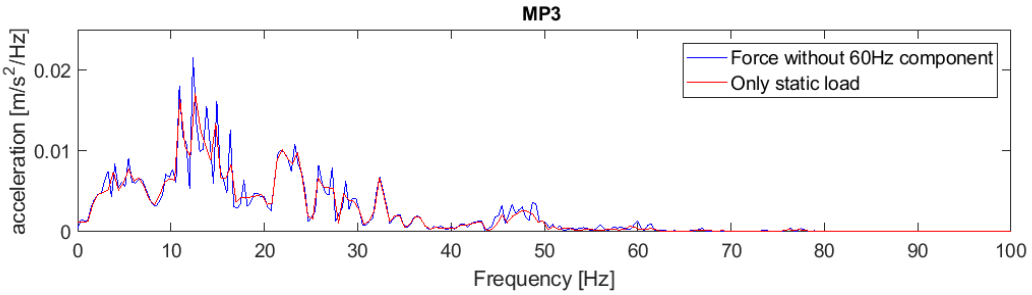

AP. C Figure 37 Comparison of acceleration spectrums in time domain between model with force including 2Hz oscillating and quasi-static component and model with quasi-static component included only at MP3

C7 – Results of models with upper layer thickness equal to 1m and 2m

In this section results of models which differ in soil layering are shown. In firth model the most upper layer is 1m thick whereas in second model thickness of top soft soil layer is increased to 2m. Acceleration are presented in time and frequency domain for locations MP1-3.

For conclusions and graphs description reader is referred to section 5.3.2.7.

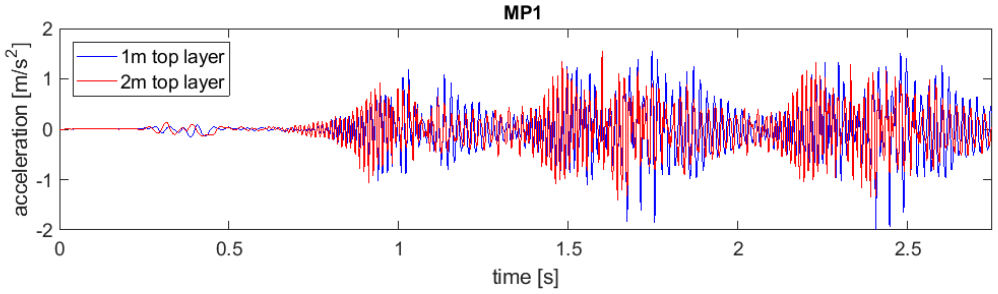

AP. C Figure 38 Comparison of accelerations between models with 1m and 2m top layer at MP1

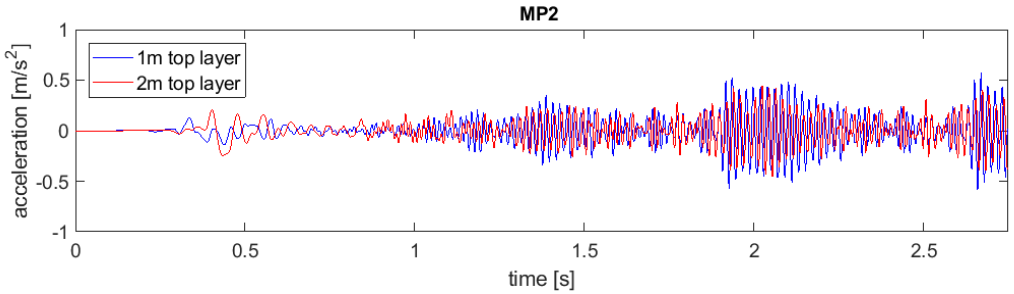

AP. C Figure 39 Comparison of accelerations between models with 1m and 2m top layer at MP2

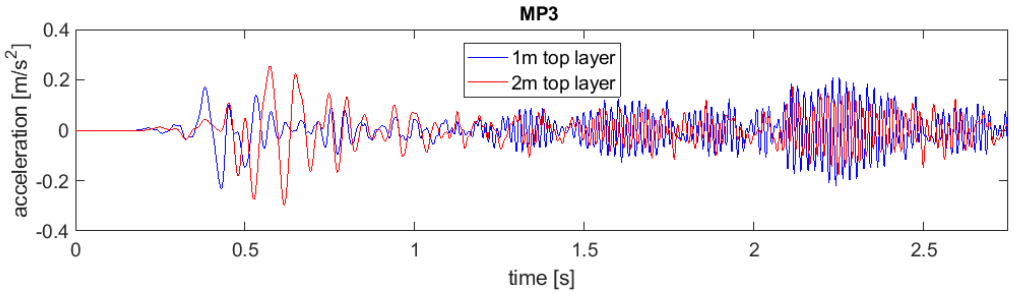

AP. C Figure 40 Comparison of accelerations between models with 1m and 2m top layer at MP3

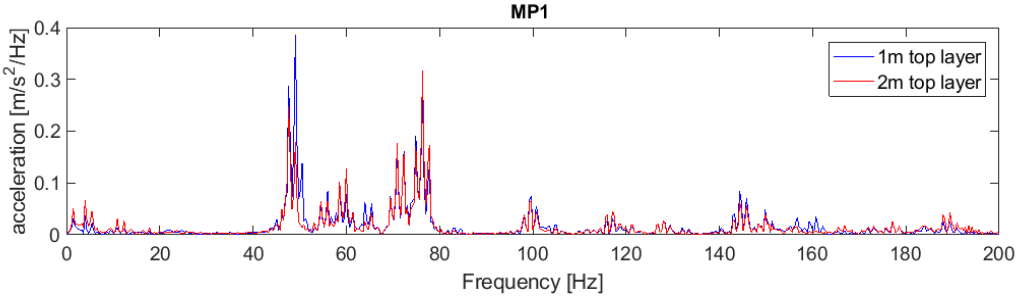

AP. C Figure 41 Comparison of spectrums between models with 1m and 2m top layer at MP1

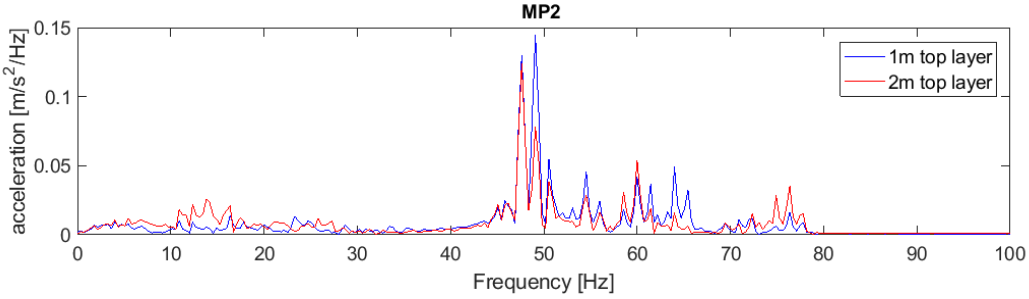

AP. C Figure 42 Comparison of spectrums between models with 1m and 2m top layer at MP2

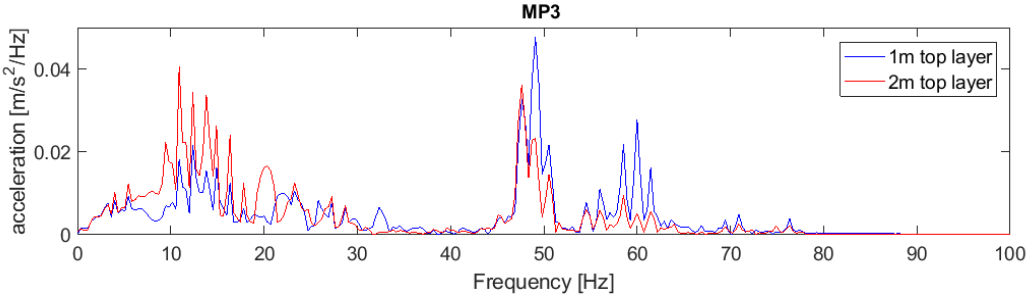

AP. C Figure 43 Comparison of spectrums between models with 1m and 2m top layer at MP3

C8 – Results of models with and without compacted sand beneath ballast

In this section results of models with and without compacted sand beneath ballast are shown. Acceleration are presented in time and frequency domain for locations MP1-3.

For conclusions and graphs description reader is referred to section 5.3.2.10.

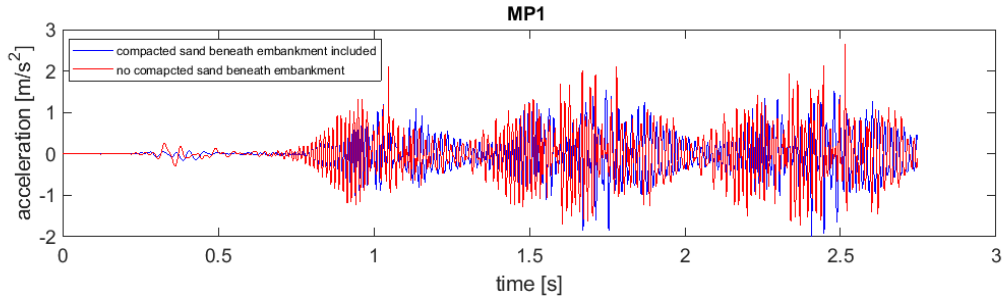

AP. C Figure 44 Comparison of accelerations between numerical models with and without compacted sand beneath the embankment at MP1

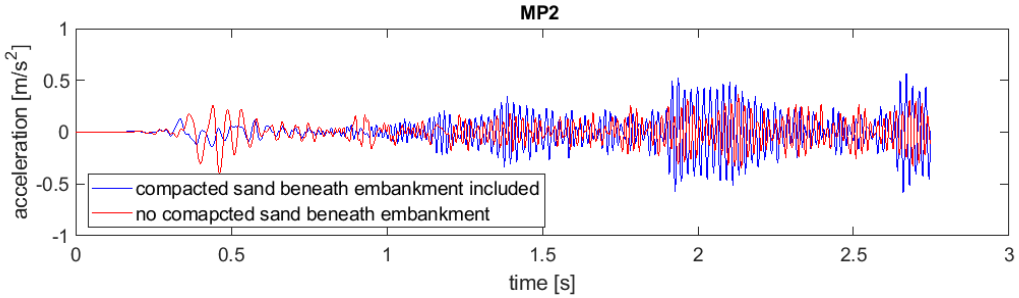

AP. C Figure 45 Comparison of accelerations between numerical models with and without compacted sand beneath the embankment at MP2

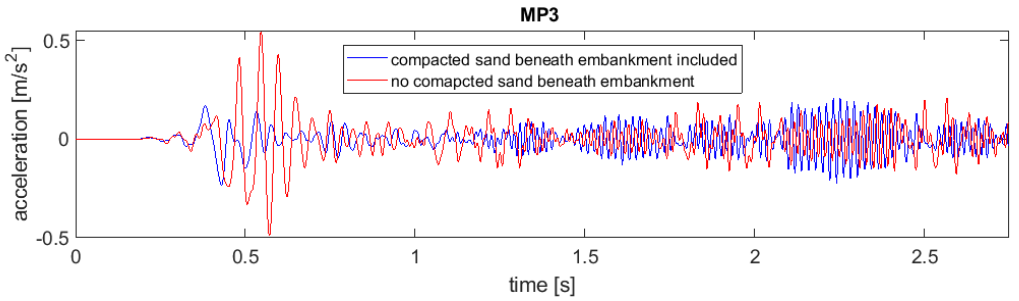

AP. C Figure 46 Comparison of accelerations between numerical models with and without compacted sand beneath the embankment at MP3

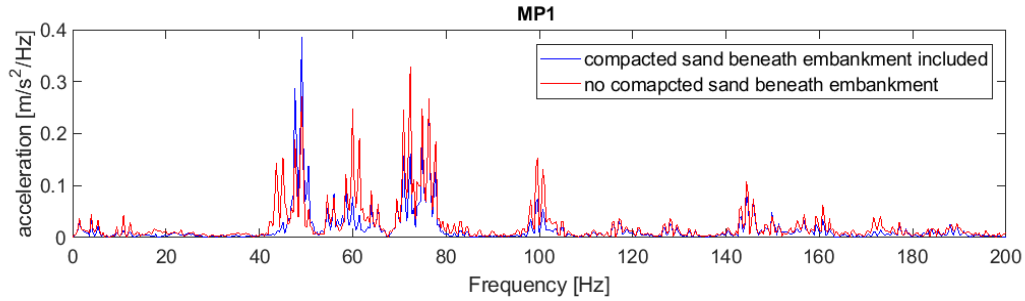

AP. C Figure 47 Comparison of acceleration spectrums between numerical models with and without compacted sand beneath the embankment at MP1

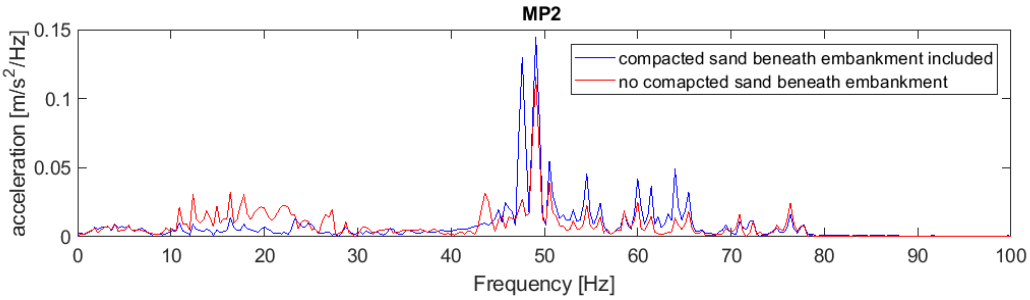

AP. C Figure 48 Comparison of acceleration spectrums between numerical models with and without compacted sand beneath the embankment at MP2

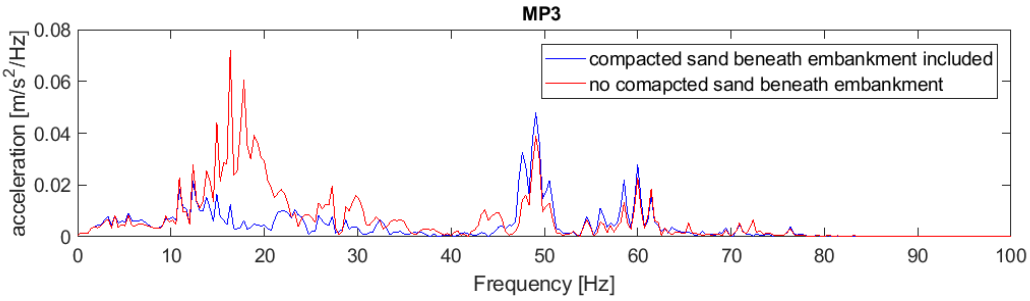

AP. C Figure 49 Comparison of acceleration spectrums between numerical models with and without compacted sand beneath the embankment at MP3

C8 – Results of models with dynamic oscillatory load equal to 5% and 2.5% of the weight of train

In this section results of models in which the dynamic oscillatory load component force is equal to 5% and 2.5% of axle load. Acceleration are presented in time and frequency domain for locations MP1-3.

For conclusions and graphs description reader is referred to section 5.3.2.11.

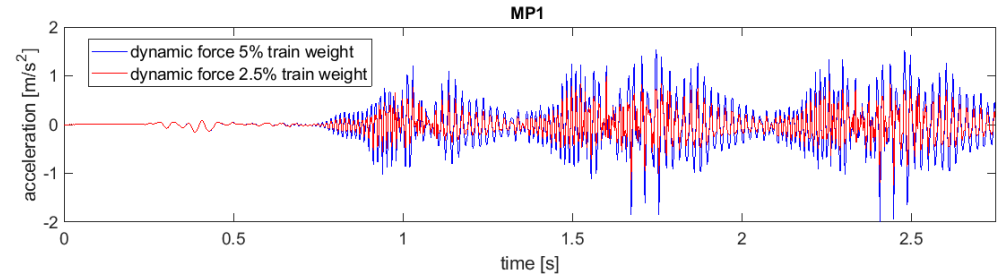

AP. C Figure 50 Comparison of accelerations of the models where dynamic force is equal to 2.5% or 5% of vehicle weight at MP1

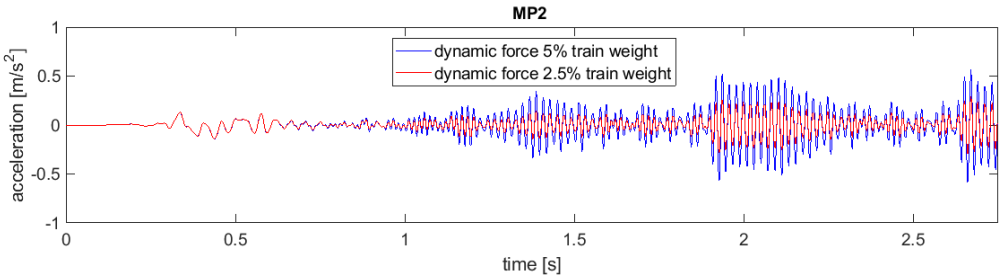

AP. C Figure 51 Comparison of accelerations of the models where dynamic force is equal to 2.5% or 5% of vehicle weight at MP2

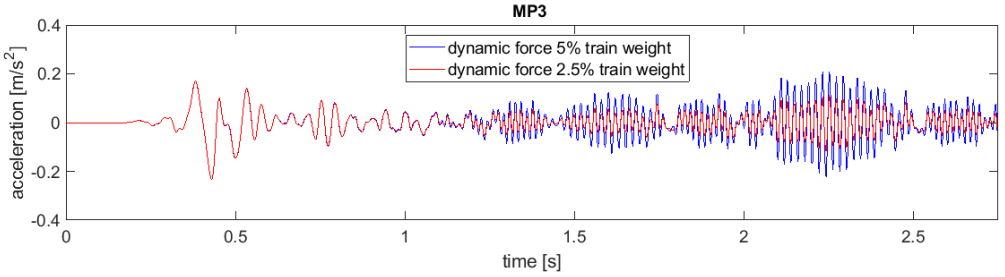

AP. C Figure 52 Comparison of accelerations of the models where dynamic force is equal to 2.5% or 5% of vehicle weight at MP3

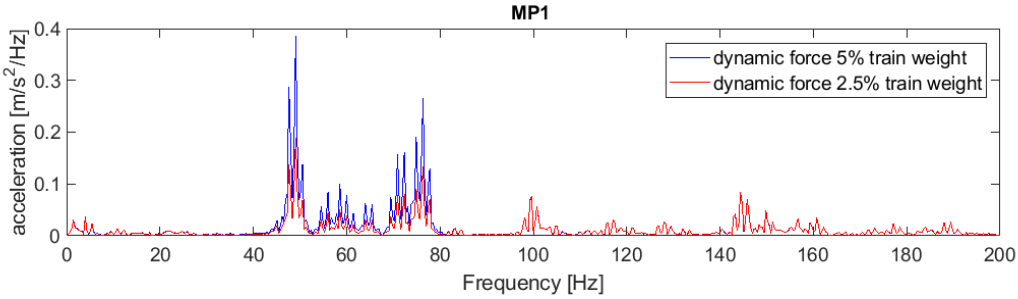

AP. C Figure 53 Comparison of acceleration spectrums of the models where dynamic force is equal to 2.5% or 5% of vehicle weight at MP1

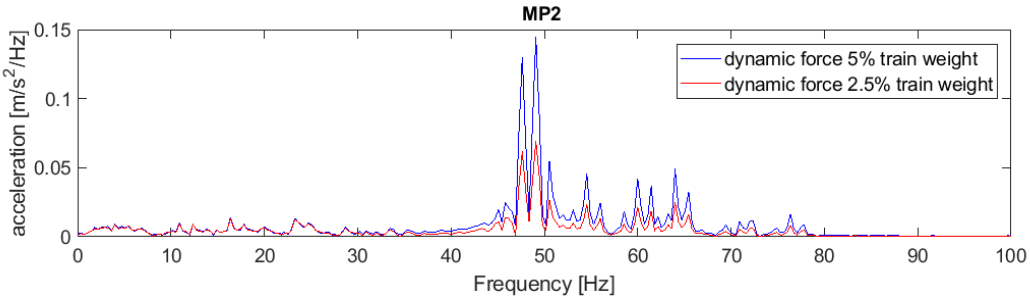

AP. C Figure 54 Comparison of acceleration spectrums of the models where dynamic force is equal to 2.5% or 5% of vehicle weight at MP2

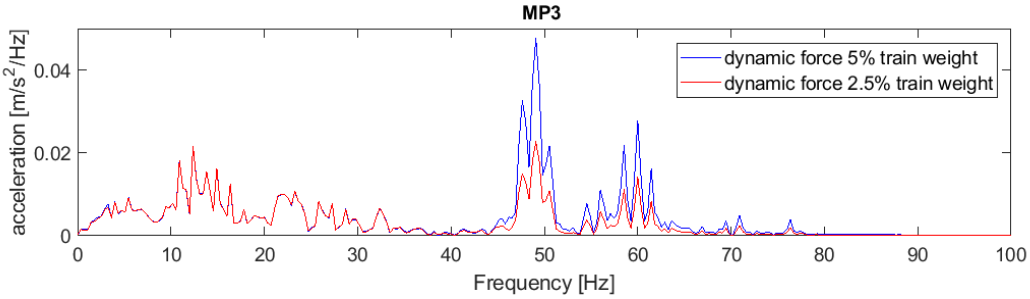

AP. C Figure 55 Comparison of acceleration spectrums of the models where dynamic force is equal to 2.5% or 5% of vehicle weight at MP3

Appendix D

Results of concrete slab variations

The overview of the content of this appendix is presented briefly in AP. D Table 1. More detailed information about each model can be found in the corresponding subsection.

Model / results analysed for specific model	acceleration		velocity		displacements in time domain
	time domain	frequency domain	time domain	frequency domain	
D1 – concrete slab thickness variation	X	X	X	X	X
D2 – concrete slab width variation	X	X	X	X	X
D3 – comparison of results for train running at 110km/h speed with and without concrete slab applied	X	X	X	X	X
D4 comparison of results for train running at 150km/h speed with and without concrete slab applied	X	X	X	X	X
D5 – comparison of results for three train speeds: 110km/h, 130km/h and 150km/h without concrete slab applied	X	X	X	X	-
D6 - comparison of results for three train speeds: 110km/h, 130km/h and 150km/h with concrete slab applied	X	X	X	X	-
D7 – Comparison of results for cracked and uncracked concrete slabs with varying damping ratio	X	X	X	X	-
D8 – scatter effect when building is included in the numerical model	X	X	-	-	-

AP. D Table 1 Overview of content of Appendix D

D1 – Concrete slab thickness variations (V1-4)

In this section results of the variations V1-4 are presented. They regard change of thickness for concrete slab of 3.5m width. Considered variations are with t = 25cm, t = 35cm, t = 50cm, t = 60cm. Graphs present acceleration in time and frequency domain, velocity in time and frequency domain and displacement in time domain for point locations MP1-3. Trains runs at speed 130km/h.

For conclusions and graphs description reader is referred to section 6.2.

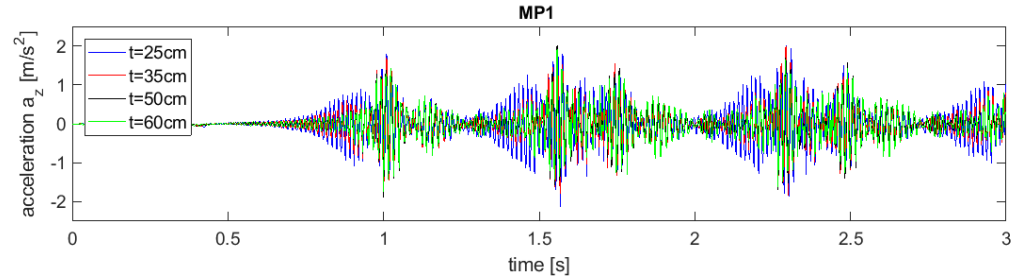

AP. D Figure 1 Acceleration for variation studies V1-4 at MP1

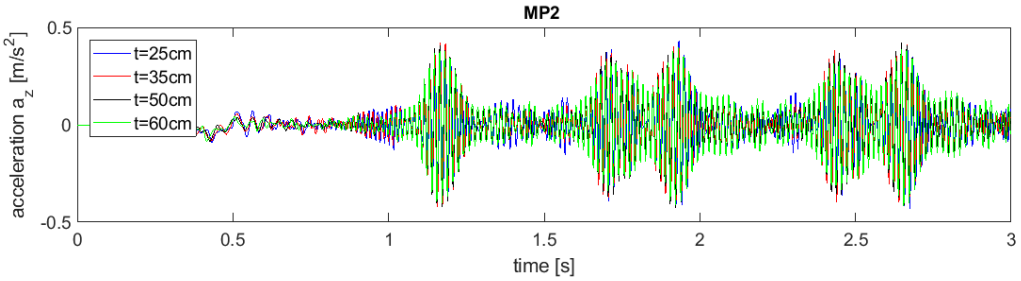

AP. D Figure 2 Acceleration for variation studies V1-4 at MP2

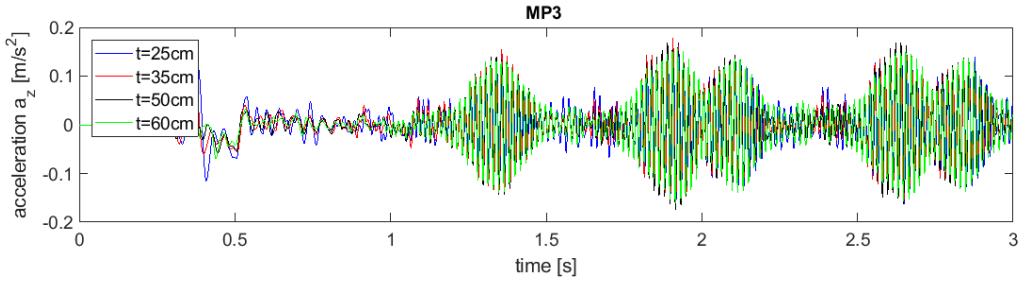

AP. D Figure 3 Acceleration for variation studies V1-4 at MP3

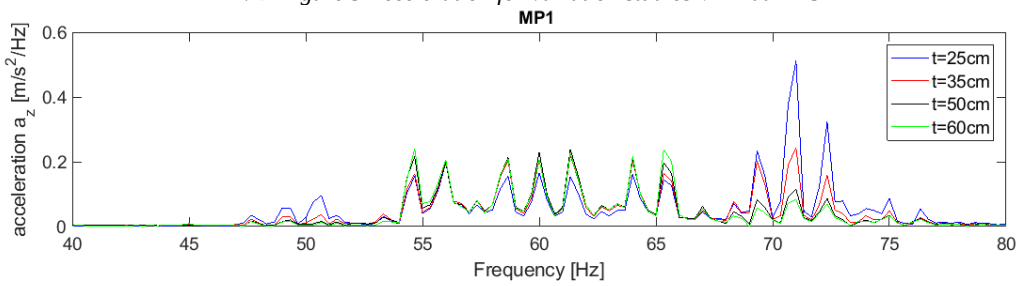

AP. D Figure 4 Spectrums of acceleration for variation studies V1-4 at MP1

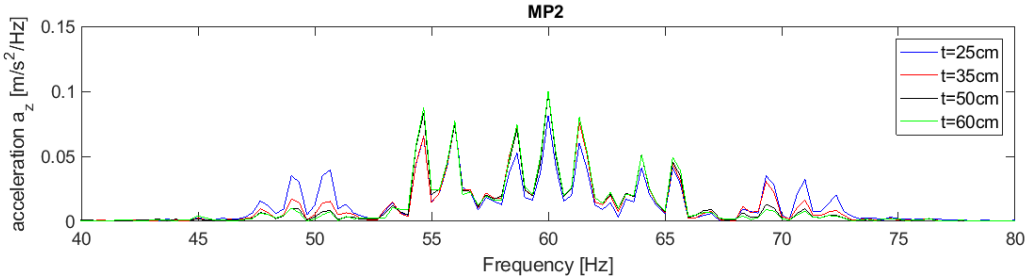

AP. D Figure 5 Spectrums of acceleration for variation studies V1-4 at MP2

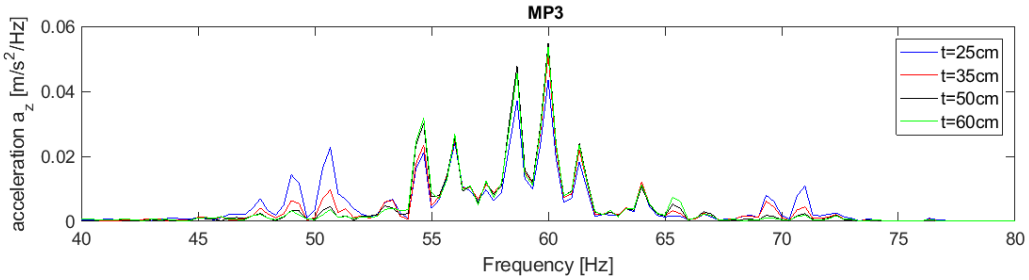

AP. D Figure 6 Spectrums of acceleration for variation studies V1-4 at MP3

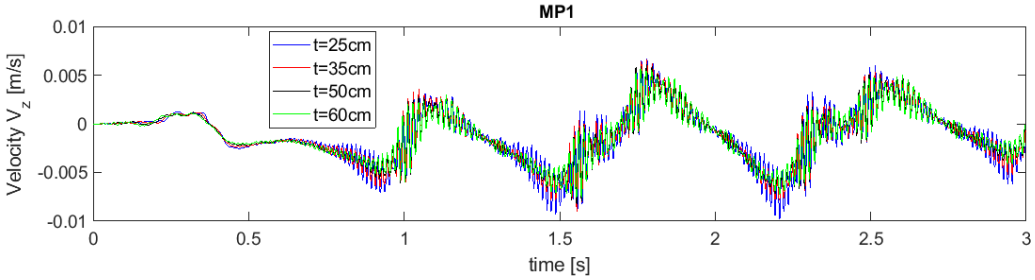

AP. D Figure 7 Velocity for variation studies V1-4 at MP1

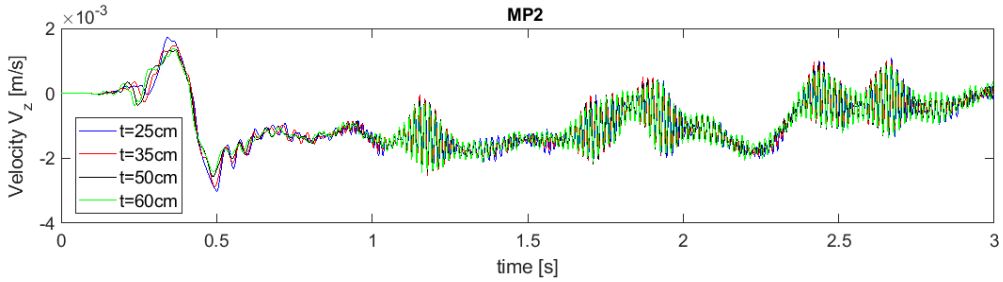

AP. D Figure 8 Velocity for variation studies V1-4 at MP2

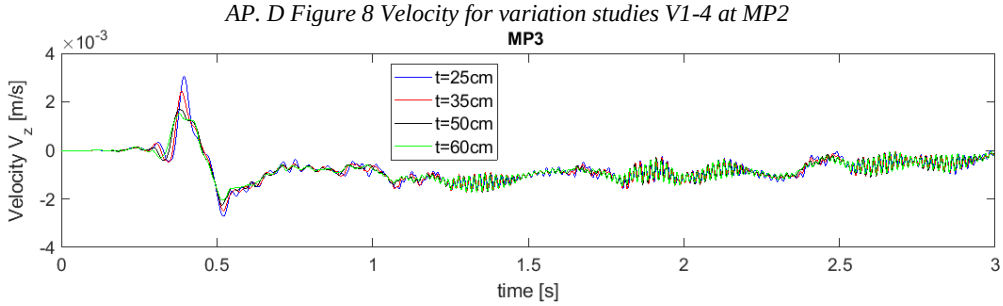

AP. D Figure 9 Velocity for variation studies V1-4 at MP3

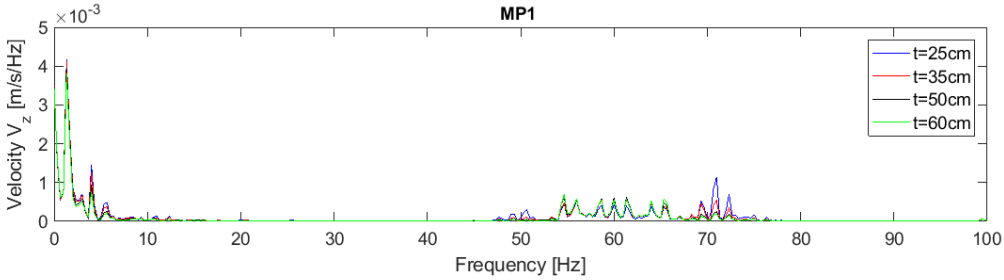

AP. D Figure 10 Spectrum of velocity for variation studies V1-4 at MP1

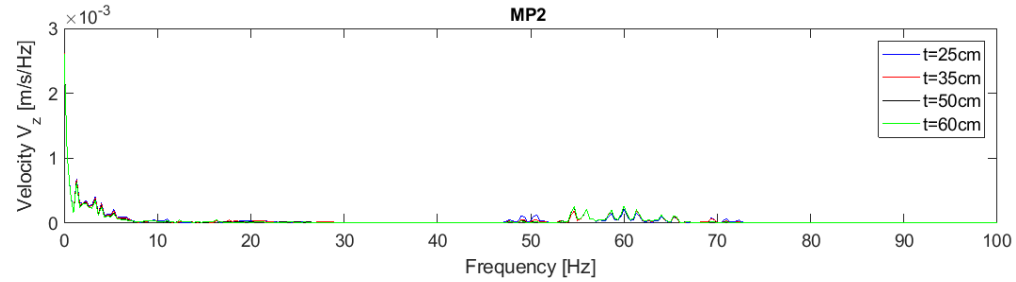

AP. D Figure 11 Spectrum of velocity for variation studies V1-4 at MP2

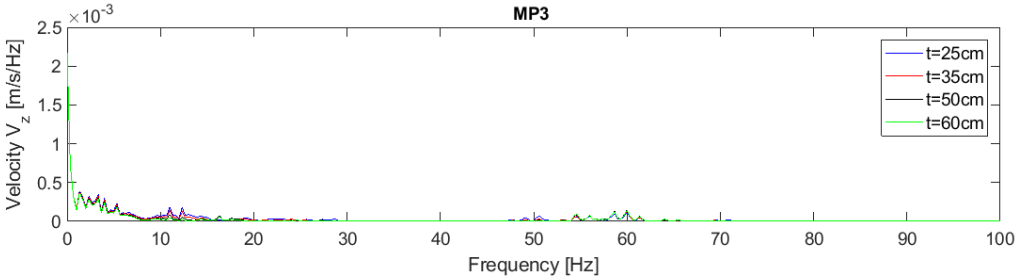

AP. D Figure 12 Spectrum of velocity for variation studies V1-4 at MP3

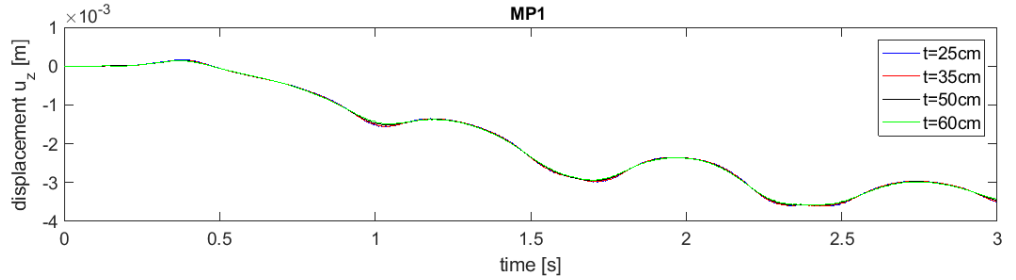

AP. D Figure 13 Displacement for variation studies V1-4 at MP1

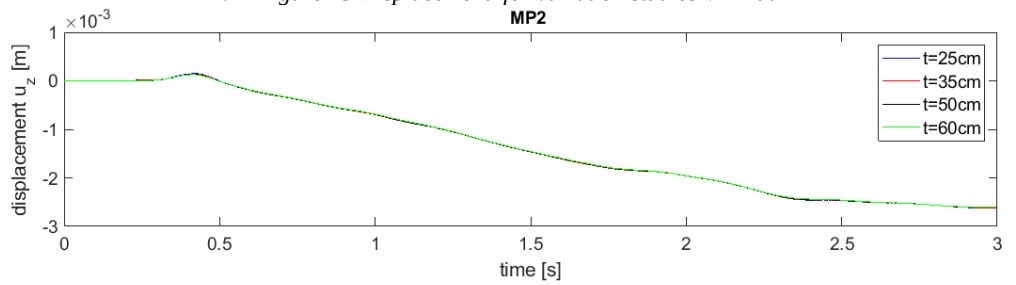

AP. D Figure 14 Displacement for variation studies V1-4 at MP2

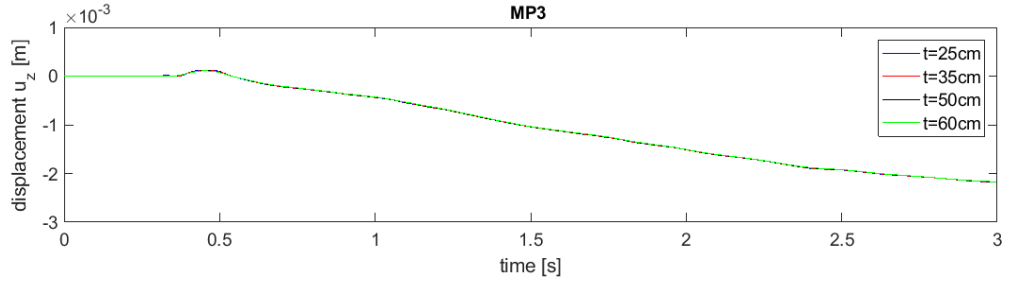

AP. D Figure 15 Displacement for variation studies V1-4 at MP3

D2 – Concrete slab width variations (V1, V5-7)

In this section results of the variations V1 and V5-7 are presented. They regard change of width for concrete slab of 0.5m thick. Considered variations are with w = 3.5m, w = 4.0m, w = 4.5m, w = 5.0m. Graphs present acceleration in time and frequency domain, velocity in time and frequency domain and displacement in time domain for point locations MP1-3. Train runs at speed 130km/h.

For conclusions and graphs description reader is referred to section 6.3.

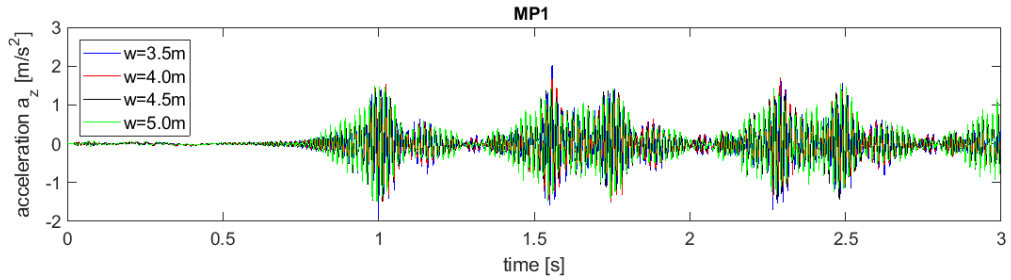

AP. D Figure 16 Acceleration for variation studies V1 V5-7 at MP1

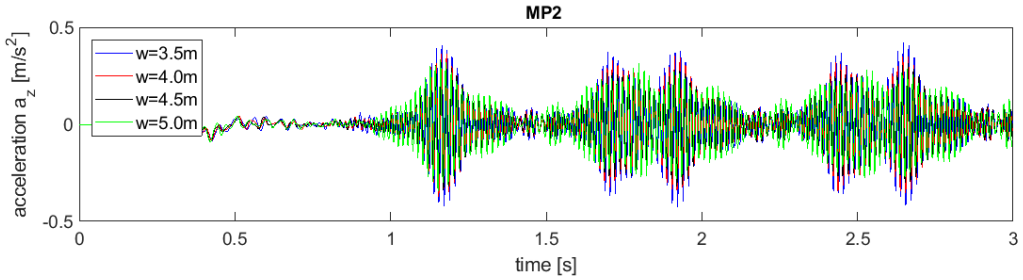

AP. D Figure 17 Acceleration for variation studies V1 V5-7 at MP2

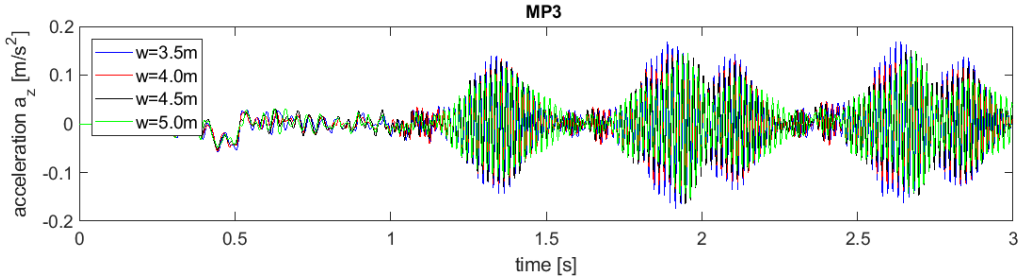

AP. D Figure 18 Acceleration for variation studies V1 V5-7 at MP3

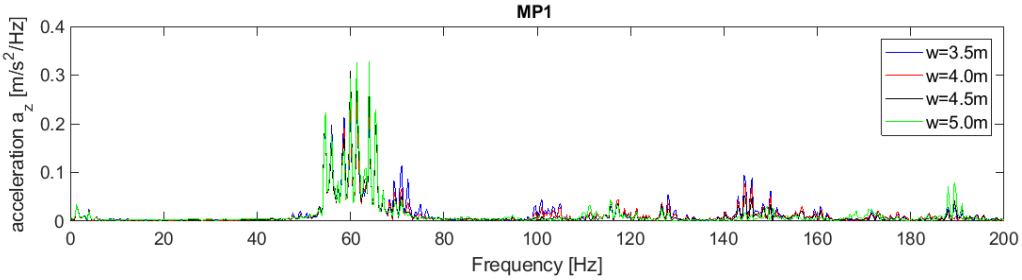

AP. D Figure 19 Acceleration spectrum for variation studies V1 V5-7 at MP1

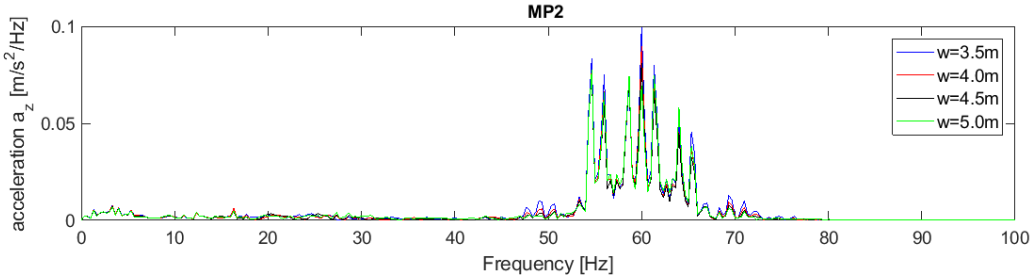

AP. D Figure 20 Acceleration spectrum for variation studies V1 V5-7 at MP2

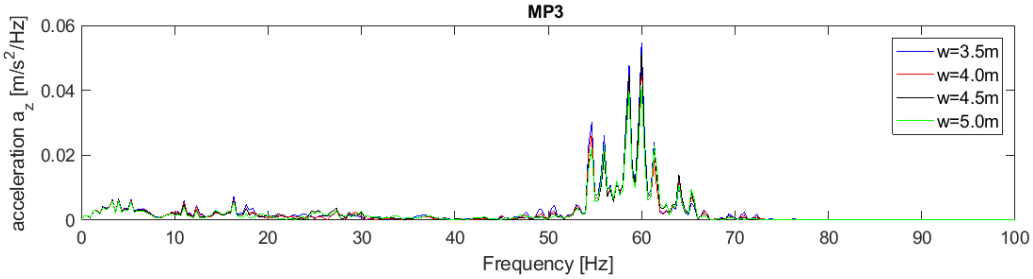

AP. D Figure 21 Acceleration spectrum for variation studies V1 V5-7 at MP3

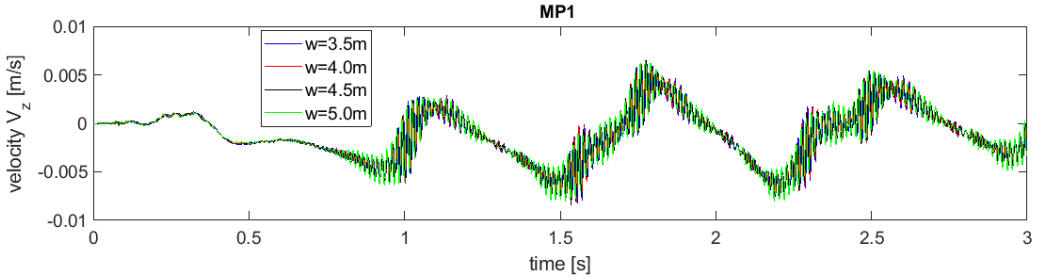

AP. D Figure 22 Velocity for variation studies V1 V5-7 at MP1

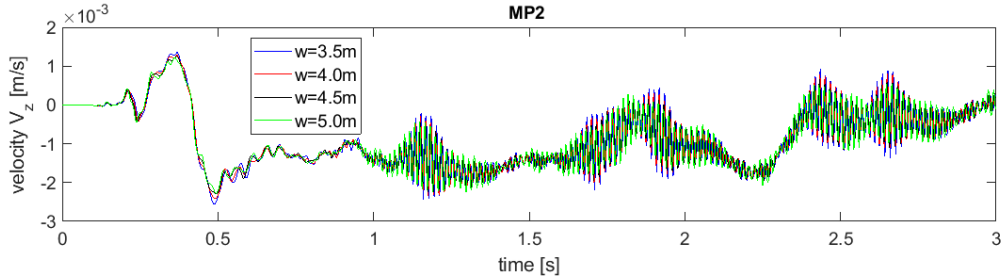

AP. D Figure 23 Velocity for variation studies V1 V5-7 at MP2

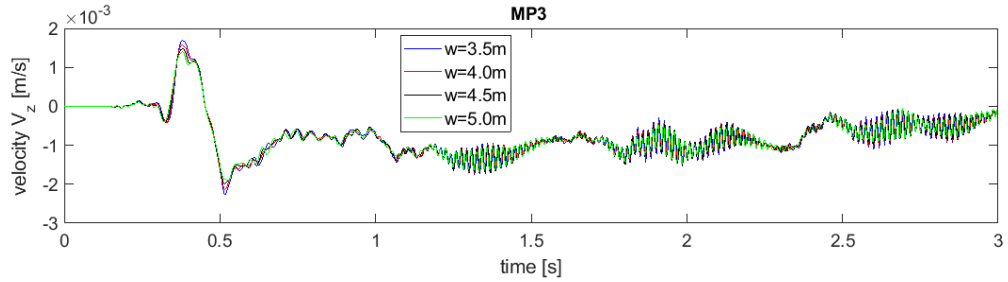

AP. D Figure 24 Velocity for variation studies V1 V5-7 at MP3

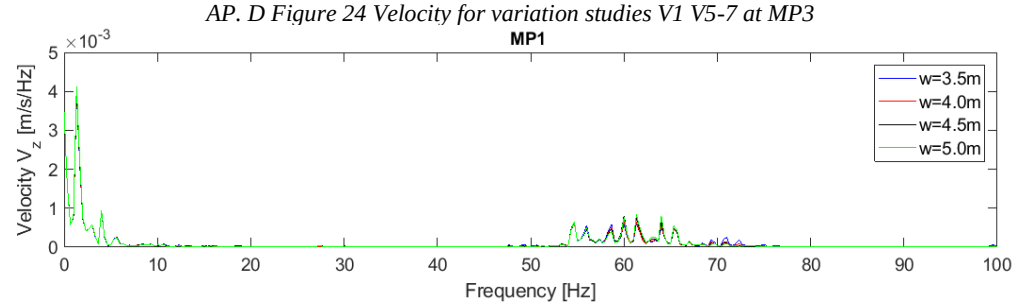

AP. D Figure 25 Velocity spectrum for variation studies V1 V5-7 at MP1

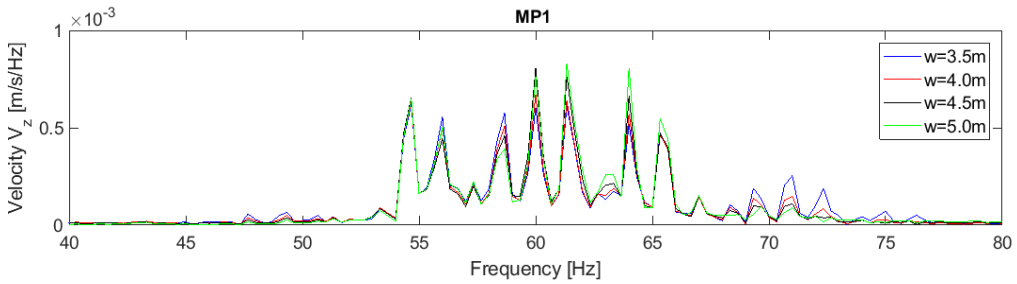

AP. D Figure 26 Velocity spectrum for variation studies V1 V5-7 at MP1 inset for frequencies 40Hz to 80Hz

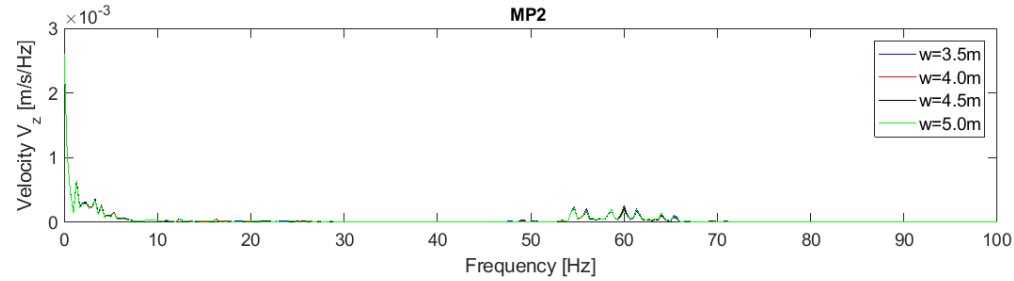

AP. D Figure 27 Velocity spectrum for variation studies V1 V5-7 at MP2

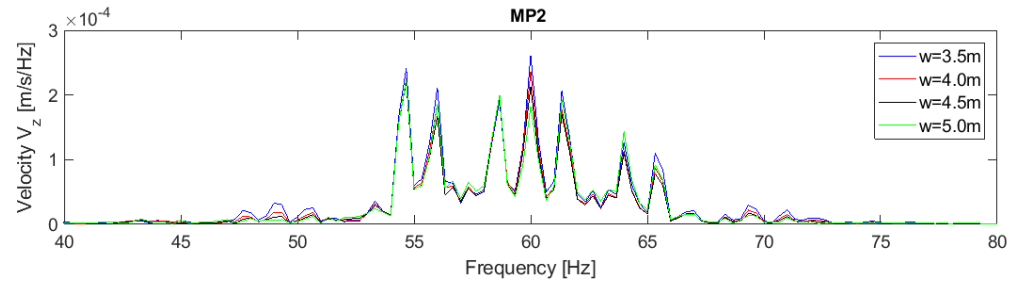

AP. D Figure 28 Velocity spectrum for variation studies V1 V5-7 at MP2 inset for frequencies 40Hz to 80Hz

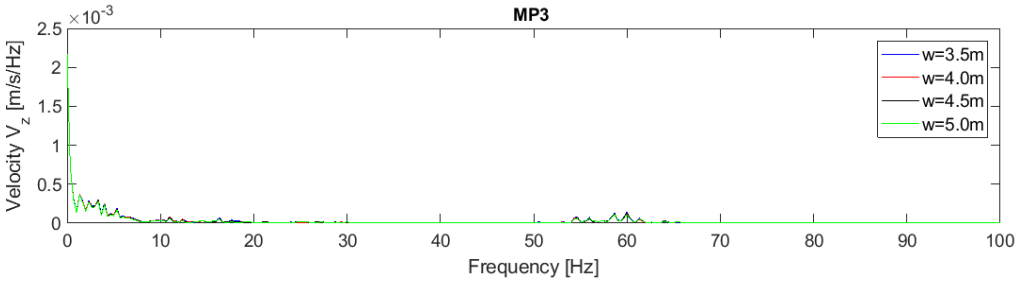

AP. D Figure 29 Velocity spectrum for variation studies V1 V5-7 at MP3

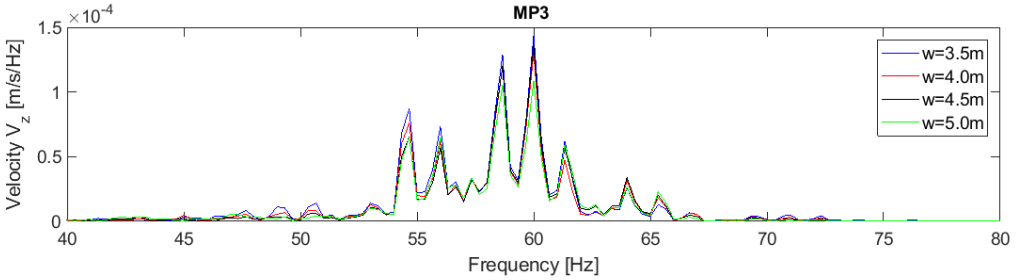

AP. D Figure 30 Velocity spectrum for variation studies V1 V5-7 at MP3 inset for frequencies 40Hz to 80Hz

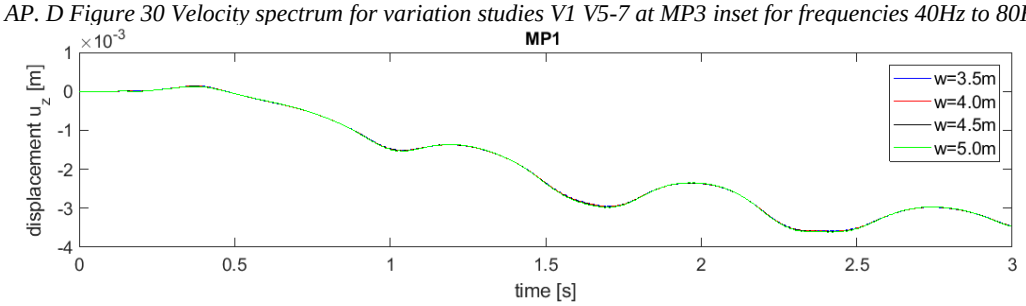

AP. D Figure 31 Displacements variation studies V1 V5-7 at MP1

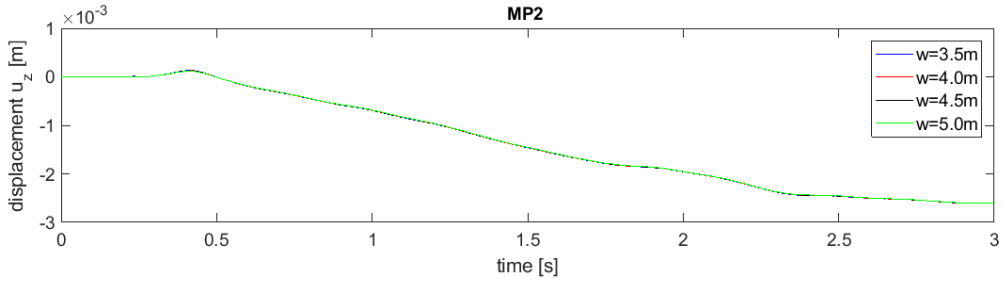

AP. D Figure 32 Displacements variation studies V1 V5-7 at MP2

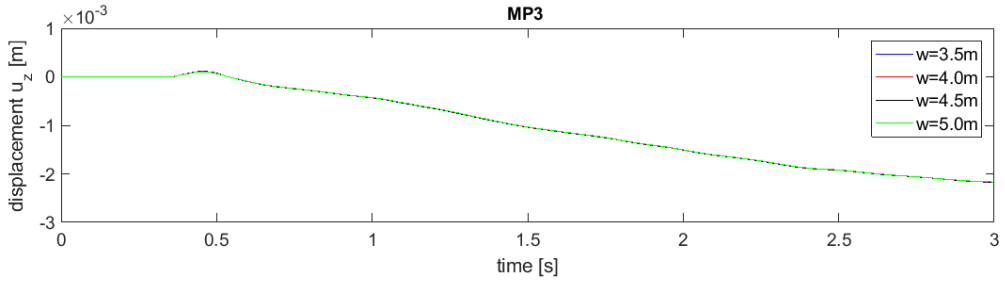

AP. D Figure 33 Displacements variation studies V1 V5-7 at MP3

D3 – Results for train running at speed 110km/h with concrete slab applied

In this section results of the models with and without concrete slab beneath ballast bed for train running at speed of 110km/h are depicted. Slab has dimensions 3.5m x 0.5m. Graphs present acceleration in time and frequency domain, velocity in time and frequency domain and displacement in time domain for point locations MP1-3.

For conclusions and graphs description reader is referred to section 6.4.1.

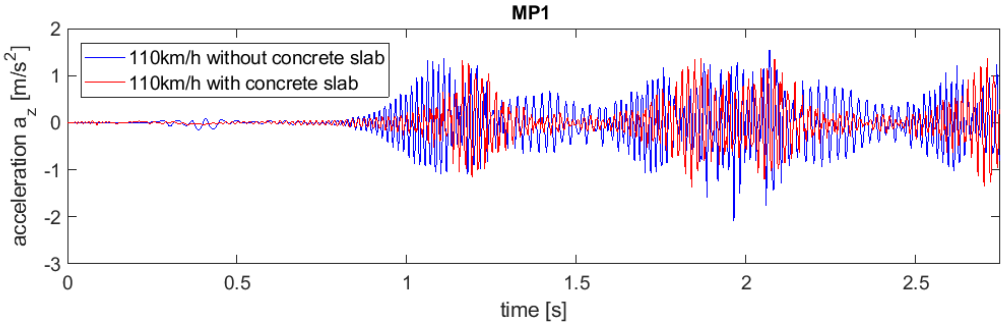

AP. D Figure 34 Acceleration at location MP1 for systems with and without concrete slab at the train speed 110 km/h

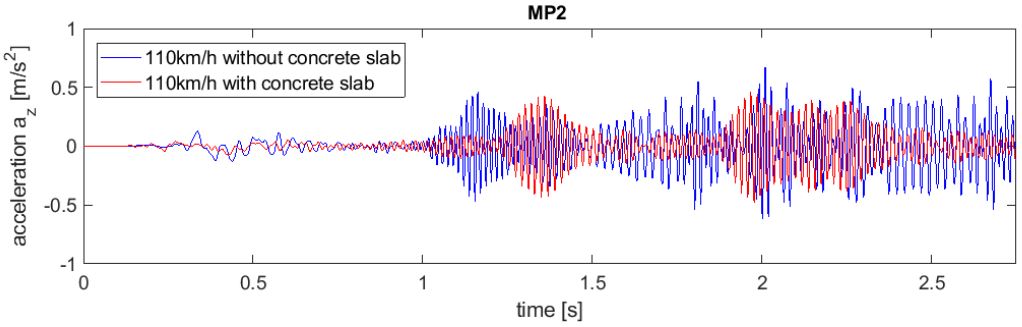

AP. D Figure 35 Acceleration at location MP2 for systems with and without concrete slab at the train speed 110 km/h

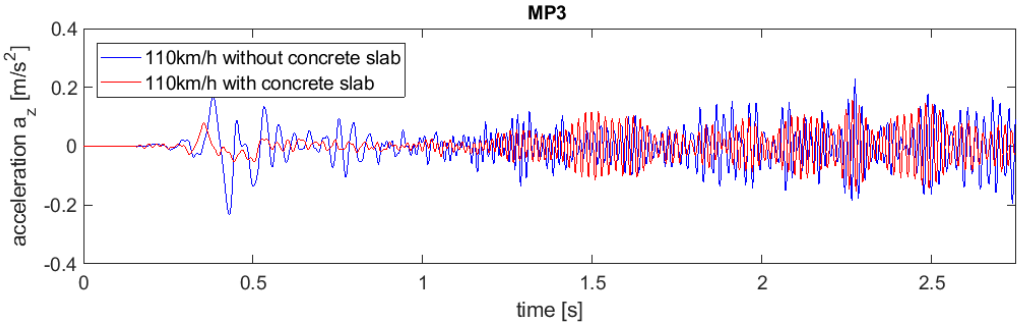

AP. D Figure 36 Acceleration at location MP3 for systems with and without concrete slab at the train speed 110 km/h

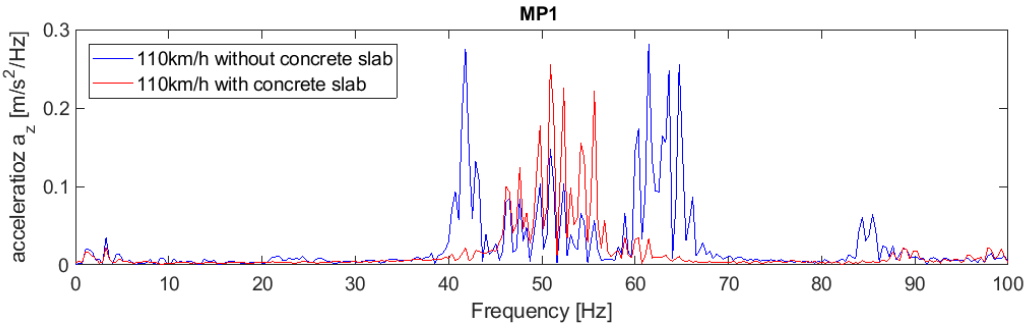

AP. D Figure 37 Spectrum of acceleration at location MP1 for systems with and without slab, train speed 110 km/h

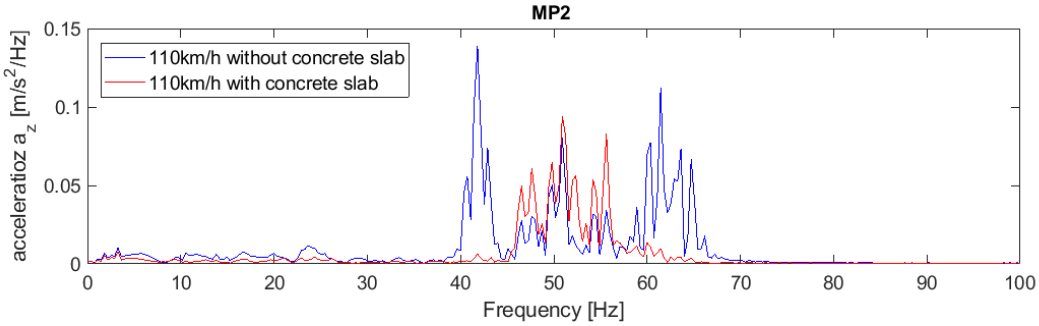

AP. D Figure 38 Spectrum of acceleration at location MP2 for systems with and without slab, train speed 110 km/h

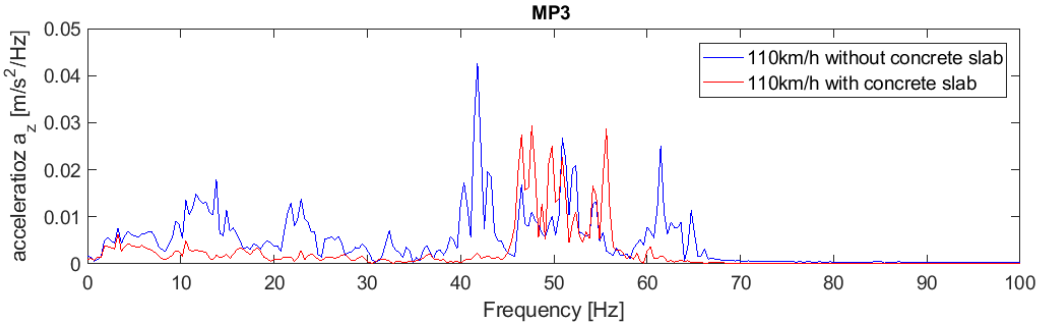

AP. D Figure 39 Spectrum of acceleration at location MP3 for systems with and without slab, train speed 110 km/h

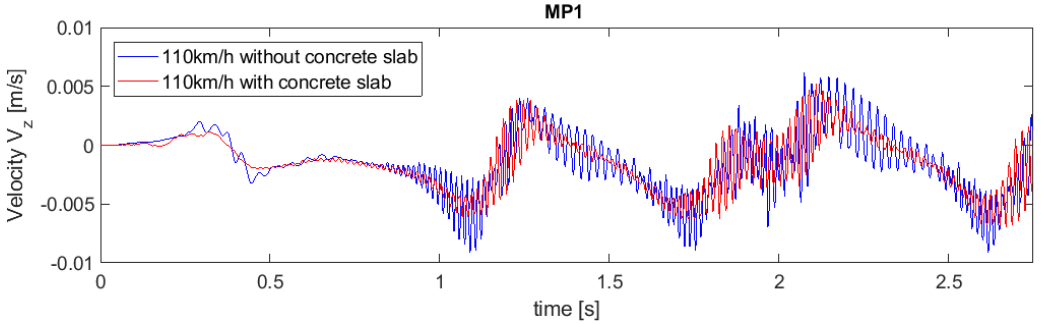

AP. D Figure 40 Velocity at location MP1 for systems with and without concrete slab at the train speed 110 km/h

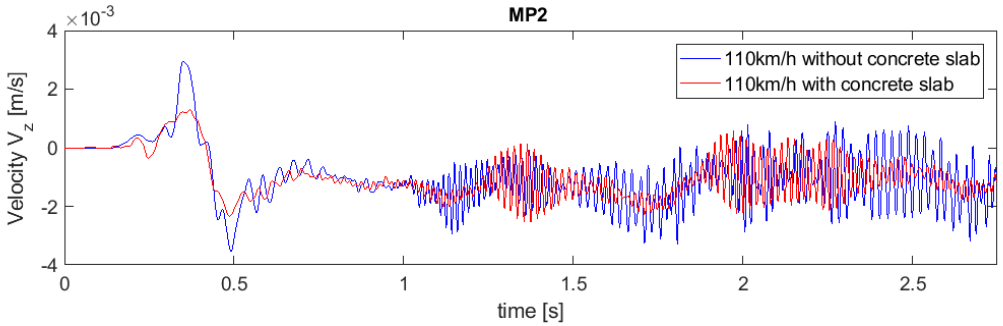

AP. D Figure 41 Velocity at location MP2 for systems with and without concrete slab at the train speed 110 km/h

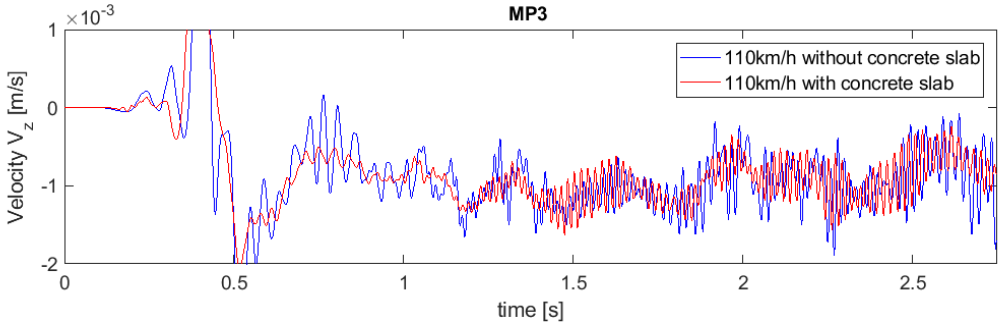

AP. D Figure 42 Velocity at location MP3 for systems with and without concrete slab at the train speed 110 km/h

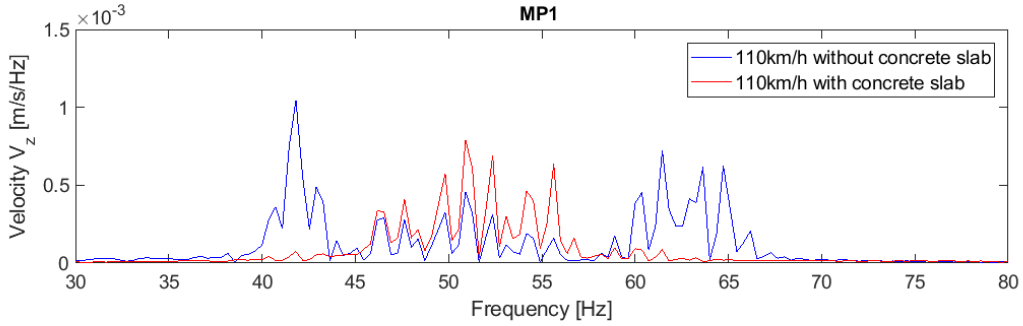

AP. D Figure 43 Spectrum of velocity at location MP1 for systems with and without slab, train speed 110 km/h

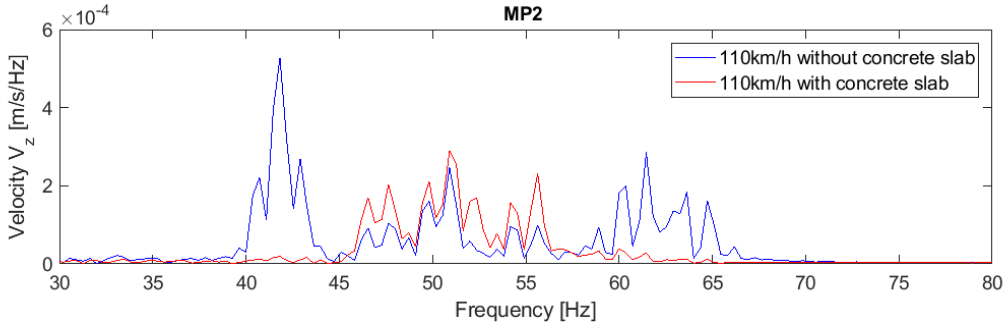

AP. D Figure 44 Spectrum of velocity at location MP2 for systems with and without slab, train speed 110 km/h

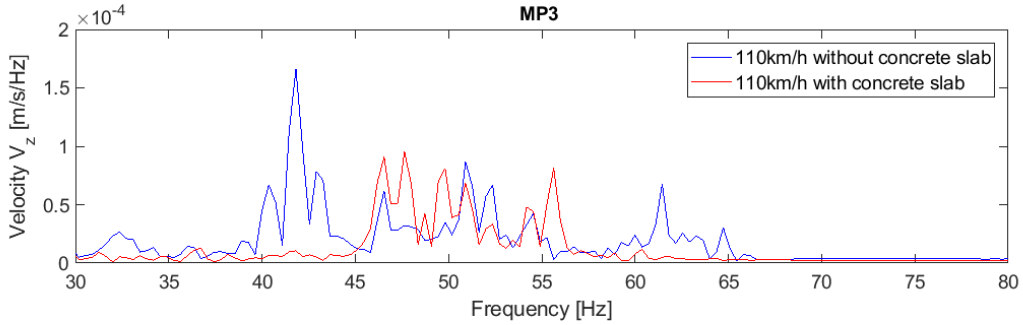

AP. D Figure 45 Spectrum of velocity at location MP3 for systems with and without slab, train speed 110 km/h

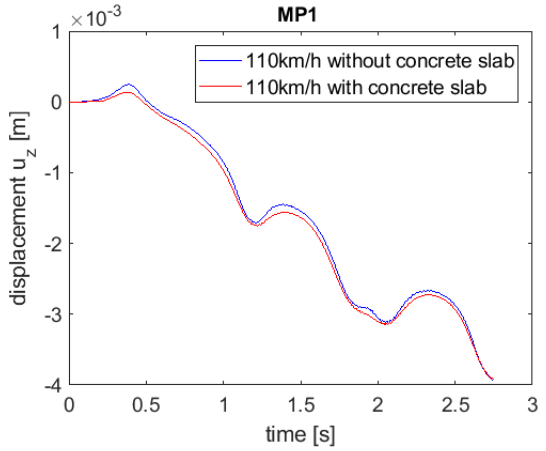

AP. D Figure 46 Displacement at location MP1 for systems with and without slab, train speed 110 km/h

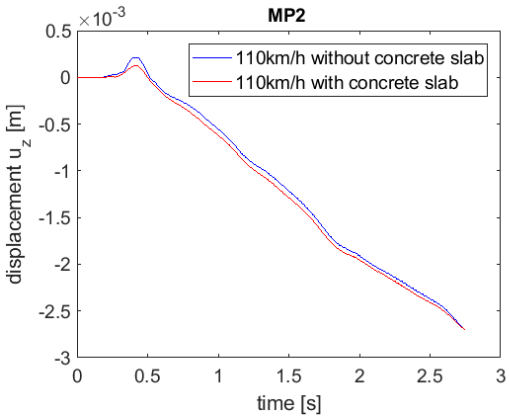

AP. D Figure 47 Displacement at location MP2 for systems with and without slab, train speed 110 km/h

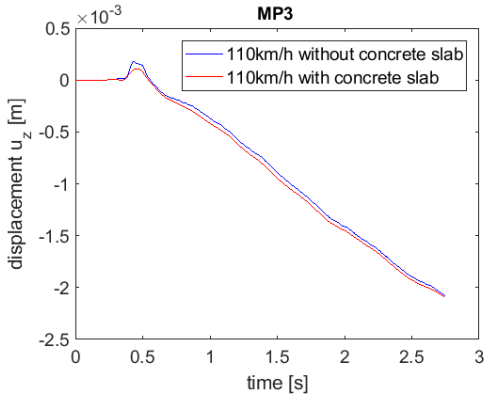

AP. D Figure 48 Displacement at location MP3 for systems with and without slab, train speed 110 km/h

D4 – Results for train running at speed 150km/h with concrete slab applied

In this section results of the models with and without concrete slab beneath ballast bed for train running at speed of 150km/h are depicted. Slab has dimensions 3.5m x 0.5m. Graphs present acceleration and velocity in time and frequency domain, for point locations MP1-3.

For conclusions and graphs description reader is referred to section 6.4.2.

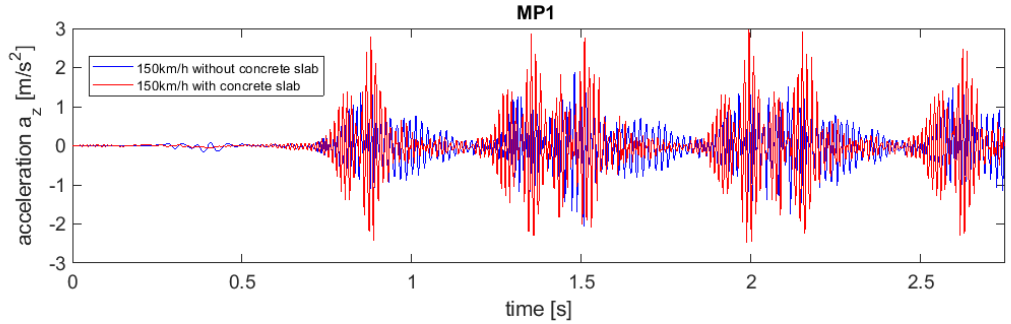

AP. D Figure 49 Acceleration at location MP1 for systems with and without concrete slab at the train speed 150 km/h

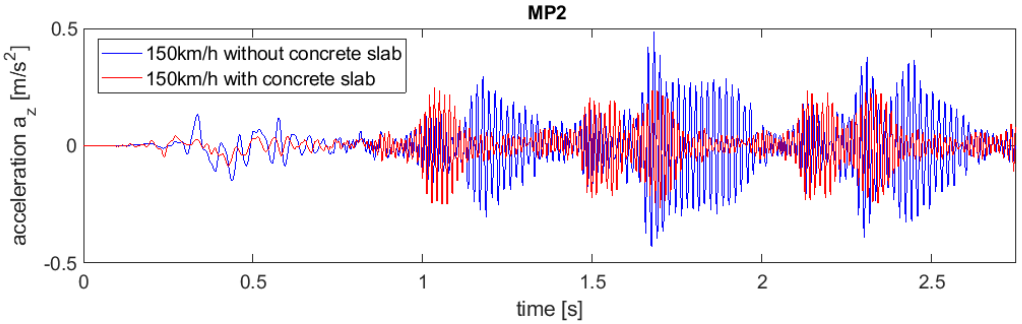

AP. D Figure 50 Acceleration at location MP2 for systems with and without concrete slab at the train speed 150 km/h

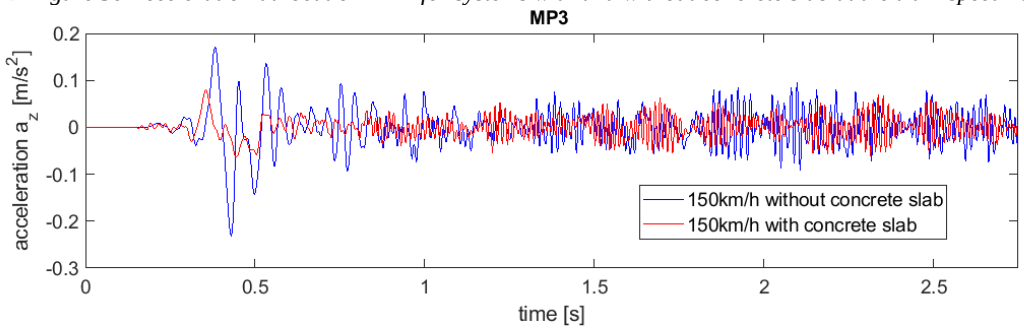

AP. D Figure 51 Acceleration at location MP3 for systems with and without concrete slab at the train speed 150 km/h

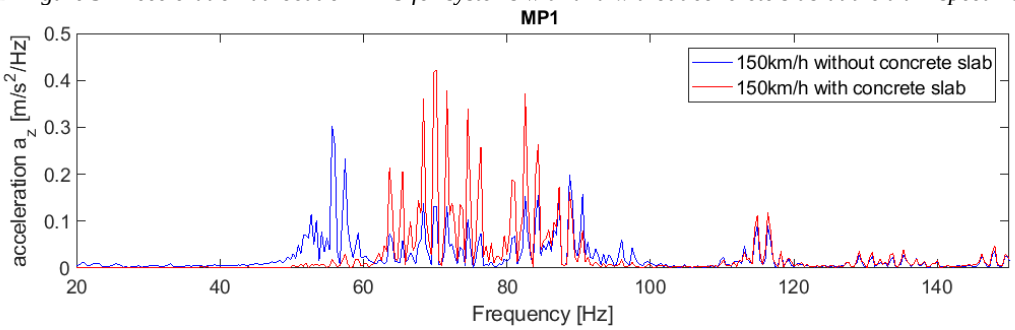

AP. D Figure 52 Spectrum of acceleration at location MP1 for systems with and without concrete slab, train speed 150 km/h

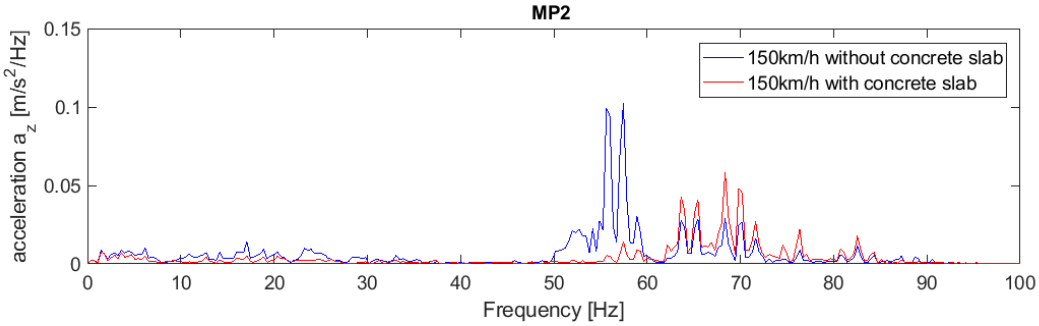

AP. D Figure 53 Spectrum of acceleration at location MP2 for systems with and without concrete slab, train speed 150 km/h

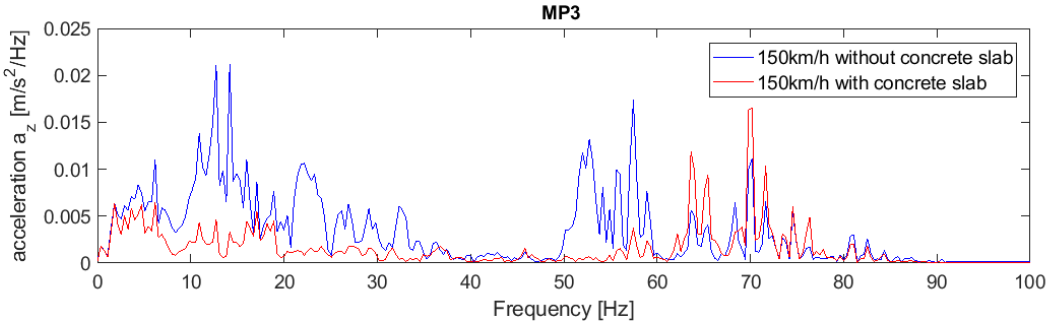

AP. D Figure 54 Spectrum of acceleration at location MP3 for systems with and without concrete slab, train speed 150 km/h

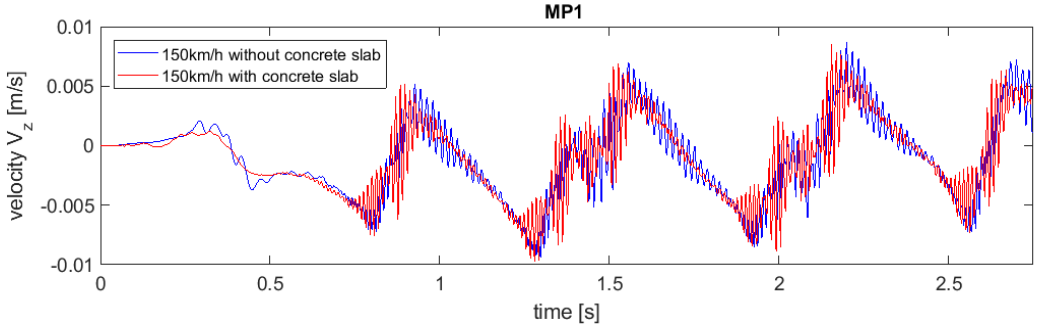

AP. D Figure 55 Velocity at location MP1 for systems with and without concrete slab at the train speed 150 km/h

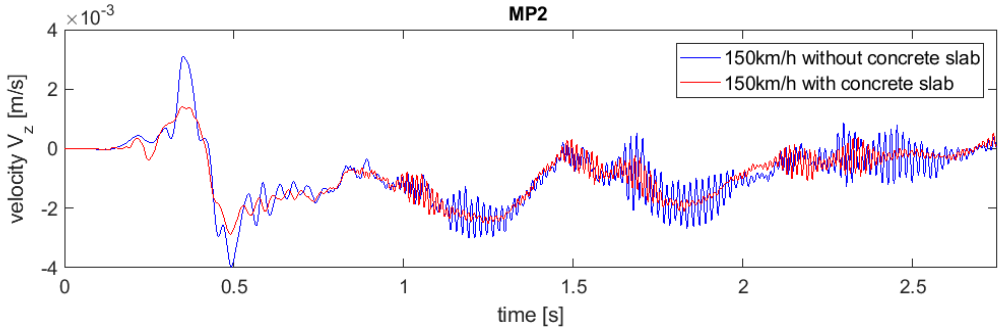

AP. D Figure 56 Velocity at location MP2 for systems with and without concrete slab at the train speed 150 km/h

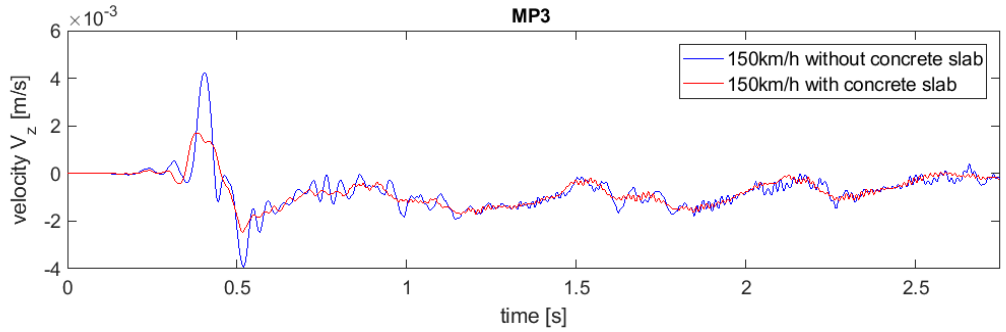

AP. D Figure 57 Velocity at location MP3 for systems with and without concrete slab at the train speed 150 km/h

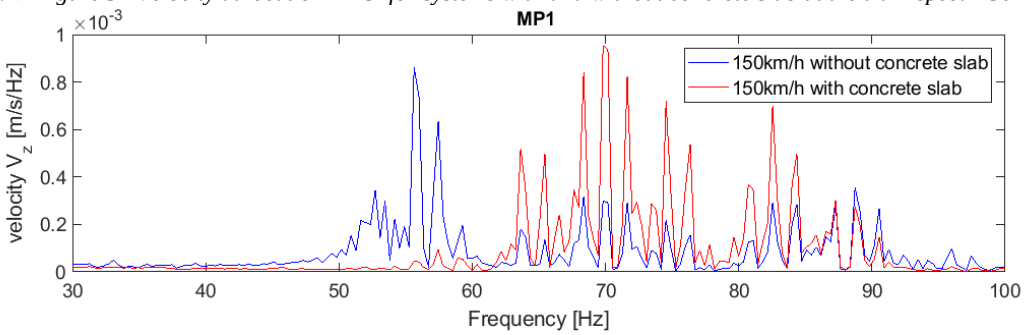

AP. D Figure 58 Spectrum of velocity at location MP1 for systems with and without concrete slab, train speed 150 km/h

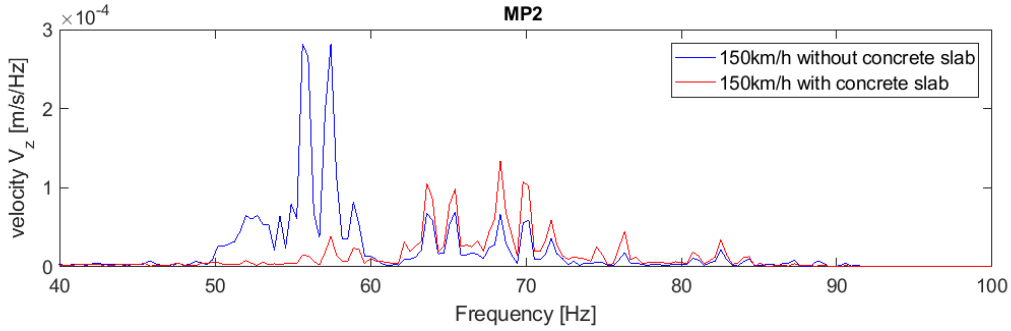

AP. D Figure 59 Spectrum of velocity at location MP2 for systems with and without concrete slab, train speed 150 km/h

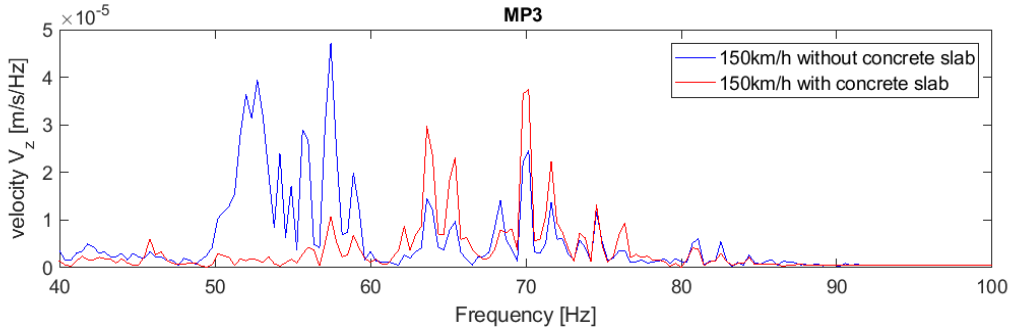

AP. D Figure 60 Spectrum of velocity at location MP3 for systems with and without concrete slab, train speed 150 km/h

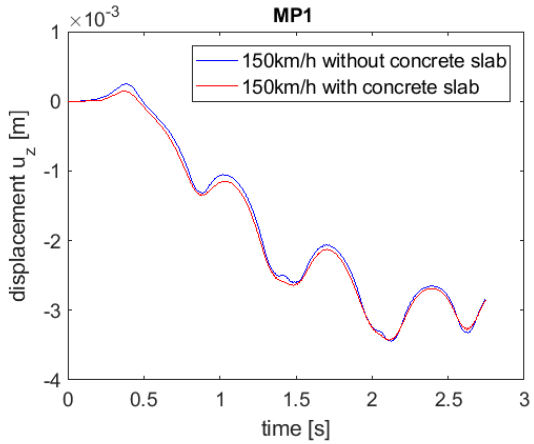

AP. D Figure 61 Displacement at location MP1 for systems with and without concrete slab, train speed 150 km/h

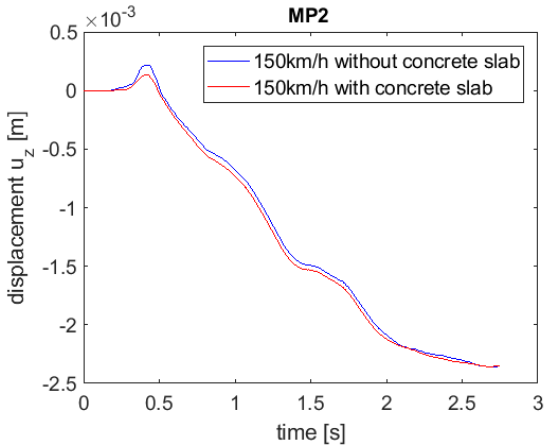

AP. D Figure 62 Displacement at location MP2 for systems with and without concrete slab, train speed 150 km/h

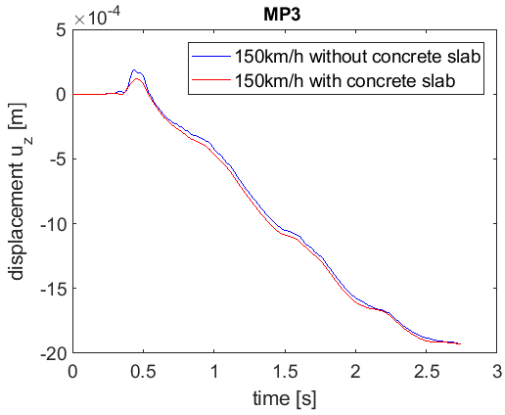

AP. D Figure 63 Displacement at location MP3 for systems with and without concrete slab, train speed 150 km/h

D5 – Comparison of results for train running at speed 110 km/h, 130km/h and 150km/h when no abatement measure is applied

In this section comparison of results of three models in which train is running at speed 110km/h, 130km/h and 150km/h is presented. In these models no concrete slab is applied. Graphs show acceleration and velocity in time and frequency domain for point locations MP1-3.

For conclusions and graphs description reader is referred to section 6.4.3.1

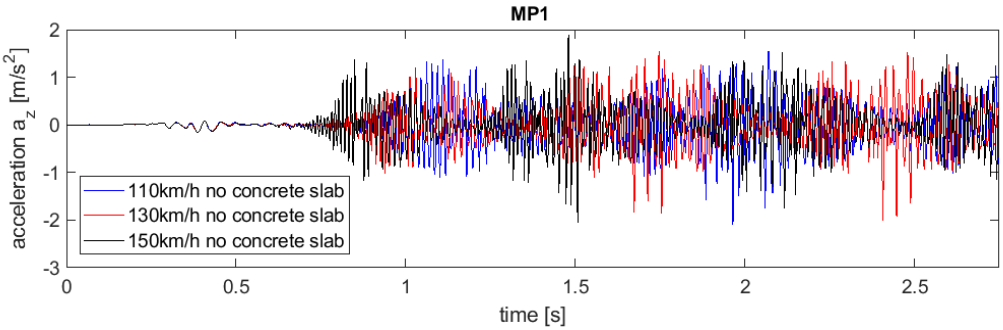

AP. D Figure 64 Comparison of accelerations in time domain for train velocities 110, 130, 150km/h when no abatement measure is used, location MP1

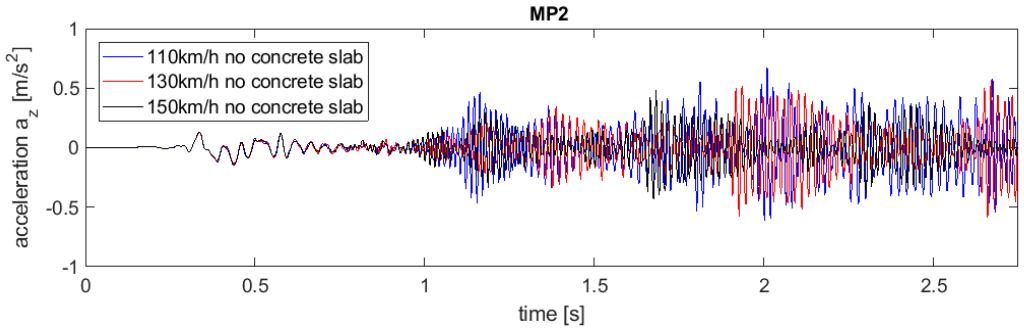

AP. D Figure 65 Comparison of accelerations in time domain for train velocities 110, 130, 150km/h when no abatement measure is used, location MP2

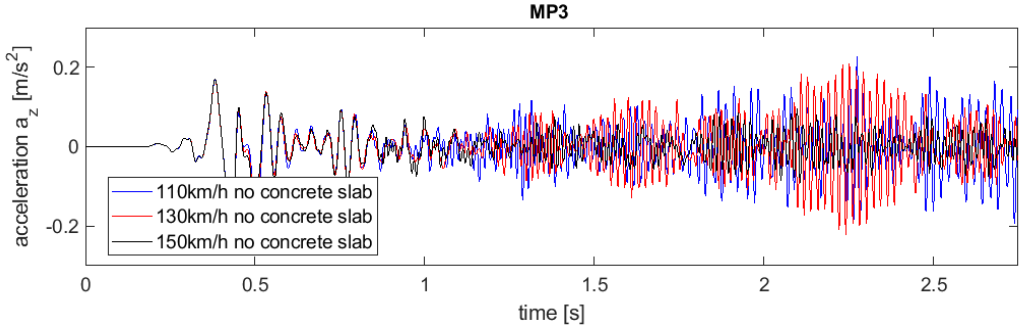

AP. D Figure 66 Comparison of accelerations in time domain for train velocities 110, 130, 150km/h when no abatement measure is used, location MP3

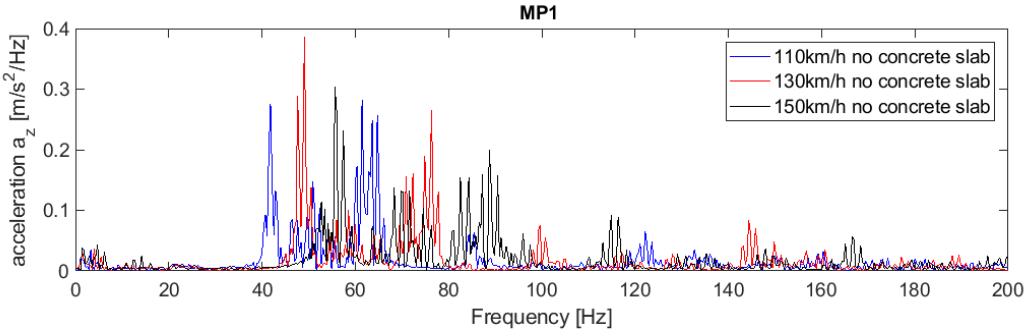

AP. D Figure 67 Comparison of spectrum of acceleration for train velocities 110, 130, 150km/h when no abatement measure is used, location MP1

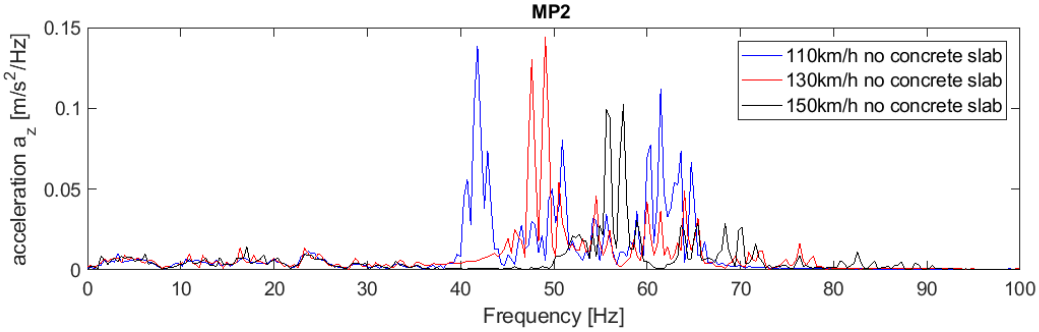

AP. D Figure 68 Comparison of spectrum of acceleration for train velocities 110, 130, 150km/h when no abatement measure is used, location MP2

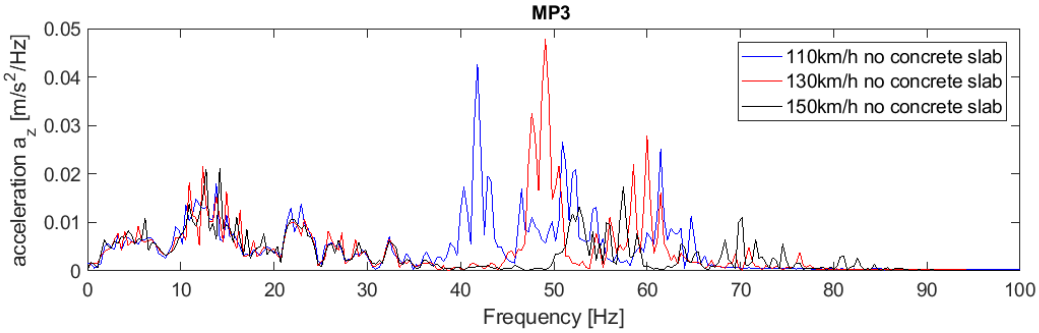

AP. D Figure 69 Comparison of spectrum of acceleration for train velocities 110, 130, 150km/h when no abatement measure is used, location MP3

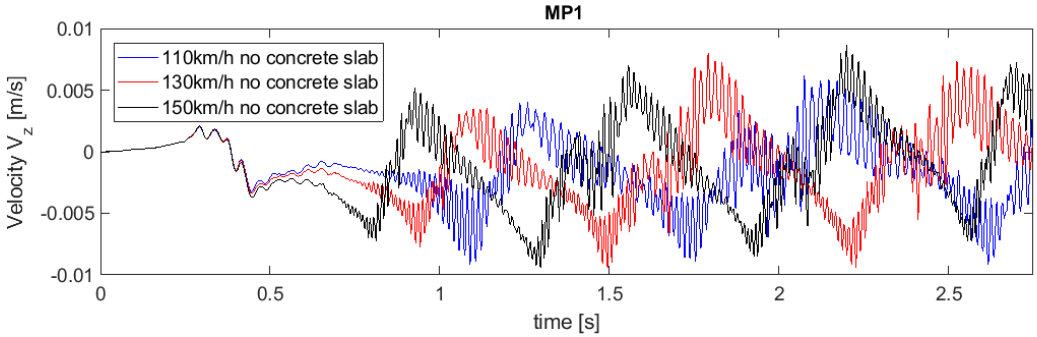

AP. D Figure 70 Comparison of velocity in time domain for train velocities 110, 130, 150km/h when no abatement measure is used, location MP1

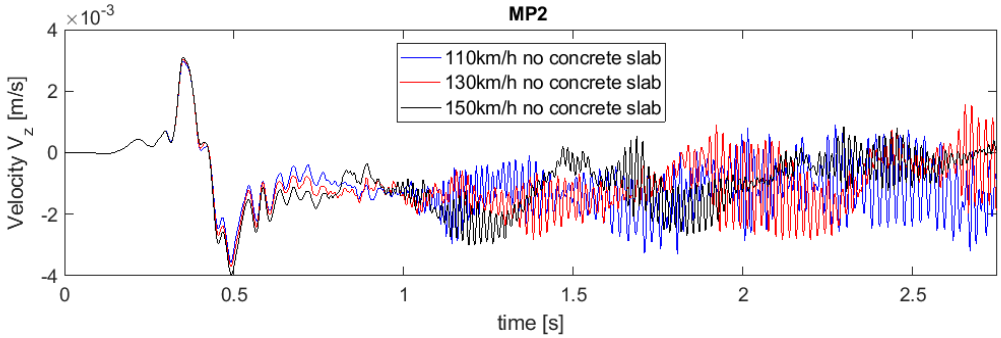

AP. D Figure 71 Comparison of velocity in time domain for train velocities 110, 130, 150km/h when no abatement measure is used, location MP2

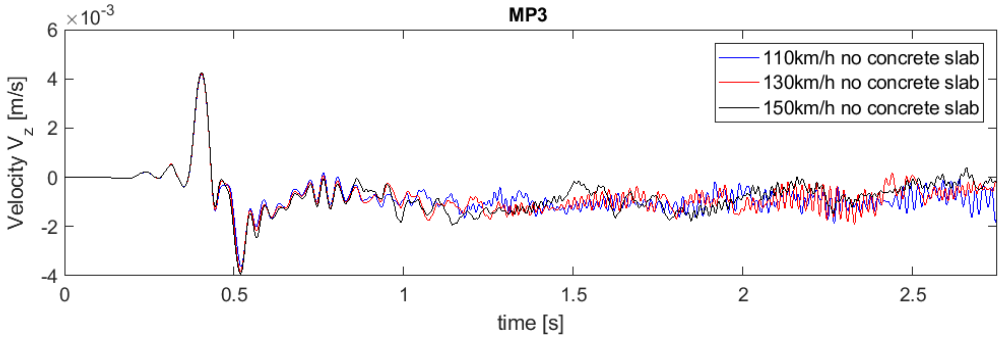

AP. D Figure 72 Comparison of velocity in time domain for train velocities 110, 130, 150km/h when no abatement measure is used, location MP3

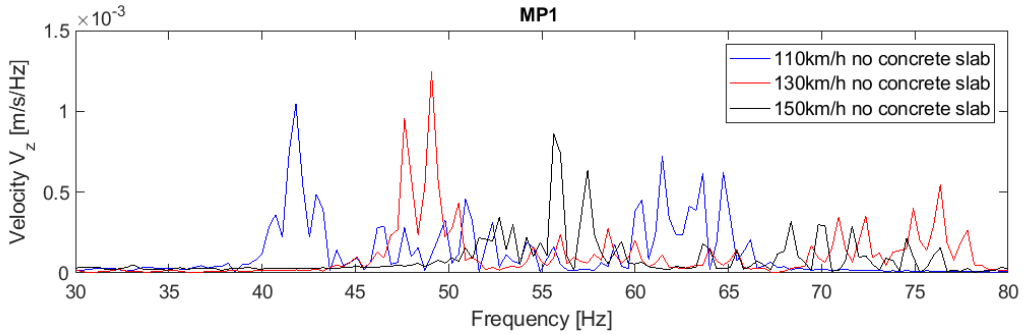

AP. D Figure 73 Comparison of spectrum of velocity for train velocities 110, 130, 150km/h when no abatement measure is used, location MP1

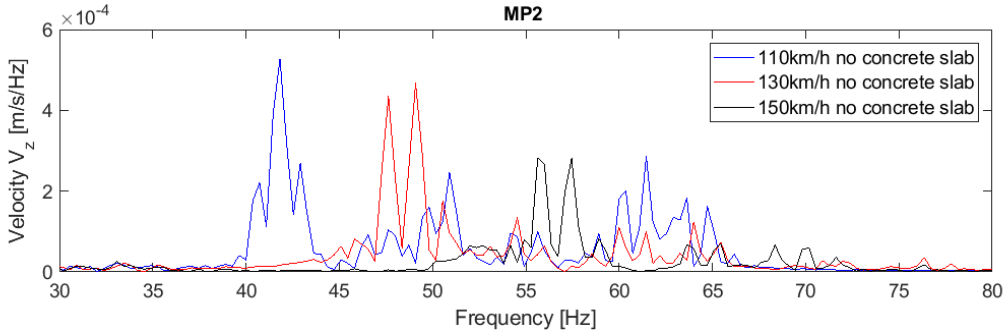

AP. D Figure 74 Comparison of spectrum of velocity for train velocities 110, 130, 150km/h when no abatement measure is used, location MP2

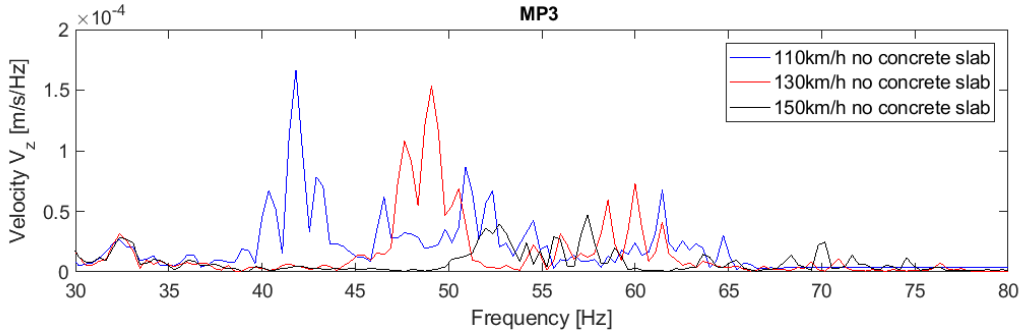

AP. D Figure 75 Comparison of spectrum of velocity for train velocities 110, 130, 150km/h when no abatement measure is used, location MP3

D6 – Comparison of results for train running at speed 110 km/h, 130km/h and 150km/h when abatement measure is applied

In this section comparison of results of three models in which train is running at speed 110km/h, 130km/h and 150km/h is presented. In these models concrete slab of dimensions 3.5m x 0.5m is present. Graphs show acceleration and velocity in time and frequency domain for point locations MP1-3.

For conclusions and graphs description reader is referred to section 6.4.3.2.

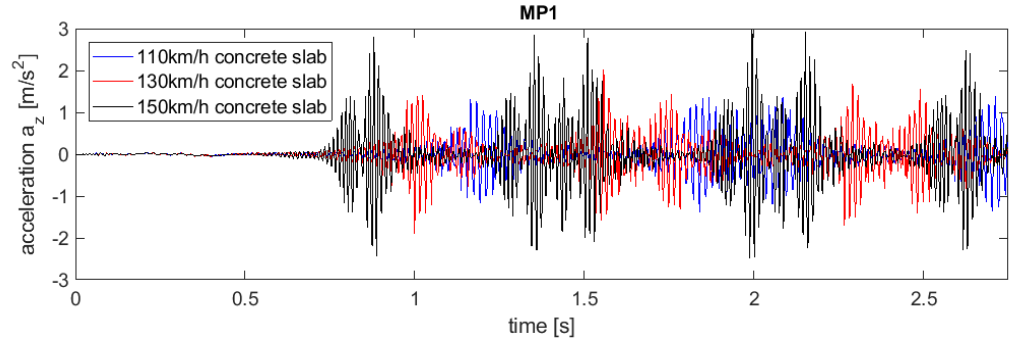

AP. D Figure 76 Comparison of accelerations in time domain for train velocities 110, 130, 150km/h when abatement measure is used, location MP1

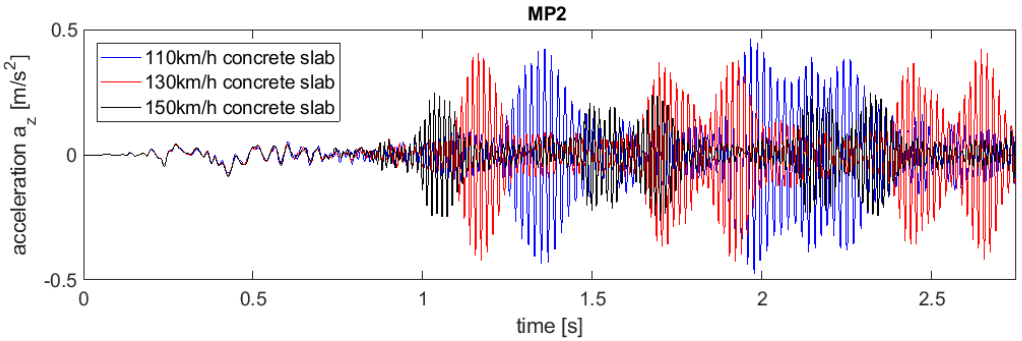

AP. D Figure 77 Comparison of accelerations in time domain for train velocities 110, 130, 150km/h when abatement measure is used, location MP2

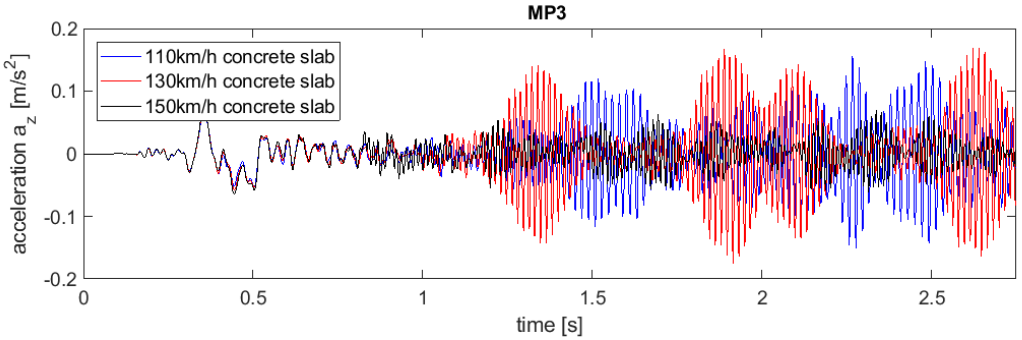

AP. D Figure 78 Comparison of accelerations in time domain for train velocities 110, 130, 150km/h when abatement measure is used, location MP3

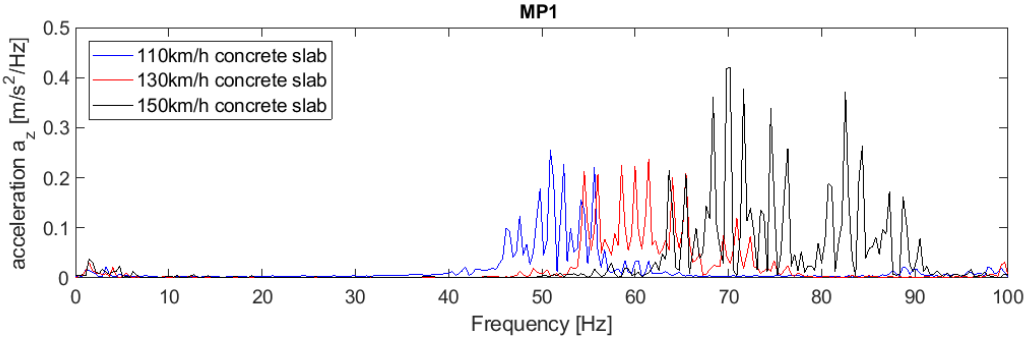

AP. D Figure 79 Comparison of spectrum of acceleration for train velocities 110, 130, 150km/h when abatement measure is used, location MP1

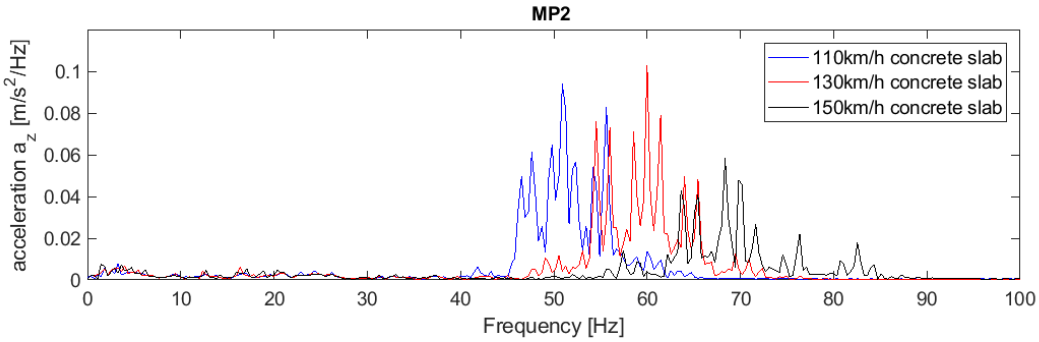

AP. D Figure 80 Comparison of spectrum of acceleration for train velocities 110, 130, 150km/h when abatement measure is used, location MP2

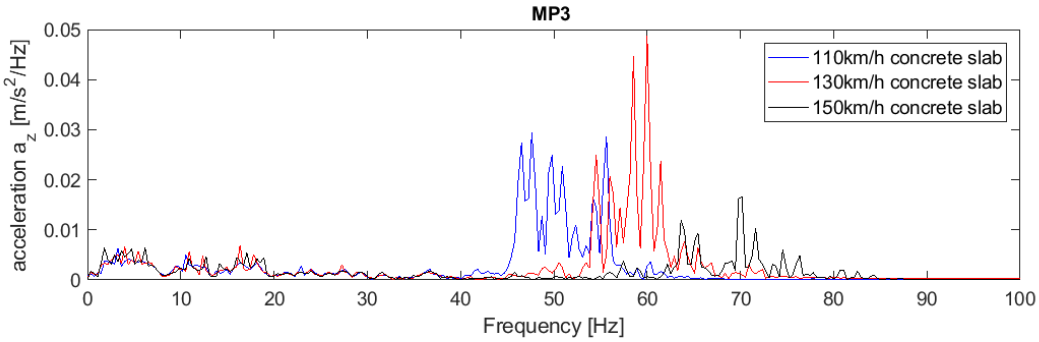

AP. D Figure 81 Comparison of spectrum of acceleration for train velocities 110, 130, 150km/h when abatement measure is used, location MP3

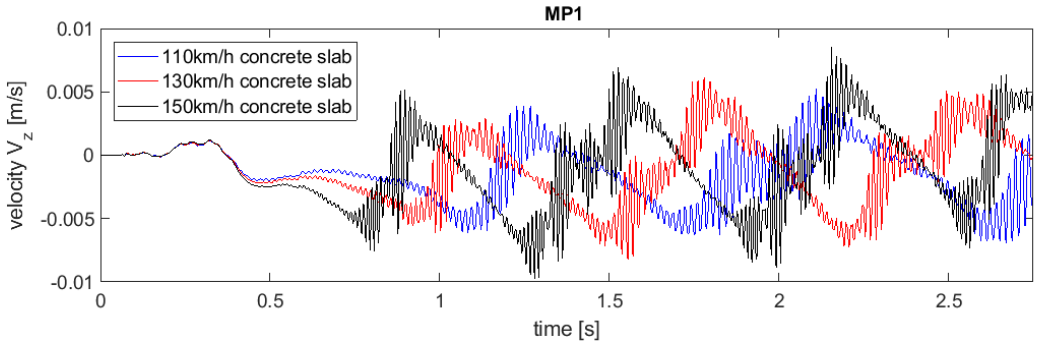

AP. D Figure 82 Comparison of velocity in time domain for train velocities 110, 130, 150km/h when abatement measure is used, location MP1

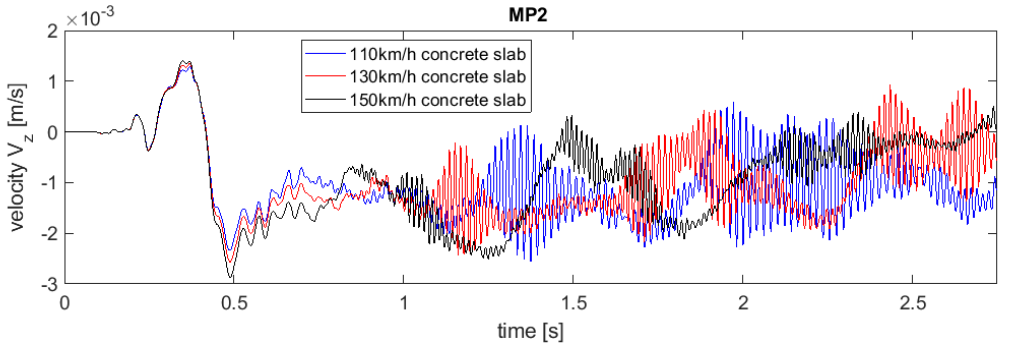

AP. D Figure 83 Comparison of velocity in time domain for train velocities 110, 130, 150km/h when abatement measure is used, location MP2

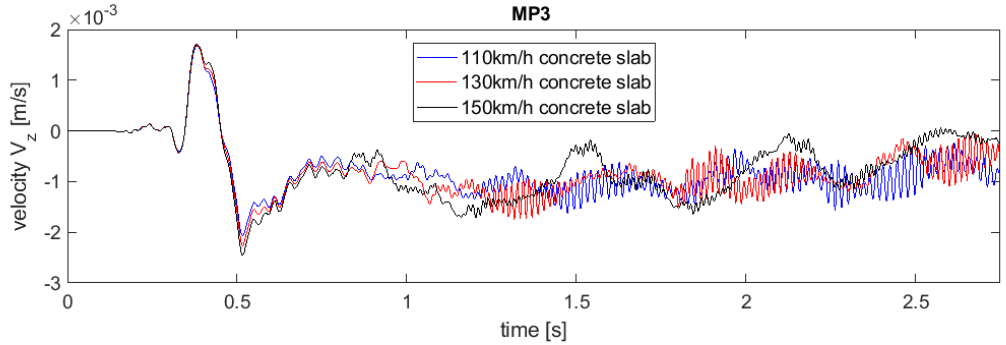

AP. D Figure 84 Comparison of velocity in time domain for train velocities 110, 130, 150km/h when abatement measure is used, location MP3

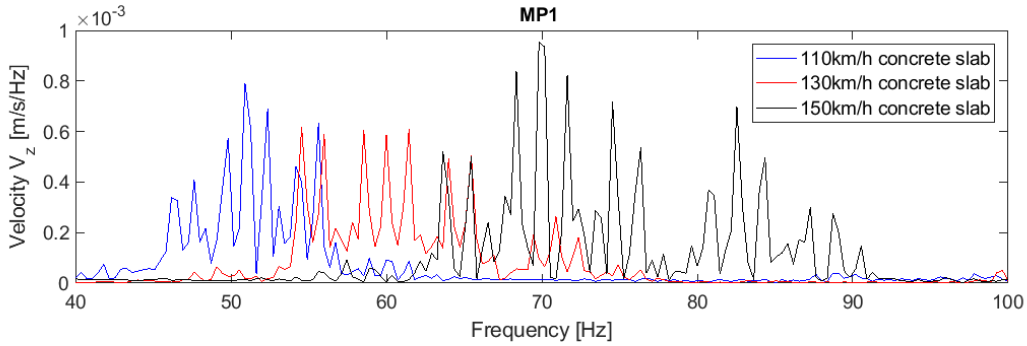

AP. D Figure 85 Comparison of spectrum of velocity for train velocities 110, 130, 150km/h when abatement measure is used, location MP1

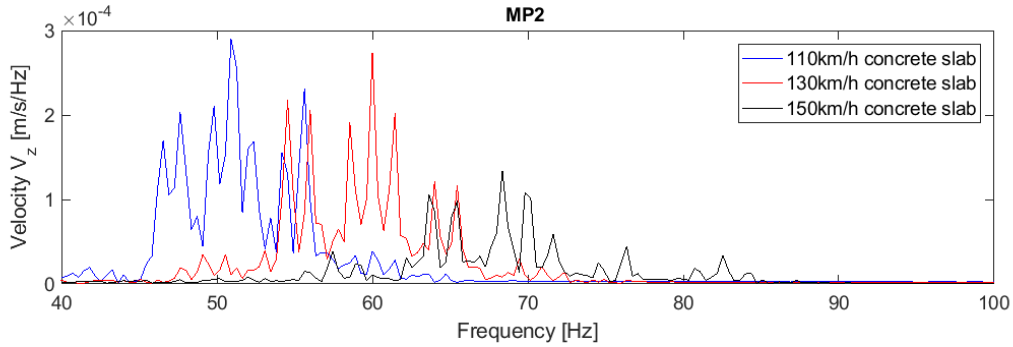

AP. D Figure 86 Comparison of spectrum of velocity for train velocities 110, 130, 150km/h when abatement measure is used, location MP2

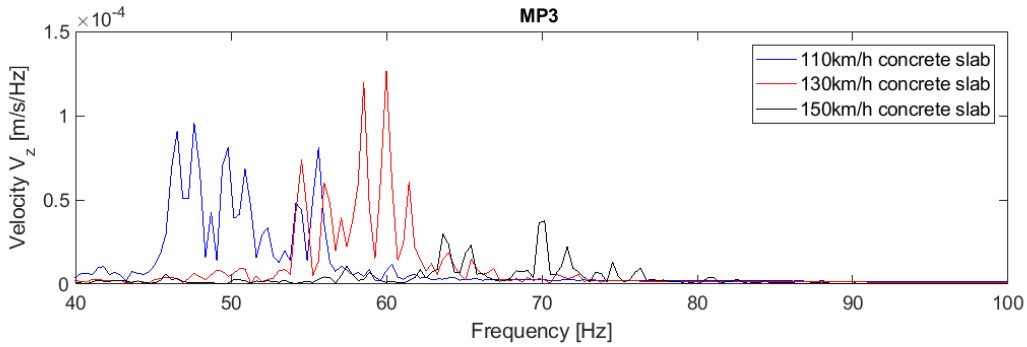

AP. D Figure 87 Comparison of spectrum of velocity for train velocities 110, 130, 150km/h when abatement measure is used, location MP3

D7 – Comparison of results when concrete slab is cracked and uncracked

This section discusses models where concrete slab is applied as the abatement measure. Comparison is made between cracked and uncracked slab cases. For uncracked concrete damping ratio is considered to be 1% but for cracked case it is 4% and 6%. Slab has dimensions 3.5m x 0.5m. Graphs depict acceleration and velocity in time and frequency domain for point locations MP1-3.

For conclusions and graphs description reader is referred to section 6.6.

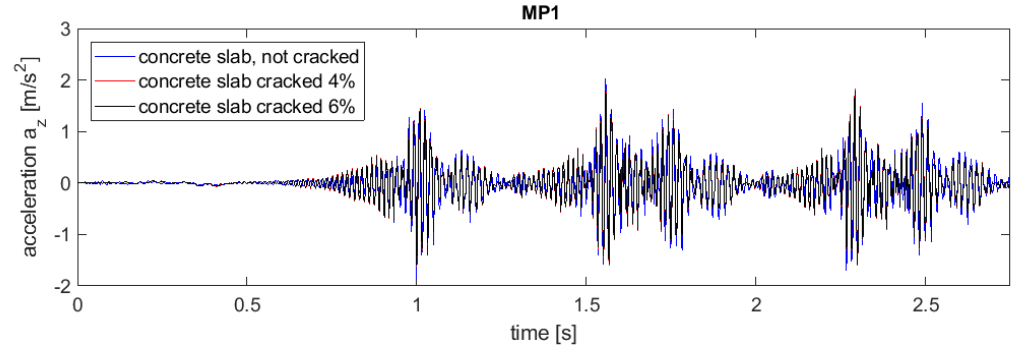

AP. D Figure 88 Acceleration for three different models of slab material properties track at MP1

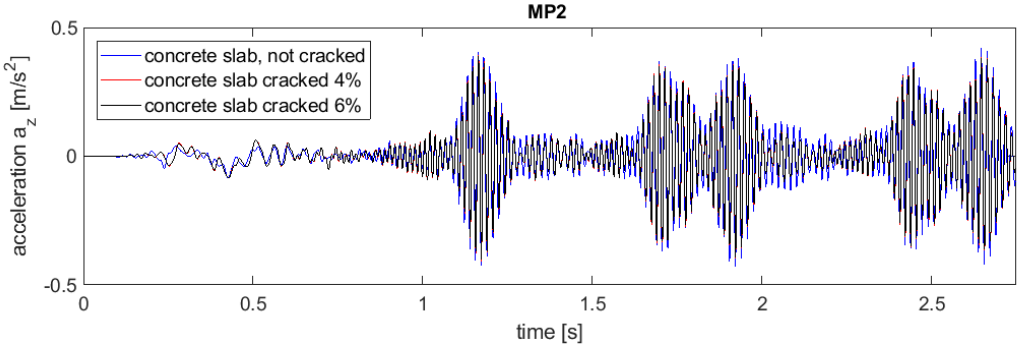

AP. D Figure 89 Acceleration for three different models of slab material properties track at MP2

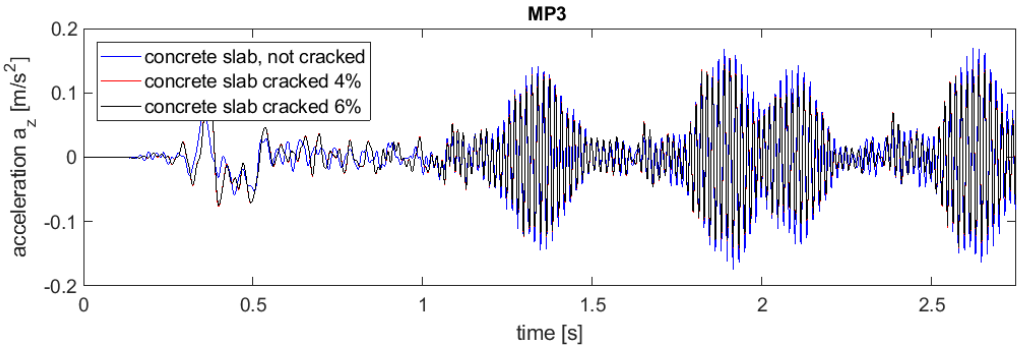

AP. D Figure 90 Acceleration for three different models of slab material properties track at MP3

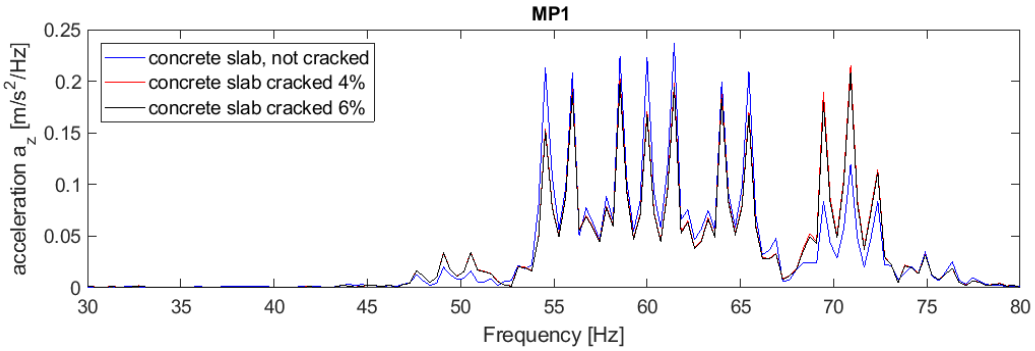

AP. D Figure 91 Acceleration in frequency domain for three different models of slab material properties track at MP1

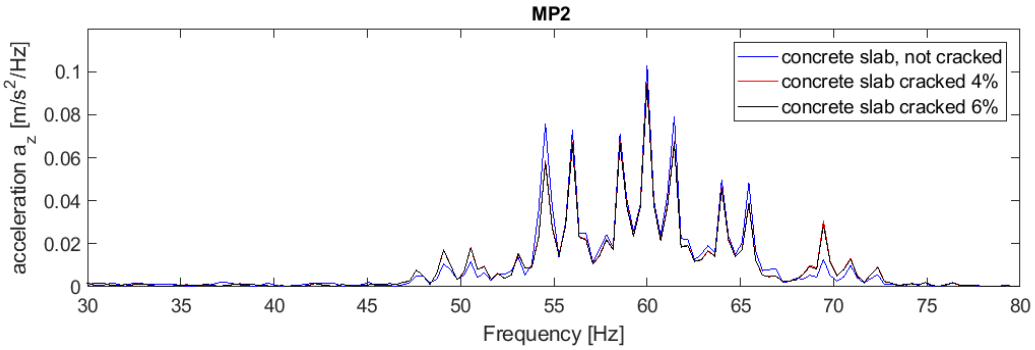

AP. D Figure 92 Acceleration in frequency domain for three different models of slab material properties track at MP2

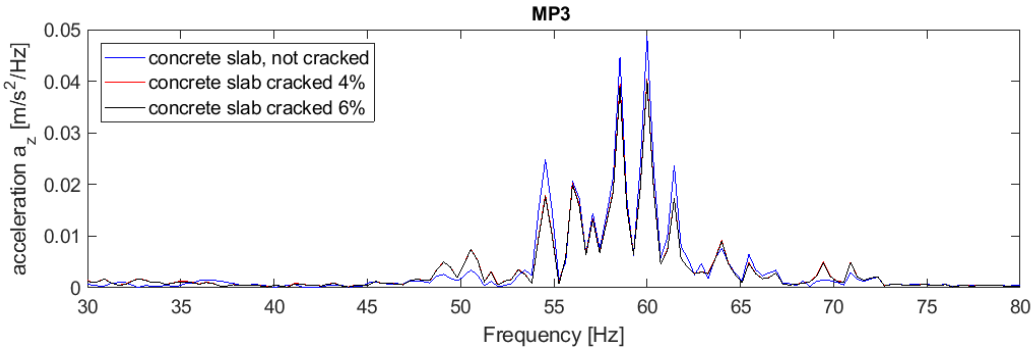

AP. D Figure 93 Acceleration in frequency domain for three different models of slab material properties track at MP3

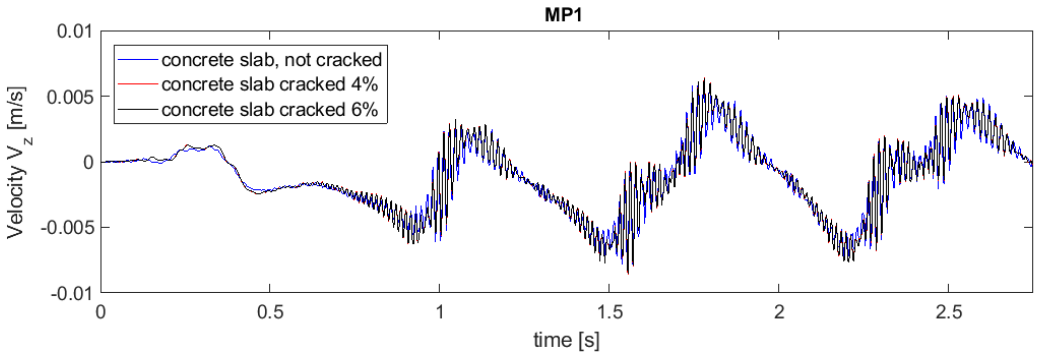

AP. D Figure 94 Velocity for three different models of slab material properties track at MP1

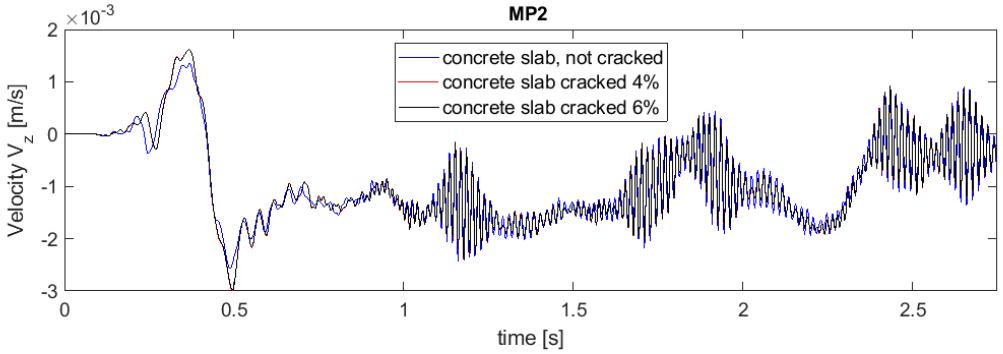

AP. D Figure 95 Velocity for three different models of slab material properties track at MP2

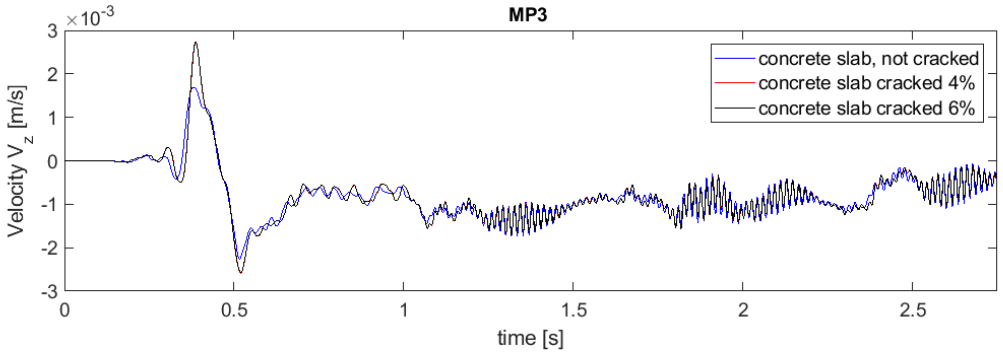

AP. D Figure 96 Velocity for three different models of slab material properties track at MP3

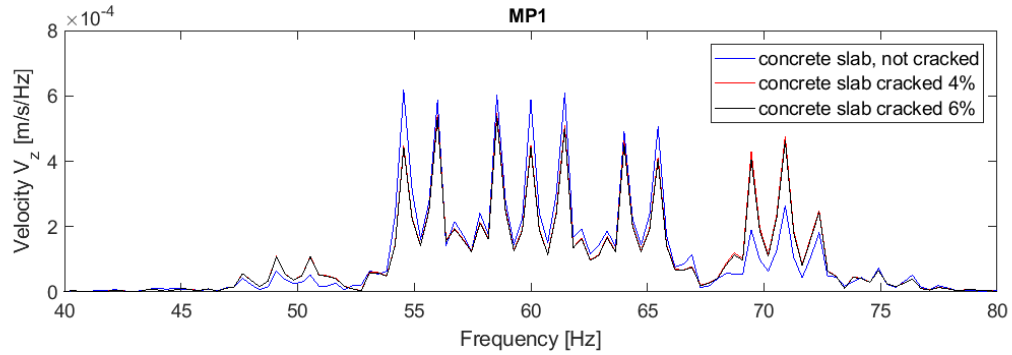

AP. D Figure 97 Velocity in frequency domain for three different models of slab material properties track at MP1

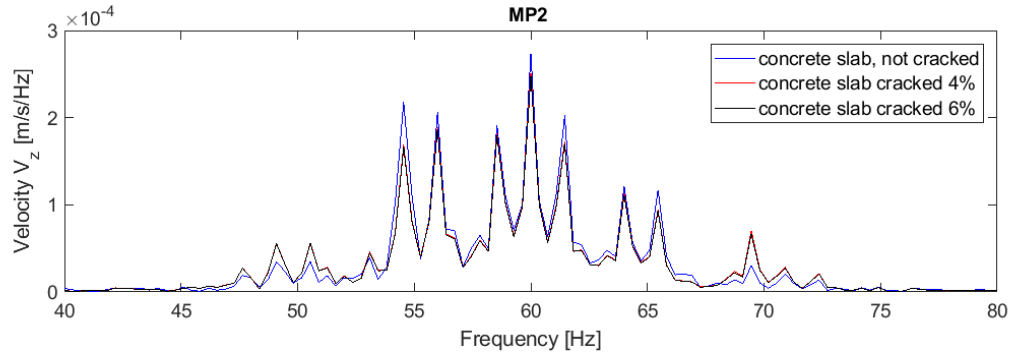

AP. D Figure 98 Velocity in frequency domain for three different models of slab material properties track at MP2

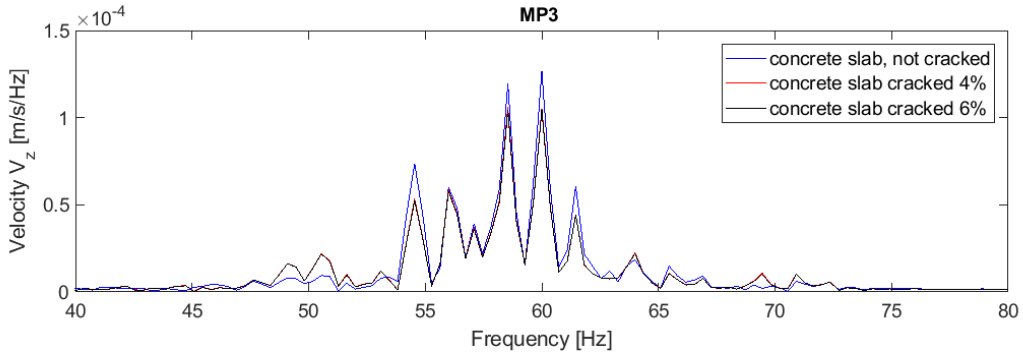

AP. D Figure 99 Velocity in frequency domain for three different models of slab material properties track at MP3

D8 - Scatter effect when building included in the numerical model

No information is available about the building. Therefore, slab in the model the foundation is assumed to be soild. It has 80cm, from which 20cm is raised above the ground level. Damping ratio of foundation is set to 1%. Concrete is uncracked. On site two buildings are present what is reflected during numerical modelling. Patameters from Table 4.1 and Table 5.2 are valid in this variation. Other relevant model parameters (e.g. rail, sleepers, soil profile and its properties etc.) are the same as in the model from section 6.5.

Walls are modelled as a plate of thickness d = 12cm, weight γ = 19kN/m^3. Height of the building is equal to 3m measuring from the foundation level.

Roof is modelled as a plate of thickness d = 40cm. Itis assumed to be made of system Teriva 34/60 HIGH (Poznan, 2015) which 1m^2 weight is equal to approximately 350kg. Therefore, weight γ=8.58kN/m^3.

The model used to perform this simulation is presented in the AP. D Figure 100. Small red “X” indicates the position of MP3 point. It is placed between two buildings.

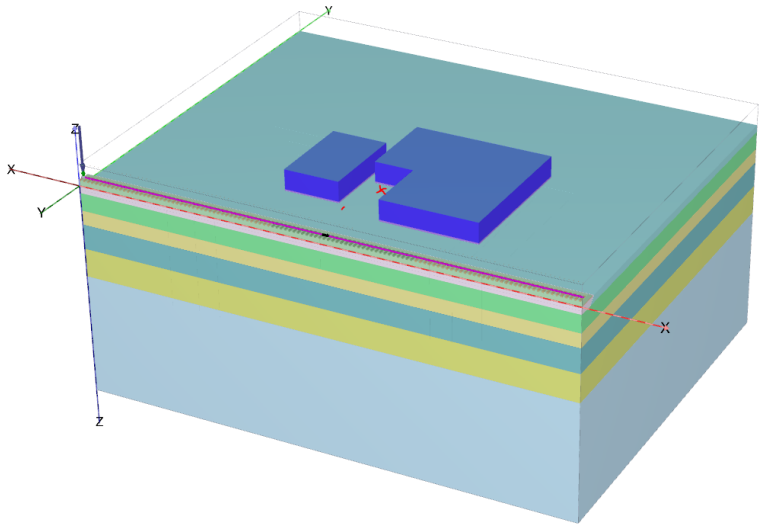

AP. D Figure 100 The overview for the model used to study scatter effect

The results of acceleration are analyzed only. They are presented from AP. D Figure 101 to AP. D Figure 108.

Discussion of the acceleration results in time and frequency domain

Small increment in accelerations is observed at point MP1 (from 2 to 2.15 m/s^2). However, for MP2 the response is smaller at some peaks but in general, very similar to the model where building was not included, thus no change in the results is observed at this location.

Next, for MP3 the reposnse is considerably smaller for the model where the building is present. That model maximum acceleration value is equal to 0.07m/s^2 while in the numerical model without structure it is 0.22m/s^2. The decrease is by 66%. This can be casued by the fact that point MP3 is shielded from incoming waves and vibrations are transferred only through the narrow soil strip.

For points MP4 (wall) and MP5 (floor) the results are very far off from the measurements. Moreover, results obtained from numerical model for MP4 and MP5 are very similar to each other. That can be the effect of sudden entrance of the load into the model. Another possible explanation might be that building is too heavy and too stiff to give noticable vibrational response.

Regarding spectrum results, the only noticeable thing is that 50Hz frequency has much smaller magnitude for point MP3 when building is included in the model.

Calculation time of this model is 6-7 days. Therefore, due to many uncertantities invloved in this iteration and long time needed to investigate this effects no more simulations are performed.

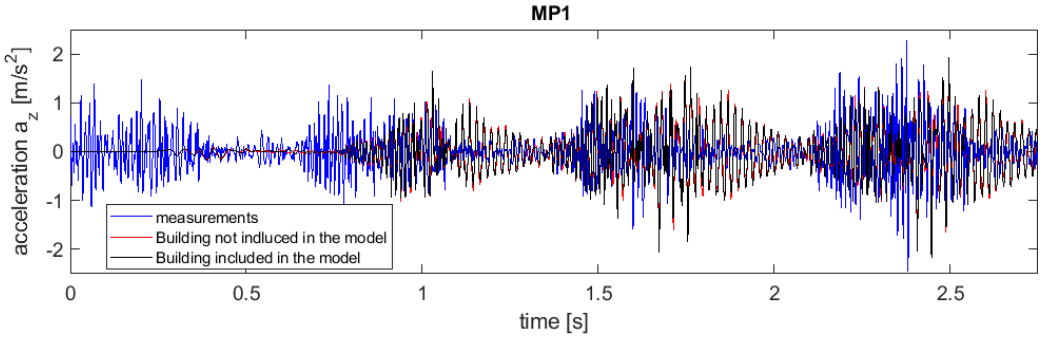

AP. D Figure 101 Comparison of acceleration from measurements and numerical model with and without building included at MP1

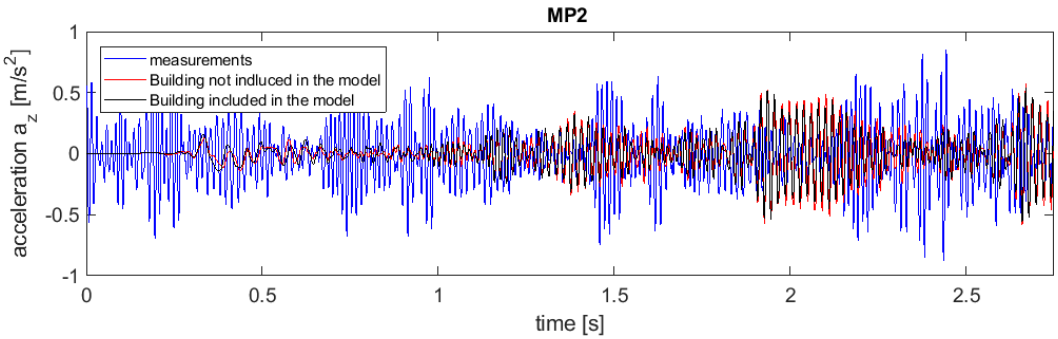

AP. D Figure 102 Comparison of acceleration from measurements and numerical model with and without building included at MP2

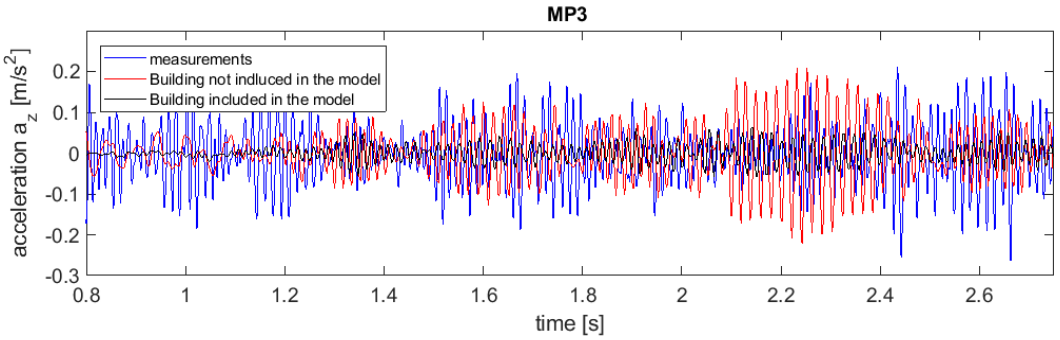

AP. D Figure 103 Comparison of acceleration from measurements and numerical model with and without building included at MP3

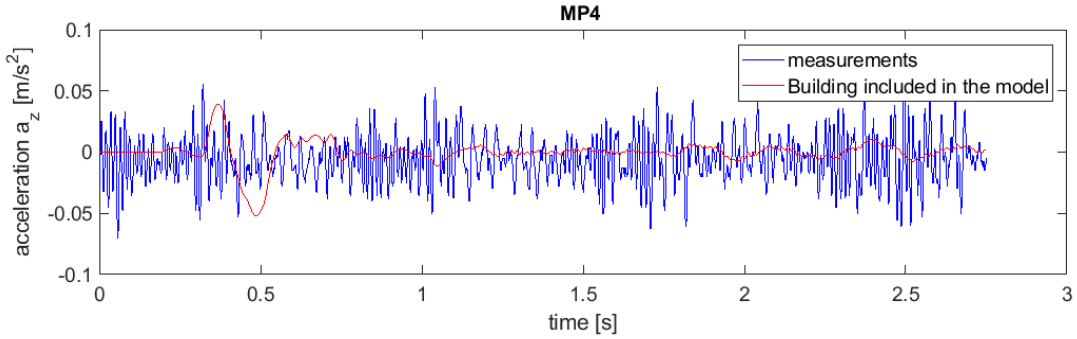

AP. D Figure 104 Comparison of acceleration from measurements and numerical model with building included at MP4

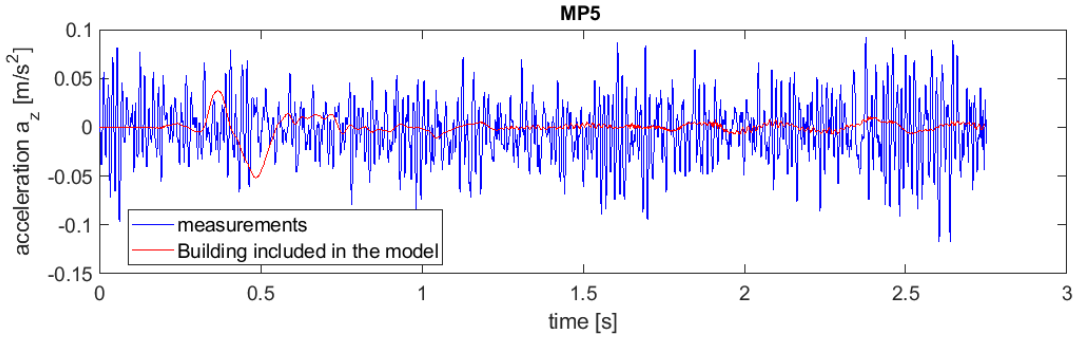

AP. D Figure 105 Comparison of acceleration from measurements and numerical model with building included at MP5

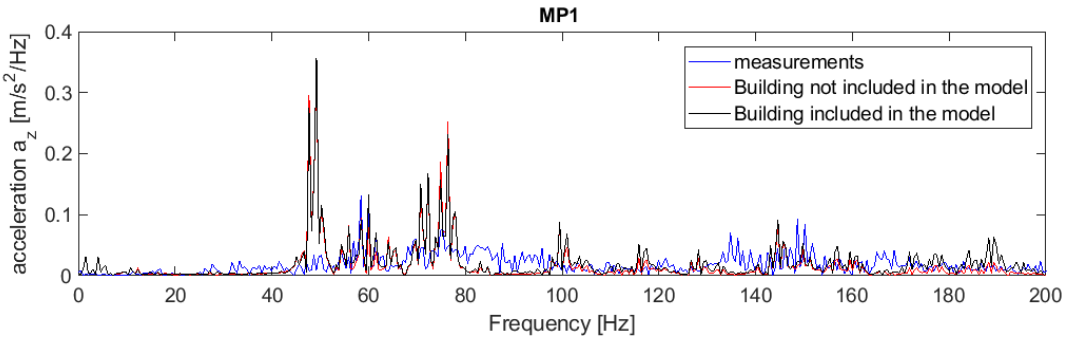

AP. D Figure 106 Comparison of acceleration spectrum from measurements and numerical model with and without building included at MP1

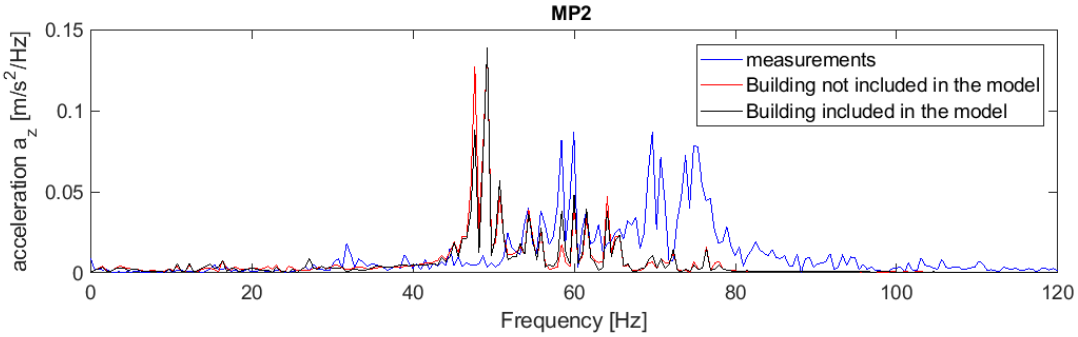

AP. D Figure 107 Comparison of acceleration spectrum from measurements and numerical model with and without building included at MP2

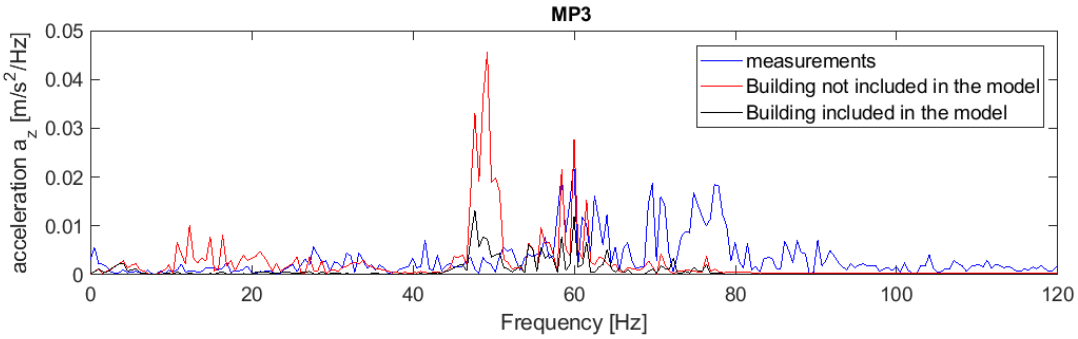

AP. D Figure 108 Comparison of acceleration spectrum from measurements and numerical model with and without building included at MP3